The Role of the K^+ Channel $K_{Ca}3.1$ in Idiopathic Pulmonary Fibrosis

Thesis submitted for the degree of

Doctor of Philosophy

at the University of Leicester

by

Katy Morgan Roach BSc (Hons)

Department of Infection, Immunity and Inflammation

University of Leicester

October 2012

Abstract

Katy Morgan Roach

The Role of the K^+ Channel $K_{Ca}3.1$ in Idiopathic Pulmonary Fibrosis

Idiopathic pulmonary fibrosis (IPF) is a common disease with a median survival of only 3 years. There is no effective treatment. IPF is characterized by myofibroblast accumulation and progressive lung scarring. The Ca^{2+}-activated K^+ channel $K_{Ca}3.1$ modulates the activity of several structural and inflammatory cells which play important roles in model diseases characterized by tissue remodelling and fibrosis. We hypothesise that $K_{Ca}3.1$-dependent cell processes are a common denominator in IPF.

$K_{Ca}3.1$ expression and function were examined in human myofibroblasts derived from IPF and non-fibrotic (NFC) donors. Myofibroblasts grown *in vitro* were characterised by western blot, immunofluorescence, RT-PCR and patch clamp electrophysiology to determine $K_{Ca}3.1$ channel expression. Wound healing, collagen secretion and contraction assays were performed using the pro-fibrotic mediators TGFβ1 and bFGF and two specific $K_{Ca}3.1$ blockers (TRAM-34, ICA-17043 [Senicapoc]).

Both NFC and IPF myofibroblasts expressed $K_{Ca}3.1$ channel mRNA and protein. Using the $K_{Ca}3.1$ channel opener 1-EBIO, $K_{Ca}3.1$ ion currents were elicited in 59% of NFC and 77% of IPF myofibroblasts tested (P=0.0411). These currents were blocked by TRAM-34 (200 nM). The 1-EBIO-induced currents were significantly larger in IPF cells compared to NFC cells (P=0.0078). TGFβ1 and bFGF increased $K_{Ca}3.1$ channel expression. TRAM-34 and ICA-17043 dose-dependently attenuated wound healing, TGFβ1-dependent collagen secretion and bFGF- and TGFβ1-dependent contraction.

We show for the first time that human lung myofibroblasts express the $K_{Ca}3.1$ K^+ channel. $K_{Ca}3.1$ channel block attenuates pro-fibrotic myofibroblast function. These findings raise the possibility that blocking the $K_{Ca}3.1$ channel will inhibit pathological myofibroblast function in IPF, and thus offer a novel approach to IPF therapy.

Acknowledgements

I would first and foremost like to say a special thanks to my supervisor Professor Peter Bradding. Throughout my three years he has been a continuous source of support, encouragement and guidance. This thesis would not have been possible without his constant enthusiasm, patience and wit, which helped to keep me motivated.

I would like to thank my colleagues within the Department of Respiratory Medicine. In particular to Dr Fiona Symon, who encouraged me to begin a PhD and Dr Glenn Cruse for his help to get my PhD off the ground. Also my PRP panel, Dr Yassine Amrani and Dr Erol Gaillard for their advice and guidance during my PhD. I am most grateful to Dr Carol Feghali-Boswick for her kind donation of the IPF fibroblasts; they were a valuable and integral part of my PhD. And to the numerous placement students who helped maintain the cells.

Finally, I would like to express my gratitude and appreciation to my family and friends. To my big sisters, Jaymie and Hayley, who I have always admired and treasured, and who kept my spirits high with their endless joviality. To my Mother and Father, Angela and Malc, who have always believed in me and made me believe that anything is possible; without you both I would never have soared this high. To my fiancé, Andrew, my rock, for your relentless love and understanding. Finally to my late Granddad and Grandma, John and Mary Morgan, your inspiration led me to strive be a doctor, and it is to “ye” both and your loving memory that I dedicate this thesis.

Table of Contents

List of Figures

List of Tables

List of Abbreviations

αSMA	Alpha smooth muscle actin
ASM	Airway smooth muscle cell
ATS	American Thoracic Society
BEGM	Bronchial epithelial growth medium
bFGF	basic Fibroblast growth factor
Ca^{2+}	Calcium
CCL	Chemokine ligand
CTGF	Connective tissue growth factor
DLCO	Diffusing capacity of the lung for carbon monoxide
ECM	Extracellular matrix
EDA	Extra domain A
EGF	Epidermal growth factor
EMT	Epithelial mesenchymal transition
FEV_1	Forced expiratory volume in the first second
FVC	Forced vital capacity
GM-CSD	Granulocyte-macropage colony-stimulating factor
HRCT	High resolution computed topagraphy
IFNγ	Interferon γ
IGF-1	Insulin like growth factor
IIP	Idiopathic interstitial pneumonias

IL	Interleukin
ILD	Interstitial lung disease
IPF	Idiopathic pulmonary fibrosis
K^+	Potassium
MGM	Myofibroblast growth medium
NFC	Non fibrotic control
NSIP	Nonspecific interstitial pneumonia
PDGF	Platelet derived growth factor
SF	Serum free
SFTPC	Surfactant protein C
TERT	Telomerase reverse transcription
TGFβ	Transforming growth factor β
TNFα	Tumor necrosis factor α
UIP	Usual interstitial pneumonia
VEGF	Vascular growth factor

1 Introduction

1.1 Idiopathic Interstitial Pneumonias

Idiopathic interstitial pneumonias (IIP) are common lung diseases of unknown etiology. Initially 5 groups of IIP were detailed by pathological classification, but this has since been reviewed and increased to 7 distinct subtypes of IIP(1). These diseases are categorised according to different clinical, radiologic and histologic classifications(2,3). The diagnosis of IIP's has been notoriously difficult as they commonly display overlapping clinical features(4). The gold standard for classification of IIP's is through histological analysis, but even then the final diagnosis is often uncertain. Many IIP's have a poor prognosis, worse than many cancers. A better understanding of the factors driving their expression is essential if we are to develop effective therapies. The most common IIP encountered clinically is usual interstitial pneumonia (UIP), which is the characteristic histological pattern of idiopathic pulmonary fibrosis, formerly known as cryptogenic fibrosing alveolitis.

1.1.1 Usual interstitial pneumonia/Idiopathic pulmonary fibrosis

Idiopathic pulmonary fibrosis (IPF) is the most common IIP, defined as a specific form of chronic fibrosing interstitial pneumonia associated with the histological appearance of usual interstitial pneumonia (UIP) on surgical lung biopsy(3).

IPF has an unknown etiology(2) and is marked by progressive lung fibrosis leading to respiratory failure. The pathogenic mechanisms involved in IPF initiation and its progression are not well understood(5), and there is no effective treatment(6,7). Prognosis is bleak with a median survival of only 3 years, worse than many cancers(8). IPF patients present with a mean age of between 60 to 65 years at diagnosis(7).

1.1.1.1 Demographics

The incidence of IPF increases with age and it is more common in men than in women(5). The prevalence of IPF in the USA was estimated to range from 4 per 100,000 persons aged 18-34, and 227 cases per 100,000 among those aged 75 years or older(5). Within the last decade the incidence of IPF has risen significantly, increasing by 11% annually in the UK(9).

There seems to be no geographical distribution to IPF, cases are reported in both rural and urban settings. Data suggests IPF targets no specific race, ethnicity or social group, however age-adjusted mortality rates seem higher among Caucasians(10). Geographical variation of age adjusted mortality rates have been observed, which is probably due to occupational or environmental exposures(3).

Mortality from IPF has been increasing in recent years, claiming more lives annually than many types of cancer(11). The crude

mortality rate for people with IPF was 180 per 100,000 persons-years(12) in the UK, gender and age being the most important determinants of survival(9). Other investigators have shown a 10% decline of Forced Vital Capacity (FVC) as another poor prognostic indicator or predictor of survival(13).

1.1.1.2 Etiology

The etiology of IPF is unknown, hence the term 'idiopathic'. The current hypothesis regarding its development is that ongoing multiple, microscopic, isolated episodes of alveoli epithelial injury lead to an abnormal wound healing response of fibrotic repair mechanisms(14). The factors initiating the injury and maintaining the inflammatory/fibrotic responses are elusive, yet there are associated risk factors(15):-

1.1.1.2.1 Cigarette smoking

Smoking has consistently been associated with IPF, and multiple studies have confirmed that the probability of developing IPF increases with the number of pack-years of smoked. However, only an association between current smoking and IPF can be seen; there is no correlation between disease state and a history of ever smokers(16).

1.1.1.2.2 Occupational and environment

Various occupational environments have been linked to the development of IPF, including several metal dusts and wood dusts(17). This risk is amplified with longer work years exposed(3). Other studies have found associated risk with occupations classed as 'dirty'(17) and an increased risk for those exposed to solvents(18). It should be noted though that the majority of these studies relied on patient questionnaires for exposure information and clinical diagnosis is often poorly defined.

Exposures in rural settings have also been linked to an increased risk in developing IPF; farming, livestock, agricultural areas and even raising birds have all been implicated(16,19).

1.1.1.2.3 Chronic aspiration

The introduction of acid into the respiratory tree as a result of gastroesophageal reflux disease plays a key role in the development of IPF(20,21). Patients with IPF have a significantly higher prevalence of increased esophageal acid exposure(20).

1.1.1.2.4 Infections

Patients with IPF have shown an increased susceptibility and incidence of virus infections such as influenza, hepatitis C(22) and Epstein-Barr virus(23). Other viruses implicated in the development

of the disease are Parainfluenza 1 and 3 virus, measles, Legionnaires disease, and human immunodeficiency virus-1 (HIV-1)(3).

1.1.1.2.5 Hereditary factors

Although a genetic marker is yet to be found, there are strong links to a familial predisposition in IPF. Familial IPF is defined as at least two members of a primary biological family having clinical features of the disease confirmed histologically(3). Supporting this hypothesis of a genetic predisposition, one study found the induction of pulmonary fibrosis in genetically susceptible mice(24). More recently mutations of telomerase reverse transcriptase (TERT) and surfactant protein C (SFTPC) have been identified in about 10% of individuals with familial pulmonary fibrosis although the predictive value of this as a test has not yet been established(25). Case studies have highlighted that a younger age of disease presentation is linked to familial IPF, and that if these cases do occur family members should also be tested(26,27).

1.1.1.3 Diagnosis of IPF

IPF patients present with symptoms of exercise-induced breathlessness and dry cough. Auscultation of the lungs reveals inspiratory crackles located in the lower posterior lung zones(13). Finger clubbing is present in approximately 50% of patients(13,28).

Guidelines on the diagnosis and management of IPF were released in 2000 by the American Thoracic Society (ATS)(3), and

more recently in 2011 by the ATS, European Respiratory Society (ERS), Japanese Respiratory Society (JRS) and the Latin American Thoracic Association (ALAT)(7). Techniques such as chest radiographs, high resolution computed tomography (HRCT) scanning and pulmonary function tests are all recommended to confirm the clinical, physiological or radiological features. However, if the patient presents with clubbing this usually suggests diagnosis of IPF as this is not found in the other forms of IIP. Commonly HRCT is performed, and if it shows classical signs or is highly suggestive of IPF then surgical lung biopsy is not necessary. If HRCT is not typical then surgical lung biopsy is recommended (dependent on the patients' health) and patterns studied in combination with HRCT. The major purpose is to distinguish UIP, the histopathological pattern of IPF from other subsets of IIP(3). Accurate diagnosis is challenging and requires the skilled integration of clinical, radiographic and histopathological findings that rarely follow the textbook criteria in appearance(6).

Histologically, the hallmark of IPF is the presence of scattered fibroblast foci(29). **See Figure 1-1**. In addition, there is a patchy distribution of temporally heterogeneous fibrosis interspersed with areas of healthy lung. Excess collagen deposition leads to fibrosis and subsequent honeycombing(2).

In the early phase of the disease chest radiographs may be normal, but in the advanced stage there is decreased lung volumes and subpleural reticular opacities that increase from the apex to the base of the lungs(30).

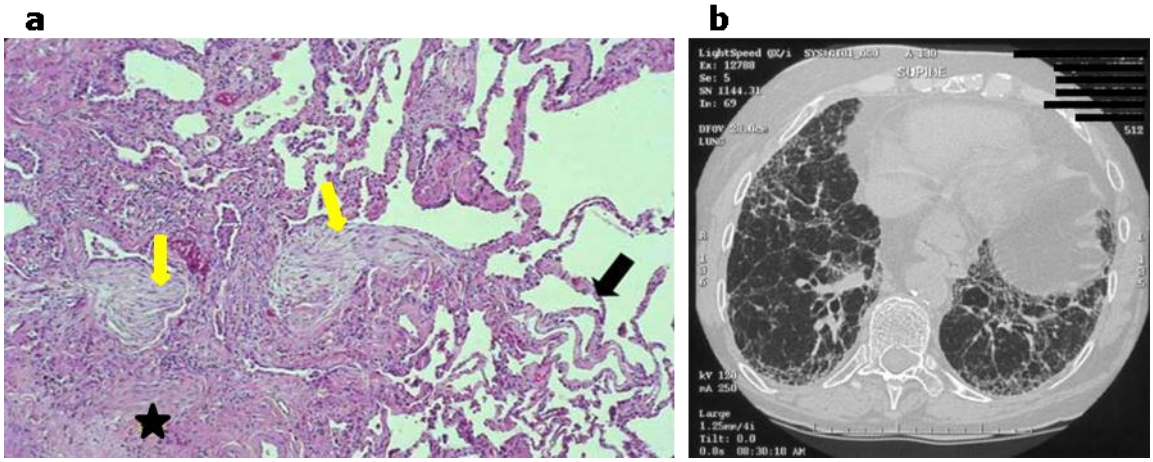

Figure 1-1. Histologic and imaging features of IPF

a) Histological features of IPF. There is patchy subpleural dense fibrosis (star), focal areas of collagen deposition and fibroblast foci (narrow yellow arrows). These abnormalities are adjacent to relatively normal appearing lung(large arrow). **b)** HRCT of IPF patient shows the presence of bi-basilar, peripheral reticular abnormality and honeycombing. Pictures taken from(31).

1.1.1.4 Treatment

IPF is a devastating diagnosis as it has no effective therapy and its prognosis is poor(32). Respiratory failure is the most common cause of death and accounting for over 80% of fatalities(5). Treatments available to IPF patients include oxygen therapy, lung transplantation, preventative therapy (Flu-vaccine) and pulmonary rehabilitation. Various attempts at treatment have been tried over the years, and early clinical trials suggested a combined prednisone and azathioprine as a safe and possibly effective regimen(33). However, many studies investigating new modes of IPF treatments, revealed patients treated with prednisone(34,35), interferon gamma-1b(36), bosentan(37), and azathioprine(38) showed no significant signs of improved lung function or survival. Those which had claimed positive outcomes to treatment, on intense scrutiny, had major flaws in experimental design such as disease definition(39), lack of randomization(39), absence of placebo(38) or small patient numbers(40). More prominently these treatments, being of little or no benefit to the patient were accompanied with serious health risks and side effects, including osteoporosis and diabetes(41). In one retrospective study, the use of corticosteroids or cyclophosphamide was associated with increased mortality(12).

After the release of the ATS guidelines in 2000, there was an overall reduction of the use of corticosteroids, but the use of cytotoxic agents increased significantly(42).

Pirfenidone has been approved for treatment in the US based on the results of 4 randomised, placebo controlled trials although not all achieved their primary outcome(43,44). This drug has anti-fibrotic and anti-inflammatory properties and may slow the decline in lung function of IPF patients and reduce the risk of disease the progression(44). However, again this drug comes with serious side effects including gastrointestinal discomfort, anorexia, skin reactions and photosensitivity(45).

Therefore, it seems unreasonable to expose patients to the treatment risks in the presence of diagnostic uncertainty(46), and lack of evidence for effective therapy. Given the potential for debilitating side effects with corticosteroid therapy (prednisone)(47) editorials and international consensus statements'(3,48) agreed that high dose corticosteroids should be discouraged in IPF. A recent study involving a triple combination therapy using prednisolone/azathioprine and N-actylecysteine was halted early, due to safety concerns(49,50). They found in a relatively short time that patients receiving the triple therapy had increased risk of death and hospitalization. Thus, prednisolone and azathioprine are no longer recommended for the treatment of IPF(51). It is evident that novel

therapies are urgently required to address this unmet clinical need(7).

1.1.1.5 Prognosis

While the average survival is between 2-3 years from the time of diagnosis, predicting survival remains particularly challenging. There have been numerous papers published on clinical and physiological predicators of survival such as age, smoking status, baseline pulmonary function(52,53). Most recently changes in FVC over 6 or 12 months has been the most important predictors of survival(53). Other methodologies have been considered, but these are less validated; DLCO(54), 6 minute walk test(55) and presence of pulmonary hypertension(56).

1.1.1.6 Pathogenesis

If we are to develop novel therapies for IPF, it is essential that we understand the underlying disease mechanisms. Early paradigms focussed on the hypothesis that lung injury in IPF produced an inflammatory response leading to secondary fibrosis, and hence treatments such as corticosteroids were used in an attempt to halt this inflammation. A more recent and popular paradigm suggests that epithelial cell injury is the initial event that triggers a series of aberrant repair pathways which lead to abnormal would healing and subsequent fibrosis(14). The epithelial injury is believed to trigger the release of numerous mediators including platelet derived growth

factor (PDGF)(57), heparin binding epidermal growth factor (HB-EGF)(58), and transforming growth factor alpha and beta (TGFα, TGFβ)(59). This leads to the release of numerous pro-fibrotic mediators, cytokines, chemokines and growth factors from many cells. Some of the cells already present or recruited to the area of injury include macrophages which release Interleukin 1 (IL-1)(60), Tumour necrosis factor (TNFα)(61), PDGF(62), HB-EGF(63), TGFα(64). Mast cells within IPF lesions express basic fibroblast growth factor (bFGF)(65) and also release IL-4(66) and IL-13(67). All these mediators and many more lead to the formation of fibroblast foci and the exaggerated deposition of extracellular matrix (ECM), driving the destruction of the lung parenchyma architecture. Mediators thought to play a key role in IPF pathophysiology are summarised in **Table 1-1**.

As the disease progresses in response to repeated injury at different sites within the lung, multifocal areas of pathology develop each at a different stage of development(68). Therefore, if these micro-injuries reoccur over a series of months and even years, the severity of the fibrosis progresses.

The proposed pathogenic fibrogenic pathway of IPF is illustrated in **Figure 1-2.**

Table 1-1. Table of Mediators involved in parenchymal fibrosis

Mediator	Cellular production	Biological effect
TGFβ1	Epithelial cells Macrophages Myofibroblasts	Promotes fibroblast to myofibroblast differentiation Initiator of EMT Stimulates and regulates collagen synthisis
bFGF	Mast cells Macrophages	ASM, endothelial and fibroblast proliferation Promotes myofibroblast to fibroblast differentiation Inducer of endothelial cell migration Promotes extracellular matrix production
IFNγ	Th1 cells Mast cells Natural killer cells	Induces leukocyte migration Inhibits fibroblast collagen secretion
TNFα	Macrophages Mast cells	Promotes fibroblast proliferation and chemotaxis Inducer of collagen synthesis
PDGF	Platelets Macrophages Mast cells Fibroblasts Epithelial cells	Promotes fibroblast proliferation ASM and fibroblast chemoattractant Survival factor for fibroblasts and ASM Sitmulates collagen production
VEGF	Platelets Fibroblasts Neutrophils Endothelial cells	Stimulates angiogenesis and vasculogenesis Decrease induces apoptosis of endothelial cells Decrease reduces angiogenesis
GM-CSF	Macrophages T cells Mast cells Fibroblasts Epithelial cells Endothelial cells	Promotes chemotaxis of T cells and macrophages Simulates accumulation of fibroblasts and myofibroblasts Reduction in GM-CSF can worsen fibrosis
EGF	Epithelial cells Endothelial cells Mast cells Macrophages	Promotes proliferation and differentiation Controls myofibroblast migration and direction Promotes cell survival
CTGF	Myofibroblasts Epithelial cells	Inducer of fibroblast proliferation Production, adhesion and contraction of ECM Strongly associated with TGFβ1
IGF-1	Macrophages	Promotes proliferation of mesenchymal cells Induces collagen synthesis

* See references, (61,67,69-74,74-100)

Mediator	Cellular production	Biological effect
CCL2	Monocytes Macrophages Fibroblasts Epithelial cells Mast cells Endothelial cells	Recruitment of circulating fibrocytes Induces fibrocyte chemotaxis
CCL3	Fibroblasts Mast cells Macrophages	Initiation and maintenance of pulmonary lesions Simulates angiogenesis
CCL4	Macrophages	Initiation and maintenance of pulmonary lesions Simulates angiogenesis
CCL5	T cells Platelets Mast cells Macrophages	Recruits T-cells, eosinophils, mast cells
CCL11	Epithelial cells Fibroblasts	Recruitment of Eosinophils Regulate myofibroblast differentiation Deposition of matrix proteins
CCL12	Epithelial cells	Fibrocyte recruitment and chemotaxis
CCL18	Monocytes Macrophages Dendritic cells	Deposition of matrix proteins Associated with high risk of disease progression
CCL22	Macrophages	Activation and recruitment of alveolar macrophages
CX3CL1	Endothelial cells	Adhesion and migration of leukocytes
CXCL5	Macrophages Hyperplastic type II cells	Regulator of angiogenic activity Found in proximity to fibroblastic foci
CXCL9	Macrophages	Abrogates TGFβ1 induced EMT
CXCL10	Monocytes Lymphocytes Endothelial cells	Chemotaxis of T cells and fibroblasts
CXCL11	Fibroblasts Leukocytes	Modulates vascular remodeling
CXC12	Monocytes	Recruitment of fibrocytes and macrophages
IL-1	Macrophages	Promotes fibroblast proliferation Induces collagen synthesis
IL-4	Mast Cells Eosinophils Lymphocytes	promotes fibroblast proliferation, chemotaxis Stimulates deposition of matrix proteins Differentiation to myofibroblast
IL-6	Epithelial cells Mast cells	Promotes collagen production
IL-8	Macrophages Fibroblasts Eipithelial cells Endothelial cells	Chemoattractant and activator of neutrophils
IL-10	Th2 cells Monocytes Macrophages B cells	Downregulates inflammatory reaction of IPF Reduces synthesis of IL-1, IL-6, IL-8 and TNFα Induces apoptosis of activated neutrophils Inhibits collagen secretion
IL-12	Macrophages	Inducer of IFNγ production
IL-13	Th2 Cells Mast Cells	Promotes collagen production Promotes fibroblast to myofibroblast differentiation Promote epitheilail cell apoptosis

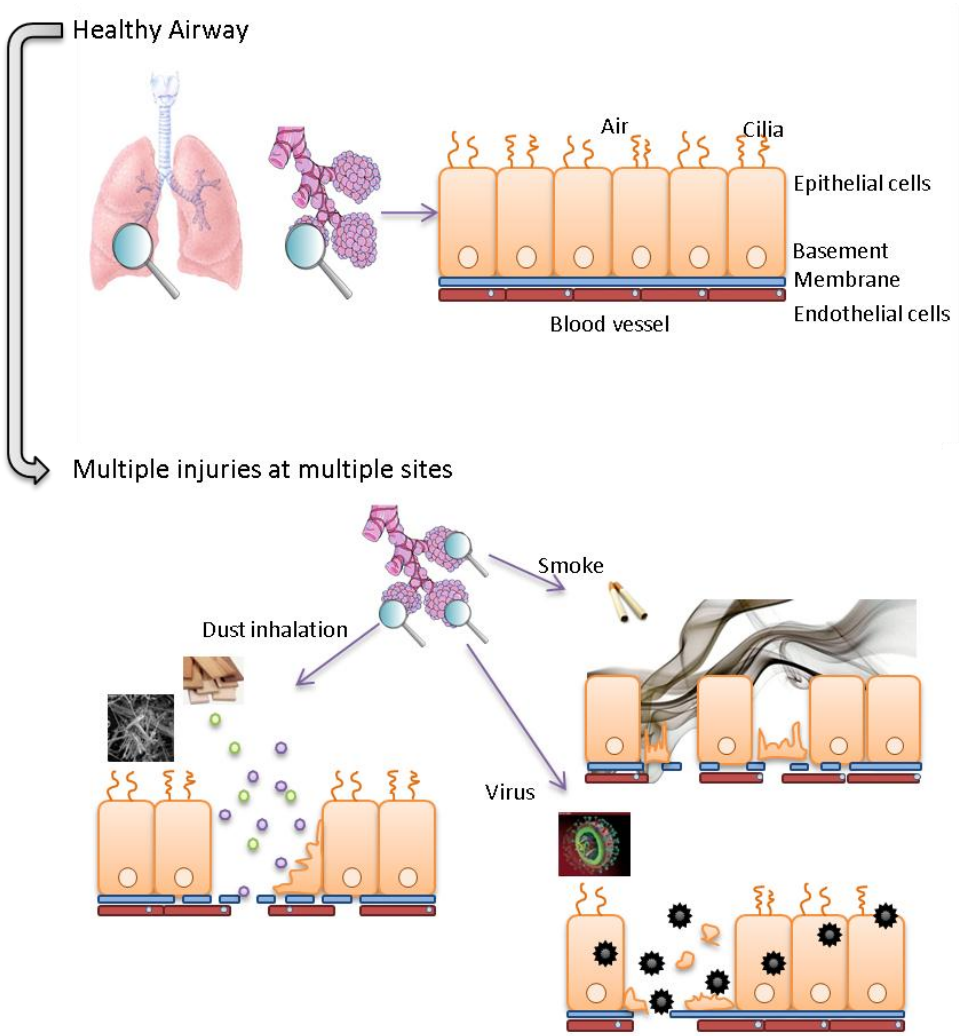

Figure 1-2. IPF Pathogenesis

The **healthy airway** shows the normal alveolar-capillary region, with intact cillia, epithelial cells, basement membrane and endothelial cells. This structure successfully separates the air from blood. However, **multiple micro-injuries at multiple sites** can arise from numerous potential risk factors such as smoking, dust or viruses which cause damage to the basement membrane, and injury to the epithelial and endothelial cells. The **response to injury** and the damage caused to the cells triggers the release of several pro-fibrotic mediators, cytokines, chemokines and growth factors. There is often some leakage of proteins and inflammatory cells into the airspace.

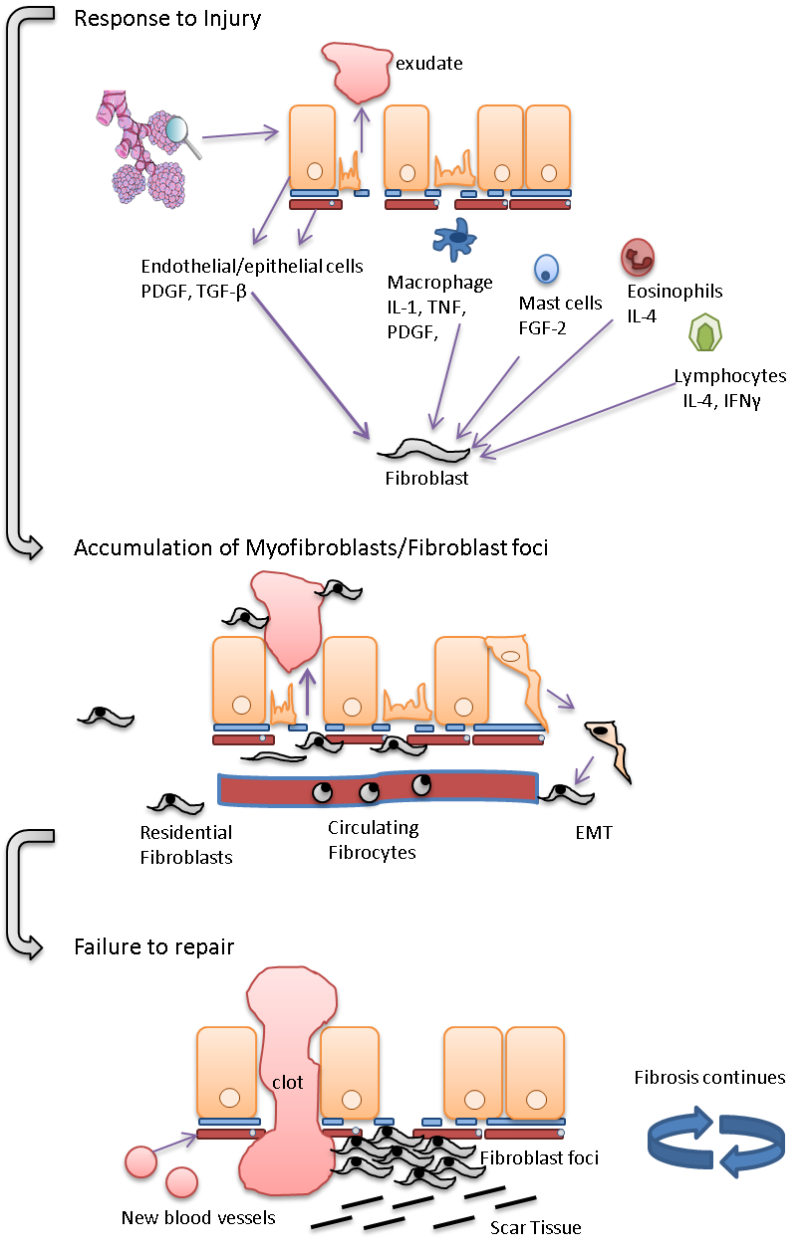

Figure 1-2 continued. IPF Pathogenesis

Therefore the response to injury leads to the accumulation of myofibroblasts/fibroblast foci within the area of injury by resident fibroblast proliferation, circulating fibrocytes or EMT. Within IPF there is a failure to repair adequately, scar tissue is formed and organization of exudate results in a clot incorporating the interstitium. The epithelial layer does not reform, the integrity of basement membrane is irretrievable and apoptosis is usually triggered resulting in a continuous fibrogenic process.

1.2 The myofibroblast

Myofibroblasts, first discovered in the 1970s(101), are the principle cell responsible for the synthesis and deposition of the fibrotic matrix in IPF(102,103). They are intermediate in phenotype between fibroblasts and airway smooth muscle, expressing α-smooth muscle actin (αSMA) and exhibiting contractile activity(70,104). Interestingly, myofibroblasts derived from IPF lungs demonstrate enhanced proliferation, differentiation, migration and collagen production(71,105,106) a process in which TGFβ1 is central.

1.2.1 Structural features of myofibroblasts

The structure of the myofibroblast is summarised in **Figure 1-3** and compared to fibroblasts and smooth muscle cells however, there is quite an overlap in these cell types(107).

The myofibroblast is a spindle or stellate looking cell, with pale eosinophilic cytoplasm and a nucleus that is elongated with indentations and small nuclei. The myofibroblast bundles control the contractility of the cell. The contractile force is transferred into the ECM via the fibronexus and fibronectin makes contact with collagen. Secretory granules containing collagen are produced by the golgi and rough endoplasmic reticulum which are both prominent ultrastructural features. Other ultrastructural features include the fusiform nucleus and cell body, aggregate of subplasmalemmal

cytoplasmic filaments and the absence of intra-cytoplasmatic intermediate type 10 nm filaments(108).

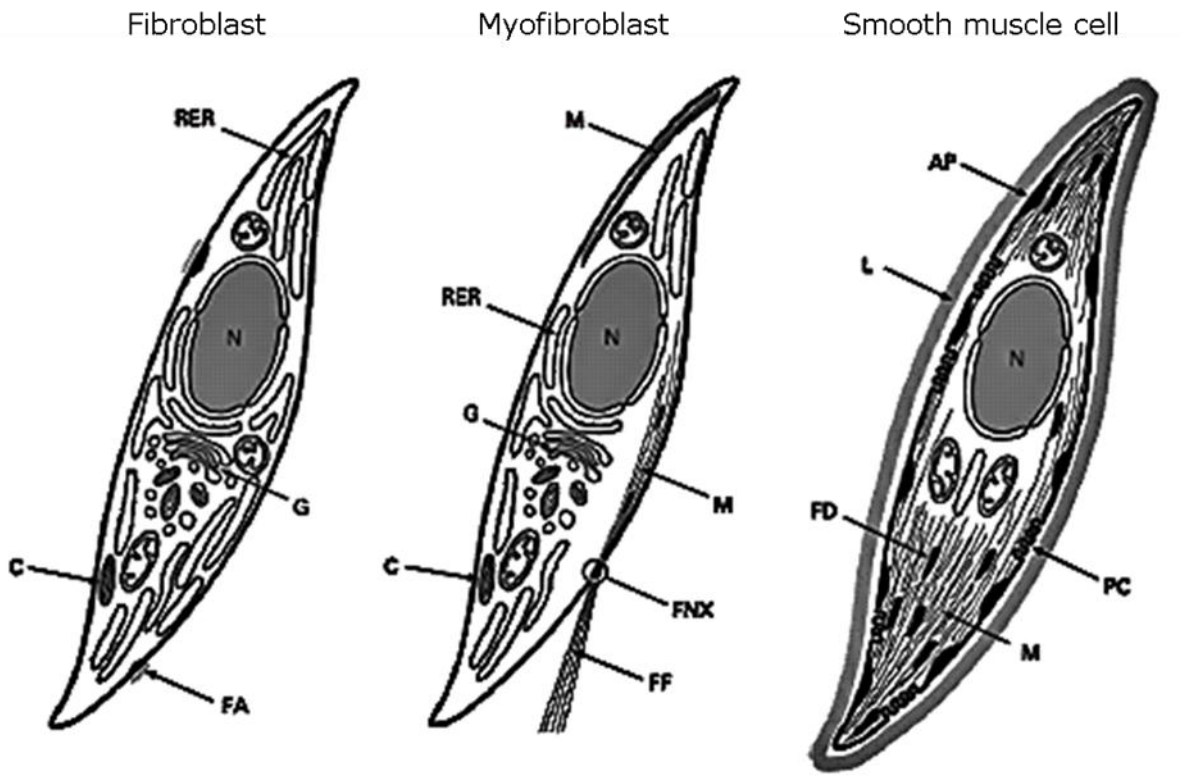

Figure 1-3. The myofibroblast structure

Diagrammatic representation of a myofibroblast in comparison with the fibroblast and smooth muscle cell. Key: AP, attachment plaque; C, collagen secretion granule; FD, focal density; FF Fibrobnectin Fibril; FNX, fibronexus; G, golgi apparatus; L, lamina; M, myofibroblast bundle; N, nucleus; RER, rough endoplasmic reticulum; SC, surface caveoloe; SPL, subplasmalemmal linear density. Figure taken from(107).

Fibroblasts, epithelial cells, fibrocytes and in some cases even smooth muscle cells have all been shown to be capable of developing a myofibroblast phenotype(69,104,109,110). Therefore, the myofibroblast is notoriously difficult to isolate and characterise. They express many of the same markers, due to their intermediate phenotype between smooth muscle cells and fibroblast,. A specific myofibroblast marker is yet to be discovered. In immunohistochemistry, the myofibroblast positively expresses markers such as:-

- αSMA – a marker specifically recognizing the αSMA isoform of actin (42KDa)(111). αSMA antibodies tend to be actin specific and do not react with other actin isoforms such as α-sarcomeric actin found in striated muscle. αSMA is expressed by airway smooth muscle cells (ASM), vascular smooth muscle cells (VSMC), myoepithelial cells, pericytes, hair follicles cells, stromal cells and myofibroblasts(112,113).
- Thy-1/CD90 - is a Glycosylphosphatidylinisotol (GPI)-anchored membrane glycoprotein of the Ig superfamily which is involved in signal transduction. It is expressed on stem cells, mast cells, myofibroblasts, fibroblasts and neuronal cells, and is an indicator of fibroblast proliferation in the myocardium(114-116).
- Fibroblast surface protein (FSP) – specifically targets fibroblast specific surface protein (43KDa) on primary fibroblasts and

fibroblast cell lines, although it is also found on tissue macrophages and blood monocytes. Neither human epithelial cells or lymphocytes express FSP(113).

- Vimentin – is a type III intermediate filament protein (57 kDa) expressed in cells of mesenchymal origin i.e. fibroblasts, myofibroblasts and endothelial cells. Vimentin is the major cytoskeletal component of mesenchymal cells and is often used as a marker for cells undergoing epithelial-mesenchymal transition(117).
- Desmin – desmin antibodies target the type III intermediate filament found near the sarcomeres. Desmin is crucial for maintenance of muscle fibres and mesenchymal cells. Smooth muscle cells are positive for desmin expression, but sarcomeres are not found in the structures of myofibroblasts(118). Fibroblasts are negative for desmin markers. Whether the myofibroblast expresses desmin(119), varies from paper to paper, some suggest that they are negative where as others suggest that as myofibroblasts develop they express the cytoskeletal protein, desmin. I believe that a likely explanation for these discrepancies is tissue-specific heterogeneity (see section **1.2.2**).

Myofibroblasts do not typically express markers such as:

- Myosin – Myosin is involved in the contractibility of muscle cells(120,121). Myofibroblasts are myosin negative, although evidence of myosin mRNA upregulation in fibroblasts has been described(122).
- CD34-The CD34 antigen is the ligand for CD62L (L-selectin). CD34 is expressed on hematopoietic stem cells, fibrocytes, progenitor cells and vascular endothelium, but not fibroblasts or myofibroblasts(123).

1.2.2 Myofibroblast transdifferentiation

There is still much debate surrounding the transdifferentiation of myofibroblasts from fibroblasts and airway smooth muscle cells. There is evidence to suggest that the genomic and phenotypic differences of a fibroblast/myofibroblast depend largely on the area of isolation. For example, fibroblasts isolated from distal human lung parenchyma have several differences in molecular expression and phenotype compared to those isolated from the airway(110,124-126). In particular, αSMA expression is markedly increased in lung parenchymal fibroblasts, suggesting that these cells are more representative of a myofibroblast phenotype(110). It is therefore vital, to consider the location of the tissue used when isolating these cells.

Characterising the cells requires the identification of both negative and positive expression of relevant antigens. A fibroblast will express fibroblast markers such as Thy-1(115), FSP, and vimentin but so will a myofibroblast. The main marker used to distinguish between the two is αSMA. However, αSMA and vimentin are also present in ASM cells. FSP though, is not expressed by ASM(127). Fibroblasts, myofibroblasts and smooth muscle cells have all been found to express collagen type 1.

Characterising the cells is clearly a difficult process therefore, if a culture of cells resembling fibroblast-like cells morphologically are positive for Thy-1, FSP, αSMA and negative for myosin, the cells are of a myofibroblast-like phenotype. If they are also negative for macrophage marker CD68, and progenitor and vessel marker CD34, it can also be concluded that there is no contamination of fibrocytes or macrophages. For an example of immunofluorescence staining see **Figure 1-4**.

A summary of the myofibroblast structure and its histological, immunohistochemical and ultrastructural features are defined in **Table 1-2** .

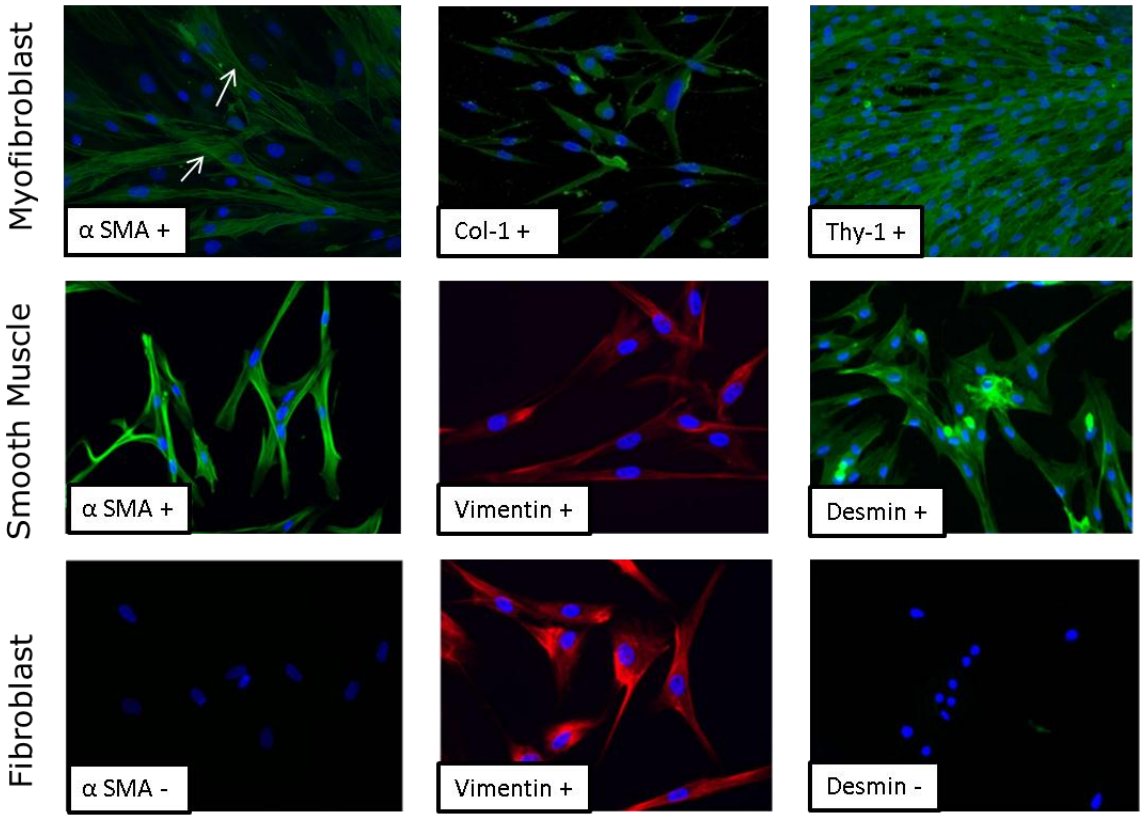

Figure 1-4. Immunofluorescent staining

This figure highlights the similarities and differences between myofibroblasts, smooth muscle cells and fibroblasts by immunofluorescence staining. White arrows clearly show the actin filament with the myofibroblast cells.

The fibroblasts and smooth muscle cells were cultured from rat coronary artery adventitia, pictures used from(128) Myofibroblast cells were grown from healthy human lung tissue at Glenfield hospital.

Table 1-2. Histological, immunohistochemical and ultrastructural definition of the reactive myofibroblast

Structure
Spindle or stellate cell
Pale eosinophilic cytoplasm
Vesicular elongated nuclei with slight indentations and small nucleoli
Abundant extracellular matrix
Immunophenotype
Vimentin positive
α-smooth muscle actin positive
Smooth muscle myosin negative
Thy-1 positive
Desmin negative
Fibronectin positive
Calponin positive
H-caldesmon negative
EDA positive
CD34 negative
Ultrastructure
Fusiform nucleus
Prominent rough endoplasmic reticulum
Golgi apparatus producing collagen secretion granules
Peripheral myofilaments
Fibronexus junctions (no lamina)
Fibronectin Fibrils
Gap junctions.
Myofibroblast bundles

Table adapted from(129).

1.2.3 Factors regulating myofibroblast function

1.2.3.1 Myofibroblast proliferation

Fibroblast proliferation occurs in both normal wound repair and fibrosis formation. In normal wound healing, fibroblasts proliferate and grow in order to provide cells needed for the synthesis of new ECM proteins. Fibroblast proliferation is controlled by combinatorial signalling pathways involving the TGFβ1/connective tissue growth factor (CTGF) pathways, but also signalling events induced by HB-EGF and IGF-2 activated receptors(130). Many studies have reported that TGFβ1 induces proliferation of fibroblasts although, the effect is not direct and believed to occur via a post TGFβ1 receptor mechanism mediated by CTGF(82,130,131). Levels of TGFβ1 are substantially increased in the IPF lung and it is believed to be a key pro-fibrotic mediator within idiopathic pulmonary fibrosis, based on in vitro and in vivo animal studies(69,72,132-135). bFGF, a growth factor released primarily by macrophages and mast cells, contributes to excessive fibroblast proliferation(136) and regulates smooth muscle cell proliferation(137). Proliferation of renal fibroblasts is induced by TGFβ1, but shown to be mediated indirectly by bFGF(72).

Tryptase, a secretory granule-derived serine proteinase within mast cells and released upon degranulation is capable of stimulating fibroblast proliferation(138). Mast cell numbers directly correlate to the degree of fibrosis(139)and activated mast cells infiltrate area of

fibrosis(140). PDGF has also been implicated in myofibroblast proliferation(141).

It should be noted, that all studies refer to the proliferation of the fibroblast rather than the myofibroblast. The common presumption is that it is the fibroblast that proliferates and then differentiates into the myofibroblast, which may then migrate to areas of injury, contract wounds and release ECM proteins(130,140).

1.2.3.2 Myofibroblast migration

The ability to migrate is a fundamental property of fibroblasts and myofibroblasts. Myofibroblast migration is evident in many types of fibrosis(142,143). Within a classical wound, such as a cut, fibroblasts/myofibroblasts migrate to the area of injury to secrete ECM and contract the wound(144). Once their role is complete they undergo apoptosis(145). A similar process occurs in lung tissue following injury, for example, the scarring which can occur after infection. However, the unknown tissue insult within IPF tissue is characterised by the ongoing activation of alveolar epithelial cells, provoking continual myofibroblast accumulation, and a failure of the cells to apoptose resulting in the formation of myofibroblast foci(15). Damage to the epithelial cells initiates the release of several chemokines, resulting in fibroblast/myofibroblast migration and these are listed in **Table 1-1**. IPF fibroblasts exposed to CCL21 showed significant migratory responses, where as normal fibroblasts were not

affected by exposure(146). bFGF promotes migration though the PI3-kinase, Rac1 and JNK pathways(147).

1.2.3.3 Myofibroblast secretion

Myofibroblasts mediate fibrosis though secretion of chemokines, cytokines, growth factors, and ECM proteins.

Myofibroblasts secrete growth factors such as TGFβ1, TGFα, EGF, bFGF and the inflammatory cytokines, IL-β all of which are discussed in **Table 1-1**. The growth factors secreted by myofibroblasts have three common functions and some can induce all three: 1) initiate or increase migration 2) induce proliferation of epithelial or parenchymal cells, and even self-stimulated proliferation(72,148) and 3) induce differentiation(69). The secretion of these growth factors and cytokines by myofibroblasts can be stimulated through several pathways including SMAD2/3 phosphorylation, ras/MEK/ERK cascade, and Jak-Stat pathways(149)

Human lung fibroblasts and myofibroblasts are the primary source of pulmonary ECM production(150). ECM production is essential in normal wound healing as it acts as a scaffold during tissue development and repair. Through binding to cell receptors, ECM components initiate intracellular signalling events, and bind to growth factors promoting epithelial and parenchymal cell migration, proliferation and differentiation(151,152). Once the repair is complete, the secretion is inhibited(153). In pulmonary fibrosis

however, the fibroblasts and myofibroblast fail to undergo apoptosis(154) and their secretion is not inhibited leading to the abundance of ECM found in the IPF lung(59,102).

ECM molecules secreted by myofibroblasts include collagens, glycoproteins (such as laminins, fibronectin and tenascin), and proteoglycans. Collagen is the main ECM protein secreted in fibrosis(155). Myofibroblasts secrete at least five collagens of the collagen superfamily; types I, III, IV, V and VIII(71,156,157). These consist mainly of the fibrillar collagens which have a rope-like structure and assemble into ordered polymers called collagen fibrils forming the basal lamina, however type IV is different and forms the basic two dimension network of all basal laminae(158). Of the collagens found in the lung, collagen type I and III are the most abundant and also the most abundantly secreted by myofibroblasts(159), implicating them as the key source. Myofibroblast production of collagen is increased by pro-fibrotic growth factors, including TGFβ1(71,150), bFGF(160) and CTGF(82).

1.2.3.4 Myofibroblast differentiation

Myofibroblasts can differentiate from numerous sources including fibrocytes(161), epithelial cells(162) and resident fibroblasts(163). The myofibroblast may also have the ability to differentiate into or transdifferentiate from a smooth muscle cell(164).

The key stages in differentiation are driven by numerous growth factors, but particularly TGFβ1 (104). PDGF released from wounds also acts as a mitogen or chemoattractant for surrounding cells(77). Fibroblasts begin to develop stress fibres containing cytoplasmic actin and TGFβ1 released at the site of injury and by fibroblasts themselves induces the synthesis of extra domain A (EDA) fibronectin(165) via a SMAD-3 dependent mechanism(166). EDA fibronectin assists in the synthesis of α-SMA which becomes incorporated into the stress fibres forming the myofilament bundles with focal densities(107,167). Fully differentiated myofibroblasts express increased amount of proteins associated with fibroblasts but also express a variety of new proteins, which include αSMA, EDA fibronectin, vinculin, paxillan, talin, tensin(168)

1.2.3.5 Myofibroblast contraction

One of the key differences between a fibroblast and a myofibroblast is the latter's ability to contract. Contractility is an vital feature in wound healing, as it allows the development of tension which promotes tissue repair and wound closure(169,170). The myofibroblast is capable of generating contractile forces due to αSMA, which is expressed in myofibroblast stress fibres and by the fibronexus adhesion complexes connecting intracellular actin with extracellular fibronectin fibrils(167). These are shown in **Figure 1-3**. In fibrosis however, the myofibroblast attempts to repair perceived

defects and re-establish mechanical integrity, but it never truly regenerates the damaged tissue. This leads to the formation of contracted collagenous scar tissue (171)

TGFβ1 is the pivotal growth factor contributing to myofibroblast contractility. TGFβ1 causes fibroblast differentiation discussed in section **1.2.3.4,** where upregulation of αSMA occurs and stress fibres are formed. Many studies have shown how stimulating myofibroblasts in vivo causes increased contraction(104,144,172). More recently, evidence has shown that the myofibroblasts, through contraction can directly liberate and activate latent TGFβ1 from pre-existing and self-generated deposits in the ECM(171).

1.2.3.6 Myofibroblast apoptosis

The abundance of myofibroblasts and fibroblast foci found in IPF is due to the myofibroblasts resistance to apoptotic stimuli. In normal wound healing, wound resolution is terminated and myofibroblasts removed by apoptosis(101). Apoptosis is triggered by a reduction in growth factor expression, increased ECM turnover and nitric oxide generation. IL-β1 is a significant inducer of high levels of nitric oxide production in fibroblasts, therefore inducing apoptosis(173).

In fibrosis, growth factor expression does not reduce. In particular, there is persistent TGFβ1 expression and ECM deposition, both counteracting apoptotic processes. TGFβ1 can induce p38 mitogen activated protein kinase pathway activation with subsequent

activation of the pro-survival phosphatidylinositol 2 kinase AKT pathway(174). TGFβ1 can also protect against IL-β1-dependent apoptosis by inhibiting nitric oxide synthesis(175). Interestingly, a selective susceptibility of myofibroblasts to nitric oxide induced apoptosis has been found(175). Nitric oxide is not only associated heavily with apoptosis, but its production is associated with a significant decline in αSMA in smooth muscle cells and therefore, potentially myofibroblast contractility(176). In summary, TGFβ1 has the ability to promote myofibroblast differentiation and create apoptosis-resistant myofibroblasts.

1.3 The role of the myofibroblast in lung biology

1.3.1 Role of the myofibroblast in normal lung

After tissue injury, the recognised functions of a myofibroblast include: playing a critical role in wound healing through cell to cell and cell to matrix interactions(144); maintaining and regulating the ECM, interstitial fluid volume, cellular pressure, and determining the levels of tissue contraction needed for optimum function(170,177,178). They also produce and respond to mediators and modulate ECM metabolism, wound contraction and scar resolution.

1.3.2 Role of the myofibroblast in disease

After tissue injury, the dysregulated or inappropriate function of the myofibroblast is associated with many pathologies in which diminished or excess ECM deposition(179), or inappropriate tissue contraction, is a feature(101,177). The myofibroblast was confirmed as the key source of collagen gene expression in fibrotic lesions by the use of combined *in-situ* hybridization for pro-collagen type 1 messenger RNA and immunostaining for αSMA(103). It is a highly synthetic cell producing both collagen type I and III, fibronectin, and proteoglycans(15,180). As well as contributing to ECM deposition, myofibroblasts release several pro-inflammatory mediators; IL-6, IL-8, and the CC chemokine, monotype chemotactic protein-1 (CCL2) and release pro-fibrotic mediators TGFβ1, (CTGF) and (PDGF)(15,69,180,181). All these mediators are heavily involved in inflammatory and remodelling. They pose the possibility that in some disease scenarios, myofibroblasts are capable of recruiting immune cells themselves thus, intensifying the response and potentially aggravating the fibrotic process.

1.3.3 Role of the myofibroblast in IPF

The failure of IPF to resolve, as seen in patients with progressive disease, correlates with the persistence of the myofibroblast(102). In normal wound healing myofibroblasts undergo apoptosis but in IPF

they are highly resistant to apoptosis leading to myofibroblast accumulation(154,183-185). The accumulated myofibroblasts (fibroblast foci) persist through all stages of pulmonary fibrosis and deposit an abundance of ECM and contribute to remodelling(186). It is the myofibroblast that likely accounts for the hyper-contractile properties and low compliance of the fibrotic lung. This dual role of the myofibroblast, as the main source of ECM and tissue contraction, make it the key cell in two processes that represent the hallmark of IPF and therefore, pivotal in the pathogenesis of pulmonary fibrosis.

1.4 Theories for myofibroblast accumulation in IPF

Expansion of the myofibroblast population and the formation of fibroblast foci, in the lung, are one of the central characteristics of IPF. Myofibroblasts exist as several morphological phenotypes, ranging from the non-contractile fibroblast to the α-SMA stress fibre-containing contractile myofibroblast(177). Even an intermediate phenotype has been suggested and termed proto-myofibroblast. Myofibroblasts can differentiate into myofibroblasts, and this process to some extent is reversible. Evidence has also suggested that airway smooth muscle cells have the ability to differentiate into a synthetic phenotype that is virtually interchangeable with a

myofibroblast(124). There are three key mechanisms that appear to contribute to the myofibroblast pool in IPF.

1 Proliferation of resident cells

The increased myofibroblast population in IPF lung appears to be generated in part by the proliferation of existing fibroblast populations(180), as a result of exposure to fibrogenic cytokines and growth factors. Cultured fibroblasts proliferate in response to stimulation with PDGF(187), TGFβ1, bFGF(72) to name a few and differentiate into myofibroblasts when exposed to TGFβ1(104), IL-13(99) or IL-4(188). Also, nuclear localisation of Ki67, a marker of proliferation, is evident in fibroblast-like cells within fibroblastic foci in IPF(189). Fibroblast migration into alveoli also contributes to the myofibroblast pool(190).

2 Recruitment of fibroblast progenitors (fibrocytes)

There is also evidence for the recruitment of bone-marrow derived circulating fibrocytes as progenitors for interstitial lung fibroblasts, in response to injury(191). Fibrocyte numbers in peripheral blood are significantly elevated in patients with IPF and increased further during acute disease exacerbations. High numbers of fibrocytes are a marker of poor prognosis(192). Fibrocytes are CD34+ and collagen I+ cells that develop αSMA expression and contractile activity in tissue culture. Their recruitment to sites of wound repair and fibrosis

has been demonstrated in many diseases and experimental models(193) including mouse radiation- and bleomycin-induced fibrosis(194,195). Patients with IPF had tenfold more fibrocytes in their peripheral circulation than healthy control subjects(196), and fibrocytes were recruited to the lungs of SCID mice in response to bleomycin(197). Importantly, fibrocytes are evident in the lungs of patients with IPF, but not healthy controls(161). One study has suggested that circulating fibrocytes recruited through the CXC4/CXCL12 axis, contribute to the expansion of the myofibroblast pool in IPF(161). Both CCL2 and CXCL12 have been implicated as key recruiters of fibrocytes into the lung, TGFβ1 again being the driving force behind differentiation(88). In asthma, following TGFβ1 stimulation fibrocytes have increased expression of αSMA, a marker of both myofibroblasts and airway smooth muscle(198).

3 Epithelial Mesenchymal Transition

Lastly, the theory of epithelial-mesenchymal transition (EMT), whereby type II alveolar epithelial cells can undergo a phenotypic, reversible switching to activated myofibroblast-like cells, known as transdifferentiation(106,178,199). It has been suggested, that certain injuries may induce EMT rather than apoptosis in type II alveolar epithelial cells, and TGFβ1 is a key mediator of this(178). EMT has also been implicated in many other diseases, such as renal fibrosis(200), tumour progression(198), and although the

mechanisms of EMT in IPF are currently unclear, there is increasing evidence supporting an EMT-like process in IPF(180,198,201). Changes to alveolar cells consistent with EMT have been demonstrated in human (A549) and rat cells exposed to TGFβ1(69,202), a mouse model of pulmonary fibrosis(203), and in human IPF tissue with cells expressing both epithelial and mesenchymal markers(202).

1.5 Growth factors regulating myofibroblast function and their role in IPF

One of the leading mechanisms driving pulmonary fibrosis is the exaggerated responses to a spectrum of pro-fibrogenic growth factors. It is crucial to understand the individual roles of these mediators and how they modulate events at a cellular level.

Growth factors can originate from a variety of sources including immune and inflammatory cells; endothelial cells, epithelial cells, fibroblasts, myofibroblasts, smooth muscle cells, platelets and mast cells. However, it is the interactions of these growth factors with the myofibroblast that are crucial. As the myofibroblast is the key driving force of the aberrant wound healing and increased ECM deposition.

1.5.1 Transforming Growth Factor-Beta

Transforming growth factor Beta (TGFβ1) is a member of the TGFβ super family that includes over 40 members. There are 3 mammalian isoforms, TGFβ1, β2, β3, encoded by separate genes with distinct and related functions(204). The most prevalent and characterised in IPF is TGFβ1. TGFβ1 is secreted from many cell types, including epithelial cells, platelets, activated macrophages and lung parenchymal cells(133). Many processes which are central to the pathogenesis of IPF, have been linked to TGFβ1. TGFβ1 induces mesenchymal/epithelial cells to differentiate into myofibroblasts and synthesize collagen by activating the cytoplasmic transcription factors Smad 2 and 3(205). It has also been shown to induce myofibroblast differentiation during wound healing by regulating αSMA expression(104). TGFβ1 is stored and secreted as an inactive molecule and is primed for activation following injury. Activation requires protease-dependent/independent mechanisms, which lead to over production and amplification of TGFβ1 dependent pathways(206). TGFβ1 has a profound effect on epithelial cells, fibroblasts and myofibroblasts, and it has a crucial role in the pathogenesis of IPF. Many studies have looked into inhibiting TGFβ1, but due to its pleiotropic nature and roles in normal tissue homeostasis, blocking TGFβ1 could be extremely problematic(133). Therefore, finding a target that can inhibit the effects of TGFβ1, and its role in fibrosis may be more attractive. Currently the only

available drug targeting TGFβ1 activity is pirfenidone, which inhibits TGFβ1 gene expression and attenuates TGFβ1 mediated collagen synthesis and fibroblast mitogenesis(43). As discussed earlier though, its ability to halt IPF progression is questionable. See **Figure 1-5** for TGFβ1 pathway signalling.

1.5.2 Basic Fibroblast Growth Factor

There are 20 mammalian fibroblast growth factors, and of these basic fibroblast growth factor (bFGF also referred to as FGF-2) is implicated in the fibrotic process(207). The FGF's are heparin binding proteins, and FGF signal transduction is facilitated by interactions with cell surface associated heperan sulphate proteoglycans. bFGF is a potent chemotactic and mitogenic factor for both smooth muscle (208) and myofibroblasts(209). Its importance in cell migration was highlighted when bFGF-deficient endothelial cells lacked the normal migratory response to mechanical wound healing(210). Not only does bFGF have mitogenic properties, it is also a potent growth factor for myofibroblasts, controlling ECM production and myofibroblast differentiation(160,208).

High levels of bFGF have been found in the bronchoalveolar lavage fluid and lung tissue of patients with acute lung injury and fibrosis(211). bFGF has been located in the lungs of patients who have died from acute lung injury, and localised to macrophages in the airspaces containing fibroblastic proliferation(73). bFGF is

secreted by alveolar macrophages(73), fibroblasts, human T lymphocytes(212) and endothelial cells. However, the key cell implicated in secreting bFGF, in the IPF lung, is the mast cell. Mast cells are the most common cell expressing bFGF in IPF(65,211), and not only are their numbers increased in IPF, they are activated and undergoing degranulation. Furthermore, their presence is associated with both the degree and the location of the fibrosis(65). bFGF release is likely to be during the mast cell degranulation(213).

Current therapies in development for the inhibition of bFGF are few. However, the TOMORROW study is a clinical trial using a tyrosine kinase receptor inhibitor (BIBF 1120) in IPF patients. This drug inhibits signal transduction through the bFGF, VEGF and PDGF(78,79). See **Figure 1-5** for bFGF pathway signalling.

1.5.3 Platelet Derived Growth Factor

Platelet derived growth factor (PDGF) was one of the first growth factors characterised. There are five different isoforms of PDGF, which activate cellular responses through two different receptor tyrosine kinases, alpha and beta types. PDGF regulates cell growth and division and plays a significant role in angiogenesis and uncontrolled angiogenesis(57,187).

PDGF may play a key role in IPF, as it is one of the most potent chemoattractants, proliferative signals and survival factors for

fibroblasts, myofibroblasts and smooth muscle cells(205). As well as these properties PDGF also induces collagen synthesis in myofibroblasts(214).

In the early fibro-proliferative process, PDGF is produced by platelets, however later on macrophages(215), parenchymal, epithelial(216), endothelial(217) and fibroblast cells have all been implicated in its release. Currently, there are 3 drugs targeting the PDGF in fibrosis. Pirfenidone reduces PDGF levels in bleomycin-induced lung fibrosis(218). Imatinib, inhibits the PDGF receptor tyrosine kinase and was thought to have strong anti-fibrotic potential; however recent trials showed that after 96 weeks, it did not affect patient survival or lung function in IPF(219). Finally, BIBF 1120 is discussed above.

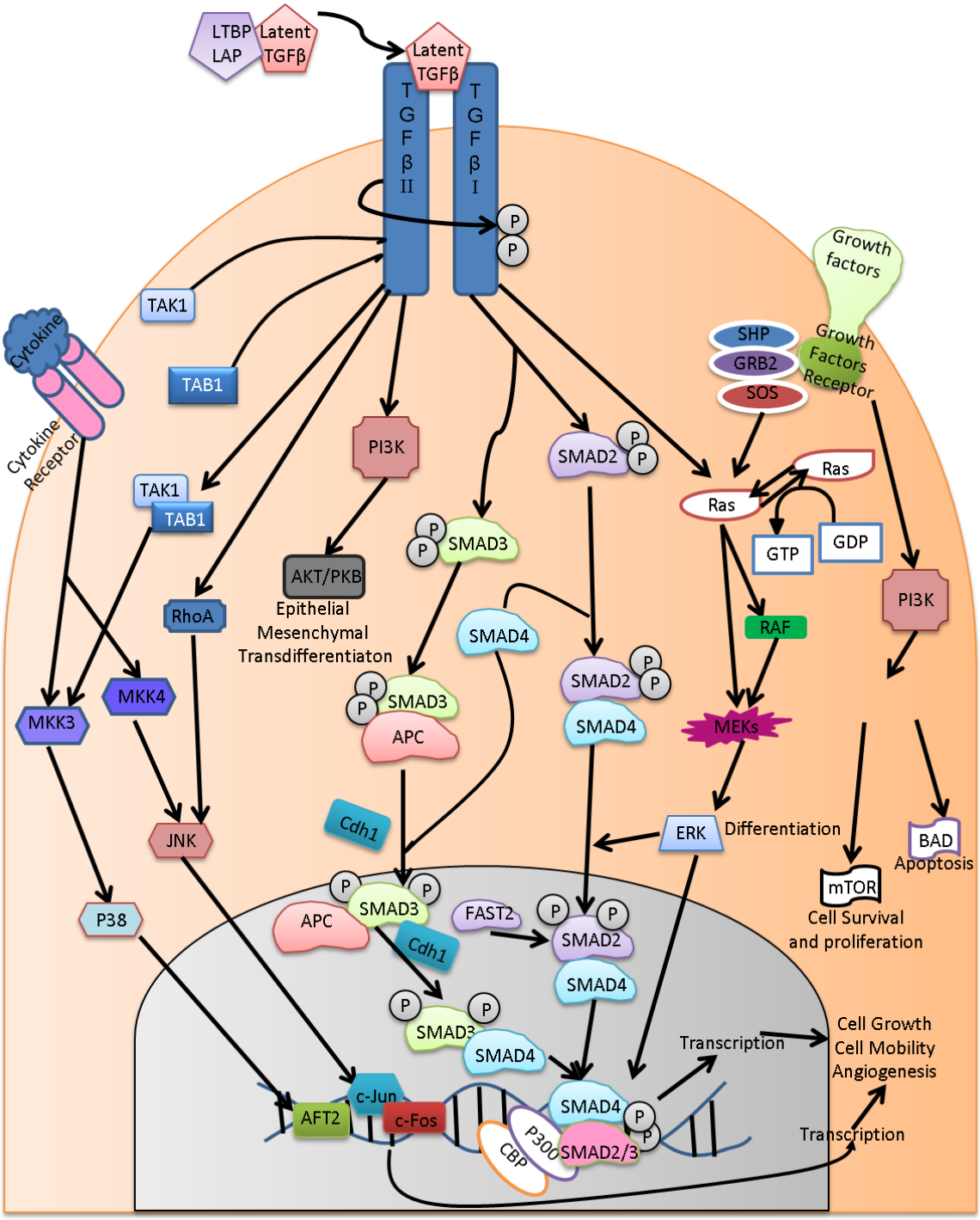

Figure 1-5. TGFβ1, growth factors and cytokine pathways

TGFβ1 is first activated from large latent complexes comprised of LTBP/LAP (Latency Associated peptide). TGFβ1 binds to the TGFβ type II receptor, which leads to the recruitment of TGFβ type I receptor. The activated TGFβI receptor phosphorylates its downstream targets, SMAD 2 and SMAD 3

(Sma and Mad related family) these tranduce signals, form hetero-oligomeric complexes with SMAD 4 and translocate to the nucleus where they interact with other transcription factors (FAST 2 (Forkhead Activin Signal Transducer 2), P300 and CBP(CREB Binding Protein), APS (Anaphase promoting complex) and Cdh1 (Cadherin 1)) at DNA binding sites where they regulate gene expression through transcription and mediate biological effects of TGFβ1.

TGFβ1 also induces other signalling pathways, which include activation of MKK's (MAP kinase Kinase) and MEK's(MAPK/ERK Kinase) pathways (JNK, p38 and ERK) through upstream mediators Rho A, Ras, TAK1 (TGFβ1 Activated Kinase), Tab1 (TAK1 binding protein). Eventually interacting with other transcription factors at DNA sequence specific binding sites ATF2 (Activating Transcription Factor 2), where they mediate the biological effects of TGFβ1 through gene transcription.

TGFβ1 and other growth factors, bFGF and PDGF activate PI3K (Phosphatidylinositol-3-Kinase) signalling pathways, which via AKT/PKB (Protein Kinase B) can lead to EMT, cell proliferation and survival through mTOR (mammalian Target Of Rapamycin), or apoptosis though BAD (Bcl-2-Associated Death promoter). Picture adapted from (220-223)

1.6 Ion channels

The passage of ions is a crucial component in the activity of living cells. The plasma membrane is composed from two layers of tightly packed lipid molecules, making it impermeable to polar molecules, like amino acids or to charged particles such as, K^+ or Na^+ ions, therefore hydrophilic charged particles cannot pass across it. To circumvent this problem, cells use protein molecules that sit within the membrane to transport ions and other charged molecules. Ion channels form one of these groups of proteins and facilitate the rapid movement of ions across the membrane(224). They provide a high conducting, hydrophilic pathway across the hydrophobic interior of the membrane and play a vital role in basic cell physiological functions including, generation of electrical activity in nerves and muscle, and cell proliferation, migration, adhesion, secretion and apoptosis. Ion channels therefore, have critical roles in the function of all cells, tissues and organs, and thus whole organisms(225).

Ion channels are often comprised of an assembly of protein subunits. One common structure is a tetramer where four principal channel proteins are assembled and to create a central aqueous pore. The aqueous pore catalyses the reaction of transporting charged molecules across a low dielectric medium. The pore can be considered to be either opened or closed which occurs as a result of conformational changes, a process known as gating. See **Figure 1-6**.

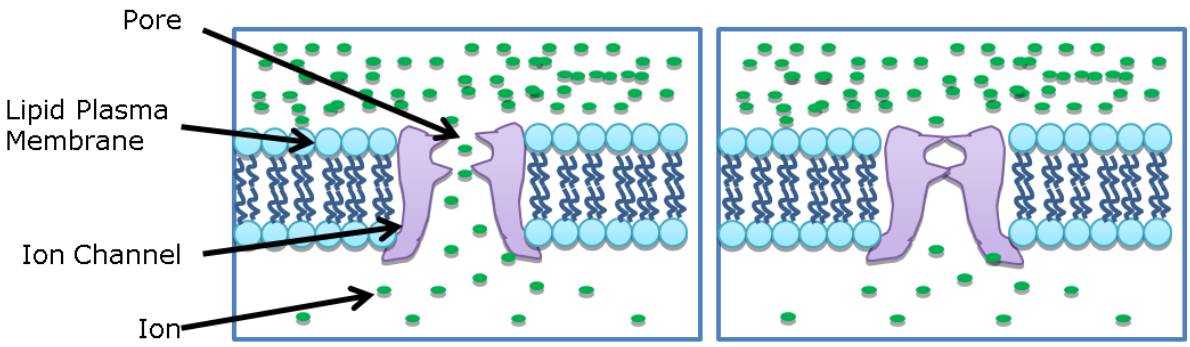

Figure 1-6. Ion channel gating

This figure shows an ion channel within the plasma membrane. The pore is either open or closed and the conformational change between closed and open is called gating.

Ion channels usually show selectivity in the ions to which they are permeable. They can discriminate between the sizes and charges of the permeant molecule. Some will only permit specific ions to pass through, for example Na^+, Ca^{2+}, Cl- or K^+ ions whereas others are less selective permitting broader groups of ions, such as mixed cations. However, it is worth noting that ion channel selectivity is conceptually distinct from ion channel gating and that ion channels are commonly described in terms of their ionic selectivity and gating properties(224).

1.7 Types of channels/gating

There are many different types of ion channels and these are classified according to either their gating activity or selectivity. Their gating activity is governed by external factors for instance chemical and physical modulators, which help to determine the different groups of ion channels. There is a standardised nomenclature used for ion channels such that they appear as $Ion_{(gate)}$ family.member e.g. $K_v1.3$ represents K^+ selectivity, voltage-gated, family 1, sub-member 3). The different types of ion channels are as followed:-

1.7.1 Voltage gated channels

Voltage gated channels are activated by changes in membrane potential due to the presence of a voltage sensor. They have a crucial role in both neurons and muscle cells by allowing a rapid and co-ordinate depolarization in response to a voltage change, and then subsequent repolarisation. Generally, ions will travel down their electrochemical gradient, and this type of channel tends to be highly specific for a particular ion. Examples of these voltage gated channels are the Na^+ and K^+ voltage-gated channels of nerve and muscle cells, and the $K_v1.3$ channel which is essential for human lymphocyte function(226).

1.7.2 Ligand-gated channels

These ion channels have increased permeability through the binding of a specific ligand for example neurotransmitter or ATP and cyclic nucleotides. Ligand gated channels tend to have a radical permeability meaning that when the pore is closed no ions can pass, but when a ligand has bound, up to $1x10^7$ ion can pass. There are three superfamilies of ligand gated channels. These are the anionic Cys-loop receptors, i.e. GABA, the Cationic Cys-loop receptors, i.e. Nicotinic acetylcholine and the ionotropic glutamate receptors, i.e. AMPA.

1.7.3 Ca^{2+} activated

Some channels open in response to increases in cytoplasmic Ca^{2+} ion concentrations, these are known as Ca^{2+} activated channels(224). These mainly consist of Ca^{2+}, K^+ and Cl- channels which have a pivotal role in cell volume, cell proliferation/differentiation, intracellular Ca^{2+} concentration and intracellular pH. Ca^{2+}-activated K^+ channels are ideally suited to maintaining a hyperpolarised cell membrane potential when depolarizations occurs as a result of Ca^{2+} influx(227). Examples of Ca^{2+} -activated channels include the $K_{Ca}2.0$ and 3.1 families.

1.7.4 Excitable/non excitable cells

Excitable cells, such as nerve and muscle cells conduct tiny electrical impulses, known as action potentials. Resting excitable cells have an electrical charge across the plasma membrane, whereby the interior of the cell is negative with respect to the exterior, known as resting potential. The resting potential arises from the activities of the sodium/potassium ATPase and facilitated diffusion and is often around -70mV for excitable cells. Certain stimuli can cause a depolarization of the cell membrane decreasing the charge of the membrane and reducing the resting potential. If the potential is reduced to the threshold voltage then an action potential is generated by the cell. These processes are largely controlled by ion channels, making ion channels essential for cell functioning. The role of ion channels propagating action potentials in excitable cells has been well documented.

In contrast, there are cells which cannot propagate an action potential, known as non-excitable cells, which express numerous ion channels carrying K^+, Cl-, and Ca^{2+}. Non excitable cells include leukocytes, and structural cells such as myofibroblasts, epithelial cells and endothelial cells. The ion channel expression within non-excitable cells is variable and is dependent on the cell subset, and the state of cell activation and differentiation. Ion channels are required for many processes in these cells for instance

proliferation(228,229), secretion of cytokines(230), regulation of cell volume, migration(231,232), apoptosis(233) and the mechanisms of resistance to chemotherapeutic agents(234).

1.8 Ca^{2+} activated K^+ channels

Ca^{2+} activated potassium channels (K_{Ca}) are a large family of K^+ channels found throughout the central nervous system and in many cell types.

1.8.1 The role of K_{Ca} channel

Influx of extracellular Ca^{2+} is an essential requirement for the activity of many cellular processes including, cell activation, differentiation and proliferation(235). Increases in intracellular Ca^{2+} are brought about by Ca^{2+} influx through plasma membrane Ca^{2+} channels or Ca^{2+} released from intracellular stores(236). Ca^{2+} acts both as a ubiquitous allosteric activator and an inhibitor of intracellular enzymes in the cytosol, organelles and nucleus(237). Depletion in intracellular Ca^{2+} can have detrimental effects on the cell leading to the inhibition of DNA synthesis, protein synthesis and nuclear transport. K_{Ca} channels have a fundamental role in Ca^{2+} signalling through their ability to maintain a negative membrane potential during cell activation(238). When K_{Ca} channels are activated they cause membrane hyperpolarization that in turn increases Ca^{2+} entry by increasing the driving force (electrical gradient) of Ca^{2+} and

thereby creates a rise in the intracellular Ca^{2+} concentration. In addition, inwardly rectifying CRACM/Orai channels conduct larger currents at negative membrane potentials(239).

The first demonstration that Ca^{2+} ions regulate K^+ flux was provided by Gardos studying red blood cells. He found that a rise in intracellular Ca^{2+} ions in red blood cells opened the Gardos (K^+) channel, leading to a loss of potassium and causing cell dehydration(240). The Gardos channel has subsequently been shown to be the intermediate conductance Ca^{2+}-activated K^+ channel $K_{Ca}3.1$ (formerly known as IK1, $K_{Ca}4$ and $IK_{Ca}1$).

1.8.2 Types/Functions

Three families of K_{Ca} channels have been identified that differ in their amino acid sequences and exhibit different single channel conductance and pharmacological profiles. They have a specific role in each of the pharmacological processes they influence(241), and are subdivided according to the size of their single channel conductance(224).

1.8.3 Large conductance K_{Ca} channels

Large conductance Ca^{2+} activated K+ channels (BK, $K_{Ca}1.1$) are characterised by their large unitary conductance usually between 100-250 pico-siemens (pS) and are gated by both voltage and

Ca^{2+}(242). Their main role is to serve as feedback modulators for the activity of voltage-dependent Ca^{2+} channels with which they co-exist, within both neurons and smooth muscle cells(241). Under physiological conditions, $K_{Ca}1.1$ channels are activated by depolarization and elevated internal Ca^{2+}. The BK structure consists of 10 transmembrane spanning domains, with the Ca^{2+} sensitive domain located between segments 9-10. This region is termed the Ca^{2+} bowl(243) and is highly selective for Ca^{2+}. There is the possibility that more than one Ca^{2+} binding region could contribute to channel activation(241). These channels can be blocked by scorpion peptides, charybdotoxin and iberitoxin, although charybdotoxin is not selective for $K_{Ca}1.1$.

1.8.4 Small conductance K_{Ca} channels

Small conductance Ca^{2+} activated K+ channels (SK, $K_{Ca}2.1$-2.3) are characterised by a small unitary conductance usually between only 4-14pS and are gated solely by internal Ca^{2+} ions(244). These channels have a fundamental role in excitable cells. Upon activation $K_{Ca}2$ channels cause membrane hyperpolarisation and inhibit cell firing(241). They are activated by an increase of intracellular Ca^{2+} to between 200-500nM(245), and are more sensitive to Ca^{2+} then $K_{Ca}1.1$ channels, due to the calmodulin binding domain located on the C- terminus of the protein. This channel can be blocked by the bee venom peptide, apamin(242).

1.8.5 Intermediate conductance K_{Ca} channels

The intermediate conductance Ca^{2+} activated K^+ channel ($K_{Ca}3.1$) has a unitary conductance between 20-85pS and like $K_{Ca}2$ channels, is gated solely by internal Ca^{2+} ions(244), through a calmodulin binding domain. It is approximately 50% homologous to $K_{Ca}2$ channels, due to their similar pore regions(246). This channel was originally termed the Gardos channel(240). Since its discovery, it has had many names including $K_{Ca}3.1$, SK4, IK, IK1, $IK_{Ca}1$. This channel is discussed in more detail below:

1.9 $K_{Ca}3.1$

The $K_{Ca}3.1$ channel is encoded in humans by the KCNN4 gene located on chromosome 19q13.2(247). $K_{Ca}3.1$ channel proteins are activated by intracellular Ca^{2+}, causing membrane hyperpolarization and promoting Ca^{2+} influx(248). This is prominent feature of the $K_{Ca}3.1$ channel as it means that during cell activation a negative membrane potential can be maintained(244,249,250). $K_{Ca}3.1$ channels are expressed to differing extents depending on the cell subset and the state of activation and differentiation(250). The $K_{Ca}3.1$ channel structure, gating, expression, role, and role in disease are discussed below;

1.9.1 $K_{Ca}3.1$ structure

$K_{Ca}3.1$ is a homotetrameric protein produced by the KCNN4 gene. Each subunit comprises of 427 amino acids(244). It has a unitary conductance between 32-39pS and is said to be sensitive to a submicromolar Ca^{2+} concentration of 100-300nM(242). An important feature of $K_{Ca}3.1$ channels is their voltage-independent activity as they do not possess a voltage sensing domain(244). This means that $K_{Ca}3.1$ channels do not inactivate at negative membrane potentials and can therefore induce a robust hyperpolarisation response (towards the K^+ equilibrium potential of −80 mV)(244,251). One of the most vital parts of the $K_{Ca}3.1$ channel structure is the calmodulin binding domain as this acts as the Ca^{2+} sensor and is responsible for the sensitivity of $K_{Ca}3.1$ to Ca^{2+} (245). $K_{Ca}3.1$ channels are thus opened by a rise in cytosolic free Ca^{2+} $[Ca^{2+}]$, due to Ca^{2+} calmodulin mediated cross linking of subunits in the channel tetramer(245). The structure of $K_{Ca}3.1$ channel is illustrated in **Figure 1-7**.

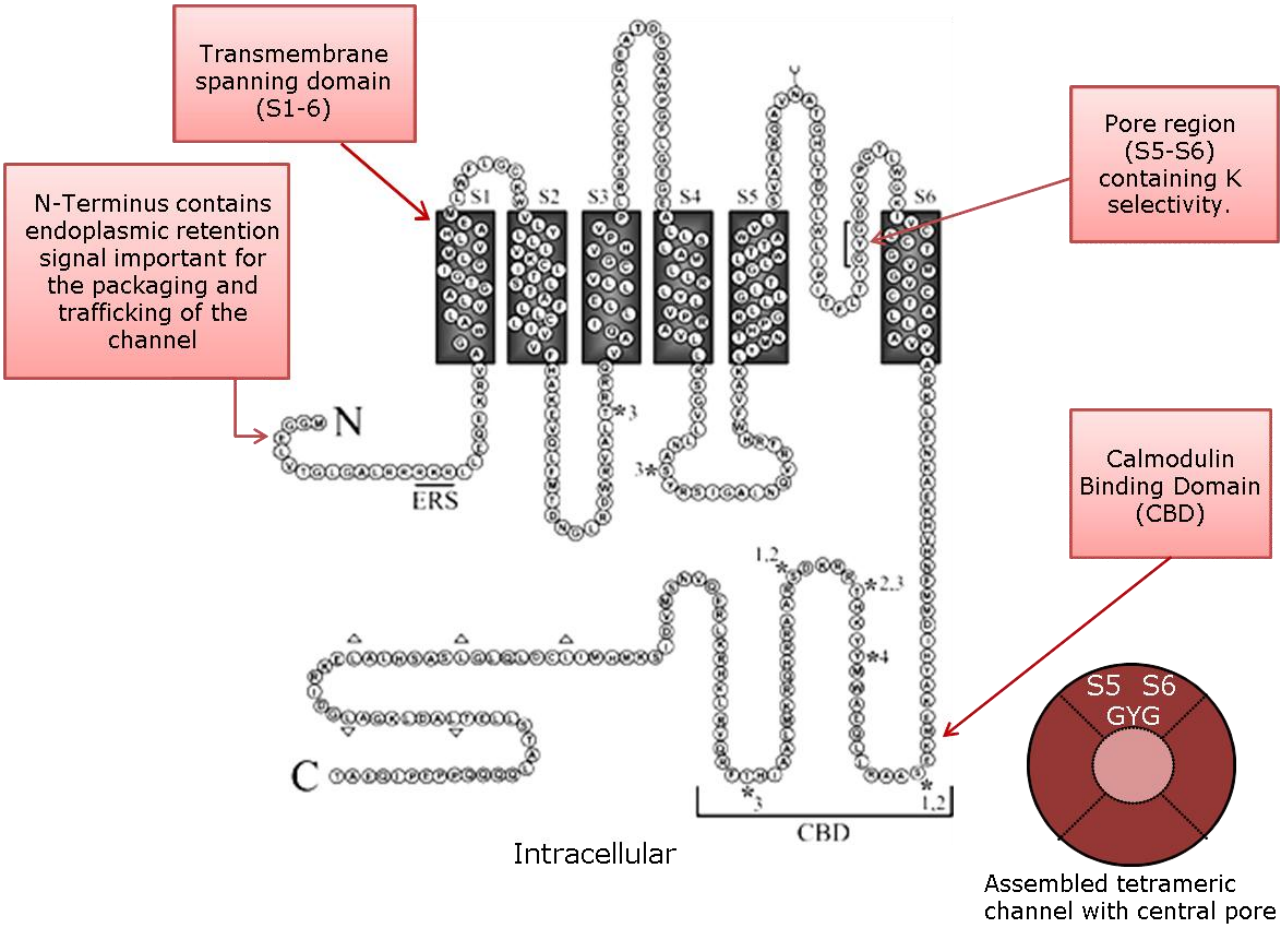

Figure 1-7. The $K_{Ca}3.1$ channel structure

There are 6 transmembrane spanning domains. The pore region is located between S5 and S6 and contains the K^+ selective amino acid sequence GYG making it highly selective for K^+ ions(246). The N termini and C termini are both located intracellularly, although there is an N-linked glycosylation site on S5 located extracellularly(246). The carboxyl- terminus, as well as containing the retention signals for protein sorting, also contains the calmodulin binding domain. Four of these structures are assembled tetramerically to form an ion channel with a central pore. Picture adapted from(242,246).

1.9.2 Gating

To enable the functional study of $K_{Ca}3.1$ channels several tools have been identified which either act as potent activators, or channel blockers.

1.9.2.1 Activators

In order to determine the presence of functional $K_{Ca}3.1$ channels within cell subtypes, pharmacological activators are often used *in vitro. C*urrently there are no known physiological $K_{Ca}3.1$ channel openers other than Ca^{2+}. A number of benzimidazolones and benzothiazoles have been illustrated as reliable K_{Ca} activators, and exert their effect by increasing the sensitivity of the calmodulin binding domain(250). More specifically, 1-ethyl-2-benzimidazolinone (1-EBIO) activates heterologously expressed $K_{Ca}3.1$with an EC_{50} of 30 μM, and achieves maximal K^+ currents at 100 μM in the presence of 100 nM free Ca^{2+}, which is below the resting Ca^{2+} concentrations of most cell types(238,252,253). However, 1-EBIO is not specific to $K_{Ca}3.1$ channels, it also activates $K_{Ca}2.x$ channels.

A similar compound to 1-EBIO, 5,6-dichloro-1-ethyl-1,3-dihydro-2H-benzimidazol-2-one (DC-EBIO), is 10-fold more potent in activating $K_{Ca}3.1$ than 1-EBIO(254). More recently riluzole derivatives have been developed, SKA-20 and SKA-31 which are also potent and selective $K_{Ca}3.1$ openers(255). Another opener mentioned in

literature is NS309, which is even more potent than DC-EBIO(256). Their structures are demonstrated in **Figure 1-8**.

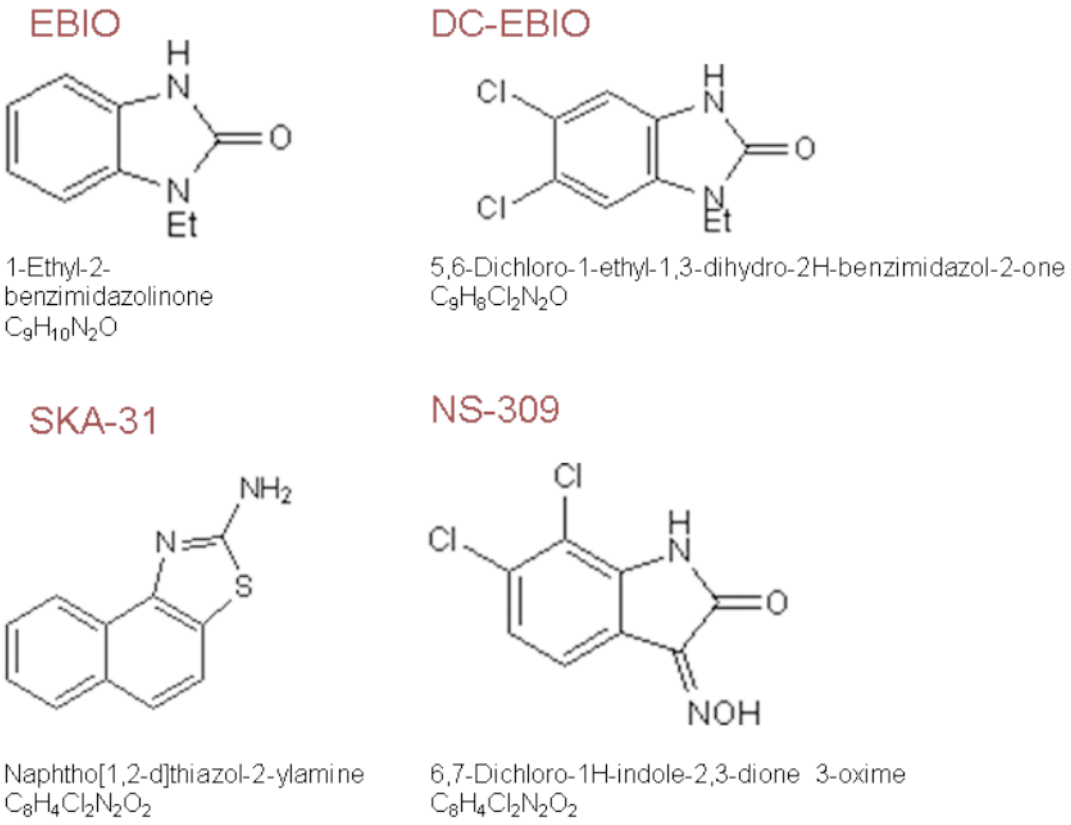

Figure 1-8. K_{Ca} activators

The structure of 1-ethyl-2-benzimidazolinone (EBIO, 5,6-dichloro-1-ethyl-1,3-dihydro-2H-benzimidazol-2-one (DC-EBIO), SKA-31 and NS-309. All are $K_{Ca}3.1$ channel openers(255),(254).

1.9.2.2 $K_{Ca}3.1$ channel blockers

Small molecule $K_{Ca}3.1$ channel blockers fall into two distinct structural classes; triphenylmethyls and dihydropyridine-like compounds. However, dihydropyridines are not used as investigative tools because they have strong cardiovascular effects which can lead to reflex cardiac stimulation(257). $K_{Ca}3.1$ is also blocked by certain toxins.

Charybdotoxin is a 37 amino acid neurotoxin present in the venom of the scorpion *Leiurus quinquestriatus* var. *hebraeu*. It results in a potent block of apamine-insensitive Ca^{2+} activated K^+ channels and is also reversible. Charybdotoxin binds to a site on the external surface of the channel(258). This is not selective for $K_{Ca}3.1$ channels, as it can also block $K_{Ca}1.1$ with a similar potency(230,259,260).

Maurotoxin is another K^+ channel blocker isolated from the venom of the Tunisian chactoid scorpion *Scorpio maurus palmatus*. It is a peptide toxin of 34 amino acids cross linked by four disulphide bridges. Although similar to charybdotoxin this peptide is not specific for $K_{Ca}3.1$ channels inhibiting many of the SK channels (SK1, SK2).

Clotrimazole is an azole antimycotic compound which blocks $K_{Ca}3.1$ channels and mammalian cytochrome P450 enzymes. Clotrimazole is effective in rheumatoid arthritis(261) and sickle cell anaemia(262). However, there are many side effects associated with

this drug and oral administration is difficult due to the drug being poorly absorbed and having a short half-life(263). Therefore, the off target side-effects of clotrimazole have limited its use. Development of a compound that is more potent and selective for the $K_{Ca}3.1$ channel might be of clinical benefit. There have been 2 drugs derived from clotrimazole which specifically target the $K_{Ca}3.1$ channel and these are discussed below;

1 TRAM-34 (1-[(2-Chlorophenyl)diphenylmethyl]-1H-pyrazole) is a highly specific $K_{Ca}3.1$ channel blocker derived from clotrimazole(250,264). The main difference between clotrimazole and TRAM-34 is the change of imidazole to pyrazole, a difference that also improves the metabolic stability(264). TRAM-34 is highly selective for $K_{Ca}3.1$ by binding to the internal residues below the selectivity filter(264), unlike charybdotoxin which binds to the external pore. The $K_{Ca}3.1$ IC_{50} values of clotrimazole are in the 25 – 387 nM range while TRAM-34 is more potent with an IC_{50} value of 20 nM(257).

2 ICA-17043 (bis(4-fluorophenyl)phenyl acetamide) (Senicapoc) has been developed more recently and is even more potent than TRAM-34 and clotrimazole with an IC_{50} of just 11 nM(257). ICA-17043 was specifically developed to inhibit Gardos channel activity in sickle cell anemia, and has been

used in phase 2 and phase 3 clinical trials where it was safe and well tolerated(265,266).

The structure of TRAM-34 and ICA-17043 are shown in **Figure 1-9.**

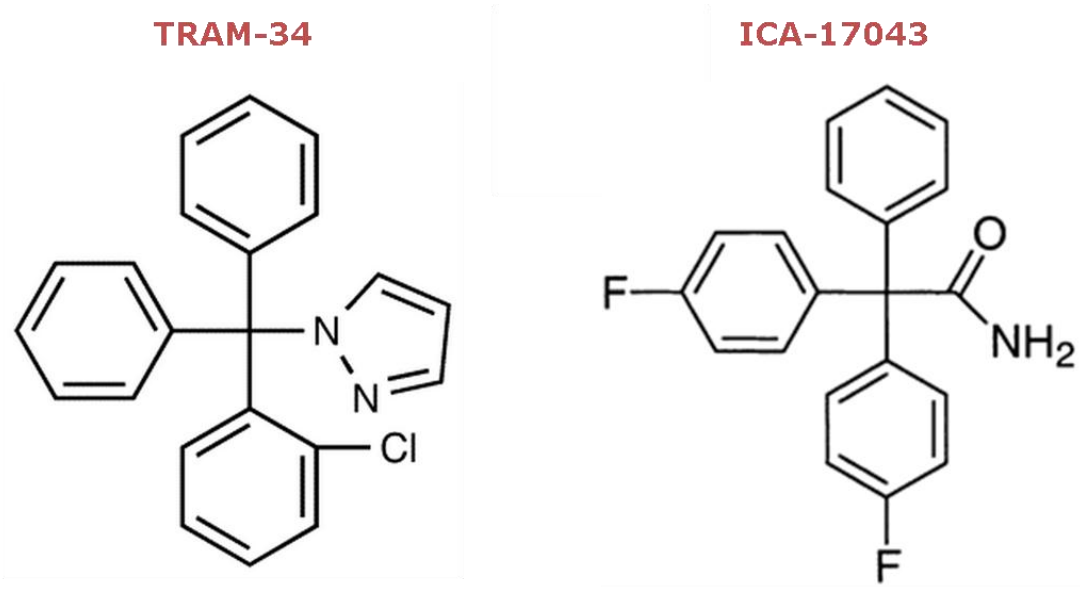

Figure 1-9. Structure of $K_{Ca}3.1$ channel blockers

The chemical structures of TRAM-34 and ICA-17043, which are both $K_{Ca}3.1$ channel blockers.

1.9.3 Cellular expression and biological roles of $K_{Ca}3.1$ channels

1.9.3.1 Lymphocytes

$K_{Ca}3.1$ channels are differentially expressed on three CD4+ T cell subsets; naive (CCR7+/CD45RA), central memory (CCR7+CD45RA-) and effector memory (CCR7-CD45RZ-), and also on CD8 cells and B cells. Channel expression is highly dependent on their state of cell activation(230,267). Following activation naive and central memory T cells transcriptionally upregulate the $K_{Ca}3.1$ channel. When the T cell voltage-gated K^+ channel $K_v1.3$, is blocked T cells quickly become insensitive to this block because they upregulate $K_{Ca}3.1$ during activation, consequently relying on $K_{Ca}3.1$ for cell proliferation and cytokine secretion(267,268). Thus, $K_{Ca}3.1$ channels are potentially important in T cell proliferation and cytokine release. A possible role proposed for $K_{Ca}3.1$ channel blockers, is as a target for Th2 responses implicated in the immunopathology of asthma(250).

1.9.3.2 Endothelial cells

$K_{Ca}3.1$ channels have been identified and characterised within endothelial cells through patch clamp physiology(251). They play pivotal roles in endothelial cell proliferation and vascular tone(251). Evidence indicates that $K_{Ca}3.1$ is heavily involved in endothelial hyperpolarization and endothelium-derived hyperpolarizing factor (EDHF)-type responses in skeletal muscle arterioles however, it

should be noted that this study did use $K_{Ca}3.1$ deficient mice and wild type mice(269). Endothelial cells stimulated with basic fibroblast growth factor (bFGF) and vascular endothelial growth factor (VEGF) express increased amounts of $K_{Ca}3.1$ channel mRNA. More interestingly the same study showed that $K_{Ca}3.1$ channel was essential for bFGF and VEGF induced proliferation by using $K_{Ca}3.1$ channel blockers TRAM-34 and charybdotoxin(270). Literature indicating $K_{Ca}3.1$ channel blockers may be capable of inhibiting angiogenesis in endothelial cells.

1.9.3.3 Mast cells

Many studies have now confirmed the expression of $K_{Ca}3.1$ in human lung, blood and bone-marrow derived mast cells (238,271-273). In human lung mast cells (HLMC) $K_{Ca}3.1$ channel activity plays a critical role in their migration(274) and degranulation(238). $K_{Ca}3.1$ channels in HLMC open following IgE-dependent activation, resulting in enhanced Ca^{2+} influx and histamine release(238). In further support of this, a mouse model showed that $K_{Ca}3.1$-deficient mice have significantly less Ag-induced Ca^{2+} influx and release of beta-hexosaminidase, a marker of mast cell degranulation(271). These mice also exhibited reduced anaphylactic responses to allergen. Blockade of the $K_{Ca}3.1$ channel proved to be essential in human mast cell migration(274), HLMC treated with TRAM-34 or charybdotoxin had significantly attenuated migration compared with control cells

towards TNFα-stimulated asthmatic ASM supernatants (272,274). These studies conclude that the $K_{Ca}3.1$ is integral for the functioning of mast cells and that blocking the $K_{Ca}3.1$ channel could have considerable potential for mast cell mediated diseases, for example asthma.

1.9.3.4 Smooth muscle

Human airway smooth muscle cells (ASM) from both healthy subjects and asthmatic patients express the $K_{Ca}3.1$ channel at the mRNA, protein and functional level(275). The same study showed that bFGF and TGFβ1-stimulated ASM cells had increased expression of $K_{Ca}3.1$ of mRNA, protein and functional channels and that pharmacological blockade of the channel contributed to cell growth arrest(275). Similarly, epidermal growth factor (EGF)-stimulated vascular smooth muscle cells (VSMC) had significantly elevated levels of $K_{Ca}3.1$ expression, indicating a role of $K_{Ca}3.1$ channel in VSMC proliferation(276). Studies suggest that the $K_{Ca}3.1$ channels play a significant role in vascular pathologies(242). A rat model of restenosis following balloon catheter injury, found a markedly increased expression of the $K_{Ca}3.1$ in VSMC after 2 weeks and 6 weeks of daily in vivo administration of TRAM-34 internal hyperplasia was reduced by up 40%(276). Similarly, a swine model demonstrated TRAM-34 delivered directly into the coronary artery wall at the time of injury, *via* coated balloon catheter, prevented the

upregulation of $K_{Ca}3.1$ mRNA expression and effectively prevented acute VSMC phenotypic modulation post angioplasty and limiting restenosis(277). Furthermore, *in vivo* therapy with TRAM-34 and clotrimazole significantly reduced VSMC proliferation and migration, and T cell activity in ApoE(-/-) mice(278), highlighting the contribution of the $K_{Ca}3.1$ channel to atherosclerosis. This study also showed that the daily administration of TRAM-34 induced no side effects to any major organs following a 28 day toxicity study. These studies emphasise the potential importance of a therapeutic blockade of $K_{Ca}3.1$ for the prevention of restonosis and atherosclerosis(242). It is worth noting that VSMC, whose phenotype are extremely similar to the myofibroblast, are heavily involved in these vascular proliferative diseases.

1.9.3.5 Myofibroblast/fibroblast

Fibroblast cell lines express a K_{Ca} channel with biological properties of the $K_{Ca}3.1$ channel(279), and more recently channel blockers such as charybdotoxin were shown to suppress fibroblast FGF-induced proliferation(280). A mouse study has shown that the expression of $K_{Ca}3.1$ channels were increased in total renal tissue following unilateral ureteral obstruction (UUO, a model of kidney fibrosis) which was paralleled by a rise in collagen-1, FSP-1, collagen-III and TGFβ1, in comparison to control tissue(281). *It is yet to be proven if*

human lung-derived fibroblasts and myofibroblasts express the K_{Ca}3.1 channel.

A mouse model of renal fibroblast proliferation and the development of interstitial fibrosis in the kidney showed a time dependent increase of K_{Ca}3.1-like K^+ currents in isolated fibroblasts following bFGF stimulation reaching a maximum after 24 hours. More importantly they showed by *in vitro* proliferation studies that TRAM-34 dose-dependently decreased bFGF- induced proliferation induced mice and that K_{Ca}3.1 deficient mice had significantly fewer numbers of myofibroblasts and decreased collagen expression in their ECM when compared to control wild type mice(281).

These findings suggest a pivotal role of K_{Ca}3.1 in the proliferation, differentiation and collagen secretion of myofibroblasts, a significant feature of IPF, but more prominently the potential role of TRAM-34 as a treatment.

K_{Ca}3.1 is therefore, an attractive pharmacological target as it appears to play a minor role in normal physiology but contributes significantly to tissue remodelling and fibrosis(266). Encouragingly, K_{Ca}3.1 knockout mice are viable, of normal appearance, did not show any gross abnormalities in any major organ and produced normal litter sizes(276,282,283). K_{Ca}3.1 blockers are feasible as potential therapies with studies showing that high doses of TRAM-34 administered to mice and rats over many weeks are well

tolerated(281). Humans administered the orally available $K_{Ca}3.1$ blocker, ICA-17043, for up to 48 weeks in phase 2 and 3 clinical trials of sickle cell disease showed only minor side effects to the drug(265). There is the potential for the rapid investigation of $K_{Ca}3.1$ blockade in clinical trials of IPF and other fibrotic lung diseases.

1.10 Summary

In summary, many of the cells heavily involved in tissue remodelling express the $K_{Ca}3.1$ channel and rely on its function for cell activities such as proliferation, activation, differentiation, adhesion, migration and mediator release. In vivo models suggest that $K_{Ca}3.1$ activity makes a significant contribution to diseases characterised by tissue remodelling and fibrosis, but plays only a minor role in healthy physiology. This makes $K_{Ca}3.1$ an attractive therapeutic target for fibrotic diseases, many of which are currently untreatable.

1.11 Hypothesis

We hypothesise that $K_{Ca}3.1$ channels in human lung myofibroblasts play a key role in the development of pulmonary fibrosis, and therefore have potential as novel targets for the treatment of IPF.

1.12 Aims

The specific aims of the research are to examine:

- The expression of $K_{Ca}3.1$ channels in human lung myofibroblasts derived from patients with IPF and non fibrotic controls.
- The expression of $K_{Ca}3.1$ in the lungs of patients with IPF and non fibrotic controls.
- The effects of $K_{Ca}3.1$ blockade on myofibroblast differentiation, proliferation, migration and secretory responses (chemokines and collagen).

2 Materials and Methods

2.1 Primary cell isolation and culture

All experiments were performed using primary human lung myofibroblasts and bronchial epithelial cells. All non-fibrotic control (NFC) patients gave written informed consent and the study was approved by the Leicestershire, Northamptonshire and Rutland Research Ethics Committee 2. Written informed consent was also obtained from all IPF subjects, in accordance with the responsible University of Pittsburgh Institutional Review Board.

2.1.1 Human myofibroblasts

Non-fibrotic control (NFC) myofibroblasts were derived from healthy areas of lung from patients who underwent lung resection for the removal of carcinoma at Glenfield Hospital. No morphological evidence of disease was found in the tissue samples used for myofibroblast isolation. IPF myofibroblasts were derived from patients undergoing lung biopsy for diagnostic purposes at the University of Pittsburgh Medical Centre, and were subsequently shown to have IPF on histological examination.

2.1.1.1 Myofibroblast isolation and culture

Myofibroblasts were grown from explanted lung tissue from both sources under identical conditions. Small fragments of lung tissue, approximately 1-2 mm^3, were placed into 6 well plates. Tissue was left to adhere to the plates for 1 hour in an incubator at 37°C in 5%

CO_2/95% air. Once adherent, 2 mls of Myofibroblast Growth Medium (MGM) was added very gently to the well and the plate was placed back into the incubator. MGM consisted of Dulbecco's Modified Eagles Medium (DMEM)(GIBCO) with glucose(4.5 g/L) and GlutaMAX^{TM}, supplemented with 10% Fetal Bovine Serum (FBS)(GIBCO), 5 ml Antibiotic/Antimycotic solution (AA, 100 U/ml penicillin, 100 µg/ml streptomycin, 0.25 µg/ml amphotericin)(GIBCO), and 100 µM nonessential amino acids (GIBCO)(284,285). The 6 well plates were monitored for cell growth and every 2 days the MGM changed. On day 7 when there was substantial cell growth the tissue and media were discarded. Cells in the wells were washed twice with Hanks Balanced Salt Solution (HBSS)(GIBCO) and detached using 0.25% Trypsin EDTA (GIBCO). The cells were centrifuged at 302 x g for 7 minutes to form a cell pellet. The pellet was re-suspended in 1 ml of MGM and the cells counted using the Trypan blue method(286). This allows the assessment of cell viability by the exclusion of the trypan blue dye. Once counted the cells were re-seeded into T75cm^2 flasks at a seeding density of 15 x 10^4 and this was deemed passage 1. When cells were 80-90% confluent they were washed, harvested, counted and re-seeded until they reached the suitable passage for experiments. Cells were washed and fed every 3 days. As IPF cells were not received until they were at passage 2, cells were studied at passages 4-5 for functional studies (**Figure 2-1**)

For a number experiments MGM was used without the addition of 10% FBS, herein referred to as serum free media (SF media), and a number of experiments employed myofibroblast media only containing 2% FBS, herein referred to as 2% MGM.

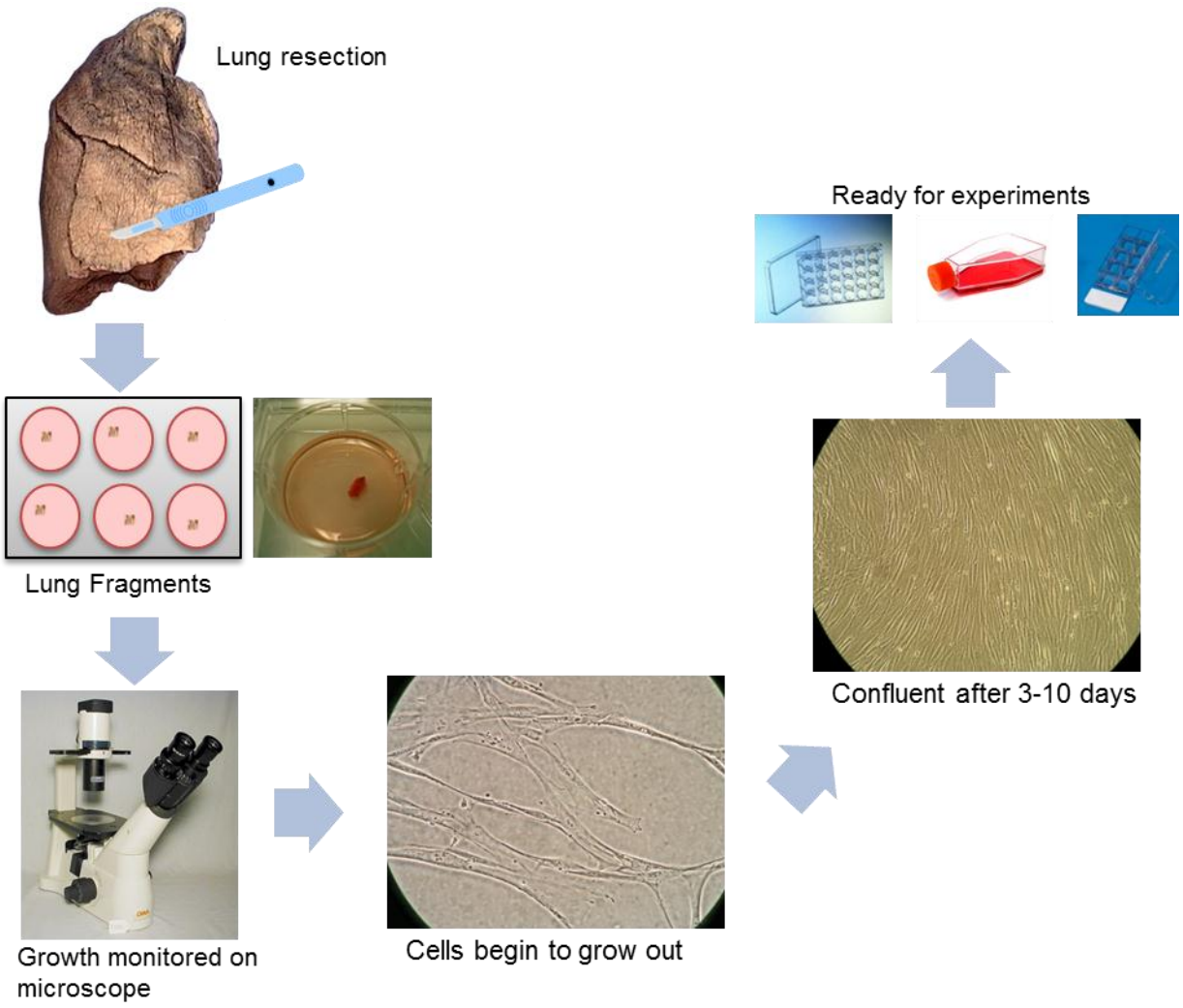

Figure 2-1. Myofibroblast isolation

Lung fragments were cut from lung resection tissue and placed into 6 well plates. Growth of cells was monitored and the media changed accordingly. When confluent the cells were passaged into relevant containers ready for experiments.

2.2 Myofibroblast characterization

To confirm the cells isolated from NFC and IPF patients were myofibroblasts, immunofluorescence was employed for characterisation. Flow cytommetry was used to assess αSMA expression.

2.2.1 Characterisation by immunofluorescence

Myofibroblasts were harvested from 80-90% confluent monolayers using 0.25% trypsin EDTA, the cells were then spun down at 302 x g for 5 minutes to form a cell pellet. The cells were re-suspended, counted and seeded at 2 x 10^4 cells per well into Lab-Tek™ II 8 well chamber slides (Nunc). They were placed in an incubator at 37°C in 5% CO_2/95% air and grown to confluence for 3—7 days. Cells were then rinsed with 1x Phosphate Buffered Saline (PBS)(Sigma-Aldrich) and fixed using ice-cold methanol (Sigma-Aldrich) for 20mins on ice. Slides were air dried and a blocking solution of 3% BSA/PBS added to each well for 30 minutes. The blocking solution was removed and the following primary antibodies applied for 90 minutes, a summary of antibodies used can be found in **Table 2-1**: mouse monoclonal (mAb) anti-α-smooth muscle actin FITC-conjugated (αSMA) (F3777, 10 µg/ml, Sigma-Aldrich, Dorset, UK) and isotype control mouse IgG_{2a} FITC-conjugated (X0933, 10 µg/ml, Dako, Ely, UK); mouse mAb anti-fibroblast surface protein (FSP) (F4771 4 µg/ml, Sigma-

Aldrich) and isotype control mouse IgM (M5909, 4 µg/ml, Sigma-Aldrich); mouse mAb anti-fibroblast antigen THY-1 (CP28, 3 µg/ml, Calbiochem, San Diego, CA) and isotope control IgG_1 (X0931, 3 µg/ml, Dako); rabbit polyclonal anti- $K_{Ca}3.1$ antibody (P4997, 8 µg/ml, Sigma-Aldrich), and isotype control rabbit polyclonal IgG (550875, 4 µg/ml, BD pharmagen, San Diego, CA); control rabbit polyclonal collagen type 1 antibody (AB745, 20 µg/ml, Millipore, Watford, UK) isotype control rabbit polyclonal IgG (550875, 20 µg/ml BD pharmigen). Mouse mAb CD68 antibody (6.4µg/ml, Dako), and CD34 R-PE antibody (0.5µg/ml, Catlag) and isotype control IgG1 R-PE was also used. After 90 minutes the cells were washed three times with PBS/0.05% Tween20 (Sigma-Aldrich) and then secondary antibodies indirectly labelled with FITC or R-PE (Dako) were applied for a further 90 minutes where appropriate. The cells were washed again three times with PBS/0.05% Tween20 and counterstained with 4',6-diamidino-2-phenylindole (DAPI)(Sigma-Aldrich). Finally the cells were washed a six times using 1 x PBS, mounted with photo bleach-retardant mounting medium (DakoCytomation fluorescent mounting medium) and cover-slipped. Original images were captured on an epifluorescent microscope (Olympus BX50, Olympus UK Ltd, Southend–on-sea) and counted using Cell F imaging software (Olympus UK Ltd). Matched exposures were used for isotype controls.

Cells stained were counted by 2 blinded observers. To assess counting repeatability, n=4 donors were counted by 2 blinded

observers who demonstrated good agreement (intraclass correlation of 0.645, Cronbach's Alpha, P=0.008).

Antibody	**Monoclonal/ Polyclonal**	**Working Concentration**	**Isotype Control**
$K_{Ca}3.1$	Polyclonal	4 µg/ml	IgG Rabbit
αSMA FITC	Monoclonal	11 µg/ml	IgG2a FITC
1B10	Monoclonal	4 µg/ml	IgM
Thy-1	Monoclonal	3 µg/ml	IgG1
Col-1	Polyclonal	20 µg/ml	IgG Rabbit
CD68	Monoclonal	6.4 µg/ml	IgG1
CD34 RPE	Monoclonal	0.5 µg/ml	IgG1 RPE

Secondary Antibody conjugated
Swine anti rabbit FITC
Anti mouse IgG FITC
Anti mouse IgG RPE

Table 2-1. Summary of antibodies used for myofibroblast characterisation

The upper table summarises the primary antibodies used for myofibroblast characterisation, their working concentration and the appropriate isotype control. Colours represent the corresponding secondary antibodies used, shown in the lower table.

2.2.2 Flow cytometry

To confirm characterization results and the strong expression of αSMA, human lung myofibroblasts were analysed by flow cytometry. The myofibroblasts were grown to confluence in T75cm^2 and washed twice with HBSS. The cells were harvested using 0.25% trypsin EDTA, centrifuged at 227 x g for 8 mins, the supernatant removed and cells then fixed by re-suspending them in 1 ml of 4% paraformaldehyde (PFA) for 15 minutes on ice. Following fixation the cells were permeabilized in 1 x PBS/0.5% BSA and 0.1% saponin (Sigma-Aldrich). Cells were split equally between FACS tubes, and centrifuged at 227 x g for 8 minutes. Supernatants were removed and cells were re-suspended in 100 µl of 1 x PBS/0.5% BSA and 0.1% saponin containing either 23 µg/ml anti- αSMA FITC-conjugated mAb (Sigma-Aldrich) or isotype control IgG2a FITC conjugated (DAKO). The FACS tubes were covered in foil and left on ice for 30 minutes. They were then washed with 1 ml 1 x PBS/0.5% BSA and 0.1% saponin and centrifuged at 227 x g for 8 minutes. The supernatant was removed and the cells re-suspended in 300 µl of 1 x PBS/0.5% BSA and 0.1% saponin and mixed thoroughly. αSMA expression was assessed by flow cytometry (FACScan, CellQuest software: BD Biosciences) and quantified as fold difference in geometric mean fluorescent intensity (GMFI) compared with isotype control.

2.3 $K_{Ca}3.1$ expression in human lung myofibroblasts

To assess the presence of the $K_{Ca}3.1$ channel, the expression in both mRNA and protein from human lung myofibroblasts was investigated. Also investigated was the functional activity of the channel within the cells.

2.3.1 A quantitative Real Time Polymerase Chain Reaction(qRT-PCR)

Quantitative real time polymerase chain reaction (qRT-PCR) is a widely used, highly sensitive technique that can determine the quantity of small amounts of mRNA within a cell or tissue. A strand of mRNA is reverse transcribed into its DNA complement (cDNA) and the resulting cDNA is amplified using standard PCR, a method that allows the exponential amplification of short DNA sequences. A fluorescent dye such as SYBR green is often used as this binds to the amplified cDNA, hence providing a method of quantification of cDNA through the measurement of fluorescence.

This method was employed to detect whether $K_{Ca}3.1$ mRNA was present within human lung myofibroblasts and whether there was a difference found in the amount $K_{Ca}3.1$ mRNA from NFC and IPF patients. We have also used this technique to assess whether the quantity of $K_{Ca}3.1$ mRNA changes following stimulation with the pro-fibrotic growth factors TGFβ1 and bFGF.

2.3.1.1 Myofibroblast cell preparation for qRT-PCR

To examine the expression of $K_{Ca}3.1$ mRNA in human lung myofibroblasts, cells were grown to confluence, harvested using trypsin-EDTA, centrifuged at 227 x g for 7 mins, supernatant removed and washed using PBS/0.1% BSA. Cells were centrifuged again at the same speed, counted and re-suspended in 1 ml of RNALater® RNA Stabilization Reagent (Qiagen) per 10^6 cells. The cells were stored at 4°C for 24 hours and then transferred to the -20°C freezer until needed.

To study the effects of transforming growth factor (TGFβ1)(R&D Systems, Abingdon, UK) or basic fibroblast growth factor (bFGF)(R&D System) on $K_{Ca}3.1$ mRNA expression, cells were grown to confluency, placed in SF medium for 24 hours and stimulated with TGFβ1 (10 ng/ml) or bFGF (10 ng/ml) for 24 hours. Cells were then prepared by the same method as above. Stimulated cells were compared to non-stimulated cells of the same passage, and in the same RT-PCR experiment.

2.3.1.2 Isolation of RNA from myofibroblast cells

To remove RNALater® cells were centrifuged at 2862 x g for 8 minutes and supernatant removed. Myofibroblast RNA was isolated from the cells using the QIAShredder spin columns and RNeasy Plus Kit (Qiagen, West Sussex, UK) according to manufacturer's instructions. Final RNA concentration was measured using a

bioanalyser, the NanoDrop (Thermofisher) and samples reconstituted with Ultrapure (Milli-Q) H_2O to contain 100 ng/µl of RNA.

2.3.1.3 qRT-PCR primers

$K_{Ca}3.1$ gene (KCNN4) expression was analysed with the gene-specific Hs_KCNN4_1_SG QuantiTect® Primer Assay primers (QT00003780, Qiagen). These primers are specific to $K_{Ca}3.1$ mRNA and detect the NM_002250 transcript, amplifying across exons 4/5, and have a final product length of 130 base pairs (bp). Exact primer sequences could not be obtained from Qiagen. The internal normaliser gene used was β-Actin (ACTB) and initially β-Actin primers (forward primer, 5'-TTCAACTCCATCATGAAGTGTGACGTG-3', reverse primer, 5'-CTAAGTCATAGTCCGCCTAGAAGCATT–3') were used which have a final product length of 310 bp. However, due to consumption we switched to using gene specific Hs_ACTB_1_SG QuantiTect® Primer Assay primers (QT00095431, Qiagen). These are specific to ACTB, detecting the NM_001101 transcript, spanning exons 3/4 and producing a final product length of 146 bp. Only results using the same primers were compared, therefore the change in primers did not affect the results. All expression data was normalized to β-Actin and corrected using the reference dye ROX.

2.3.1.4 qRT-PCR

Gene expression was quantified by quantitative RT-PCR using the Brilliant SYBR® Green QRT-PCR 1-Step Master Mix (Strategene,

Amsterdam, the Netherlands). For the assay 12.5 µl of 2 x SYBR® QRT-PCR mastermix was added to each tube of a 96 well qRT-PCR plate (ThermoScientific). 7 µl of PCR grade water was added to each well and 2.5 µl of the appropriate primers. 1 µl of reference dye ROX and 1 µl of Stratascript Reverse Transcriptase (RT)/RNase block enzyme mixture were also added to the well. Finally 1 µl of myofibroblast RNA at a concentration of 100 ng per reaction tube was added. All reactions were performed in triplicate. Wells were also set up to include a no template control (NTC) which would contain no template RNA and also a no RT control which contained everything but the RT/RNase block mixture.

The plates were sealed using optically clear tube caps (8x strips)(Agilent technologies) and centrifuged at 302 x g for 1 minute to eliminate bubbles caused by pipetting as these could interfere with the fluorescent reading of the plate. The 96 well plates were transferred to the Mx3000P™ quantitative PCR machine (Stratagene) for analysis. The protocol was set to read fluorescence for both SYBR Green and ROX, the reference dye. The cycling conditions were set as follows;

Initial Reverse Transcription		30 mins	@ 50°C
Inactivation of RT		10 mins	@ 95°C
Denaturation	30 Secs	@ 95°C	Repeat for 50 cycles
Annealing	30 Secs	@ 60°C	
Extension	31 Secs	@ 72°C	
Melting curve	30 secs @ 90°C		
	30 secs @ 60°C		
	30 secs @ 90°C		
	30 secs @ 60°C		

Fluorescent readings were taken at the end of the extension step. A melting curve cycle was performed at the end and the fluorescence read continually throughout the 2nd 90°C to determine the melting point of the cDNA products. Only experiments where a distinct single peak was observed with a melting temperature different to that of the no template control were used.

2.3.1.5 Agarose gel

To prepare a 1.5% agarose gel, 0.75 g of agarose (Sigma) was added to 50 mls of Tris base, acetic acid and EDTA (TAE) buffer. The mixture was placed into a microwave at 700 Watts until all the agarose had completely dissolved. The mixture was left to cool and then 2 µl of Ethidium Bromide added. The mixture was carefully poured into a gel mould containing a comb. Once set the comb was lifted to leave the loading wells, and the mould placed into the gel tank and approximately 1 L of TAE added.

2 µl of blue/orange 6x loading dye (Promega, Wisconsin, USA) was added to each PCR product and 10 µl loaded into the agarose gel. 10 µl of a 100bp DNA ladder (Promega) was also loaded into the gel. The tank was then connected to the power pack and the gels left to run at 80V for 1 hour. Gels were viewed on an IllumoVision camera (Syngene, Cambridge, UK) and pictures taken. This allowed confirmation that the product amplified in the QRT-PCR reaction was the expected length for both the $K_{Ca}3.1$ channel (130 bp) and β-Actin (310 bp) by comparing the products against a DNA ladder.

2.3.2 Western blot

Western blot is a universal technique used to detect specific proteins within a sample by using gel electrophoresis to separate proteins by their structure and/or molecular weight. The proteins are then transferred to a membrane and stained with specific antibodies to target the protein which can be detected using chemiluminescent agents and visualised using photographic film. Western blot analysis was used to confirm whether the $K_{Ca}3.1$ protein was present within human lung myofibroblasts.

2.3.2.1 $K_{Ca}3.1$ protein isolation

To examine the expression of $K_{Ca}3.1$ protein in human lung myofibroblasts, cells were grown to confluence, harvested using trypsin-EDTA, centrifuged at 227 x g for 7 mins, the supernatant

removed and the cells then washed using PBS + 0.1% BSA. Cells were centrifuged again and the PBS removed. 500 µl of RIPA lysis buffer (1 ml of RIPA buffer, 10 µl protease inhibitor, 10 µl PMSF and 10 µl of sodium orthovanadate) was added to the cells and re-suspended, with care taken to ensure there were no bubbles. The cells and buffer were left on ice for 30 minutes. If the mix was still viscous after 30 minutes, the cells were lysed further using a needle and syringe to disrupt the cells. This mix was then centrifuged at 13,416 x g for 15 minutes. The supernatant was removed and transferred into a fresh eppendorf. The cell pellet was discarded as this only contained cell debris.

2.3.2.2 Determining concentration of protein

The amount of protein isolated from the cells was determined using the Bio-Rad DC Protein Assay (Bio-Rad Laboratories Ltd, Hertfordshire, UK). This assay determines the concentration of protein through the reaction of protein with an alkaline copper tartrate solution and folin reagent, based on the Lowry assay(287). Using the Bio-Rad reagents, six protein standard solutions were prepared in duplicate with Bovine Serum Albumin (BSA) ranging from 0 mg/ml to 1.45 mg/ml. Samples were prepared with a 1 in 10 dilution in Radio-Immuno-Precipitation Assay (RIPA) buffer. Working reagents were prepared according to the manufacturer's instructions and the reagents were then added to both the standard solutions and

the samples. They were then vortexed and left to incubate for 15 minutes. The standards and samples were transferred to cuvettes and measured using a spectrophotometer set at an absorbance of 750 nm.

As this is a colorimetric assay a standard curve was produced using the average of each BSA standard absorbance, plotting the protein concentration (mg/ml) against the absorbance. The sample concentration was then determined from the linear equation and the sample absorbance. The samples were diluted to a final concentration of 1 µg/µl using RIPA buffer.

2.3.2.3 Protein electrophoresis and membrane blotting

Firstly, it was necessary to perform sodium dodecyl sulphate polyacrylamide gel electrophoresis (SDS-PAGE). SDS polyacrylamide gels were prepared by adding 7.5 mls of 12% resolving gel (3.6 mls H_2O, 6.72 mls Tris pH 8.8, 180 µl 10% sodium dodecyl sulphate (SDS), 400 µl ammoiniaperoxysulphate (APS), 7 mls 30% acrylamide, and 10 µl of tetramethylethylenediamine (TEMED)) between glass plates and layering isobutanol on top. The resolving gel was left to set for 15 minutes at room temperature. Isobutanol was removed and the top of the gel rinsed with distilled H_2O (dH_2O). A stacking gel (3.68 mls H_2O, 625 µl Tris pH 6.8, 50 µl 10% SDS, 100 µl 10% APS, 665 µl 30% acrylamide and 8 µl TEMED) was then added to the top of the resolving gel and a comb placed in it. This

was allowed to set at room temperature for 40 minutes. The comb was removed and the plates were set in the gel running units and the running buffer (10X running buffer containing 30.3 g Tris, 144 g glycine, 10 g SDS and 1000 mls dH_2O, pH was adjusted to 8.3) was added.

Protein samples were prepared as follows. 2 x SDS loading buffer containing DTT reducing agent (100 mM Tris-Cl pH 6.8, 0.2% bromophenol blue, 20 % glycerol and 200mM dithiothreitol (DTT)) was added at a 1:1 dilution to the protein sample and the sample denatured by heating at 99°C for 10 minutes. Protein samples were loaded into the gel, 10 µl of SeeBlue® plus 2 pre-stained marker (Invitrogen) was loaded as this allows visualisation of proteins of different molecular weight during the electrophoresis and western transfer. Also loaded was MagicMark™ XP western protein standard (Invitrogen) which allows visualisation of protein standard bands on the photographic film. Two gels were made and the protein and markers loaded exactly the same, one gel was used for the detection of the $K_{Ca}3.1$ protein and the second for β-actin. The gel was run at 100 V, 400 mA for 2 hours.

Following electrophoresis the gels were removed from the tank, glass plates detached and the stacking gel removed. The gels were placed in transfer buffer (transfer buffer contained 1.54 g Tris, 14.4 g glycine, 100 mls methanol and made up to 1000 ml using dH_2O) for

15 minutes. Immobilion-P transfer membrane (Sigma-Aldrich) was cut to size and soaked in 100% methanol for 15 seconds then milli-Q grade water for 2 minutes, and finally transfer buffer for 10 minutes. Blotting paper was briefly soaked and a transfer sandwich was constructed on the transfer device, layering blotting paper, the membrane, then the gels and finally more blotting paper on top. The bubbles were rolled out and the transfer lid secured. The transfer was performed by running at 15 V for 30 minutes. The sandwich was disassembled and the membrane removed, the gel and blotting paper were discarded. The membrane was placed into 100% methanol for 15 seconds and dried for 10 minutes. The membrane was then washed in dH_2O for 2 minutes.

2.3.2.4 Detection of proteins

Membranes were blocked in tris buffered saline (TBS)(Tris 30.3 g, NaCl 90 g and 1 litre of H_2O, and pH adjusted to 7.5) containing 5% Milk (Marvel) and 0.1% Tween20 (Sigma-Aldrich) for 1 hour at room temperature. The membranes were then transferred to a container containing the primary antibodies which had been prepared in TBS/5% milk/0.1% Tween20, and left overnight at 4°C. The following primary antibodies were used: rabbit polyclonal $K_{Ca}3.1$ P4997 (Sigma-Aldrich) at a concentration of 0.8 µg/ml, rabbit polyclonal KCNN4 AV35098 (Sigma-Aldrich) at a concentration of 1 µg/ml, and a gift antibody from GSK, M20, dilution of 0.2µg/ml The second

membrane was used as a loading control for each sample protein, with β-Actin HRP antibody (Santa Cruz) used at a concentration of 10 ng/ml. This was also incubated overnight at 4°C. The membranes were washed the following morning with TBS containing 0.1% Tween20 for 10 minutes; this was done 3 times in total. Secondary polyclonal goat anti rabbit immunoglobulin conjugated with horseradish peroxidase (HRP)(Dako) was applied to both membranes at a concentration of 1.25 mg/ml diluted with the blocking solution. The membranes were incubated with the secondary antibody for 1 hour at room temperature. Following this the membranes were washed a further 3 times using TBS containing 0.1% Tween20. The membranes with immunolabelled proteins were visualized using the Amersham Enhanced ChemiLuminescence (ECL) western blot detection system (GE Healthcare Life Sciences, Buckinghamshire, UK) within a dark room. This detection system relies on the emission of light following HRP plus hydrogen peroxide catalysing the oxidation of luminal. ECL reagents 1 (luminal) and 2 (peroxide) were added at a 1:1 ratio onto the membrane and left for 1 minute before being removed. The membrane was wrapped in Saranwrap and along with blue sensitive X-Ray film (Fuji) the membrane and film were pressed together for the appropriate exposure time. The film was then developed using Curix60 processor (AGFA Healthcare, South Carolina, USA).

2.3.3 Patch clamp electrophysiology

The patch clamp technique allows single or multiple ion currents to be measured across biological membranes. In our study I have used the whole cell patch clamp technique which measures the currents of multiple channels across the whole cell membrane.

2.3.3.1 Whole cell patching

The whole cell variant of the patch clamp technique was used (273,288). Patch pipettes were made from borosilicate fibre-containing glass (Clark Electromedical Instruments, UK) and the tips were heat polished, typically resulting in resistances of 4-8 MΩ .

2.3.3.2 Patch clamp solutions

The standard pipette solution contained KCl 140 mM; $MgCl_2$ 2 mM; HEPES 10 mM; Na^+-ATP 2 mM; GTP 0.1mM (pH 7.3 adjusted using KOH).

The standard external solution contained NaCl 140 mM; KCl 5 mM; $CaCl_2$ 2 mM; $MgCl_2$ 1 mM; HEPES 10 mM (pH 7.3, adjusted using NaOH).

2.3.3.3 Cell preparation

Myofibroblasts were grown in 24 well plates and harvested using 0.25% trypsin EDTA. The cells were then centrifuged at 302 x g for 5 minutes to form a cell pellet, and re-suspended in 200 µl of MGM.

Where appropriate, cells were serum starved for 24 hours and stimulated with TGFβ1 10 ng/ml or bFGF 10 ng/ml for 24 hours before harvesting. For recording, myofibroblasts were placed in 35 mm dishes containing standard external solution.

2.3.3.4 Patch clamp protocol

Whole-cell currents were recorded using an Axoclamp 200A amplifier (Axon Instruments, Foster City, CA), and currents were evoked by applying voltage commands to a series of potentials in 10 mV steps from -120 to 100 mV and a holding potential of –20 mV. The currents were digitized, stored on computer and analysed using pClamp software (Axon instruments). Capacitance transients were minimized using the capacitance neutralization circuits on the amplifier. Drugs were added directly to the recording chamber. To elicit $K_{Ca}3.1$ currents the $K_{Ca}3.1$ opener 1-Ethyl-2-benzimidazolinone (1-EBIO; Tocris, Avonmouth, UK) was used at a final concentration of 100 μM. To block the currents the highly specific $K_{Ca}3.1$ channel blockers TRAM-34 (a gift from Prof. Heike Wulff, University of California, Davis, CA) and ICA-17043 (Senicapoc) were used.

2.4 Immunohistochemistry – Paraffin embedded lung

Paraffin embedded ILD disease tissue was received from the Pathology Laboratory at Glenfield hospital, Leicester. The tissue had been removed originally for diagnostic purposes. The use of this

tissue was approved by the North West Ethics Committee and the patients gave written informed consent for its use. NFC tissue was removed during surgical resection for lung cancer.

In short, for paraffin embedding, the lung tissue was placed in a series of processing reagents including, Industrial Methylated Spirits (IMS), Histoclear and finally into paraffin wax. Paraffin sections were cut using a rotary microtome (Leica microsystems) at 4 μm and mounted onto positively charged microscope slides (Thermo-Scientific). Sections were deparaffinised using xylene, ethanol and IMS baths and placed in antigen retrieval solution containing 0.01M citric acid, pH 6 (Sigma), and micro-waved for 30 minutes at 700 watts. The slides were placed in distilled water and then in endogenous peroxidase inhibitor (0.1% sodium azide (NaN_3) and 0.3% hydrogen peroxide (H_2O_2)) for 30 minutes. After a wash with TBS, culture blocking medium was added to each section for 30 minutes and then primary antibodies to the following antigens were applied: αSMA (mouse mAb,1A4, 0.7 μg/ml, Dako), mast cell tryptase (mouse mAb AA1, 0.085 μg/ml, Dako), fibroblast marker Thy-1 (mouse mAb CP28, 3 μg/ml, Calbiochem), anti-fibroblast surface protein (FSP)(mouse mAb 1B10, 4 μg/ml, Sigma), collagen type 1 (mouse mAb 5D8-G9, 7.5 μg/ml, Millipore) and appropriate isotype controls. Rabbit polyclonal antibody $K_{Ca}3.1$ (P4997, 4 μg/ml, Sigma-Aldrich) was also used. Appropriate isotype controls were performed using the isotype at the same concentration as the specific

primary antibody. Primary antibodies were left on sections overnight. Sections were then washed with TBS and secondary antibodies, polyclonal rabbit anti mouse immunoglobulins/biotinylated (E0413, 2.4 mg/ml, Dako), polyclonal swine anti rabbit immunoglobulins/biotinylated (E0431, 2.9 mg/ml Dako) were incubated for 1 hour at room temperature. Sections were washed with TBS and 200 µl of avidin/biotin peroxidase complex (Vectorstain elite ABC Kit, Vector Labs, Peterborough, UK) was applied for 1 hour. Sections were washed again with TBS and 200 µl of DAB (3, 3'-diaminobenzidine) substrate which produces a dark brown colour was applied for 10 minutes. Slides were rinsed with TBS and washed under running water for 5 minutes. Sections were then counterstained with Mayers haematoxylin (Sigma-Aldrich) and cover slipped using DPX mountant (Sigma-Aldrich). Staining was assessed using Cell-F image software analysis (Olympus UK Ltd).

2.5 Cell proliferation assay

To assess cell proliferation the MTS assay was used which is a well-documented, non-radioactive, colorimetric method(289).

2.5.1 Cell preparation

Myofibroblasts were seeded in triplicate in 96-well flat-bottomed plates at 2 x 10^3 cells per well in 10% FBS media until 60% confluent and placed in SF medium for 24 hours. TRAM-34 (20 and 200 nM)

and ICA-17043 (10 and 100 nM) were then added (final DMSO concentration 0.1%), and the cells stimulated with either 1, 10 100 ng/ml TGFβ1, 10 ng/ml bFGF plus 2% FBS or 10% FBS alone for 72 hours. Control wells contained either 0.1% DMSO or SF medium. A control well containing no cells for each condition was also included.

2.5.2 MTS protocol

Cell proliferation was assessed using the MTS assay at 0 and 72 h after stimulation. CellTiter 96 Aqueous one solution containing the tetrazolium compound MTS, [3-(4,5-dimethylthiazol-2-yl)-5-(3-carboxymethoxyphenyl)-2-(4-sulfophenyl)-2H-tetrazolium] (Promega, Madison, WI, USA) was added to each well and incubated at 37°C for 3 hours. The absorbance of each well was read at 490 nM for 0.1 seconds using a microplate reader (Wallac 1420 Victor^{TM} multi-label counter, PerkinElmer Inc).

2.6 Repair Response assay

Cells were grown to confluence in 6 well plates with regular medium and then replaced with SF medium. Grid lines were drawn onto the bottom of each well and after 24 hours, 3 artificial wounds were created in each well, using a 200 µl pipette tip to scratch the confluent cell monolayer, see **Figure 2-2**. This created a cell free area. The medium was removed and the well was washed three times. TRAM-34 (20 and 200 nM), ICA-17043 (10 and 100 nM),

TRAM-7 (200 nM) and TRAM-85 (200 nM) were then added in a final DMSO concentration of 0.1%, and the cells stimulated with either 10 ng/ml bFGF or 10% FBS alone for 48 hours.

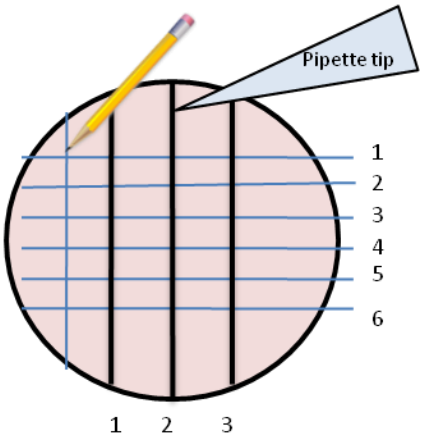

Figure 2-2. Creating the myofibroblast wound

Grid lines were drawn onto the bottom of a 6 well plate, 1 vertical line on the left hand side and 6 horizontal, equal distances apart. A pipette tip was then used to score 3 vertical wounds through the confluent myofibroblast monolayers. Photos were taken and labelled according to the grid and wound number.

Control wells contained 0.1% DMSO and culture medium alone. Cells migrating and proliferating into the wound were observed and photographs taken at 0, 6, 24, 30 and 48 hours. To determine the best way to measure the photos 2 different techniques described in the literature were adopted. The first to measure the area of the wound at each time point and the second to measure the distance of the wound, see **Figure 2-3**. The two methods were compared using Bland-Altman method which showed a bias of -0.13 indicating that the two methods were producing similar very results. I then performed the rest of the analysis using the area method as this was a slightly quicker technique.

In each experiment, wound healing was measured by analysing the area of the scraped wound. Wound healing was quantified as a percentage of the starting area of the wound scraped. Data presented represents the mean measurement from 2 different scratches. Repeatability of wound measurement was assessed by 2 blinded observers in n=3 subjects with excellent agreement (intraclass correlation of 0.969, Cronbech's Alpha, $P<0.000$).

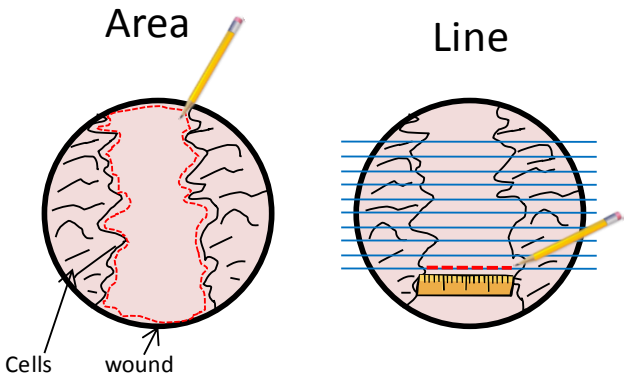

Figure 2-3. Measuring the wound

The wound was measured by two different methods the first by measuring the area of the wound at each time point. The second was to draw 10 pre-set lines across the photograph and measure the length of the wound on each line and then take the average.

2.7 Collagen secretion assay

To measure collagen secretion from myofibroblasts we used the Sircol assay (Biocolor, County Antrim, UK). This is a well-documented technique(148,290) which can assess the rate of newly synthesised fibrillar collagens (types I, II, III, V and XI) deposited in cell supernatants.

2.7.1 Supernatant preparation

For these experiments, cells were grown to confluence in 24 well plates and placed in SF media. After 24 hours, the media was replenished and the cells stimulated with bFGF (10ng/ml), TGFβ1 (10ng/ml), bFGF or TGFβ1 containing TRAM-34 (20 and 200 nM), and bFGF or TGFβ1 containing ICA-17043 (10 and 100 nM). Both drugs added had a final DMSO concentration of 0.1% and a control well was included containing 0.1% DMSO. Also used were TRAM-34 analogs which did not block the $K_{Ca}3.1$ channel, TRAM-7 200 nM and TRAM-85 200 nM. After 16 hours the supernatants from the 24 well plates were collected and centrifuged at 307 x g for 7 minutes to remove any cell debris.

2.7.2 Sircol assay protocol

To measure the collagen released into culture medium by treated myofibroblasts the Sircol collagen assay was used. Initially 250 µl of

cell supernatant was placed into a low-protein binding tube (Eppendorf) and 50µl of cold isolation and concentration reagent was added. Each sample was analysed in duplicate. Culture medium alone which had not been cultured with myofibroblasts was used as a control, as it is said to contain small amounts of collagen. The tubes were placed into a container of half ice and water and placed at 4°C overnight. The following day the tubes were centrifuged at 6440 x g for 10 minutes. 250 µl of supernatant was slowly removed from the top using a pipette. Collagen standards of 0, 1.25, 2.5, 5 and 7.5 µg/ml were prepared in duplicate using the Sircol collagen reference standard supplied. 500 µl of Sircol dye reagent was then added to each sample and each standard. All the tubes were mixed by inversion and then placed on a shaker for 30 minutes to allow the collagen-dye complex to form. Following this all tubes were centrifuged at 6440 x g for 10 minutes producing a pellet at the bottom. It was then necessary to remove all unbound dye carefully by inverting, draining and removing excess dye from the tube using a cotton wool bud. The pellet was then washed using 375 µl of ice-cold acid-salt wash to remove any unbound dye from the surface of the pellet. The tube was centrifuged at 6440 x g for another 10 minutes, inverted, drained and any excess fluid removed using a cotton wool tip. Finally, 125 µl of alkali reagent was added to each tube and mixed thoroughly to release the collagen bound dye into the solution. After 5 minutes the standards and samples were measured using a

spectrophotometer at an absorbance of 555 nm. The standards were used to create a standard curve, using the average of each collagen standard and plotting the collagen concentration (µg/ml) against the absorbance. The sample concentration was then determined from the linear equation; the absorbance is directly proportional to the amount of newly formed collagen in the supernatant.

2.8 Collagen gel contraction

Collagen gel contraction assays are a recognized *in vitro* model that allows examination of the physiological mechanisms of cytoskeletal re-organisation or stress fibre formation(291). This technique has been used in fibroblasts(292), ASM(293) and vascular smooth muscle cells(294). This technique was used to examine the contractility of NFC and IPF myofibroblasts.

2.8.1 Preliminary dose response assay

To determine the optimum concentration of TGFβ1, the collagen gel contraction assay was first performed using three different doses of TGFβ1, 1 ng/ml, 10 ng/ml and 100 ng/ml. The optimum concentration of collagen gel contraction was 10 ng/ml of TGFβ1; this amount was used for the following experiments.

2.8.2 Contraction assay

Cells were pre-treated for 24 hours with either SF media, 0.1% DMSO, TRAM-34 200 nM, ICA-17043 100 nM, TRAM-7 200 nM or TRAM-85 200 nM. The cells were then washed, harvested using trypsin-EDTA and re-suspended at 8.68 x 10^5 per ml in SF medium. Collagen gels were made on ice and consisted of 299 µl of PureCol type 1 collagen (Inamed Biomaterials), 37 µl of 10X DMEM (Invitrogen), and 20 µl sodium bicarbonate (Invitrogen), and impregnated with 144 µl myofibroblast cell suspension (0.125 x 10^6 per collagen gel). Gels were added to 24 well plates, coated with PBS/0.5% BSA and left to polymerize at 37°C for 90 minutes. The gels were then detached from the plastic surface to allow free contraction and re-suspended in either 500 µl SF medium or SF medium containing the stimulants TGFβ1 (final concentration of 10ng/ml) or bFGF (final concentration of 10ng/ml) where appropriate and left to incubate for 22 hours. Photographs were taken at 0 and 22 hours. The percentage contraction was assessed by measuring the collagen gel surface area at each time point using ImageJ software (http://rsbweb.nih.gov/ij/). Repeatability was evaluated in n=4 donors by 2 blinded observers who demonstrated excellent agreement in the assessment of gel size (intraclass correlation of 0.968, Cronbach's Alpha, P<0.000).

2.9 Epithelial mesenchymal transition

When basal epithelial cells were 80-100% confluent, they were washed twice using HBSS and harvested using 0.1% trypsin EDTA. The cells were centrifuged at 227 x g for 8 minutes to form a cell pellet. The cells were re-suspended in 1 ml of BEGM, counted using the trypan blue method and seeded into 8 well chamber slides (approximately 2 x 10^4 cells per well). Chamber slides were kept in an incubator at 37°C in 5% CO_2/95% air and cells grown to confluence for 3—7 days. Once approximately 80% confluent, cells were either placed in either fresh BEGM or BEGM containing 10 ng/ml TGFβ1 for 72 hours.

Cells were then washed, fixed and blocked by the same method in section **2.2.1**. Fibroblast markers used were anti-αSMA FITC-conjugated mAb (F3777, 10 µg/ml, Sigma-Aldrich) and isotype control mouse IgG_{2a} FITC-conjugated (X0933, 10 µg/ml, Dako), mouse mAb anti- THY-1 (CP28, 3µg/ml, Calbiochem, San Diego, CA) and isotope control IgG_1 (X0931, 3µg/ml, Dako). Epithelial cell markers used were rabbit mAb anti-E-Cadherin (24E10, 0.215 µg/ml, Cell Signaling, Massachusetts, USA), and polyclonal rabbit anti-Zo-1 (40-2200, 2.5 µg/ml, Invitrogen, USA). For both antibodies isotype control rabbit polyclonal IgG (550875, 2.5 µg/ml, BD pharmagen) was used. Also used was rabbit polyclonal anti- $K_{Ca}3.1$ antibody (P4997, 8 µg/ml, Sigma-Aldrich). Primary antibodies were incubated

for 90 minutes and then appropriate secondary antibodies indirectly labelled with FITC or R-PE (F0313, Dako) were applied for a further 90 minutes. Cells were counterstained with 4',6-diamidino-2-phenylindole (DAPI, Sigma-Aldrich). Cells were mounted with fluorescent mounting medium and cover-slipped. Original images were captured on an epifluorescent microscope (Olympus BX50, Olympus UK Ltd) and counted using Cell F imaging software (Olympus UK Ltd). Matched exposures were used for isotype controls.

The results from this experiment were inconclusive, more time was required to perfect the technique, optimize antibodies and optimize conditions. Due to these reasons the results are not shown.

2.10 Effects of bFGF and $K_{Ca}3.1$ inhibition on myofibroblast differentiation

To investigate the differentiation of the human lung myofibroblasts we analysed the expression of αSMA following stimulation with the growth factor bFGF (a known differentiator of fibroblasts) and following $K_{Ca}3.1$ block using Tram-34 and ICA-17043. Fibroblasts have few or no αSMA filaments, therefore if a myofibroblast differentiates towards a fibroblast phenotype this can be characterised by the loss of αSMA.

2.10.1 The effects of TRAM-34 and ICA-17043 on myofibroblast αSMA expression

Myofibroblasts were harvested from 80-90% confluent monolayers using 0.25% trypsin EDTA, the cells were centrifuged at 302 x g for 5 minutes to form a cell pellet. The cells were re-suspended, counted and seeded at 2 x 10^4 cells per well into Lab-Tek™ II 8 well chamber slides (Nunc).They were placed in an incubator at 37°C in 5% CO_2/95% air and grown to confluency for 3—7 days. When 80% confluent the growth medium was replaced in each well with a different condition; either with SF medium, SF medium containing 0.1% DMSO, SF media containing TRAM-34 20 nM or 200 nM, and SF media containing ICA-17043 (10 nM or 100 nM). The final DMSO concentration was 0.1%. Analogs of TRAM-34, TRAM-7 and TRAM-85 that do not block the $K_{Ca}3.1$ channel were used at 200 nM. Cells were stimulated with each condition for 48 hours.

2.10.2 The effects of bFGF on myofibroblast αSMA expression

Myofibroblasts were harvested from 80-90% confluent monolayers using 0.25% trypsin EDTA, the cells were centrifuged at 302 x g for 5 minutes to form a cell pellet. The cells were re-suspended, counted and seeded at 2 x 10^4 cells per well into Lab-Tek™ II 8 well chamber slides (Nunc). They were placed in an incubator at 37°C in 5%

CO_2/95% air and grown to confluence for 3—7 days. When 80% confluent the growth medium was replaced in each well in either SF medium alone or SF medium containing bFGF at a concentration of 10 ng/ml. Cells were incubated for 48 hours.

2.10.3 Measuring αSMA expression by Immunofluorescence

Immunofluorescence was performed as described in section **2.2.1**, following 48 hours stimulation. Primary antibodies used were mouse mAb anti-α-SMA FITC-conjugated (10 μg/ml) and isotype control mouse IgG_{2a} FITC-conjugated (10 μg/ml). Original images were captured on an epifluorescent microscope (Olympus BX50, Olympus UK Ltd, South end–on-sea) and counted using Cell F imaging software (Olympus UK Ltd). Matched exposures were used for isotype controls. Cells expressing αSMA were counted by 2 blinded observers who demonstrated good agreement (intraclass correlation of 0.645, Cronbach's Alpha, P=0.008).

2.11 Enzyme-linked immune-absorbent assay

In this study we used sandwich Enzyme-Linked Immune-absorbent Assay (ELISA) to measure the amount of the target antigen within myofibroblast cell supernatants.

2.11.1 TGFβ1 ELISA

To detect the amount of Human TGFβ1 in cell culture supernatants we used the DuoSet® ELISA development kit (R&D systems). This kit uses a sandwich ELISA to measure the natural and recombinant human TGFβ1.

2.11.1.1 TGFβ1 ELISA sample preparation

Initially it was necessary to ascertain how much TGFβ1 the human lung myofibroblasts naturally produce. So cells were grown to 80% confluence in T75 flasks and placed in SF medium for 24 hours. The SF medium was replaced either with fresh SF medium or with MGM, after 24 hours the supernatants from the T75cm^2 flasks were collected and centrifuged at 307 x g for 7 minutes to remove any cell debris.

Once we had determined that the cells produced their own TGFβ1 we then looked to see whether K_{Ca}3.1 channel blockers inhibited this constitutive TGFβ1 production. The cells were grown to 80% confluence in T75cm^2 flasks and placed in SF medium for 24 hours. After 24 hours, the media was replenished and the cells incubated with SF media containing either 0.1% DMSO, TRAM-34 200 nM, ICA-17043 100 nM, TRAM-7 200 nM, TRAM-85 200 nM. After 24 hours the supernatant from the T75cm^2 flasks was collected and centrifuged at 307 x g for 7 minutes to remove any cell debris. Supernatants were kept frozen in -20°C freezer until required.

2.11.1.2 TGFβ1 ELISA Assay

Following the manufacturer's instructions the capture antibody mouse anti-TGFβ1 a 2µg/ml was used to pre-coat maxi-sorp 96 well Nunc plates (Thermo Scientific) which were sealed and left to incubate overnight at room temperature. The next day the plates were washed with wash buffer (0.05% Tween20 in 1 x PBS) and the remaining protein binding sites blocked using block buffer (5% Tween20 0.05% NaN_3 in PBS). TGFβ1 standards were prepared ranging from 0 pg/ml to 200 pg/ml, which were diluted in reagent diluent (1.4 g BSA, 50 µl Tween20 and made up to 100 mls using 1 x PBS). To convert latent TGFβ1 to active immunoreactive TGFβ1 it was necessary to incubate the sample with 1N HCL for 10 minutes, then neutralize with 1.2N NaOH/0.5M HEPES. After the plate was washed 3 times the standards and samples were placed into the wells in triplicates and incubated for 2 hours at room temperature. The plate was washed and then the detection antibody, biotinylated chick anti-human TGFβ1 300ng/ml antibody was added to each well. After 2 hours the plates were washed and Streptavidin HRP incubate in each well for 20 minutes. A final wash was performed to remove any unbound antibodies, and a substrate solution added. The colour develops in proportion to the amount of TGFβ1 present. The reaction was stopped using 2 N H_2SO_4. The plate was then read on a plate reader (Wallac 1420 Victor^{TM} multi-label counter, PerkinElmer Inc, Massachusetts, USA) set at 450 nM. The standards were used to create a standard curve,

using the average of each TGFβ1 standard and plotting the known TGFβ1 concentration (pg/ml) against the absorbance. The sample concentration was then determined from the linear equation. The absorbance is directly proportional to the amount of TGFβ1 present in the supernatant.

2.11.2 Chemokine ELISA

Chemokines implicated in IPF include CXCL10 (IP-10), CX3CL1 (Fractalkine), CCL11 (Eotaxin), CCL5 (RANTES). To detect the amount of these cytokines in cell culture supernatants we used the DuoSet® ELISA development kit (R&D systems). These kits use a sandwich ELISA to measure the natural and recombinant human IP-10, Fractalkine, Eotaxin and RANTES.

2.11.2.1 Sample preparation

Sample preparation was performed the same as section **2.11.1.1**, however after 24 hours, the media was replenished and each well was incubated with a different condition for 16 hours. Cells were subjected to SF media, TGFβ1 (10 ng/ml), or TGFβ1 plus either 0.1% DMSO, TRAM-34 20 nM, TRAM-34 200 nM, ICA-17043 10 nM or ICA-17043 100 nM. The same conditions were used for bFGF (10ng/ml), or IFN-γ plus TNF-α (both 10 ng/ml).

2.11.2.2 Chemokine ELISA assay

Again the ELISA assay was performed in the same way as section **2.11.1.2**. Each plate however was either coated with mouse anti human CXCL10 (IP-10) 2 µg/ml, mouse anti human CX3CL1(Fractalkine) 4 µg/ml, mouse anti human CCL11(Eotaxin) 2 µg/ml, mouse anti human CCL5(RANTES) 1 µg/ml. Appropriate standards were made (CXCL10 0-2000 pg/ml, CX3CL1 0-20 ng/ml, CCL11 0-1000 pg/ml, CCL5 0-1000 pg/ml) and cell supernatants added, however for this assay the samples did not need to be activated. Detection antibodies specific for target chemokine added (goat anti human CXCL10 50 ng/ml, mouse anti human CX3CL1 500 ng/ml, goat anti human CCL11 100 ng/ml, goat anti human CCL5 20 ng/ml).

3 Results

3.1 Characterisation of myofibroblast phenotype and effect of culture passage

3.1.1 Patient characteristics

In total, cells from 8 non fibrotic control donors and 9 idiopathic pulmonary fibrosis patients were used for the following experiments in human lung myofibroblasts. The patient clinical characteristics can be found in **Table 3-1**. The most noteworthy features are the reduced lung function of the IPF donors; the FEV_1 and FVC are both below 50% predicted. The IPF patients also have marked reduction of gas transfer; the DLCO is below 30%.

Characteristic	IPF (N=9)	Non Fibrotic (N=8)
Sex (no. of subjects)		
Male	8	3
Female	1	5
Age (yr)		
Mean	59.77 ± 3.39	69.5 ± 3.3
Range	40 - 70	58 - 80
Length of symptoms (yrs)		
Mean	4.86 ± 1.38	NA
Range	1 - 11	NA
Smoking (no. with >10 pack/years)	7	5
FEV_1 (% predicted ± SE)	39.56 ± 3.675	112.9 ± 11.04
FVC (% predicted ± SE)	45.63 ± 6.074	92.54 ± 10.51
DLCO (% predicted ± SE)	26.63 ± 3	-
PA mean (% predicted ± SE)	28.38 ± 2.570	-
Treatments		
Prednisone	7	
Mycophenolate Mofetil	5	
Azathioprine	2	
Methylprednisolone sodium succinate	2	
Tacrolimus	2	

Table 3-1. Clinical characteristics of NFC and IPF patients

This table demonstrates the clinical characteristics of the donors who provided tissue for the culture of human lung myofibroblasts.

3.1.2 Characterisation of myofibroblasts

Cultured human lung myofibroblasts displayed the typical morphology of the myofibroblast-like cells with a spindle or stellate shape (**Figure 3-1**). The phenotype of these cells derived from both the NFC and IPF donors was determined by positive immunofluorescent staining with antibodies identifying αSMA, Thy-1, Fibroblast Surface Protein (FSP), Collagen type I (**Figure 3-2**), and negative immunofluorescent staining with antibodies recognising CD68 and CD34 (**Figure 3-3**).

Initially NFC myofibroblasts were we characterized at passages, 2, 4 and 7, to investigate any differentiation or transdifferentiation that may occur. For both Thy-1 and FSP there was little variation between passage, but there was a decrease in αSMA expression at passage 7 (*$P<0.05$, Bonferroni's multiple comparison test). This decrease in αSMA expression suggests that the cells may be dedifferentiating towards a more fibroblast-like phenotype (**Figure 3-4)**.

IPF cells used in this study were not received until passage 3. All donors (NFC n=8 and IPF n=9) were therefore characterised at passages 4 or 5. FSP expression varied little between donors, with >94% of cells from all donors expressing this marker at passages 4-5. FSP is not expressed by lymphocytes, endothelial, epithelial, or vascular smooth muscles cells(127,295). There is however, evidence

of FSP expression in macrophages(295), so another fibroblast marker THY-1 was used alongside FSP. The expression of THY-1 in all donors was >85%. All donors were >97% positive for αSMA expression, and the expression of αSMA was comparable among IPF and NFC donors. We found collagen 1 staining present in 100% of cells from all donors.

No expression of the macrophage/monocyte marker CD68 or mesenchymal cell marker CD34 was found indicating no contamination of fibrocytes, monocytes or macrophages within the cultures. Overall, there was no difference between NFC and IPF cells. All isotype controls were negative **Figure 3-2** and **Figure 3-3**. These results indicate that the cells isolated from NFC and IPF donors at passages 4-5 display a myofibroblast phenotype.

Further confirmation of the αSMA expression was performed by flow cytometry using two NFC donors at passage 4. The results concluded that the cells were >99% positive for αSMA (**Figure 3-5**).

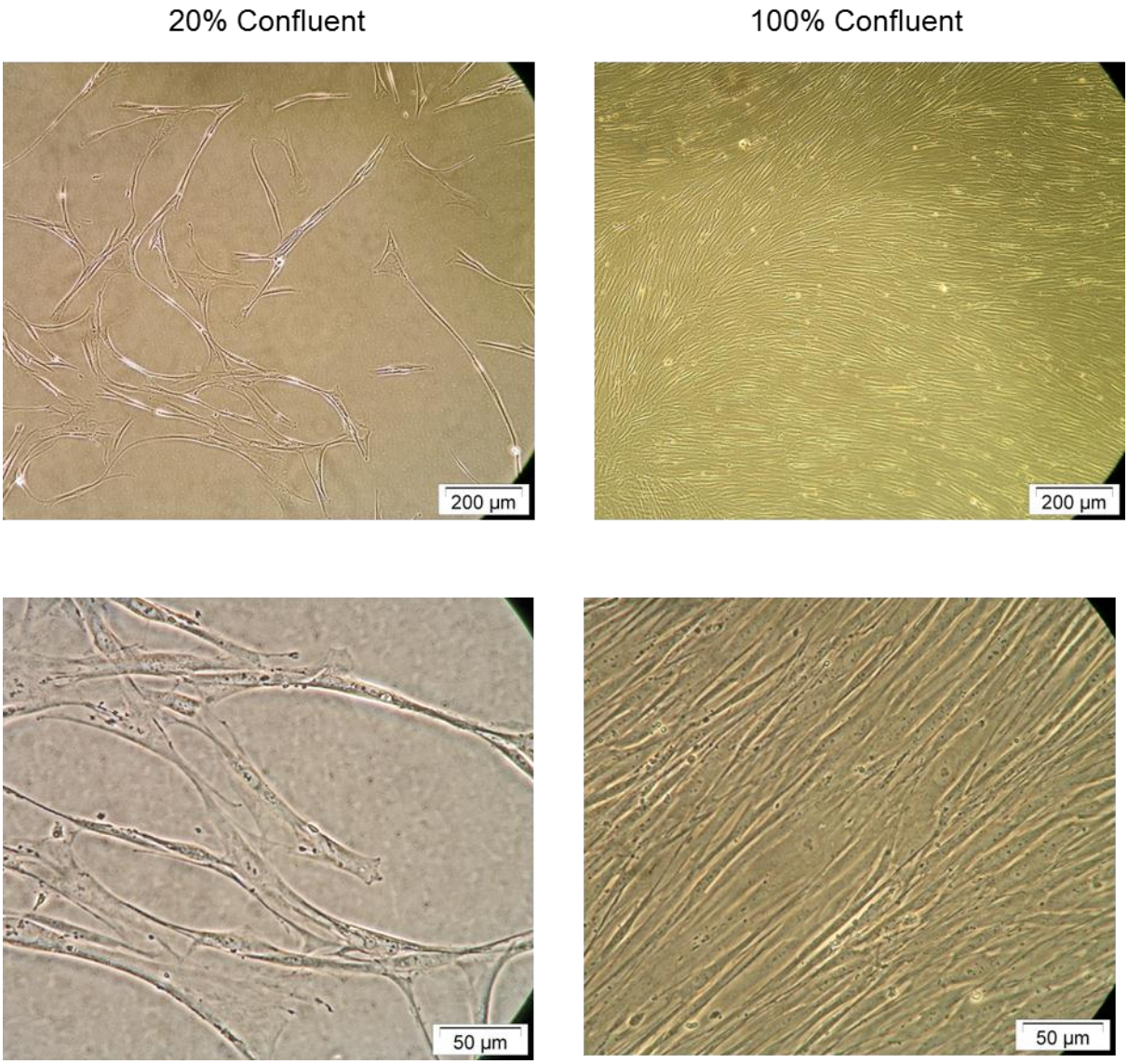

Figure 3-1. Myofibroblast morphology

Myofibroblasts in culture from 1 representative donor. At 20% confluence, the cells show the typical myofibroblast morphology, displaying both stellate and spindle structures. The nuclei are elongated and stress fibres can be identified. When 100% confluent the myofibroblasts display the typical spindle morphology, assembling side by side, occasionally overlapping and in a common direction.

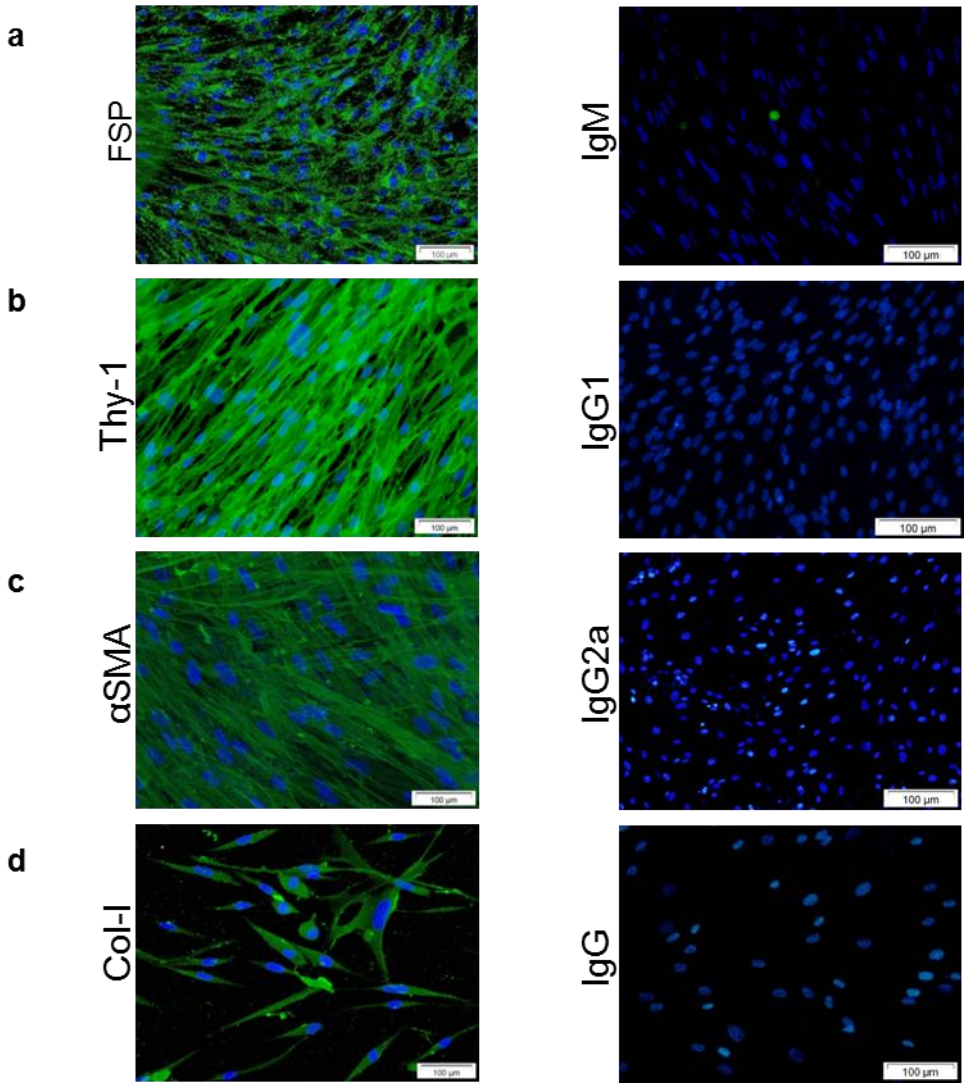

Figure 3-2. Myofibroblast characterization

Primary human lung myofibroblast cultures between passages 4 and 5 were immunostained for myofibroblast markers. Representative images are shown for: **a**) anti-fibroblast surface protein (FSP) and the mouse isotype control IgM; **b**) anti-fibroblast antigen which recognizes the fibroblast antigen (Thy-1/CD90) and the mouse isotype control IgG_1; **c**) α-smooth muscle actin, and the isotype control IgG_{2a}; **d**) collagen type 1 antibody and rabbit isotype control IgG. Nuclei are stained with DAPI.

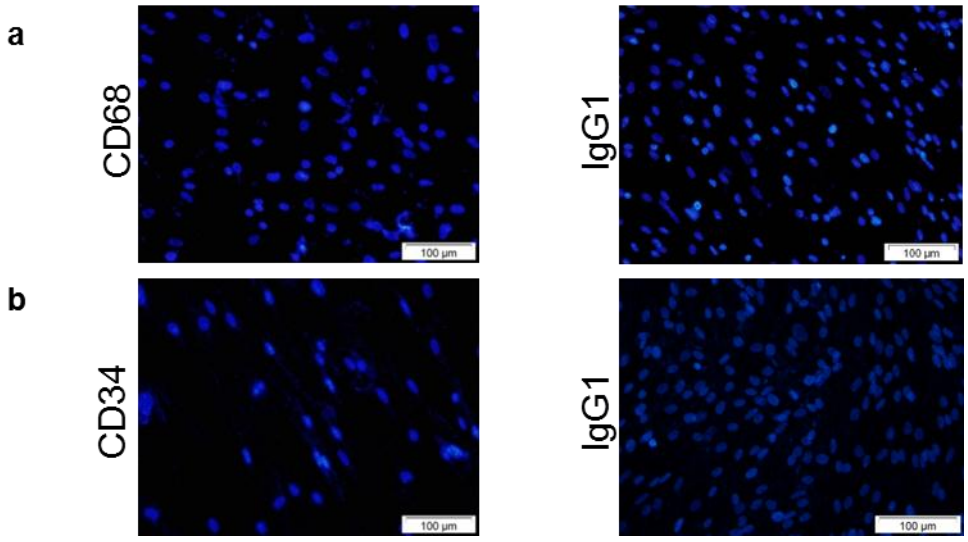

Figure 3-3. Confirmation of pure myofibroblast population

a) shows negative CD68 cell staining and corresponding isotype control IgG3, indicating that there is no contamination of monocytes or macrophage cells. **b)** CD34 antibody shows negative staining with appropriate isotype control IgG, concluding no contamination of fibrocytes.

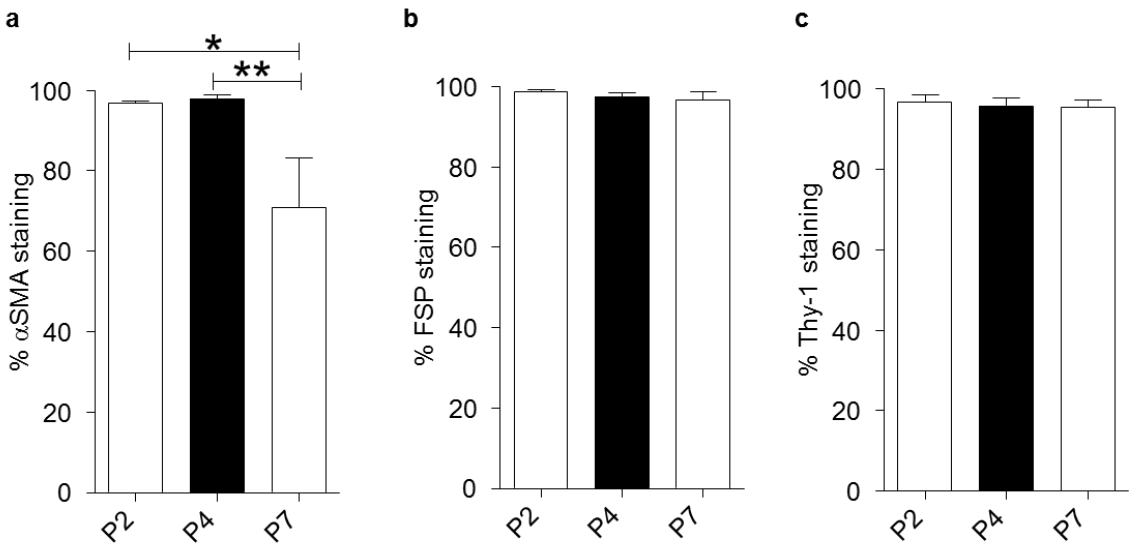

Figure 3-4. The effect passage has on myofibroblast phenotype

The above graphs show the phenotypic characterisation of cells from 5 NFC donors at passages 2, 4 and 7. **a)** the percentage cells αSMA positive. There was a significant difference of αSMA expression amongst passages *P=0.0231, repeated measures ANOVA, with post hoc testing revealing a significant difference between passage 4 and 7, **P<0.05, Bonferroni's multiple comparison test. **b)** and **c)** demonstrate the percentage of FSP and Thy-1 positive cells, respectively. No significant difference was found between passages 2, 4 and 7.

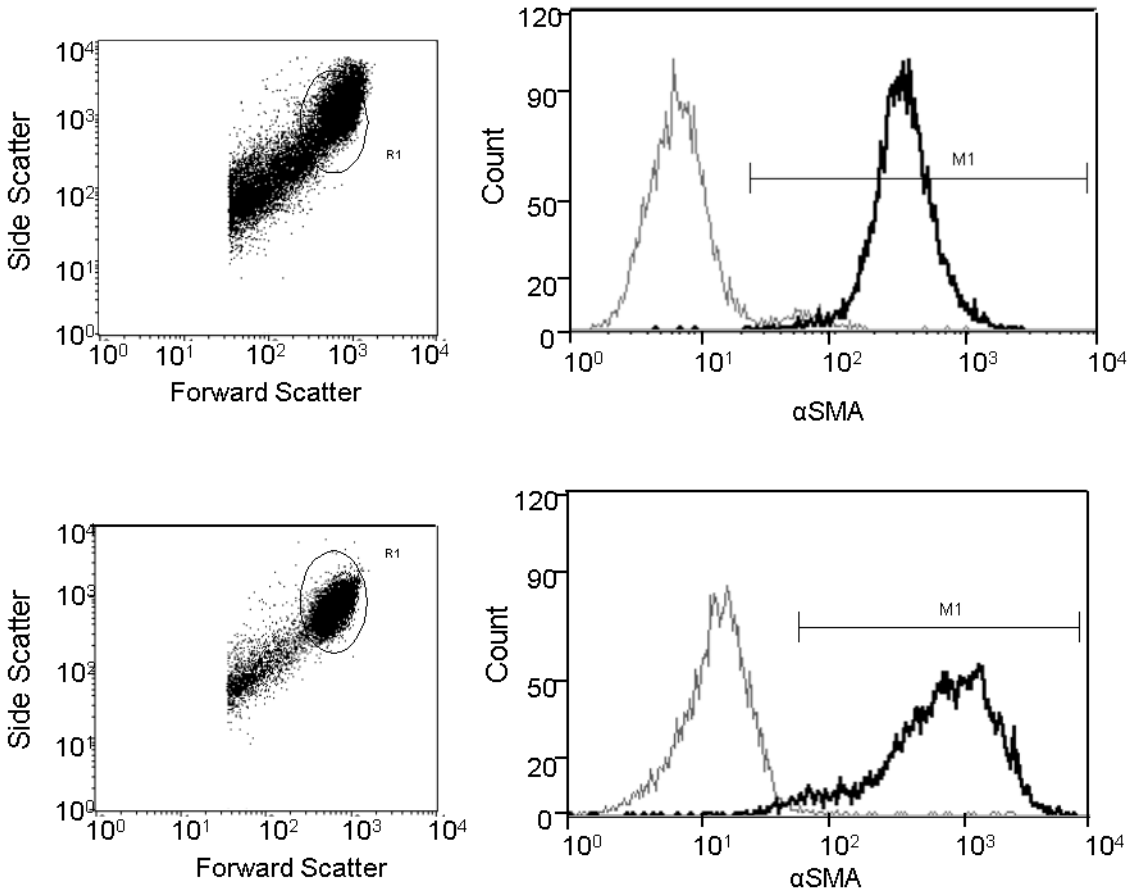

Figure 3-5. Confirmation of αSMA expression

To confirm the high expression of αSMA demonstrated by immunofluorescence, flow cytometry was performed on 2 representative donors. The left hand figures represent the scatter plots for each donor. The right hand side graphs; the light grey line represents the isotype control, the black line shows the αSMA expression where a clear shift can be seen. The results confirmed the characterization results; both donors were >99% positive for αSMA.

3.2 Evidence for expression of $K_{Ca}3.1$ at message and protein level

3.2.1 Myofibroblasts express $K_{Ca}3.1$ channel mRNA, which is up-regulated by TGFβ1 Stimulation

Initially we focused on the expression of $K_{Ca}3.1$ channel mRNA in 5 NFC donors at passage 2, 4, and 7. All passages expressed $K_{Ca}3.1$ channel mRNA **(Figure 3-6).** No significant difference in the amount of $K_{Ca}3.1$ mRNA was found between passages although passage 7 expressed larger amounts in comparison to passage 2 and 4 **(Figure 3-6)**. To visualize the PCR products they were ran on a 1.5 % agarose gel, confirming the products were the correct size and that only one product was amplified **(Figure 3-7).** All donors demonstrated similar expression of β-actin deeming it suitable to use as a normalizing gene.

As previously mentioned, the IPF cells were not received until passage 3, therefore passage 2 was unsuitable for IPF and NFC comparison. Passage 7 was unsuitable due to the reduced αSMA expression. Henceforth the cells were used at passages 4 and 5 for further qRT-PCR experiments. Donors used for experiments were chosen at random.

Both NFC (n=5) and IPF (n=5) human lung myofibroblasts expressed $K_{Ca}3.1$ mRNA **(Figure 3-8)**, and this was significantly increased in cells from NFC compared to IPF donors **(Figure 3-9)**.

Following 24 hours of TGFβ1 stimulation both NFC and IPF myofibroblasts upregulated $K_{Ca}3.1$ channel mRNA relative to β-actin. IPF myofibroblasts had a significantly higher degree of $K_{Ca}3.1$ mRNA up-regulation following TGFβ1 stimulation compared to cells from NFC donors **(Figure 3-10)**. $K_{Ca}3.1$ mRNA was up-regulated at least 8 fold in all the IPF donors after TGFβ1 exposure **(Figure 3-11)**.

Following 24 hours of bFGF stimulation IPF myofibroblasts upregulated $K_{Ca}3.1$ channel mRNA relative to β-actin. IPF myofibroblasts had a higher degree of $K_{Ca}3.1$ mRNA up-regulation following bFGF stimulation compared to NFC myofibroblasts which showed little upregulation **(Figure 3-12)**. $K_{Ca}3.1$ mRNA was up-regulated at least 4 fold in all the IPF donors after bFGF exposure **(Figure 3-13)**.

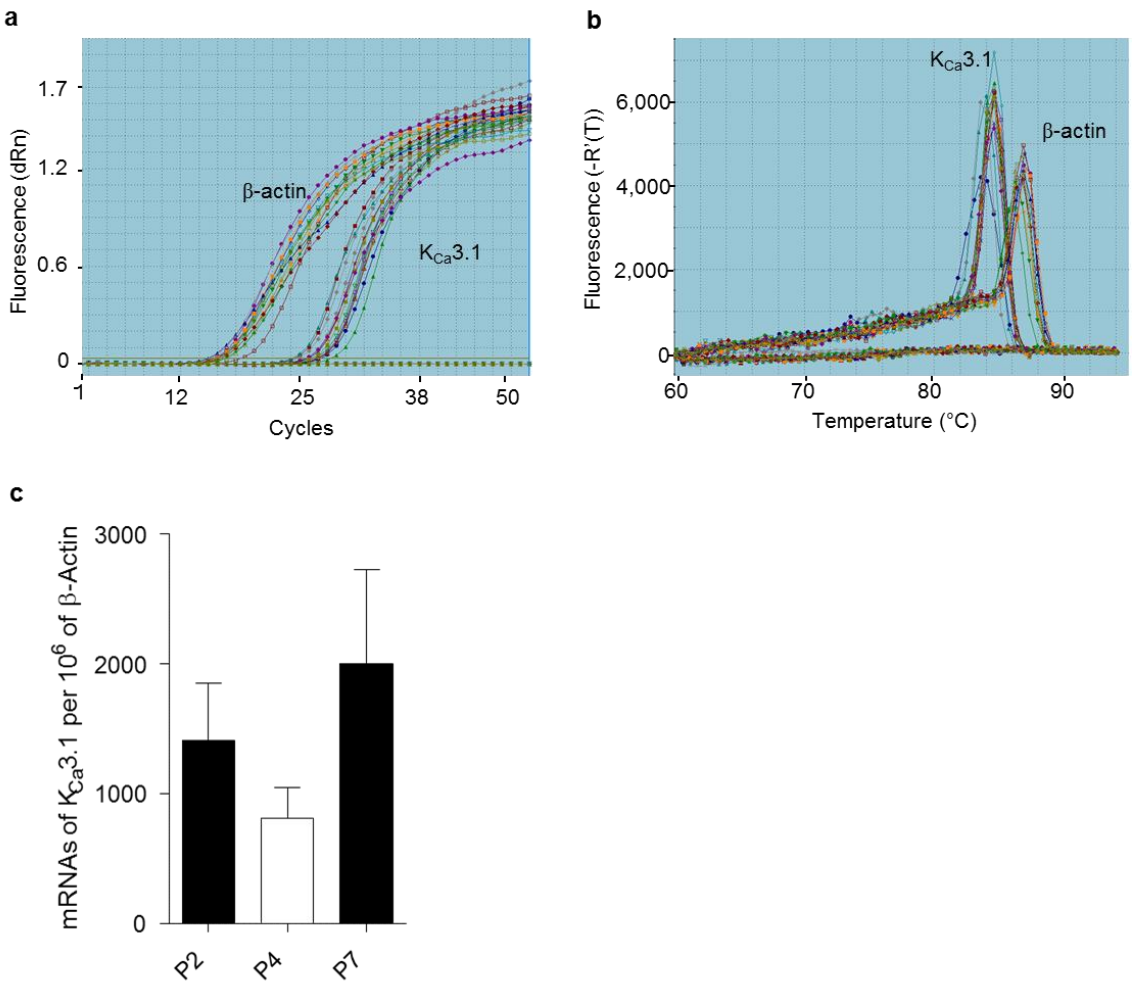

Figure 3-6. $K_{Ca}3.1$ mRNA expression compared between passages

a) Displays the amplification curve of the $K_{Ca}3.1$ and β-actin products of passages 2, 4 and 7 in 5 NFC donors. It shows that all express similar CT values and the β-actin is an appropriate normalizing gene to use. **b)** the dissociation curve of all the products, confirming one single peak for each $K_{Ca}3.1$ and β-actin, indicating that the primers were specific. **c)** the amount of $K_{Ca}3.1$ mRNAs per 10^6 of β-actin did not differ significantly between passages.

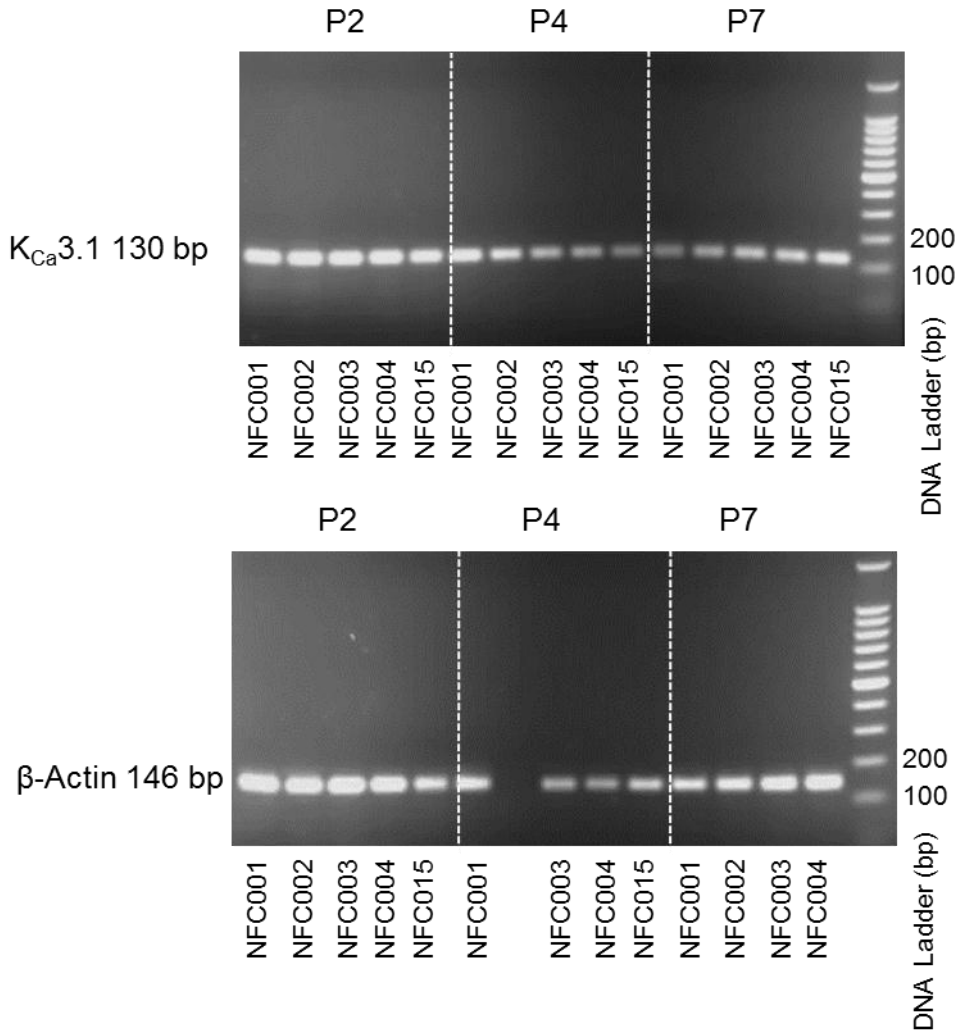

Figure 3-7. K_{Ca}3.1 RT-PCR products compared at different cell passages

Products from quantitative real-time PCR for K_{Ca}3.1 were visualized on a 1.5% agarose gel to confirm that only one product was amplified and that it was the correct size (130 bp). β-Actin was used as the normalizing control (146 bp).

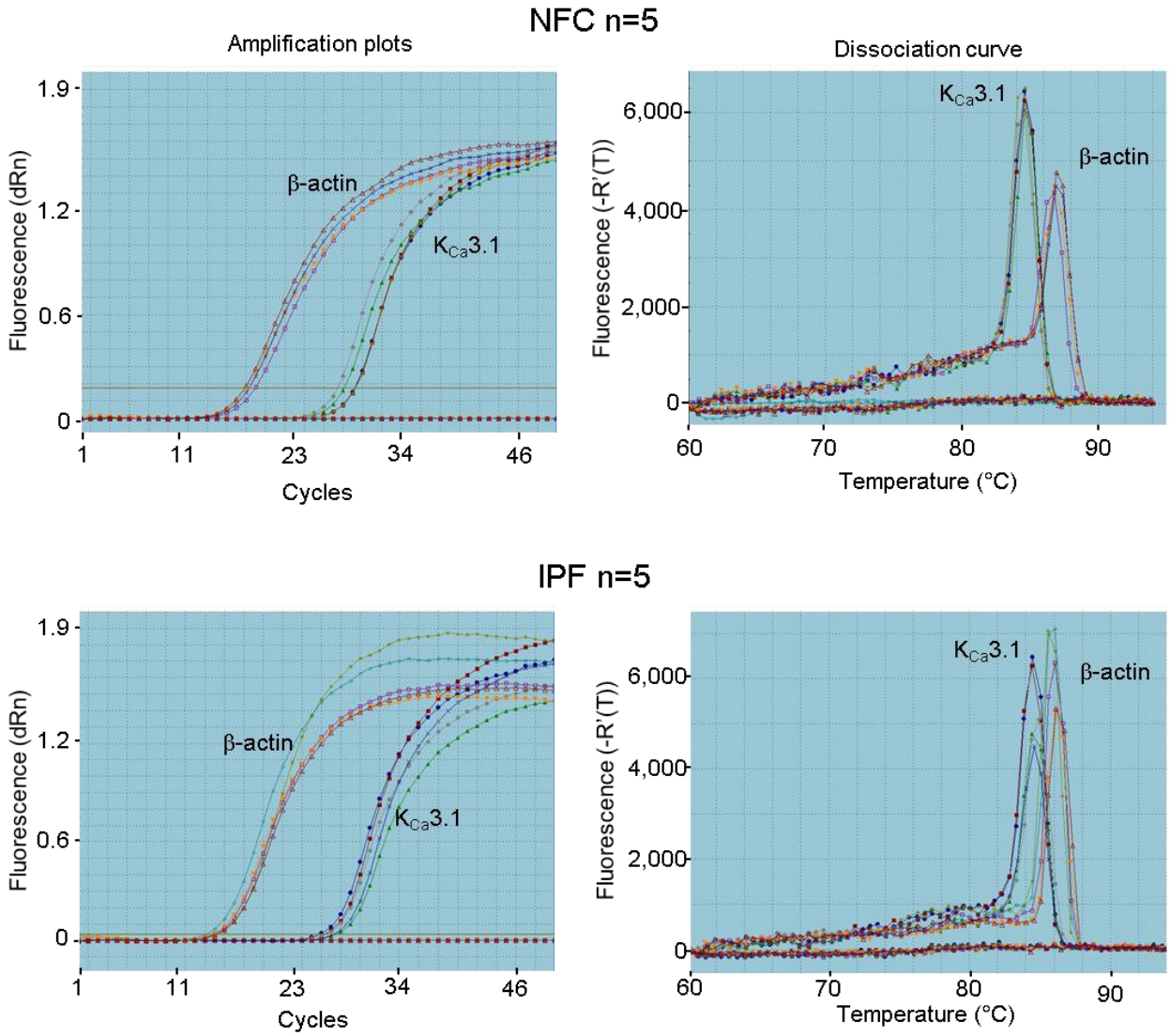

Figure 3-8. $K_{Ca}3.1$ mRNA expression by NFC and IPF donors

The top 2 graphs demonstrate the consistent expression of the $K_{Ca}3.1$ mRNA in NFC donors (n=5). The amplification plot shows the $K_{Ca}3.1$ product has a CT of approximately 24 and all donors used have similar expression. Confirmation that only one product was amplified is highlighted by the dissociation curve; a single peak is seen for both $K_{Ca}3.1$ and β-actin. The bottom 2 graphs show that IPF donors (n=5) also expressed $K_{Ca}3.1$ mRNA.

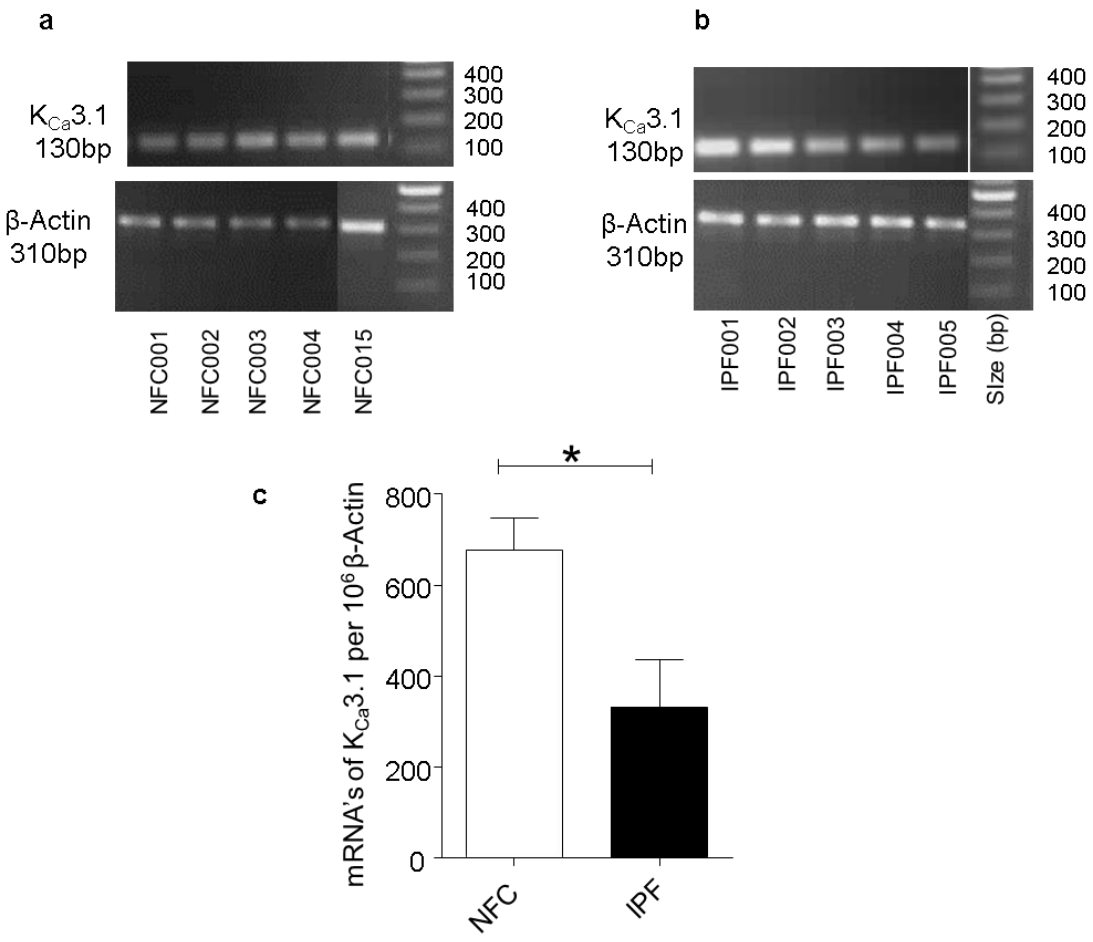

Figure 3-9. Comparison of K_{Ca}3.1 mRNA expression between NFC and IPF donors

a) and **b)** Products from quantitative real-time PCR for K_{Ca}3.1 were visualized on a 1.5% agarose gel to confirm that only one product was amplified and that it was the correct size (130 bp). β-Actin was used as the normalizing control (310bp). **c)** Quantitative real-time PCR showed that K_{Ca}3.1 mRNA expression was greater in NFC donors (n=5) than IPF donors (n=5), *P = 0.0262.

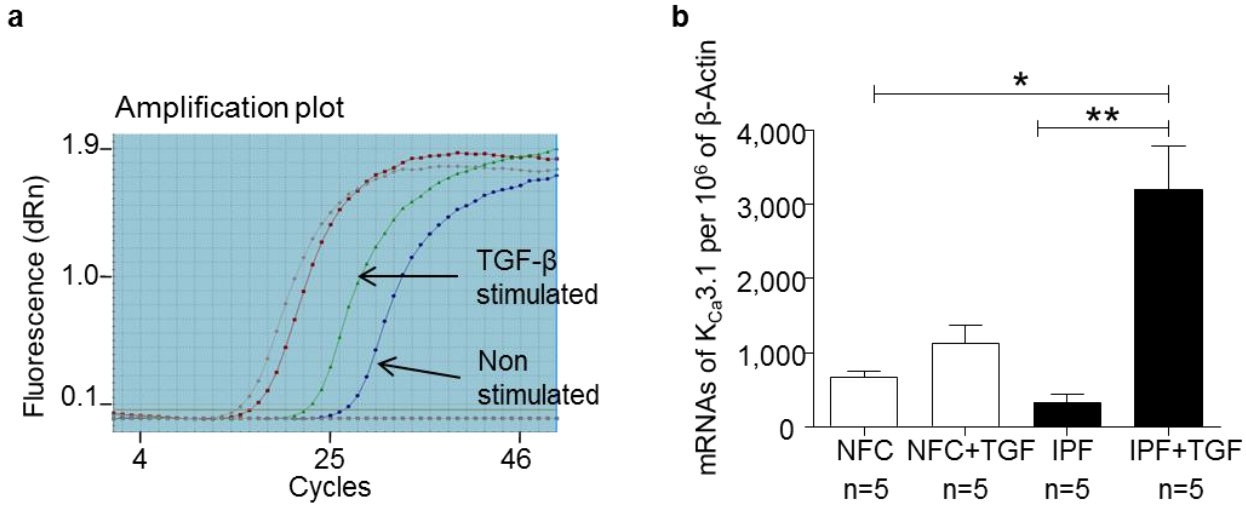

Figure 3-10. The effect of TGFβ1 on $K_{Ca}3.1$ mRNA expression

a) Quantitative real-time PCR from a representative IPF donor demonstrating increased expression of $K_{Ca}3.1$ mRNA in myofibroblasts following stimulation with TGFβ1 (10 ng/ml). *Blue*, non-stimulated $K_{Ca}3.1$; *green,* TGFβ1-stimulated $K_{Ca}3.1$; *red,* non-stimulated β-actin; *grey,* TGFβ1-stimulated β-actin. **b)** $K_{Ca}3.1$ mRNA expression increases after TGFβ1 stimulation, (*P<0.0001, 1-way ANOVA), NFC donors (n=5), IPF donors (n=5). There was a highly significant increase in IPF myofibroblasts following 24 hours of TGFβ1 stimulation (**P<0.05, Bonferroni's multiple comparison test).

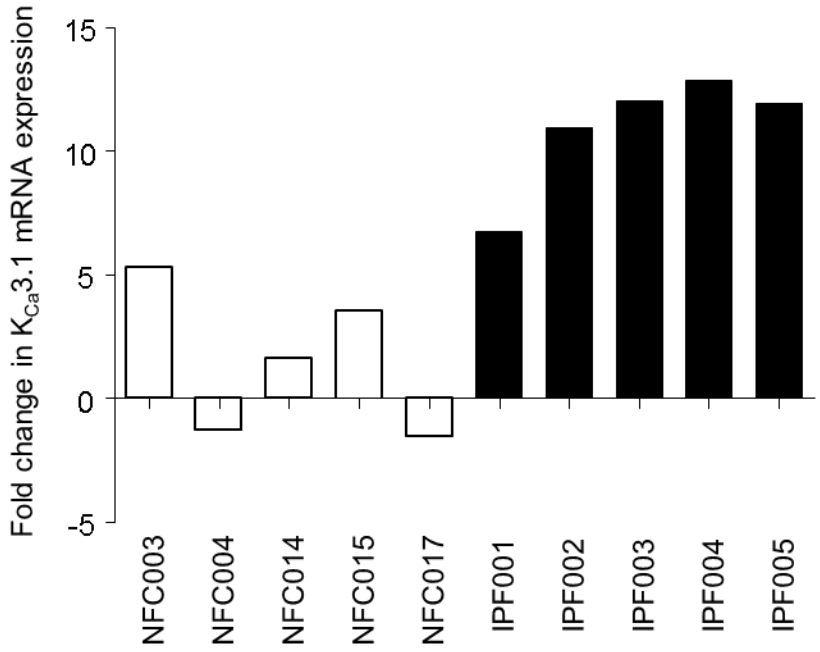

Figure 3-11. Fold change in K_{Ca}3.1 following TGFβ1 stimulation

Quantitative real-time PCR demonstrating the relative fold increase in NFC and IPF myofibroblasts after stimulation with TGFβ1. Following normalization with β-actin there is a relative fold increase in K_{Ca}3.1 expression in all IPF donors. Results were calculated using the δδCT method.

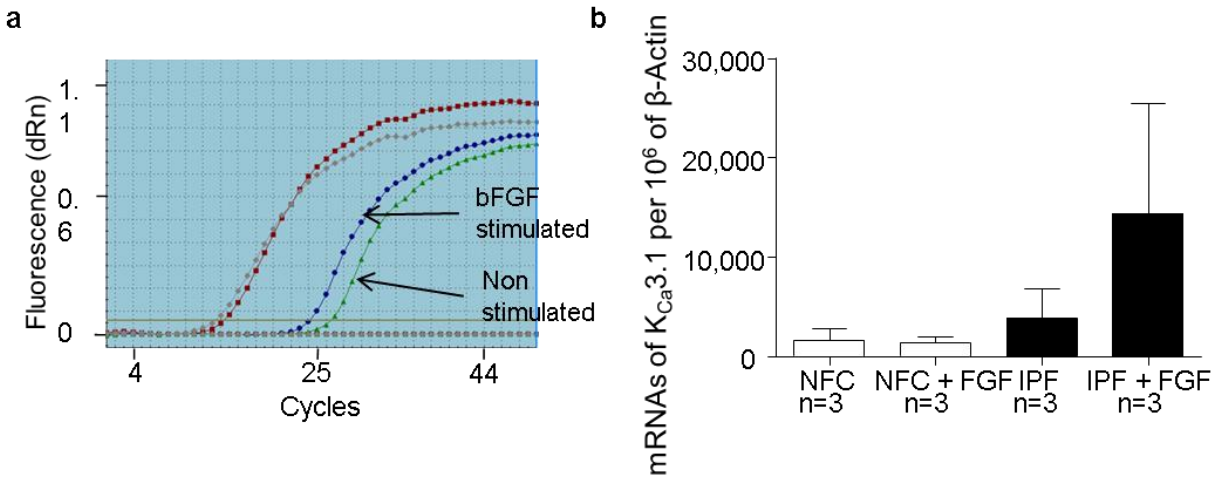

Figure 3-12. The effect of bFGF on $K_{Ca}3.1$ mRNA expression

Quantitative real-time PCR from a representative IPF donor demonstrating increased expression of $K_{Ca}3.1$ mRNA in myofibroblasts following stimulation with bFGF. *green*, non-stimulated $K_{Ca}3.1$; *blue,* bFGF-stimulated $K_{Ca}3.1$; red*,* non-stimulated β-actin; *grey,* bFGF-stimulated β-actin. **b)** $K_{Ca}3.1$ mRNA expression increases after bFGF stimulation in IPF donors (n=3), however, this was not significantly different.

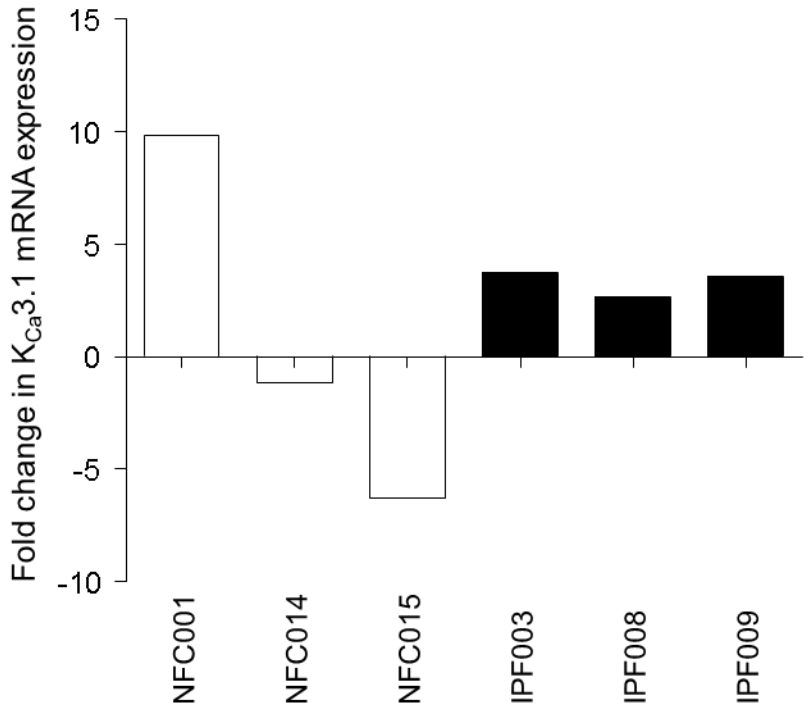

Figure 3-13. Fold change in K_{Ca}3.1 following bFGF stimulation

Quantitative real-time PCR demonstrating the relative fold increase in NFC and IPF myofibroblasts after stimulation with bFGF. Following normalization with β-actin there is a relative fold increase in K_{Ca}3.1 expression in all IPF donors after 24 hours of bFGF stimulation. Results were calculated using the δδCT method.

3.2.2 Myofibroblasts express $K_{Ca}3.1$ channel protein

$K_{Ca}3.1$ protein expression was identified by western blot analysis in myofibroblast lysates from NFC (n=6) and IPF (n=5) donors. The predicted weight of the $K_{Ca}3.1$ channel protein is 48 kDa, but larger forms of ~53 kDa and several shorter splice variants have been described(275,296-298). Using three different anti-$K_{Ca}3.1$ antibodies, M20, P4997 and AV35098, a consistent band of ~48 kDa was observed (**Figure 3-14**). M20, AV35098 and P4997 also stained bands of 53 kDa as described previously in human fibrocytes and airway smooth muscle cells(275,298), and 39 kDa, consistent with the presence of splice variants as described by others(297). The consistency in the weight of the additional bands evident with different antibodies suggests they are due to the detection of $K_{Ca}3.1$. Using the M20, P4997 and AV35098 antibodies, $K_{Ca}3.1$ protein expression was visualised in myofibroblasts using immunofluorescence (**Figure 3-15**).

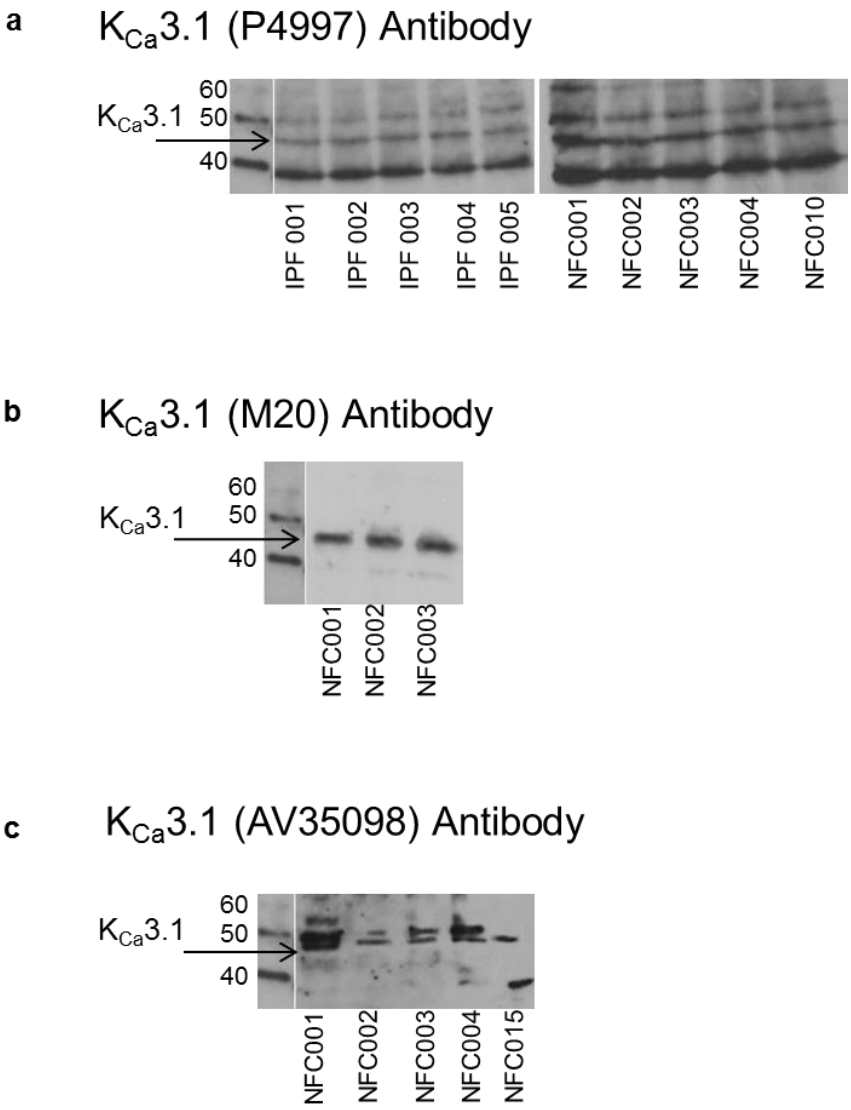

Figure 3-14. $K_{ca}3.1$ channel protein is present within myofibroblasts

Western blots from human lung myofibroblast lysates obtained using 3 different $K_{Ca}3.1$ channel antibodies, **a)** P4997 **b)** M20 and **c)** AV35098. All images show a consistent band at the predicted size for the $K_{Ca}3.1$ channel at 48 KDa in human lung myofibroblasts. An additional band at 53 kDa is present as described in other cell types.

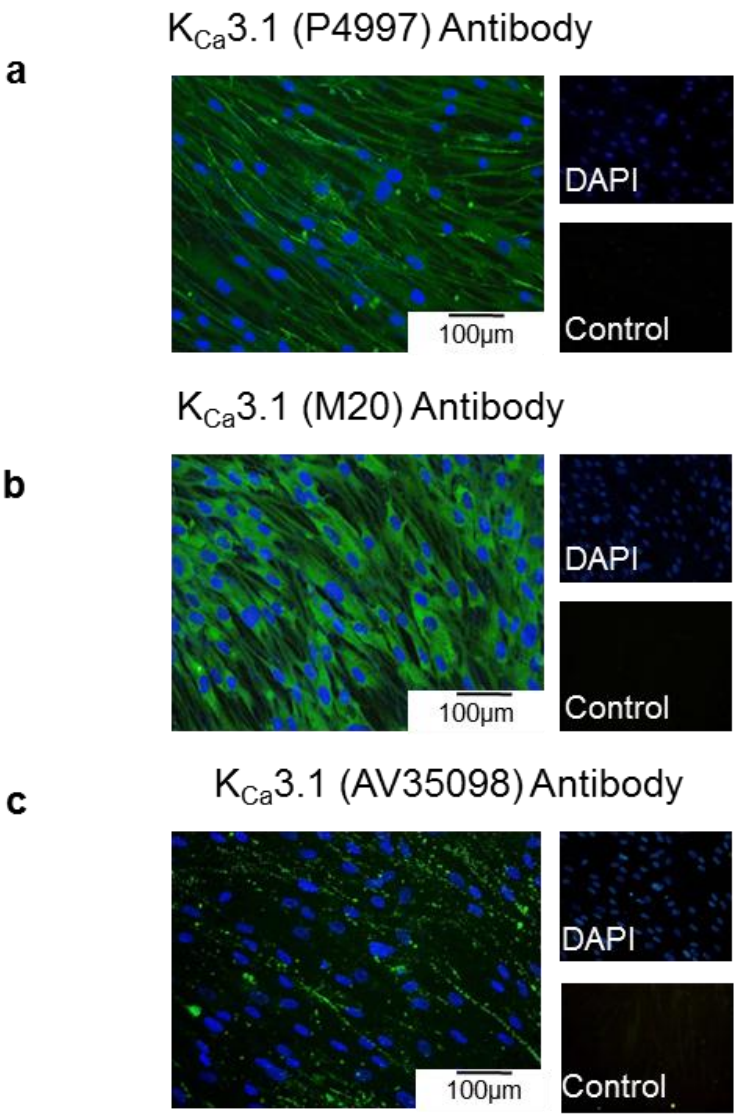

Figure 3-15. K_{ca}3.1 channel immunofluorescent staining within myofibroblasts

Illustrated is the immunofluorescent staining for K_{Ca}3.1 in human lung myofibroblasts using **a)** P4997 **b)** M20and **c)** AV35098 antibodies. DAPI nuclear staining and negative rabbit isotype control IgG are also shown.

3.3 Evidence of functional channel

3.3.1 Myofibroblasts express $K_{Ca}3.1$ channel currents which are increased in IPF

To evoke $K_{Ca}3.1$ currents in myofibroblasts the compound 1-EBIO was used, which opens $K_{Ca}3.1$ with a half maximal value of approximately 30 µmol/L, with a maximal effect at approximately 300 µmol/L(252). 1-EBIO opens $K_{Ca}3.1$ by enhancing its sensitivity to $[Ca^{2+}]_i$, and therefore, at 100 µM 1-EBIO, maximal K^+ currents are achieved in the presence of 100 nM free Ca^{2+}(252,275), which is below the resting concentration in most cells. The characteristic electrophysiological features of $K_{Ca}3.1$ channels are that the current appears immediately as voltage steps are applied and the current is sustained throughout the 100 millisecond pulse. The current does not decay, inward rectification occurs from around +40 mV, and a negative shift in reversal is seen. The voltage protocol and the raw current are demonstrated in **Figure 3-16**.

Initially whole cell currents in cells from 5 NFC donors were compared between passage 2, 4 and 7. At baseline all passages demonstrated a strong outwardly rectifying whole cell current with occasional inwardly rectifying currents with features of the Kir2.0 family (**Figure 3-17**)**.** To confirm the inwardly rectifying current was

a Kir2.0 family current 10 μM of Ba^{2+} was used (**Figure 3-18**). $K_{Ca}3.1$ currents not obviously present at baseline.

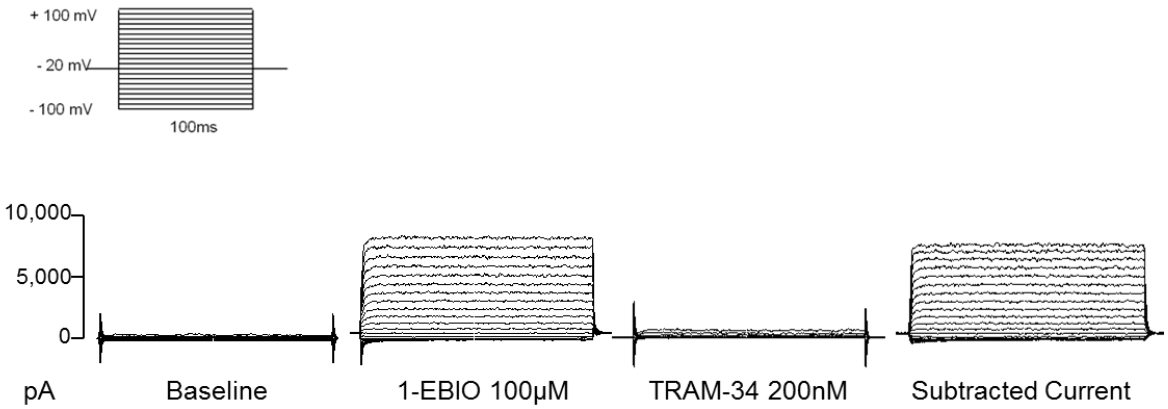

Figure 3-16. Typical features of the $K_{ca}3.1$ channel

The voltage protocol and the raw current are demonstrated showing typical electrophysiological features of $K_{Ca}3.1$ (as described in the text) in a myofibroblast. The subtracted current is the TRAM-34 sensitive $K_{Ca}3.1$ current (1-EBIO minus TRAM-34).

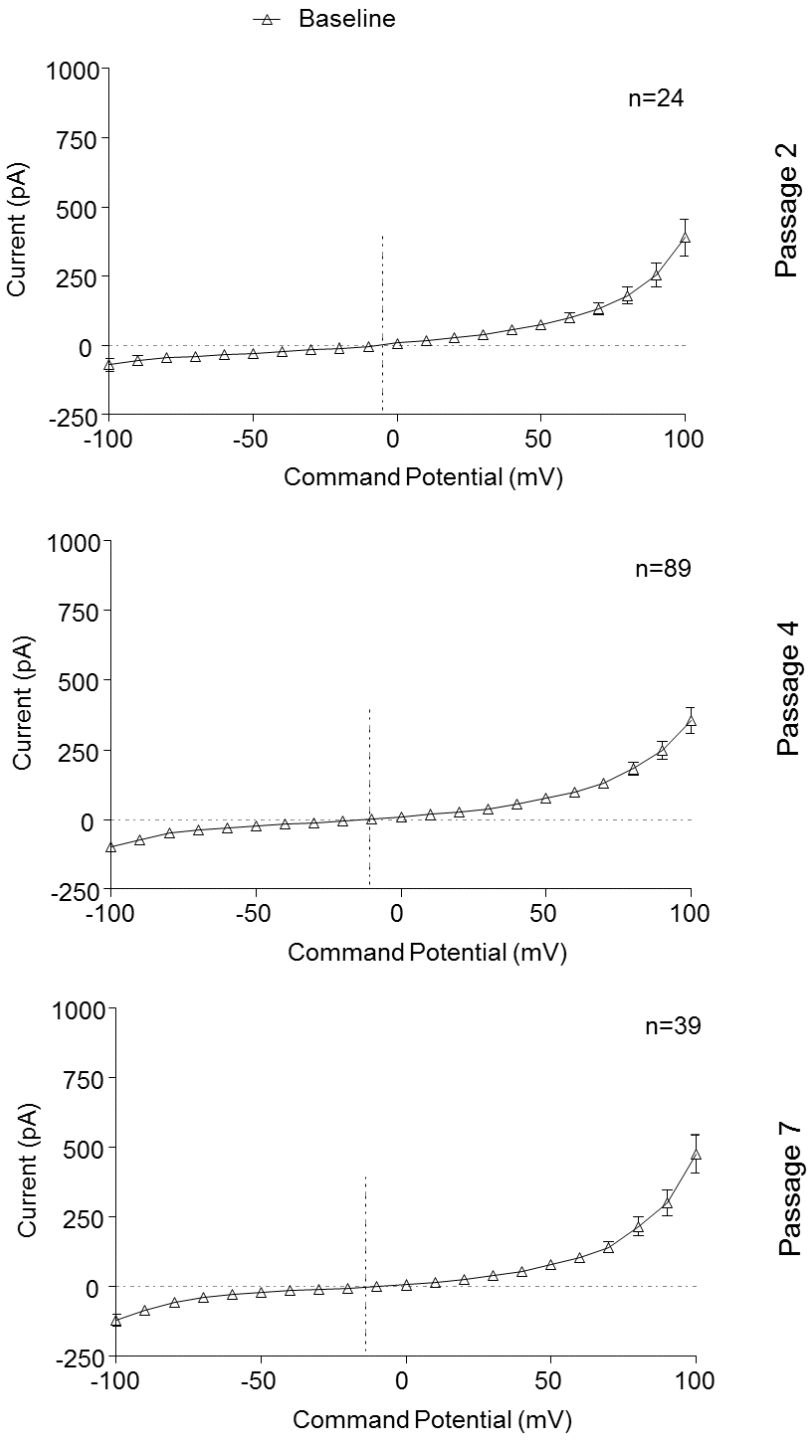

Figure 3-17. Myofibroblast Baseline Currents

Mean ± SEM current voltage curves demonstrate an outwardly rectifying current at baseline for passage 2 (n=23), passage 4 (n=89) and passage 7 (n=39). All passages displayed relatively small Kir2.0 family-like current.

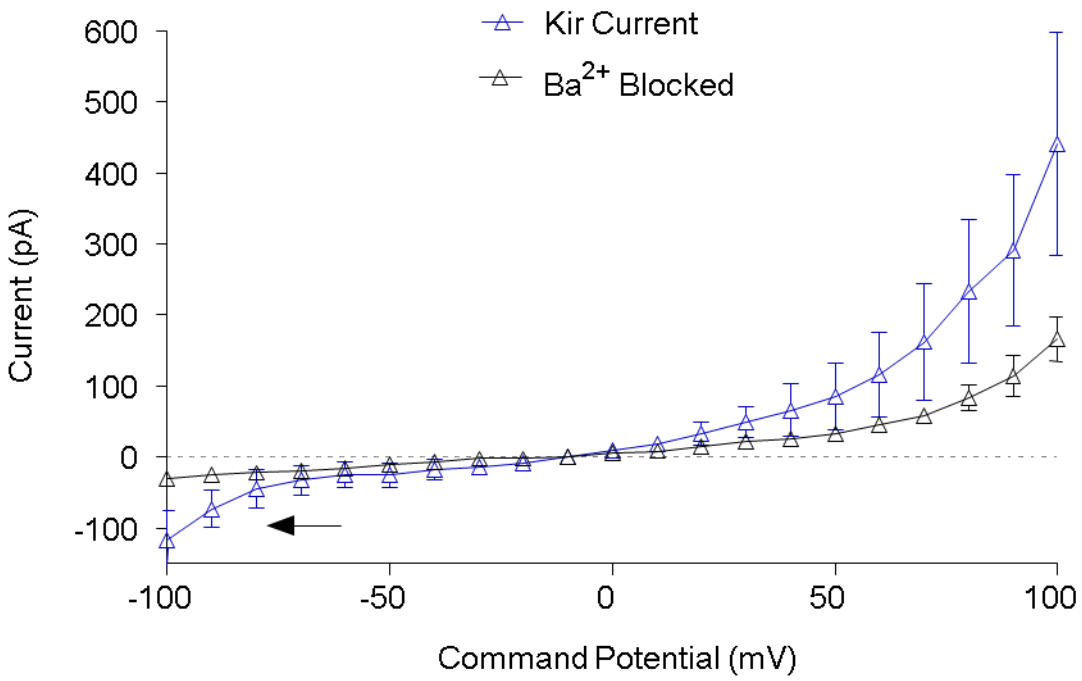

Figure 3-18. Blocking the Kir current

To identifying and confirm that the inwardly rectifying current at baseline was a Kir2.0 current, Ba^{2+} was used at 10 μM. Ba^{2+} blocked the current in n=3 cells. The Kir 2.0 current is identified with the black arrow.

When comparing the baseline currents of over 20 cells for each passage 2, 4 and 7, no difference was found in reversal potential or the size of current at +40 mV (**Figure 3-19**). Measurements of myofibroblast capacitance were unreliable due to the relatively large cell size, so it was not possible to calculate current density.

Upon the addition of 1-EBIO (100 μM) currents were frequently elicited which demonstrated the typical features of the $K_{Ca}3.1$ channel (**Figure 3-20**). When comparing the currents induced by 1-EBIO between passages, no difference in reversal potential was found, and no significant difference was found in the proportion of cells that responded to 1-EBIO with the development a $K_{Ca}3.1$ current (**Figure 3-21**). However, cells at passage 4 and 7 developed significantly larger 1-EBIO-dependent currents at +40 mV than passage 2 cells, *P=0.0150 (**Figure 3-22**).

In addition, the 1-EBIO induced current was entirely blocked in all passages by the selective $K_{Ca}3.1$ blocker TRAM-34 at a concentration of 200 nM (**Figure 3-23**). A dose dependent blockade of the $K_{Ca}3.1$ channel was recorded using TRAM-34 at 20 nM and 200 nM, with complete block occurring at 200 nM, ***P<0.0001 (**Figure 3-24**). Using another specific $K_{Ca}3.1$ blocker, ICA-17043 at 10 nM and 100 nM, also dose-dependently blocked the 1-EBIO induced $K_{Ca}3.1$ current, *P=0.0227 (**Figure 3-25**).

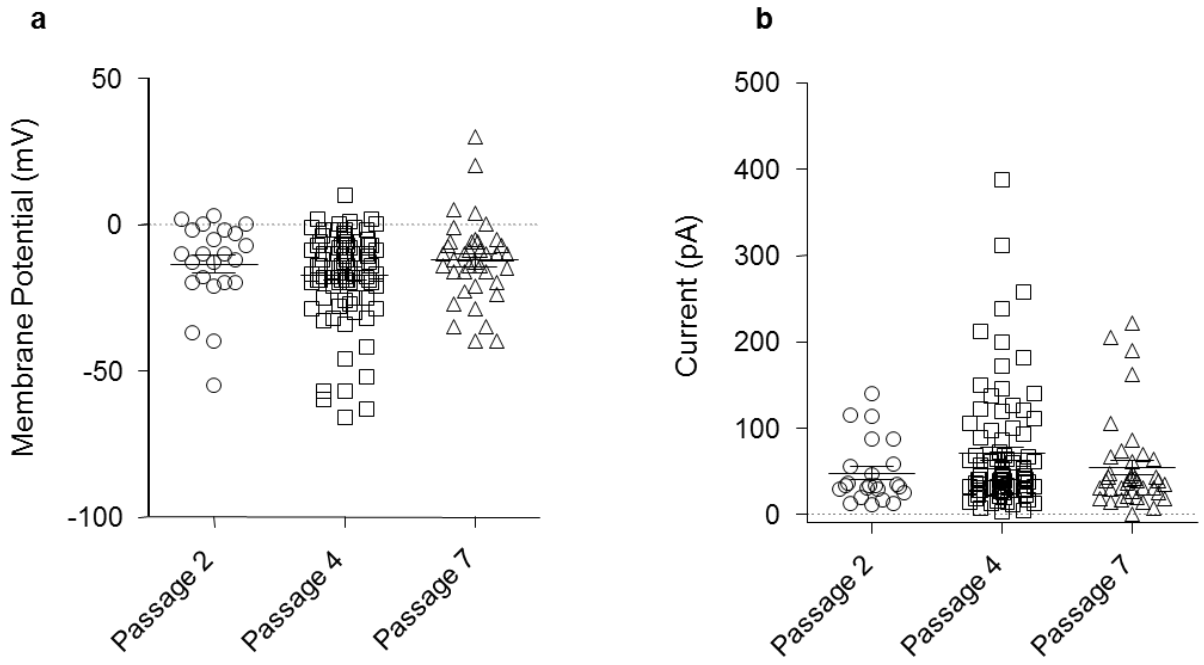

Figure 3-19. Baseline current differences between passage

No significant difference was found between passages 2 (n=23), passage 4 (n=89) and passage 7 (n=39) in the baseline reversal potential (**a**) or the size of the baseline current at +40 mV (**b**).

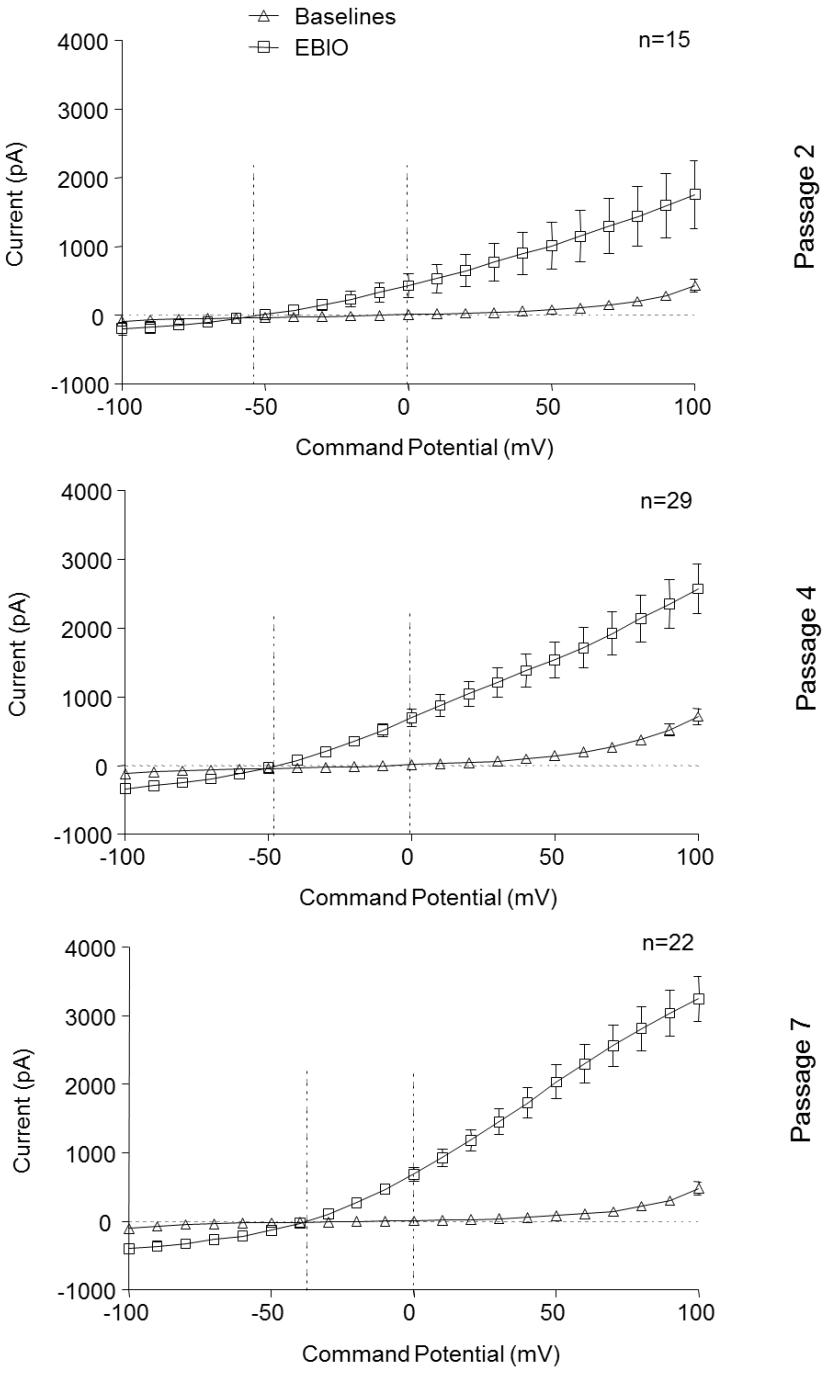

Figure 3-20. $K_{Ca}3.1$-like current was induced by 1-EBIO

The mean ± SEM current voltage curves following the addition of 1-EBIO (100 μM). Large whole cell currents with a negative reversal potential developed in all passages once the $K_{Ca}3.1$ opener 1-EBIO (100 μM) was added.

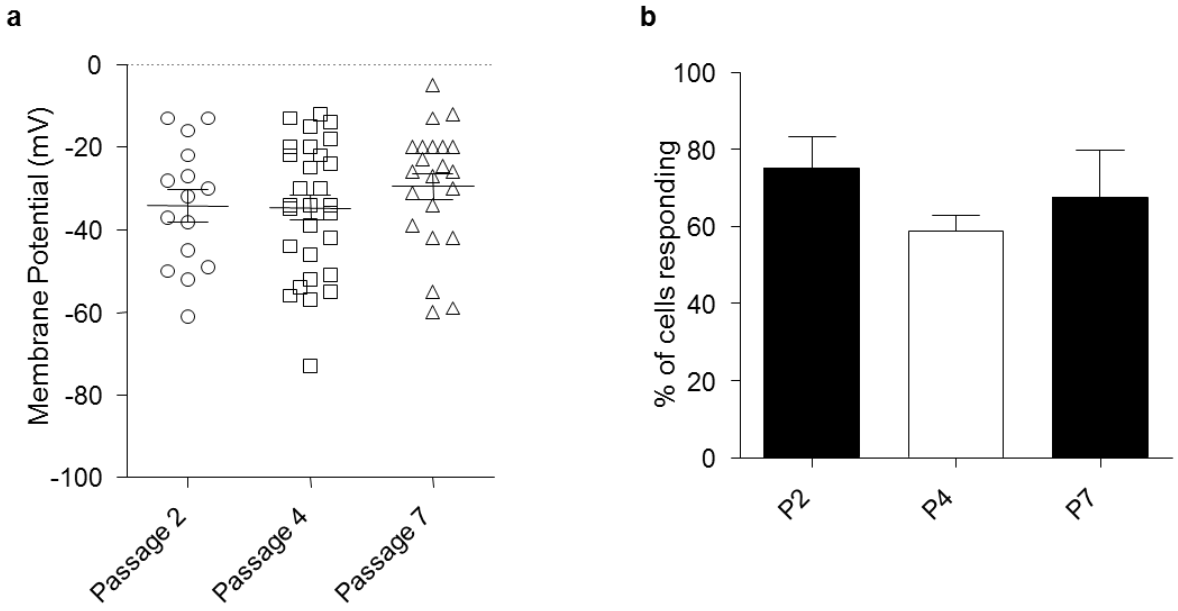

Figure 3-21. Comparison of the 1-EBIO-induced current between passages.

a) No significant difference was found in the 1-EBIO induced reversal potential between passage. **b**) There was no significant difference in the proportion of l cells responding to 1-EBIO between passages.

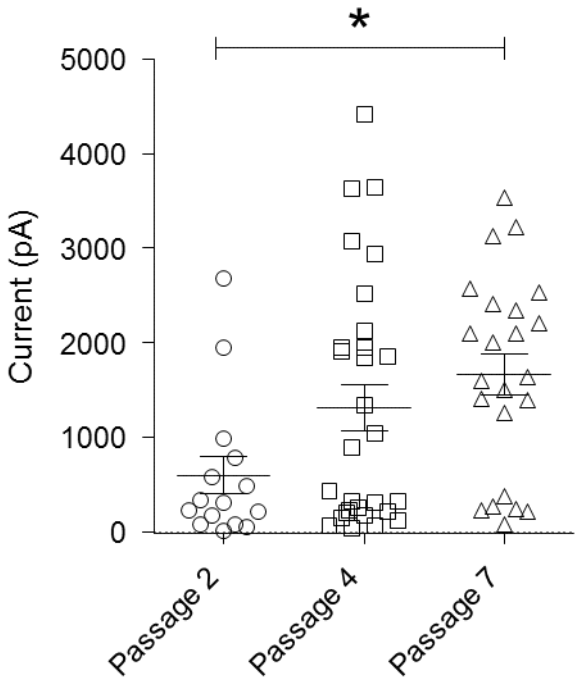

Figure 3-22. The size of the 1-EBIO-dependent current varies between passage

This graph illustrates the subtracted (1-EBIO minus baseline) 1-EBIO-dependent $K_{Ca}3.1$ current at +40 mV. There was a significant difference in current size between passage 2 (n=15), passage 4 (n=29) and passage 7 (n=23), *P=0.0150 (Kruskal Wallis test). Dunn's multiple comparison post test revealed a further significant difference between passages 2 and 7, *P<0.05.

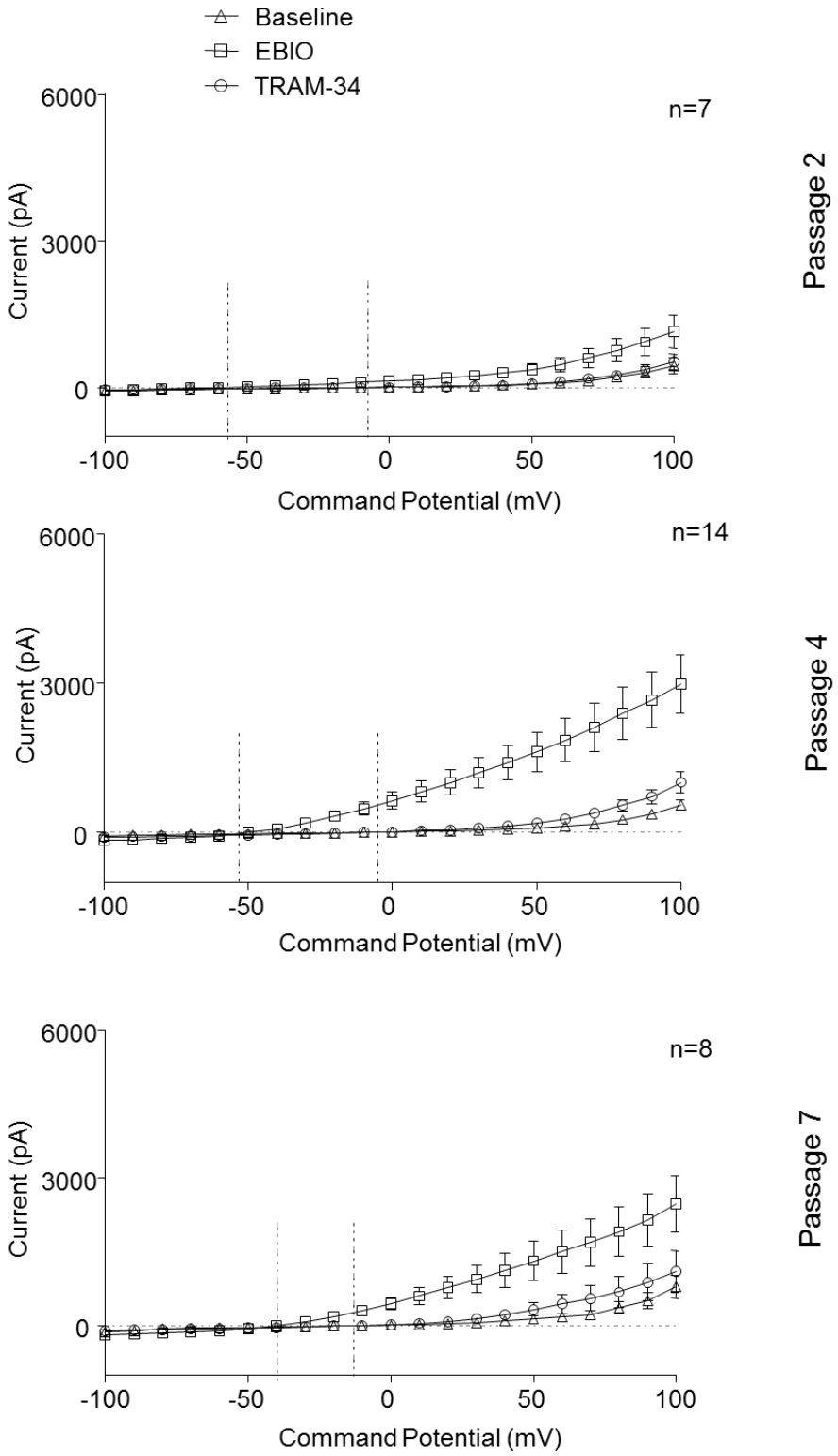

Figure 3-23. TRAM-34 blocks the 1-EBIO-induced current

To confirm the 1-EBIO induced current was $K_{Ca}3.1$, the $K_{Ca}3.1$ selective blocker TRAM-34 (200 nM) was used. The mean ± SEM current voltage curves show that TRAM-34 blocks the 1-EBIO induced currents in all passages.

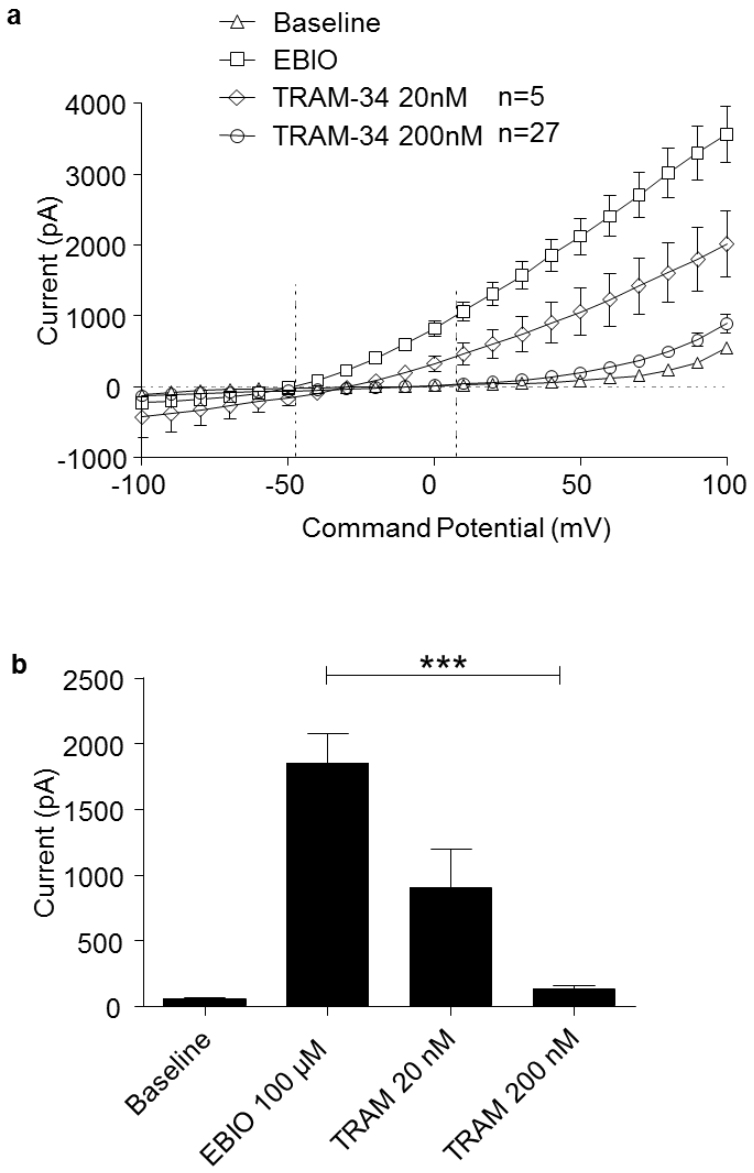

Figure 3-24. TRAM-34 dose-dependently blocks $K_{Ca}3.1$ channel currents

a) TRAM-34 at 20 nM initiates partial block of the 1-EBIO induced current and total block is achieved with TRAM-34 at 200nM. **b**) The 1-EBIO current at +40 mV was dose-dependently blocked, ***P<0.0001 (One-way analysis of variance). There was a highly significant difference between the 1-EBIO induced current and TRAM-34 at 200 nM, ***P<0.0001 (Bonferroni's multiple comparison test).

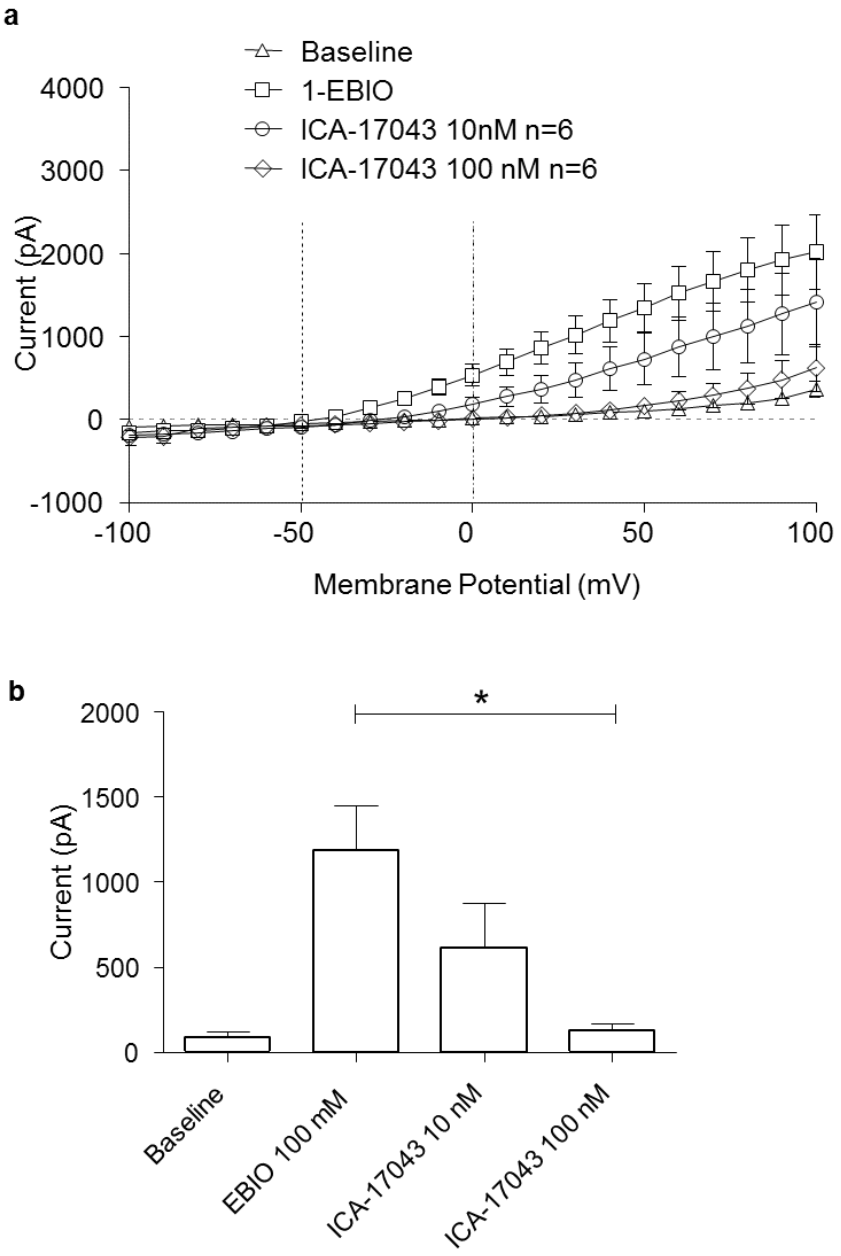

Figure 3-25. ICA-17043 dose-dependently blocks $K_{ca}3.1$ channel currents

a) ICA-17043 at 10 nM induces partial block of the 1-EBIO induced current and total block was achieved with ICA-17043 at 100nM. **b**) The 1-EBIO current at +40 mV was dose-dependently blocked, *P=0.0227 (One-way analysis of variance). Post test revealed a significant difference between the 1-EBIO induced current and ICA-17043 at 100 nM, *P<0.05 (Bonferroni's multiple comparison test).

This confirms that the 1-EBIO induced current was carried by the $K_{Ca}3.1$ channel. TRAM-34 is diluted in 0.1% DMSO, to ensure the DMSO was not causing the block 0.1% DMSO was added to n=5 cells which did not affect the 1-EBIO induced current, indicating the channel block was solely TRAM-34 dependent. The mean TRAM-34 sensitive current (1-EBIO minus TRAM-34) for each passage illustrates the characteristic current-voltage curves and raw current for the $K_{Ca}3.1$ channel (**Figure 3-16**, **Figure 3-26**).

Following these findings, further whole cell electrophysiology was conducted at passages 4 and 5.

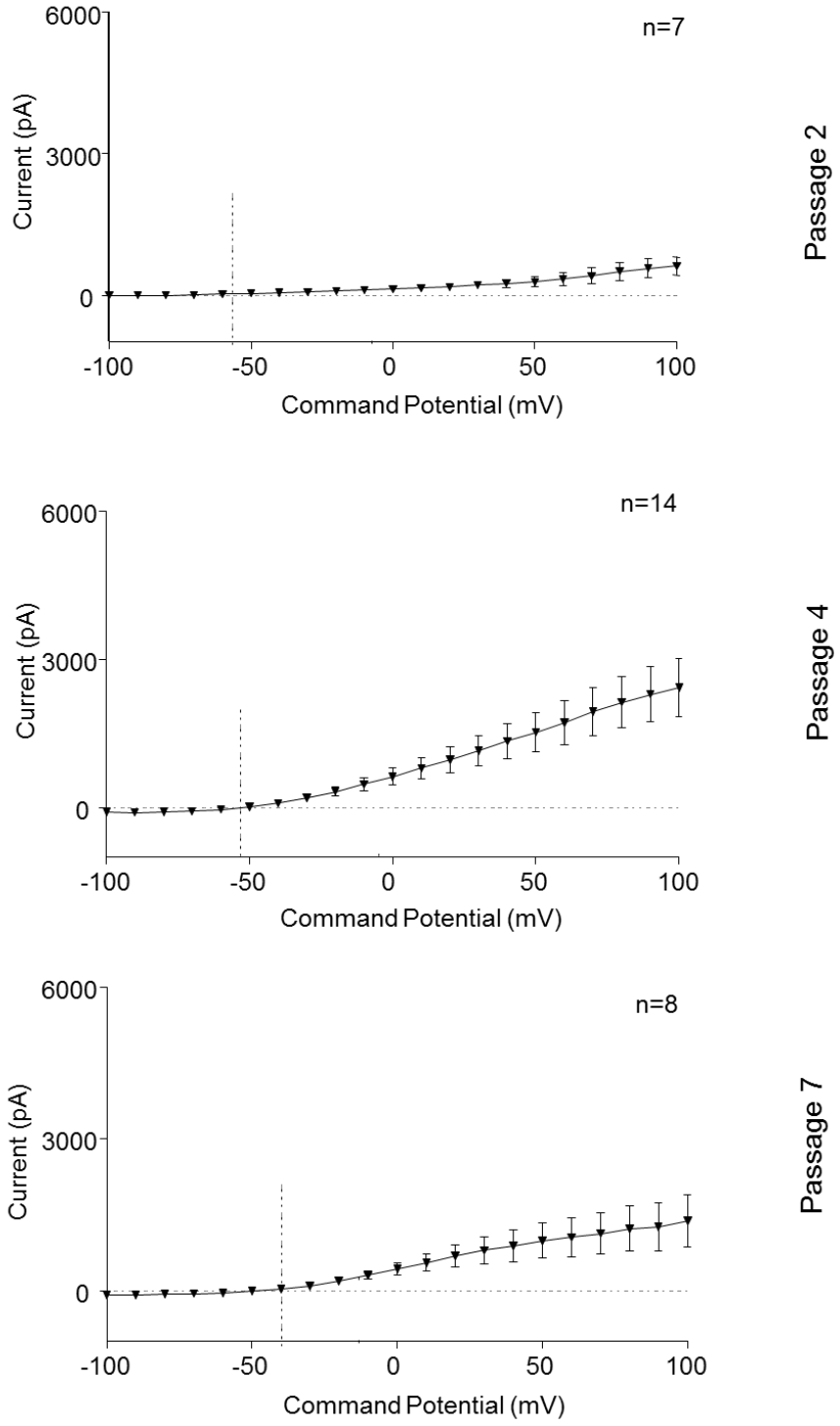

Figure 3-26. Subtracted TRAM-34 sensitive $K_{Ca}3.1$ current

The subtracted (1-EBIO minus TRAM-34) TRAM-34-sensitive $K_{Ca}3.1$ current for each passage. Passage 4 shows a notably larger TRAM-34-sensitive $K_{Ca}3.1$ current compared to the other passages however, this was not statistically significant.

3.4 Comparison of expression and function of $K_{Ca}3.1$ channel between IPF and NFC and effect of pro-fibrotic cytokines

3.4.1 Comparison of whole cell currents in NFC and IPF-derived myofibroblasts

At passages 4-5 the baseline myofibroblast whole cell recordings from NFC and IPF donors demonstrated strong outwardly rectifying currents, and occasional inwardly rectifying currents with features of the Kir2.0 family. Interestingly, 69% of IPF cells had Kir2.0-like channels open at baseline as opposed to only 42% of NFC cells. No obvious evidence of $K_{Ca}3.1$ currents was present at baseline and no difference in baseline current was found between NFC and IPF donors (**Figure 3-27**). 1-EBIO frequently elicited $K_{Ca}3.1$ currents (**Figure 3-28**) which were blocked by selective $K_{Ca}3.1$ blocker TRAM-34 (**Figure 3-29**) in both NFC and IPF donors.

Overall, the addition of 1-EBIO elicited a robust $K_{Ca}3.1$ channel current in 59% of myofibroblasts from NFC donors and 77% of cells from IPF donors (*P=0.0411, Chi squared). Also, when analysing the proportion of cells responding per donor, significantly more IPF cells responded compared to NFC (*P=0.0285, t-test) (**Figure 3-30**). When analysing responding cells, in NFC cells, baseline currents of

(mean ± SEM) 91.30 ± 14.91 pA at +40 mV increased to 1532 ± 228.4 pA following addition of 1-EBIO (n=34 cells, ***P<0.0001). In IPF cells, baseline currents of (mean ± SEM) 70.30 ± 8.18 pA at +40 mV increased to 2230 ± 187.5 pA following addition of 1-EBIO (n=40 cells, ***P<0.0001) (**Figure 3-31**). The size of the currents induced by 1-EBIO in IPF cells was significantly greater than in NFC cells (**P=0.0078) (**Figure 3-31**). Thus functional $K_{Ca}3.1$ channels were expressed more frequently and tended to be larger in myofibroblasts derived from IPF lung tissue compared to NFC tissue.

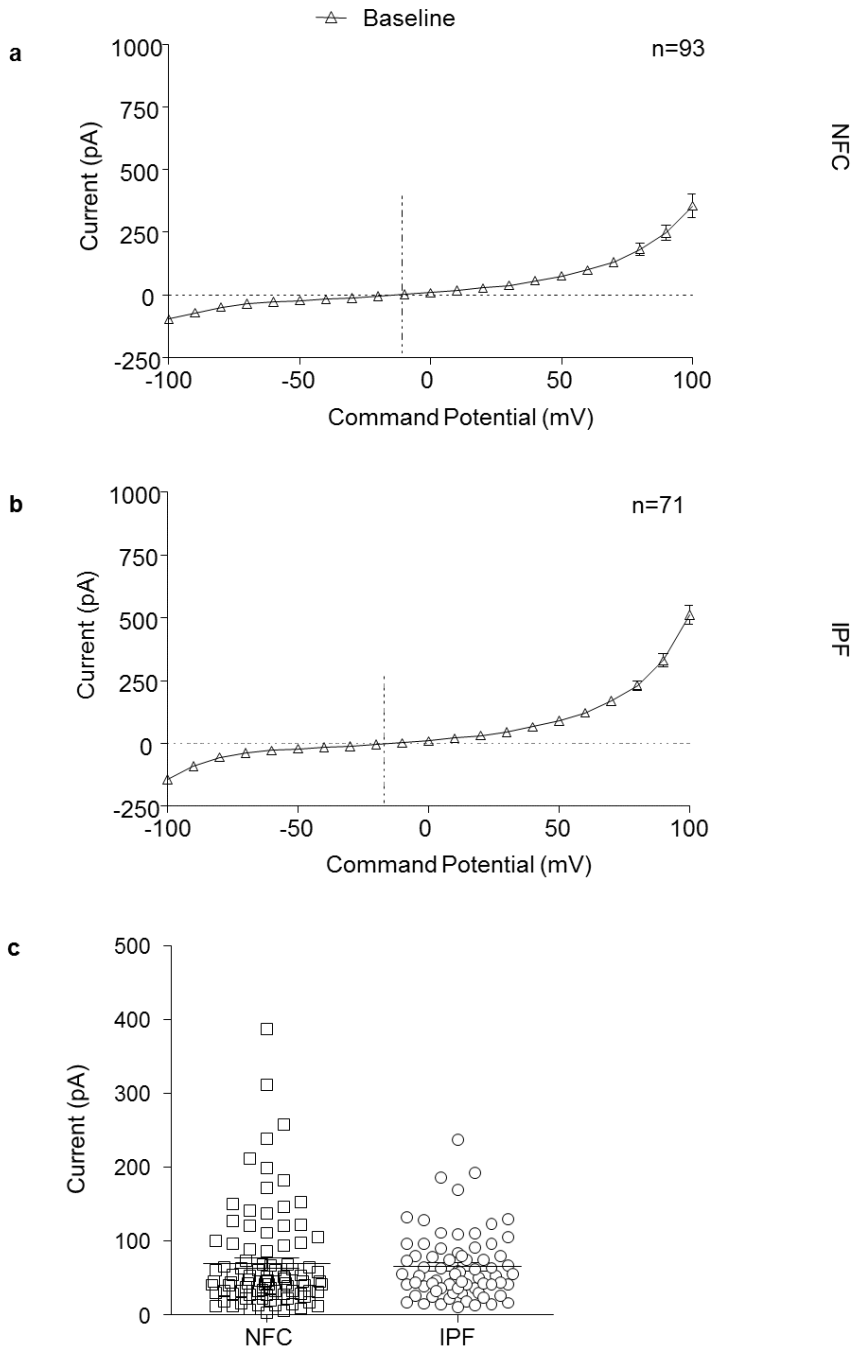

Figure 3-27. Comparison of baseline recordings in NFC and IPF myofibroblasts

a) Shows the mean baseline current of 93 NFC myofibroblast cells. **b**) Demonstrates the mean baseline current of 71 IPF myofibroblast cells. **c**) at +40 mV there was no significant difference in baseline current between NFC and IPF donors.

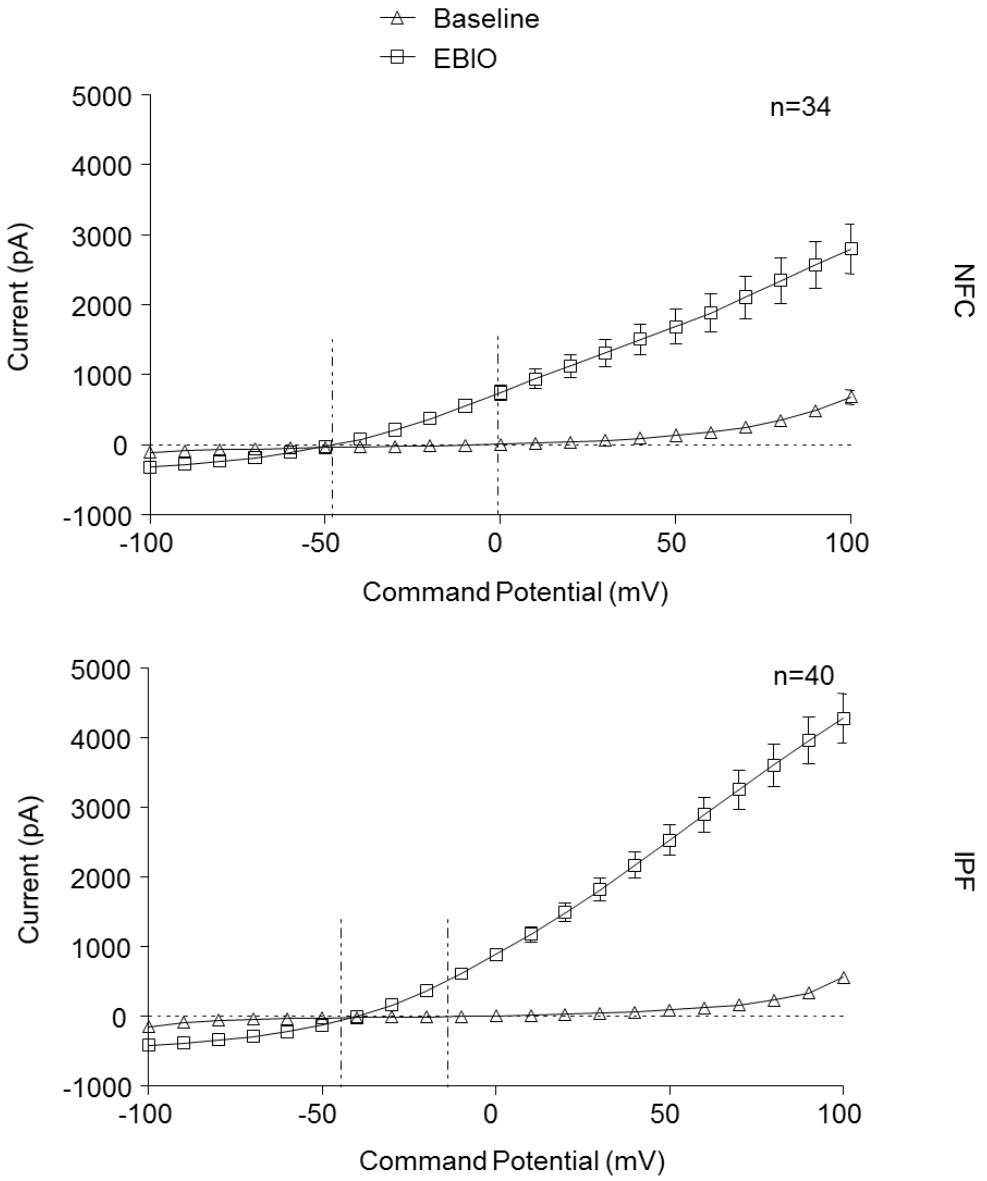

Figure 3-28. $K_{ca}3.1$ currents elicited in NFC and IPF myofibroblasts

Upon the addition of 1-EBIO (100 μM), there was a negative shift in reversal potential and a large current was elicited. Not all cells responded to 1-EBIO, the above graph shows responding cells only. The top graph displays the mean ± SEM current voltage curves for 34 NFC cells, where both the baseline and 1-EBIO current were recorded. The bottom graph demonstrates mean ± SEM current voltage curves for 40 IPF myofibroblasts. The mean IPF 1-EBIO-dependent current was notably larger than the NFC current.

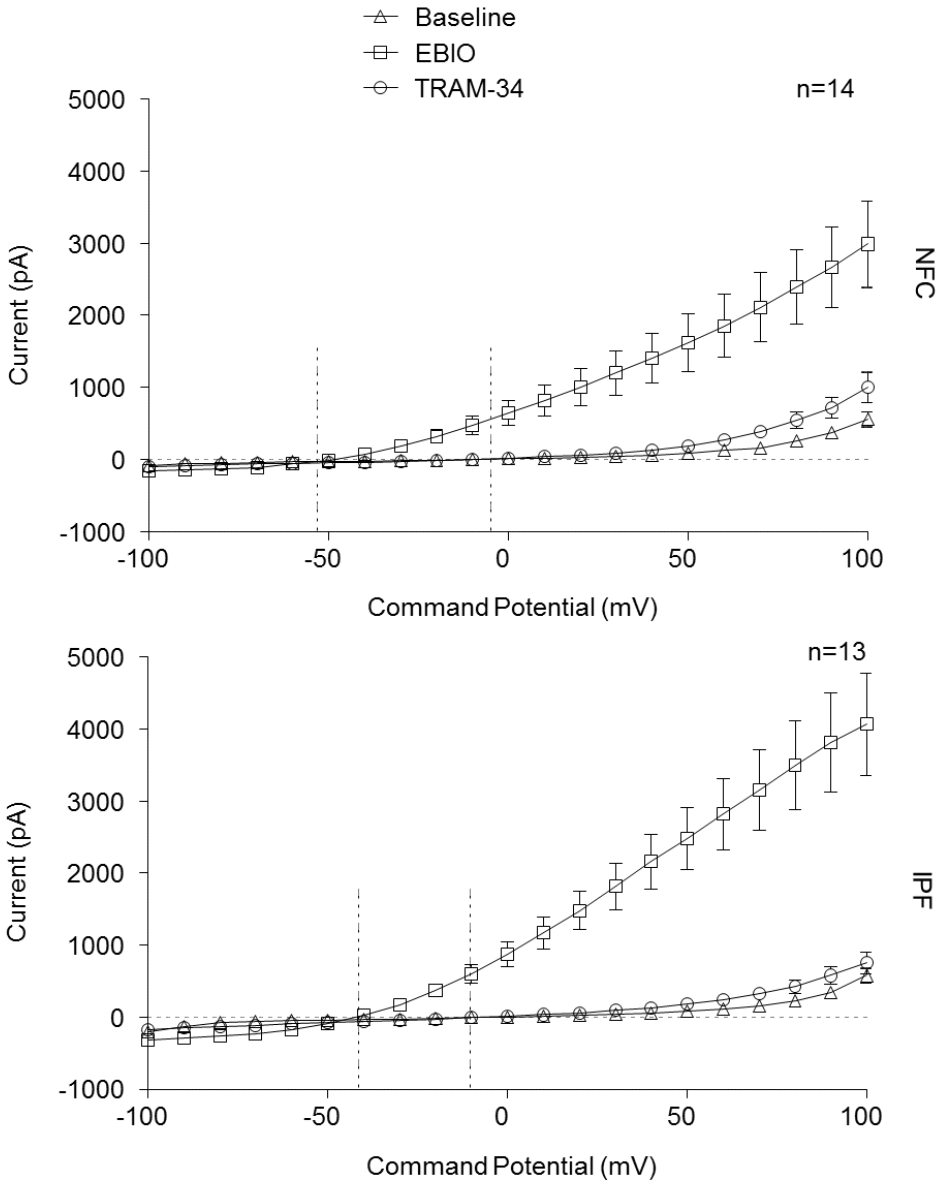

Figure 3-29. $K_{Ca}3.1$ currents blocked by TRAM-34 in both NFC and IPF myofibroblasts

1-EBIO (100 μM)-induced currents were blocked by TRAM-34 (200 nM) in both NFC and IPF donors. Both graphs show the mean ± SEM current voltage curves of individual cells where a baseline current, 1-EBIO current and TRAM-34 current were all recorded, 14 NFC cells and 13 IPF cells.

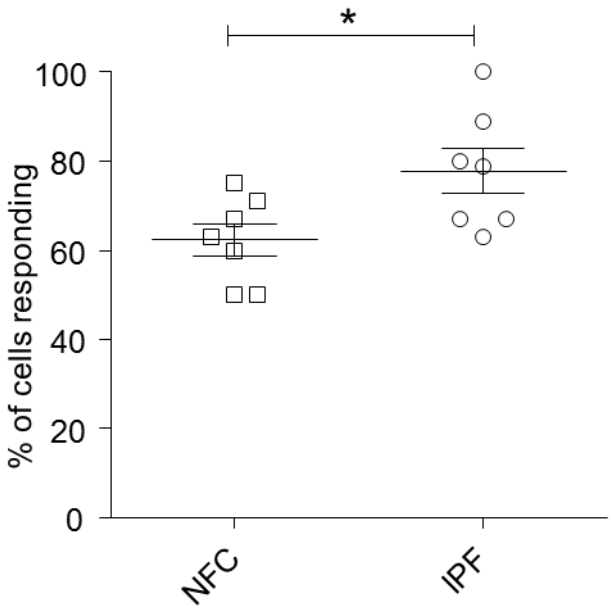

Figure 3-30. The proportion of Cells responding to 1-EBIO

This graph shows the mean percentage of cells responding for each donor, NFC (n=7), and IPF (n=7). The proportion of IPF cells responding to 1-EBIO was significantly higher than NFC donors *P=0.0285.

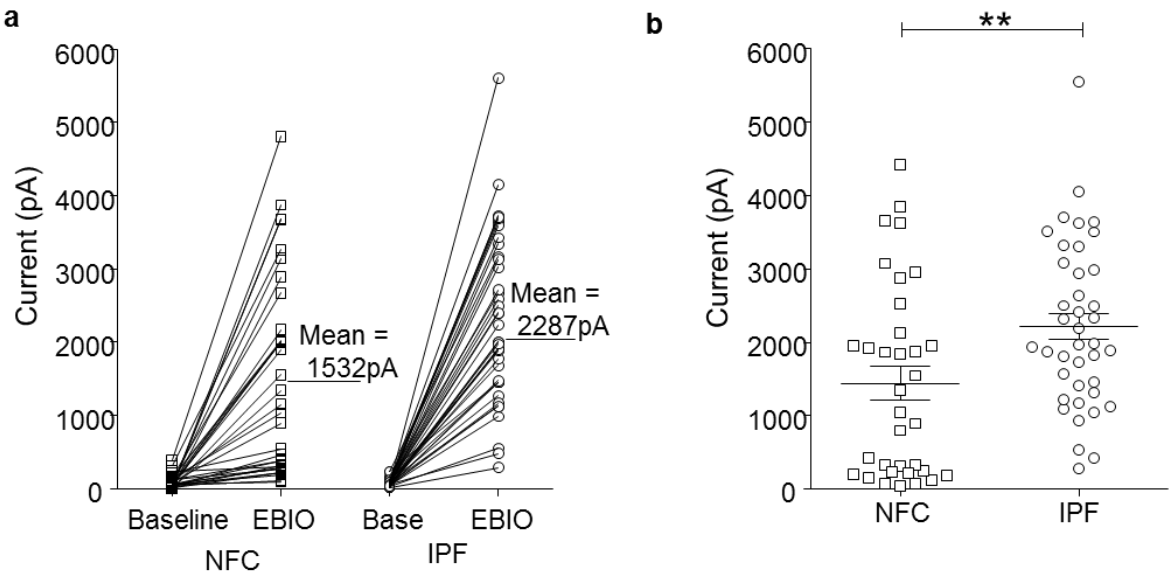

Figure 3-31. The size of the 1-EBIO induced current differs between NFC and IPF.

a) Demonstrates how the size of the current at +40 mV increases following the addition of 1-EBIO in each responding cell, (NFC n=34, IPF n=40). Following the addition of 1-EBIO a significantly larger outward current is produced (NFC ***P<0.0001, IPF ***P<0.0001). **b**) The subtracted (1-EBIO minus baseline) 1-EBIO-dependent $K_{Ca}3.1$ current at +40 mV, for each cell (NFC n=34, IPF n=40) was significantly larger in IPF cells than in NFC cells (**P=0.0078).

3.4.2 More myofibroblasts express $K_{Ca}3.1$ currents following mitogenic stimulation

After 24 hours of mitogenic stimulation with either TGFβ1 or bFGF, both NFC and IPF donors demonstrated increased functional channel expression (*P=0.0013) (**Figure 3-32**). Bonferroni's multiple comparison test revealed a significant increase in the proportion of NFC myofibroblasts that responded to 1-EBIO following bFGF stimulation **P<0.01, and confirmed that the proportion of IPF cells which responded to 1-EBIO following TGFβ1 stimulation also increased *P<0.05 (**Figure 3-32**).

Analysis of the mean current induced by 1-EBIO following TGFβ1 and bFGF stimulation highlighted that the mean currents at +40 mV were actually similar or smaller following mitogenic stimulation compared to pre-stimulation (**Figure 3-33**). However, these results taken alongside the increase in the proportion of cells responding may indicate that both TGFβ1 and bFGF increase $K_{Ca}3.1$ expression in previously non-expressing cells resulting in smaller overall current size. For example before TGFβ1 stimulation, only 77% of IPF cells responded to 1-EBIO but following 24 hour stimulation 100% cells responded to 1-EBIO.

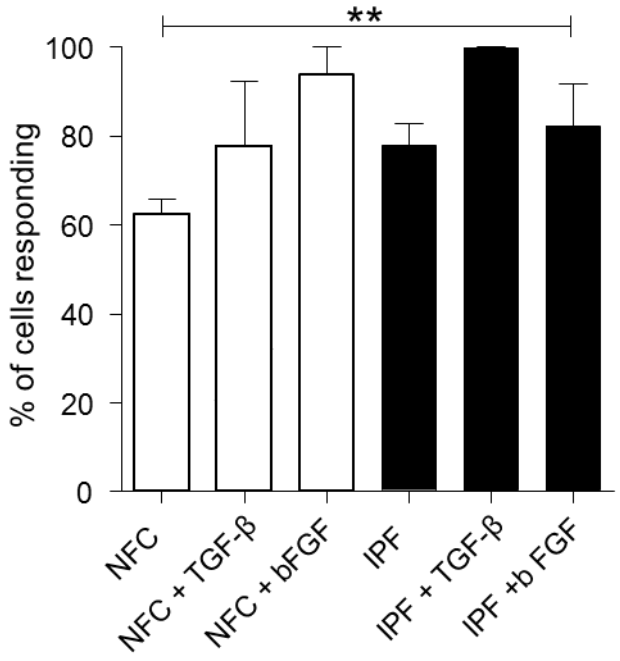

Figure 3-32. The proportion of cells responding to 1-EBIO following mitogenic stimulation

The graph illustrates the mean percentage of cells responding to the $K_{Ca}3.1$ opener 1-EBIO for each donor (NFC n=7, NFC+TGFβ1 n=3, NFC+bFGF n=3, IPF n=7, IPF+TGFβ1 n=5, IPF+NFC n=3). The One-way analysis of variance test found a significant difference among the groups (**P=0.0013). The proportion of IPF cells responding to 1-EBIO after TGFβ1 stimulation was significantly higher *P<0.05. Significantly more NFC cells responded to 1-EBIO following bFGF stimulation **P<0.01.

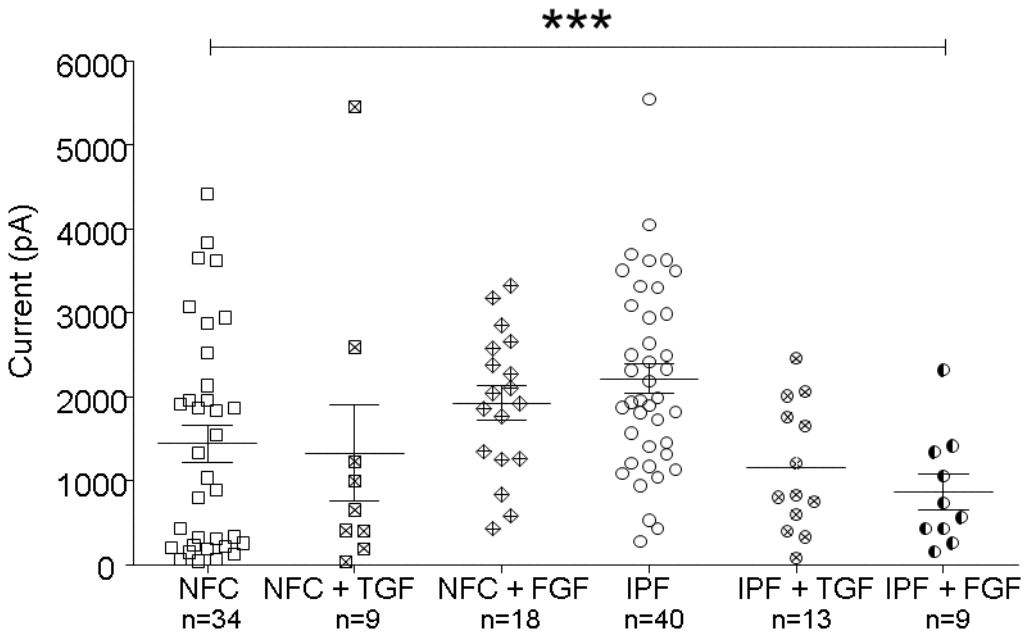

Figure 3-33. Changes to the 1-EBIO-dependent $K_{Ca}3.1$ current following mitogenic stimulation

The above graph represents the 1-EBIO dependent (1-EBIO minus baseline) current at +40mV, for each responding cell, ***P=0.0006. Following 24 hours of either bFGF (10 ng/ml) or TGFβ1 (10 ng/ml) stimulation, the currents in both NFC and IPF groups have a tendency to be smaller. Only the NFC donors after bFGF stimulation show increased current size.

3.4.3 Examination of TGFβ1 expression by human lung myofibroblasts.

The cells used in the study were αSMA positive. To determine whether the cells were producing their own TGFβ1, therefore activating themselves. TGFβ1 is known to increase αSMA actin expression(132,299,300) and the results in section **3.2.1** and **3.4.2** show TGFβ1 also increases $K_{Ca}3.1$ expression at both a mRNA and functional channel level. It was plausible therefore, that the IPF fibroblasts generate more TGFβ1 constitutively. TGFβ1 release was therefore examined in myofibroblasts from both NFC and IPF donors. Using a TGFβ1 ELISA I found that after only 24 hours, both the NFC and IPF cell supernatants contained TGFβ1, but there was no significant differences between the donors (**Figure 3-34)**.

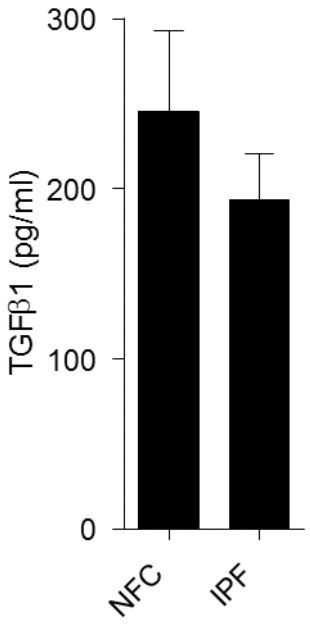

Figure 3-34. TGFβ1 secretion by human lung myofibroblasts

Supernatants collected after 24 hours from both NFC (n=3) and IPF (n=3) donors showed evidence of constitutive TGFβ1 production but no significant difference between NFC and IPF donors was found.

3.5 Evidence of in vivo expression of $K_{Ca}3.1$

3.5.1 $K_{Ca}3.1$ immunoreactivity is expressed strongly in IPF parenchymal lung tissue

So far it has been shown that the presence of the $K_{Ca}3.1$ channel mRNA, protein and functional channels in human lung myofibroblasts *in vitro*. To determine whether the $K_{Ca}3.1$ channel was expressed within human lung tissue *in vivo*, and most importantly in IPF lung tissue, immunohistochemistry was undertook on NFC and IPF lung tissue. IPF (and other ILD tissue) tissue was obtained from the pathology laboratory at Glenfield hospital and NFC control tissue from non-cancerous lung removed at the time of lung resection for carcinoma. **Table 3-2** shows the tissue donors used for the experiments and the diagnosis following lung biopsy.

There was strong immunostaining for $K_{Ca}3.1$ in NFC lung tissue, particularly in airway and alveolar epithelial cells, but also in cells within the interstitium including vessels (**Figure 3-35**). $K_{Ca}3.1$ was also expressed strongly in areas of parenchymal fibrosis in the IPF (UIP), NSIP and sarcoidosis tissues and was co-localized with areas of αSMA positivity (**Figure 3-36**). Because there is no control for parenchymal fibrosis, the magnitude of $K_{Ca}3.1$ staining between NFC and IPF tissue could not be compared. Particularly interesting was

the strong expression of $K_{Ca}3.1$ in the IPF epithelium which could hint at a possible role of $K_{Ca}3.1$ in EMT (**Figure 3-36**).

Parrafin Blocks	Diagnosis
ILD001	Sarcoidosis
ILD002	NSIP
ILD003	UIP
ILD005	UIP
ILD006	Probable UIP
ILD007	IPF end stage
ILD008	Sarcoidosis
ILD009	UIP
ILD010	NSIP
ILD012	UIP
0026J	non-malignant tissue
0002X	non-malignant tissue
0003E	non-malignant tissue
0008B	non-malignant tissue
0006BL	non-malignant tissue
0039B	non-malignant tissue
0058C	non-malignant tissue
0101B	non-malignant tissue

Table 3-2. Patient diagnosis of lung tissue

Overall a total of 10 biopsies were used with different forms of interstitial lung disease. 8 biopsies defined as non-fibrotic control lung were also used.

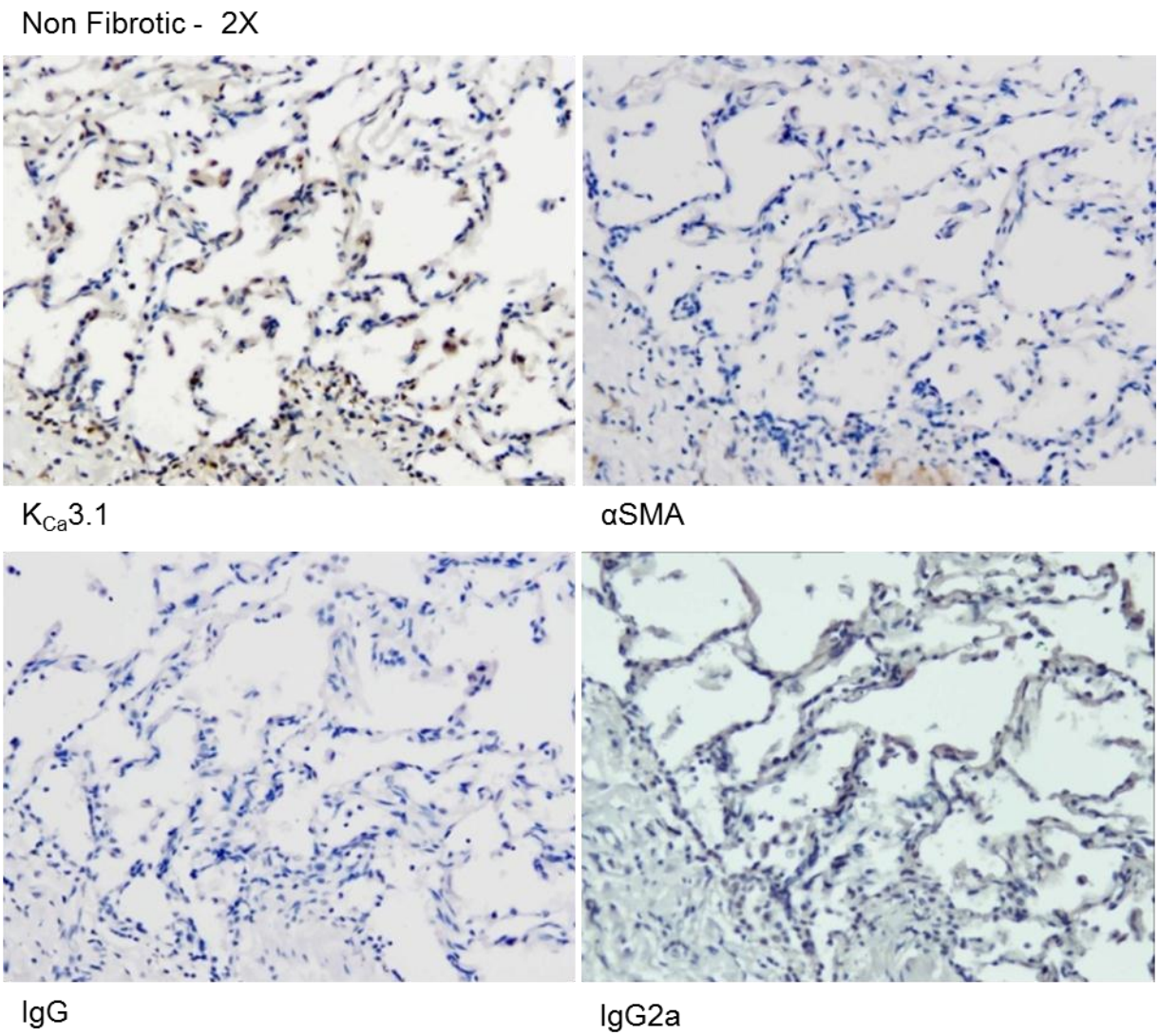

Figure 3-35. $K_{Ca}3.1$ expression in NFC tissue

This picture shows the results of the immunohistochemical staining from 1 representative NFC donor. There is $K_{Ca}3.1$ staining in non-fibrotic areas, and predictably there was little αSMA staining, both controls were negative.

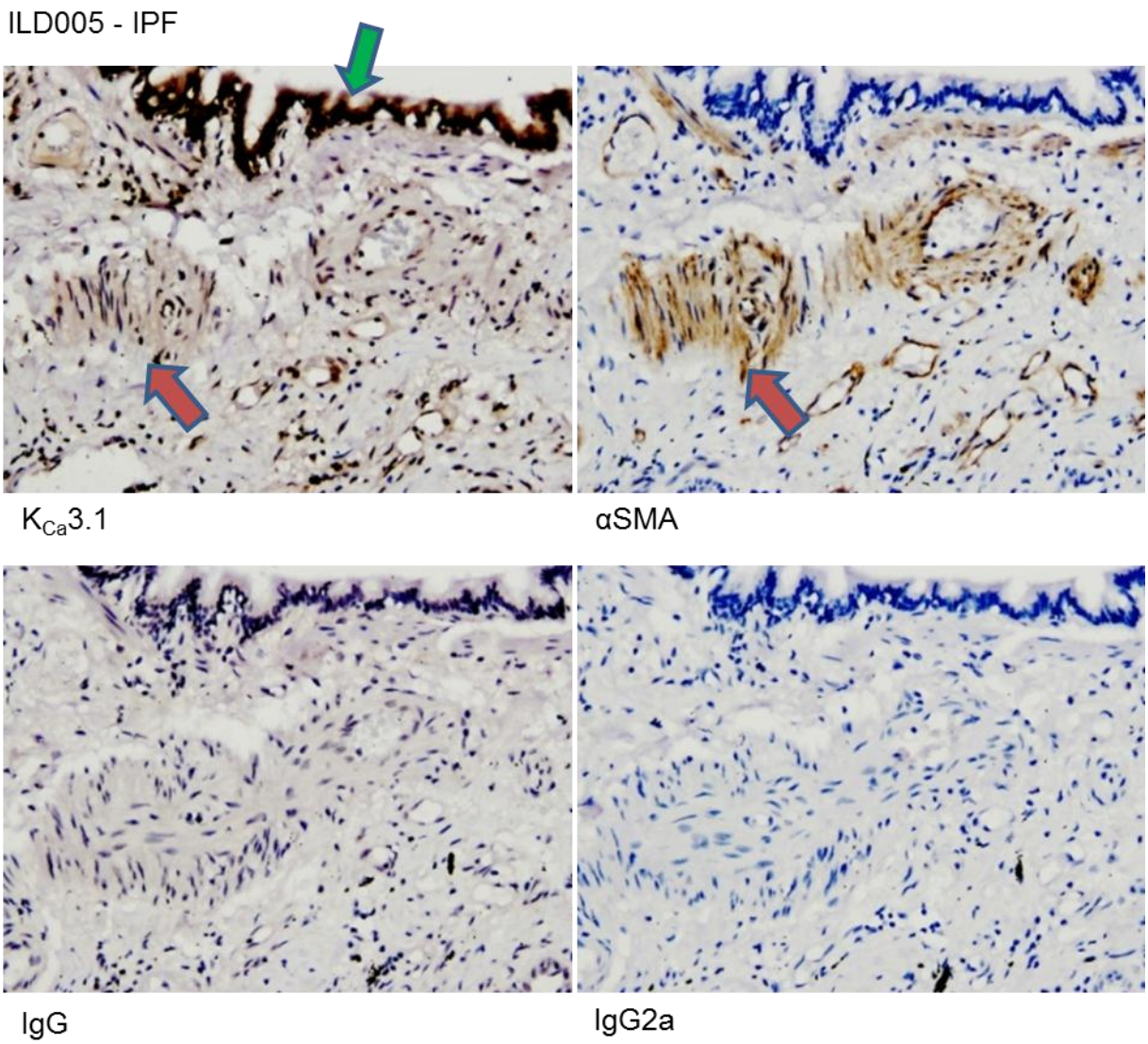

Figure 3-36 $K_{Ca}3.1$ expression in IPF tissue

Staining from 1 of the 10 IPF donors. The $K_{Ca}3.1$ staining co-localizes with αSMA staining, indicating the presence of myofibroblasts (red arrows). $K_{Ca}3.1$ staining is weak within smooth muscle bundles (red arrows). The green arrow shows strong $K_{Ca}3.1$ staining in IPF epithelium.

3.6 Role of $K_{Ca}3.1$ in modulation of myofibroblast function

3.6.1 Inhibition of $K_{Ca}3.1$ K^+ channels attenuates human lung myofibroblast function

The results presented so far confirm that the $K_{Ca}3.1$ channel is expressed by human lung myofibroblasts, the channel is functional and it is present within IPF lung tissue. However, its role in human lung myofibroblast function was unknown.

The pathology of IPF is thought to arise from an aberrant repair response following an alveolar epithelial insult(59,71). With respect to the role of myofibroblasts in this process, they potentially proliferate, migrate, contract and secrete collagen. Therefore, experiments were devised to examine the effect of $K_{Ca}3.1$ blockade on these processes.

To stimulate the cells two of the most predominant fibrotic mediators discussed in literature TGFβ1 and bFGF(59,71-73).

3.6.2 $K_{Ca}3.1$ channel inhibition fails to prevents FBS-induced myofibroblast proliferation

$K_{Ca}3.1$ channels are reported to inhibit the proliferation of T cells (264,301) and airway smooth muscle cells(275,282) but not fibrocytes(298) or mast cells(274). Stimulation with 10% FBS for 72

hours significantly increased myofibroblast proliferation over control (P=0.0003) in both NFC (n=3) and IPF (n=3) cells. The results were similar in NFC and IPF cells, and the data are presented together (**Figure 3-37**). However, $K_{Ca}3.1$ block with TRAM-34 (20 and 200 nM) or ICA-17043 (10 and 100 nM) did not decrease this (**Figure 3-37**).

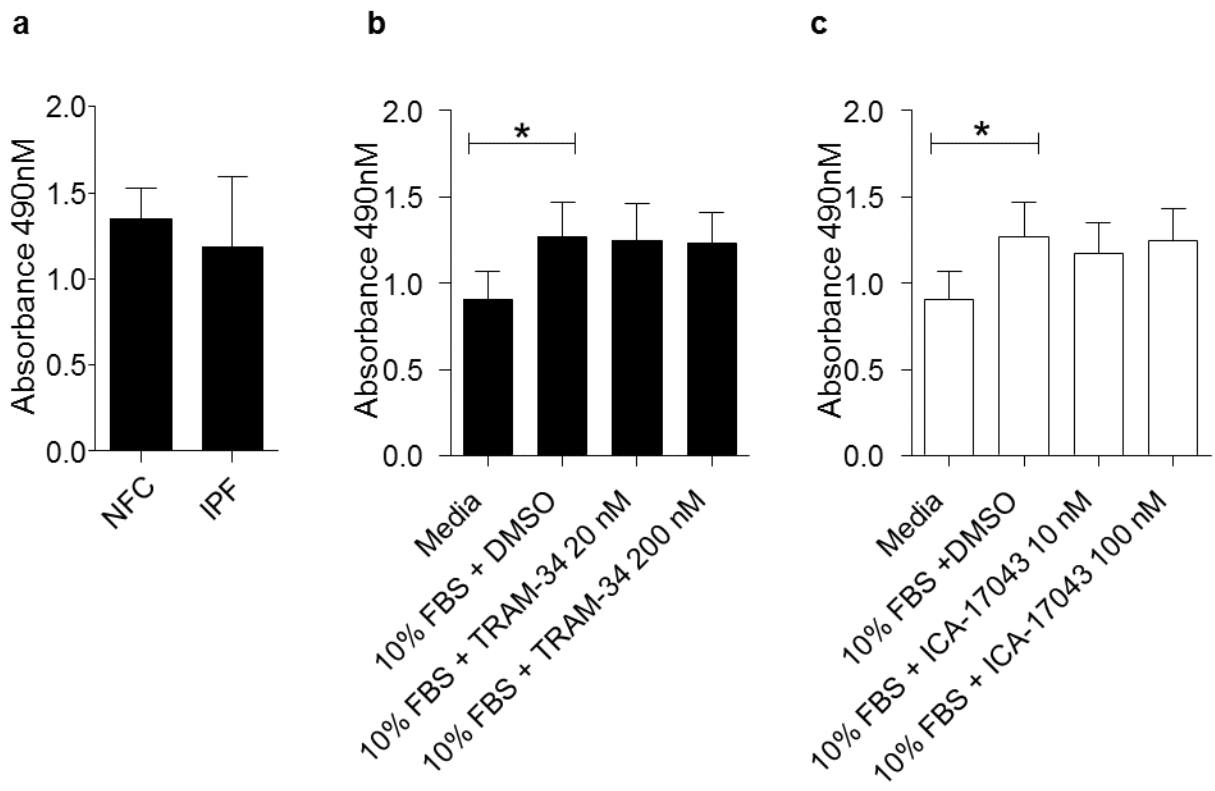

Figure 3-37. Failure to inhibit FBS induced myofibroblast proliferation

Following 24 hours of FBS stimulation, both NFC (n=3) and IPF (n=3) myofibroblasts showed an increase in proliferation compared to media alone, *P=0.0003. **a**) The results were similar in both NFC and IPF-derived cells, so the data are pooled. **b**) TRAM-34 did not significantly inhibit FBS induced myofibroblast proliferation at either 20 or 200 nM (n=6). **c**) ICA-17043 also failed to inhibit FBS induced proliferation at either 10 or 100 nM (n=6).

3.6.3 $K_{Ca}3.1$ channel inhibition does not inhibit bFGF induced myofibroblast proliferation

Next, the effects of bFGF on myofibroblast proliferation was examined. bFGF is released primarily by mast cells in IPF. Intriguingly, it has been shown to increase proliferation, though the proliferating cells have a more fibroblast morphology with less αSMA expression(70). To confirm this immunofluorescence was performed on cells following 48 hours bFGF incubation. In 3 donors, although αSMA expression did not significantly decrease the morphology was more fibroblast-like (**Figure 3-38**). This suggests that bFGF increases proliferation of myofibroblasts but it is TGFβ1 that encourages αSMA expression.

Upon stimulation with bFGF (10 ng/ml) plus 0.1% DMSO for 72 hours there was a significant increase in lung myofibroblast proliferation over control (*P=0.0022), in both NFC (n=3) and IPF (n=3) donors (**Figure 3-39**). The results were similar with NFC and IPF cells so all data is pooled. Pharmacological blockade of $K_{Ca}3.1$ with TRAM-34 (200 nM) failed to inhibit the bFGF proliferation. ICA-17043 (100 nM) inhibited the bFGF-induced proliferation, (*P=0.0291, repeated measures ANOVA). Although the result was significant the decrease was marginal (**Figure 3-39**), and in the absence of a response to TRAM-34, or in the presence of FBS, it is

unlikely that myofibroblast proliferation is inhibited by $K_{Ca}3.1$ blockade.

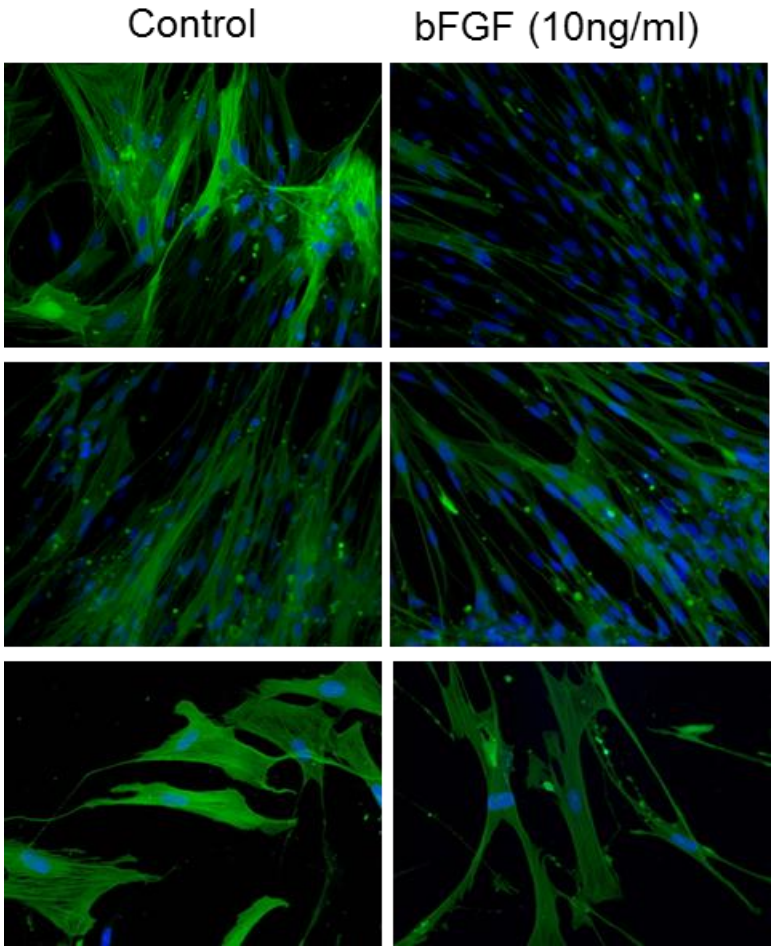

Figure 3-38. bFGF alters myofibroblast morphology

Following 48 hours of bFGF (10 ng/ml) stimulation, myofibroblasts still expressed αSMA and there was no significant difference between control and bFGF stimulated cells (n=3). However, cells appeared to be structurally different containing less stress fibres and becoming more spindle shaped.

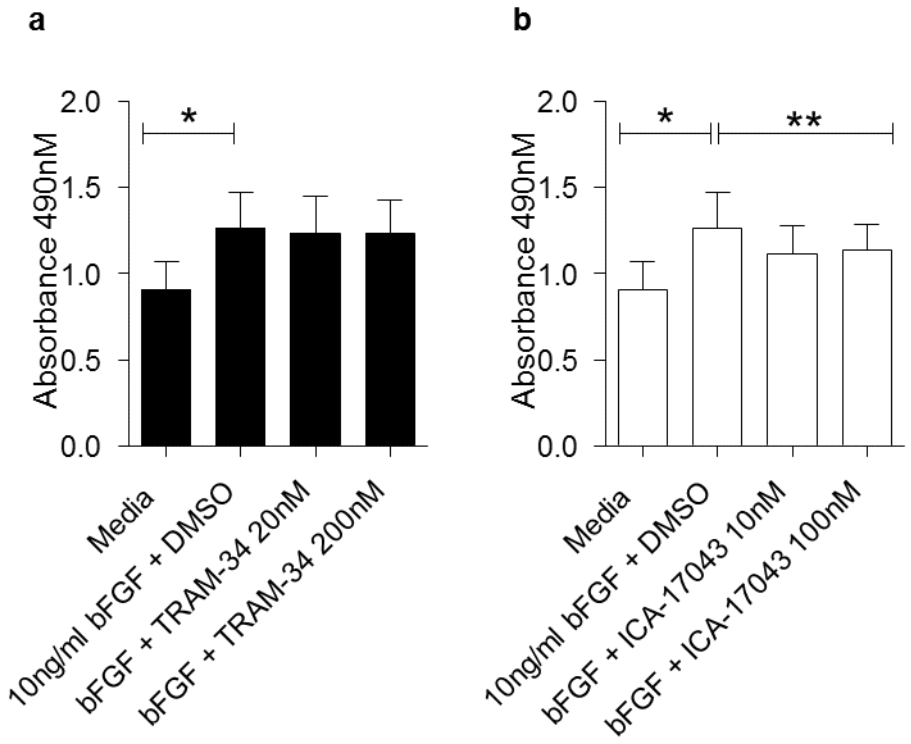

Figure 3-39. $K_{Ca}3.1$ channel inhibition of bFGF induced myofibroblast proliferation

Following 24 hours of bFGF stimulation both NFC (n=3) and IPF (n=3) myofibroblasts showed an increase in proliferation compared to media alone, *P=0.0022. **a**) TRAM-34 did not significantly inhibit bFGF induced myofibroblast proliferation at either 20 or 200 nM. **b**) ICA-17043 inhibited bFGF induced proliferation at 100 nM, **P=0.0291.

3.6.4 TGFβ1 does not induce myofibroblast proliferation

Using TGFβ1 at 1, 10 and 100 ng/ml a dose-response assay was conducted to examine the effects of TGFβ1 on myofibroblast proliferation over 72 hours. However, none of the doses increased myofibroblast proliferation. Interestingly, TGFβ1 appeared to dose-dependently decrease myofibroblast proliferation (*P=0.0202, repeated measures ANOVA). Proliferation after 72 hours using TGFβ1 at 100 ng/ml was significantly lower than media alone (*P<0.05, Bonferroni's multiple comparison test) although the effect was marginal (**Figure 3-40**). It is well documented that TGFβ1 is involved in the differentiation of fibroblasts into myofibroblasts along with the development of αSMA fibres and rod-like structures(302). As the cells used in this study are already myofibroblasts and have an αSMA positive phenotype, TGFβ1 is not likely to increase proliferation.

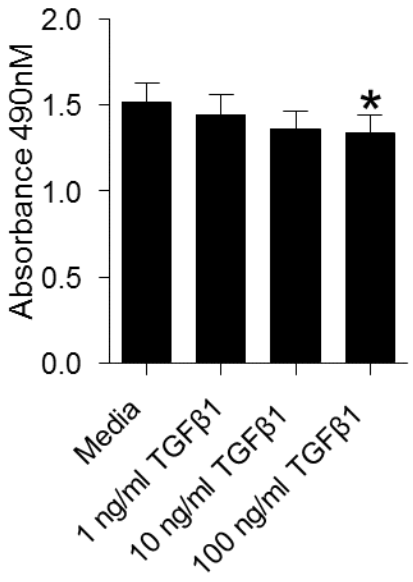

Figure 3-40. TGFβ1 appeared to dose dependently decrease myofibroblast proliferation

TGFβ1 dose dependently reduces myofibroblast proliferation (NFC n=3 and IPF n=3), P=0.0202, repeated measures ANOVA. Proliferation after 72 hours of TGFβ1 (100 ng/ml) was significantly lower than media alone, *P<0.05, Bonferroni's multiple comparison test, however, this difference is marginal.

3.6.5 Selective pharmacological blockade of $K_{Ca}3.1$ attenuates bFGF and FBS-dependent wound healing

Using a 2-D wound healing assay it was investigated whether pharmacological $K_{Ca}3.1$ inhibition with TRAM-34 and ICA-17043 had any effect on myofibroblast repair response (**Figure 3-41)**. No difference in wound repair was found between NFC or IPF cells and therefore the data shown are pooled. 0.1% DMSO was used as the vehicle control and did not alter the wound repair response.

Constitutive wound healing in the absence of FBS or bFGF was not inhibited by TRAM-34 (**Figure 3-42**). bFGF stimulation significantly increased the percentage of myofibroblast wound healing in both NFC (n=3) and IPF donors (n=3) over 48 hours compared to non-stimulated cells (P=0.002). Following the addition of either TRAM-34 or ICA-17043, the effect of bFGF-stimulated wound healing was dose-dependently attenuated (**Figure 3-43**). Thus at the 48 hour time-point wound healing was reduced by 22.2 ± 11% for TRAM-34 20 nM and 27.3 ± 9.5% for TRAM-34 200 nM compared to 0.1% DMSO control (P=0.0467 across groups). The inhibition by 200 nM TRAM-34 was equivalent to inhibition of the bFGF-dependent response by 53.3 ± 17.6%. ICA-17043 reduced wound healing by 16.9 ± 8.1% at 10 nM and 24.4 ± 6.6% at 100 nM, equivalent to inhibition of the bFGF-dependent response by 63.4 ± 13.4% (P=0.0076 across groups) (**Figure 3-44**).

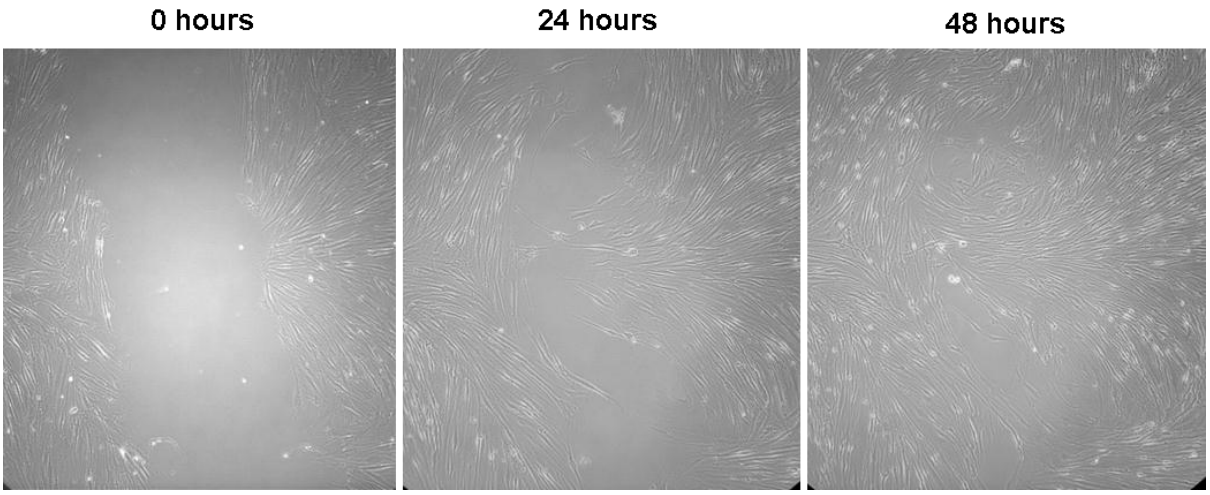

Figure 3-41. Visual example of wound healing

An example of the wound created in a confluent monolayer of myofibroblasts. At 0 hours the wound is apparent. At 24 hours the myofibroblasts have begun to proliferate and/or migrate into the wounded area, and at 48 hours the wound is almost completely healed.

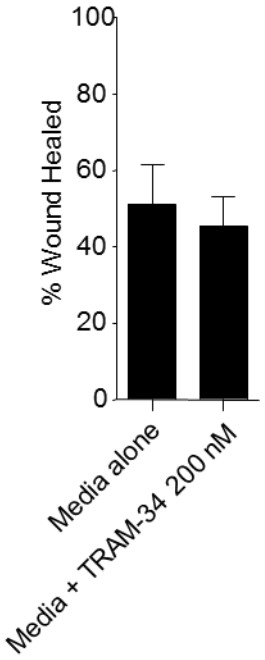

Figure 3-42. A $K_{Ca}3.1$ blockade only inhibits mitogenic wound healing

No differences in wound repair were found between media plus 0.1% DMSO vehicle compared to media plus TRAM-34 (n=4).

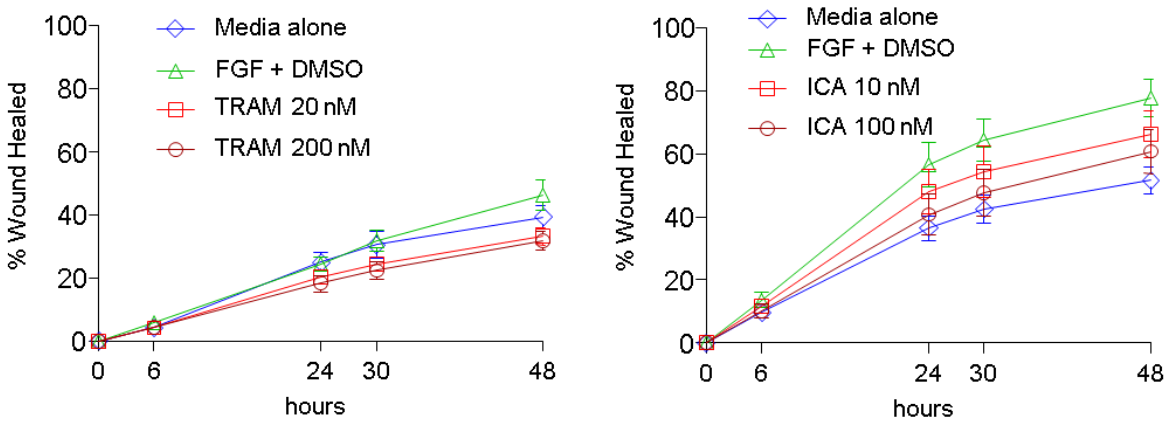

Figure 3-43. bFGF stimulated wound healing over 48 hours

Shows the wound healing response over different time points 0, 6, 24, 48 hours (both n=6). Myofibroblasts stimulated with 10ng/ml bFGF and 0.1% DMSO, showed accelerated wound healing in comparison to media alone. **a**) When TRAM-34 was added at 20nM or 200nM there was a dose dependent decrease in wound healing over the 48 hours. **b**) Similarly when the cells were subject to ICA-17043 at either 10nM or 100nM there was also a dose dependent attenuation of myofibroblast wound healing.

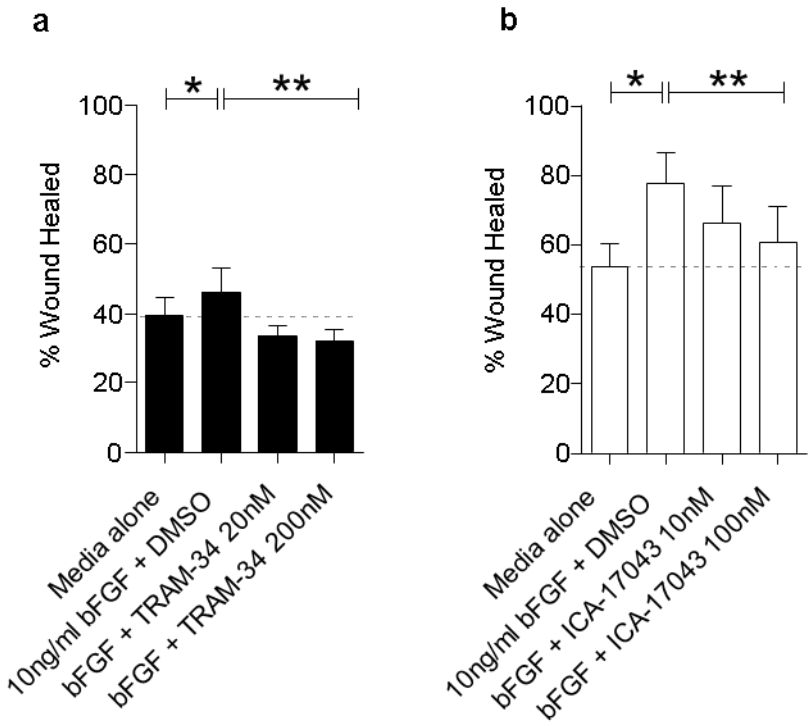

Figure 3-44. $K_{Ca}3.1$ blockade inhibits bFGF wound healing

Myofibroblasts stimulated with bFGF and 0.1% DMSO vehicle control, displayed accelerated wound repair in comparison to media alone **a**)*P=0.0399 **b**)*P=0.0073 Paired t-test (both n=6), dotted line shows baseline wound healing. There was a dose-dependent decrease in bFGF-induced wound healing over 48 hours in the presence of either **a**) TRAM-34 (20 nM and 200 nM) (**P=0.0467, repeated measures ANOVA) or **b**) ICA-17043 (10 nM and 100 nM) (**P=0.0076, repeated measure ANOVA).

Similarly, myofibroblasts stimulated with 10% FBS and 0.1% DMSO showed enhanced wound healing compared to media alone (***P<0.0001) in both NFC (n=3) and IPF (n=3) donors. This was dose-dependently attenuated by both TRAM-34 and ICA-17043 (**Figure 3-45**). In 10% FBS and 0.1% DMSO, wound healing was decreased by (mean % ± SEM), 14.7 ± 4.1% with TRAM-34 20 nM and 30.6 ± 5.4 with TRAM-34 200 nM (equivalent to inhibition of the FBS-dependent response by 75.7 ± 10.9%) (**P=0.0004, across groups). Correspondingly, ICA-17043 decreased the wound healing response by 3.1 ± 0.9 % (10 nM) and 12.9 ± 5.1% (100 nM)(equivalent to 47.9±15.3% of the FBS-dependent response) (**Figure 3-46**).

As a further control, experiments were also performed using two molecules, TRAM-7 and TRAM-85, that are structurally related to TRAM 34 but which do not have channel blocking activity. These did not inhibit FBS-dependent wound healing. (**Figure 3-47**).

In conclusion the 2-D in vitro wound repair response of human lung myofibroblasts is attenuated by $K_{Ca}3.1$ channel block.

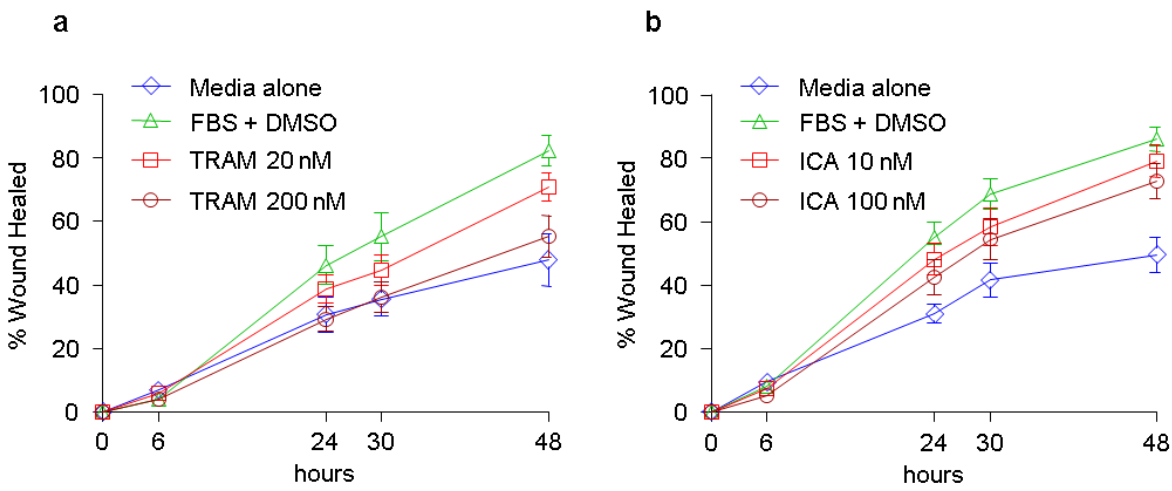

Figure 3-45. FBS stimulated wound healing over 48 hours

The FBS-dependent wound healing response over different time points 0, 6, 24, 48 hours (n=6). Myofibroblasts stimulated with 10% FBS in the presence of 0.1% DMSO, showed accelerated wound repair in comparison to media + 0.1% DMSO alone. **a**) TRAM-34 produced a dose-dependent decrease in wound repair over the 48 hours. **b**) Similarly when the cells were treated with ICA-17043 there was also a dose-dependent attenuation of myofibroblast wound repair.

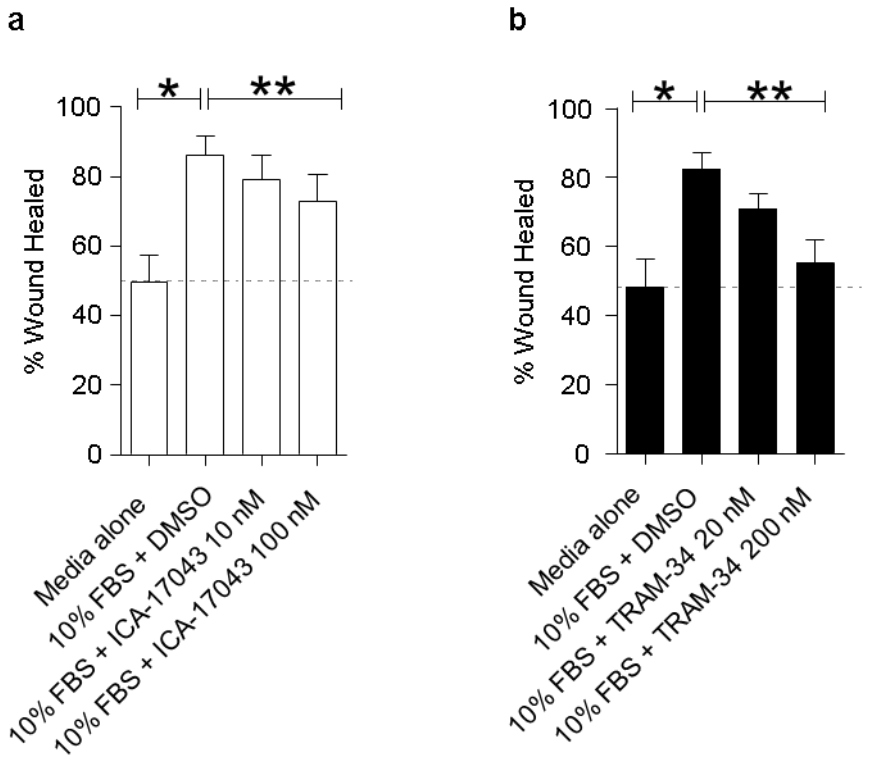

Figure 3-46. $K_{Ca}3.1$ blockade inhibits FBS wound healing

Myofibroblasts stimulated with 10% FBS and 0.1% DMSO vehicle control, showed accelerated wound repair in comparison to media + 0.1% DMSO alone **a**)*P=0.0019 **b**)*P=0.0043, Paired t-test (n=6). Dotted line represents baseline wound healing. There was a dose-dependent decrease in FBS-induced wound repair over 48 hours in the presence of either **a**) TRAM-34 (20 nM and 200 nM) (***P<0.0001, repeated measures ANOVA) or **b**) ICA-17043 (10 nM and 100 nM) (**P=0.0095, repeated measures ANOVA).

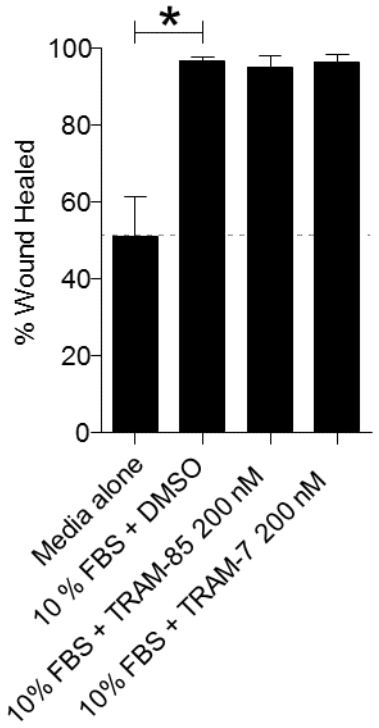

Figure 3-47. TRAM 7 and 85 have no effect on wound healing

10% FBS increases myofibroblast wound repair (*P=0.0168), but TRAM-34 isoforms, TRAM-85 (200 nM) or TRAM-7 (200 nM) do not inhibit myofibroblast wound repair (n=4).

3.6.6 TGFβ1-induced collagen synthesis is decreased following blockade of the $K_{Ca}3.1$ channel

TGFβ1 increases collagen synthesis by both human lung fibroblasts and myofibroblasts(71). **Figure 3-48** confirms this and demonstrates that TGFβ1 plus 0.1% DMSO significantly increases collagen production and secretion in both NFC (n=4) and IPF (n=4) derived human lung myofibroblasts (*P<0.05, t test) (data shown is pooled IPF and NFC which did not differ). The collagen detection assay used identifies the fibrillar collagens, types I, II, III, V and XI within supernatants, and it is these fibrillar collagens that account for the majority of excess extracellular matrix molecules accumulating in IPF tissue(2,184). There was a striking reduction in collagen production following the addition of TRAM-34 (**P=0.0161, repeated measures ANOVA) and ICA-17043 (**P=0.0038, repeated measures ANOVA), **Figure 3-48**. In contrast, no effect was seen with TRAM-7 or TRAM-85 (n=3) **Figure 3-49**. This confirms that the effects of TRAM-34 and ICA-17043 were mediated through their channel blocking activity.

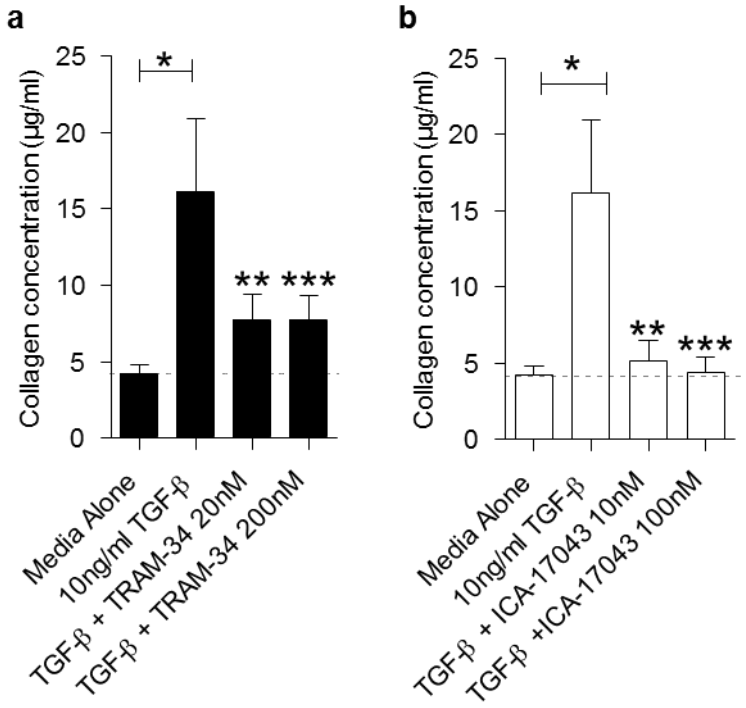

Figure 3-48. Blocking $K_{Ca}3.1$ channels decreases TGFβ1-dependent myofibroblast collagen secretion

a) and **b**) Collagen secretion was increased in myofibroblasts following TGFβ1-dependent stimulation in both IPF donors (n=4) and NFC donors (n=4), *P<0.05, Paired t test (the data shown is pooled). DMSO was used a vehicle control. Dotted line represents baseline collagen secretion **a**) The TGFβ1-induced increase in collagen secretion was inhibited by TRAM-34 20 nM and 200 nM (P=0.0161, repeated measures ANOVA) and there were significant differences found between TGFβ1 and TRAM-34 20 nM (**P<0.05, Bonferroni's multiple comparison test) and between TGFβ1 and TRAM-34 200 nM (***P<0.05, Bonferroni's multiple comparison test). **b**) TGFβ1-dependent collagen secretion was also inhibited by ICA-17043 (P=0.0038, repeated measures ANOVA), and there was significant differences found between TGFβ1 and ICA-17043 10 nM (**P<0.05, Bonferroni's multiple comparison test) and between TGFβ1 and ICA-17043 100 nM (***P<0.01, Bonferroni's multiple comparison test).

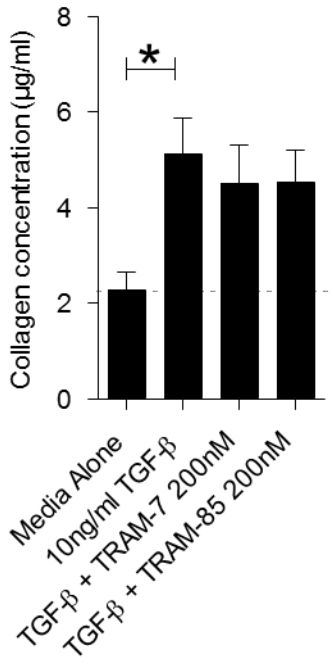

Figure 3-49. TRAM-7 and TRAM-85 do not inhibit collagen production

Collagen production was increased following the addition of TGFβ1 (10 ng/ml) plus 0.1% DMSO, *P<0.05, paired t test (n=3). However, unlike TRAM-34 and ICA-17043, the structurally related molecules that do not block $K_{Ca}3.1$ (TRAM-7 and TRAM-85 200 nM), did not inhibit collagen production by human lung myofibroblasts.

3.6.7 bFGF has no effect on collagen synthesis

Unlike TGFβ1, bFGF did not increase collagen production of human lung myofibroblasts from either NFC (n=4) or IPF donors (n=3). There was actually a statistically significant inhibition of collagen production by bFGF (*P<0.05), but the decrease was marginal and of doubtful clinical significance (**Figure 3-50**).

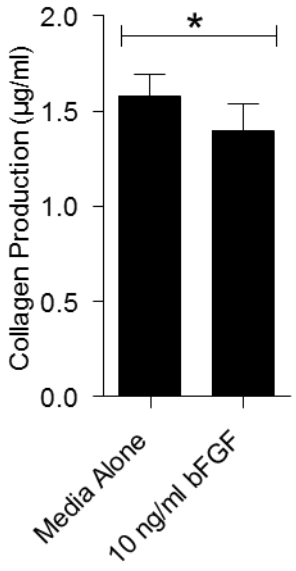

Figure 3-50. bFGF has no effect on collagen synthesis

bFGF did not increase collagen production in NFC (n=4) or IPF (n=3) myofibroblasts, *P<0.05 (data shown is pooled).

3.6.8 $K_{Ca}3.1$ inhibition attenuates TGFβ1 and bFGF induced myofibroblast contraction.

Initially dose response experiments were performed with TGFβ1 and bFGF at concentrations of 1, 10 and 100 ng/ml to assess their effects on myofibroblast contraction within collagen gels (**Figure 3-51**). Myofibroblasts cultured in collagen gels from both IPF (n=1) and NFC (n=1) donors exhibited optimal contraction following TGFβ1 stimulation at 10 ng/ml and bFGF stimulation at 10 ng/ml. There was no difference between NFC and IPF derived cells and all data are pooled.

In further experiments, TGFβ1 (10 ng/ml) stimulation increased myofibroblast contraction with the percentage decrease of initial gel area increased from (mean ± SEM) 30.6 ± 3.6% to 48.6 ± 2.4% (pooled data from NFC [n=3] and IPF [n=3] derived myofibroblasts) (**Figure 3-52**). bFGF (10 ng.ml) stimulation increased myofibroblast contraction from (mean ± SEM) 31.7 ± 3.8% to 51.2 ± 4.8% (pooled data from NFC [n=3] and IPF [n=3] derived myofibroblasts)(**Figure 3-53**). Compared to DMSO control, pre-treatment for 24 hours in the presence TRAM-34 200 nM or ICA-17043 100 nM almost completely inhibited both TGFβ1- and bFGF-stimulated myofibroblast contraction (*P<0.05, Bonferoni's multiple comparison test for both TRAM-34 and ICA-17043). In contrast, TRAM-85 was without effect (**Figure 3-54**). TRAM-34 did not inhibit

baseline constitutive myofibroblast contraction in the absence of growth factors, indicating that TRAM-34 only inhibits TGFβ1- or bFGF-dependent myofibroblast contraction. **Figure 3-55** provides a visual example of the gel contraction seen under each condition.

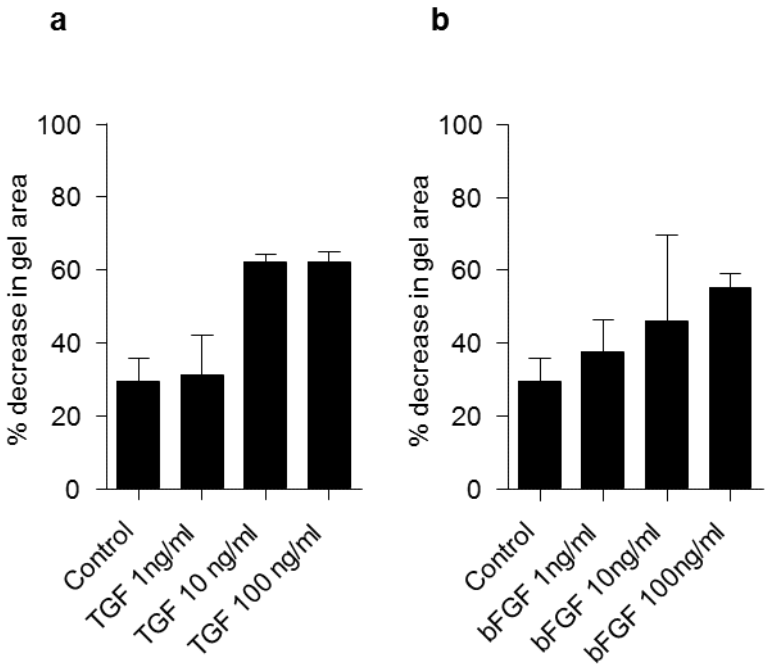

Figure 3-51. The dose response of myofibroblast contraction following growth factor stimulation

Dose response experiments were performed on 2 donors, to determine the optimum concentration of TGFβ1 and bFGF to use. As only 2 donors were used statistical analysis was not performed. For both bFGF and TGFβ1 a concentration 10 ng/ml was chosen for further experiments.

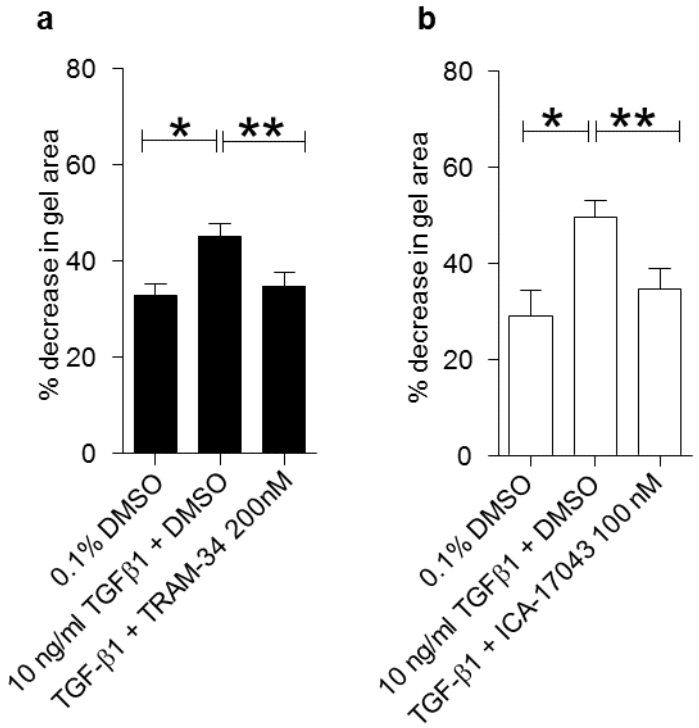

Figure 3-52. $K_{Ca}3.1$ channel block inhibits TGFβ1-dependent myofibroblast contraction

a) Myofibroblast collagen gel contraction was increased following TGFβ1 stimulation and this was inhibited by TRAM-34 200 nM in both IPF (n=3) and NFC (n=3) donors (for the pooled data shown P=0.0109, repeated measures ANOVA, *P<0.05 for TGFβ1 compared to control, **P<0.05 for TRAM-34 compared to TGFβ1, Bonferroni's multiple comparison test). **b**) TGFβ1-dependent myofibroblast collagen gel contraction was also inhibited by ICA-17043 100 nM (n=6) (for the pooled data shown P=0.0025, repeated measures ANOVA) (*P<0.01 for TGFβ1 versus control and **P<0.05 for TRAM-34 versus TGFβ1, Bonferroni's multiple comparison test).

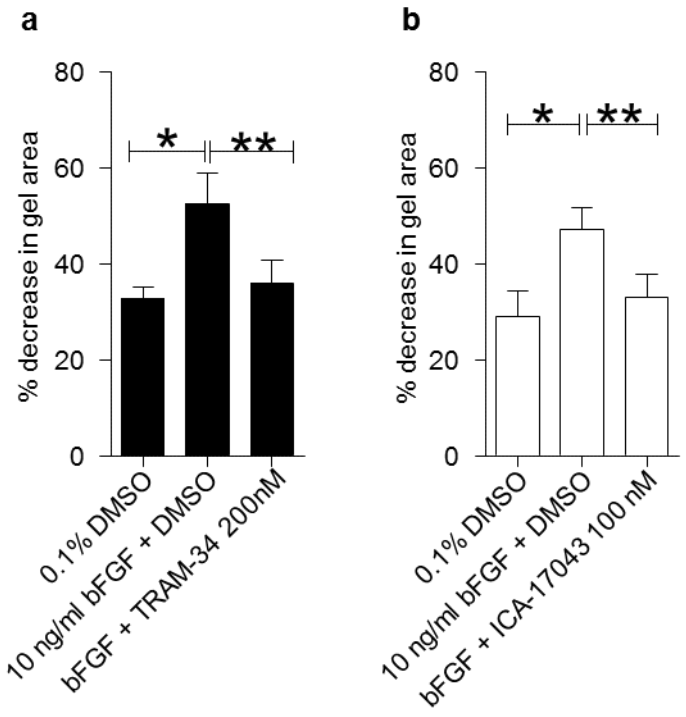

Figure 3-53. $K_{Ca}3.1$ channel block inhibits bFGF-dependent myofibroblast contraction

a) Myofibroblast collagen gel contraction was increased following bFGF stimulation and was also inhibited by TRAM-34 200 nM (for the pooled data shown P=0.0020, repeated measures ANOVA), *P<0.01 for bFGF compared to control, **P<0.01 for TRAM-34 compared to bFGF, Bonferroni's multiple comparison test. **b**) Similarly, ICA-17043 100 nM significantly reduced bFGF-dependent myofibroblast collagen gel contraction (for the pooled data shown P=0.0007, repeated measures ANOVA) (*P<0.001 for bFGF versus control and **P<0.01 for TRAM-34 versus bFGF, Bonferroni's multiple comparison test).

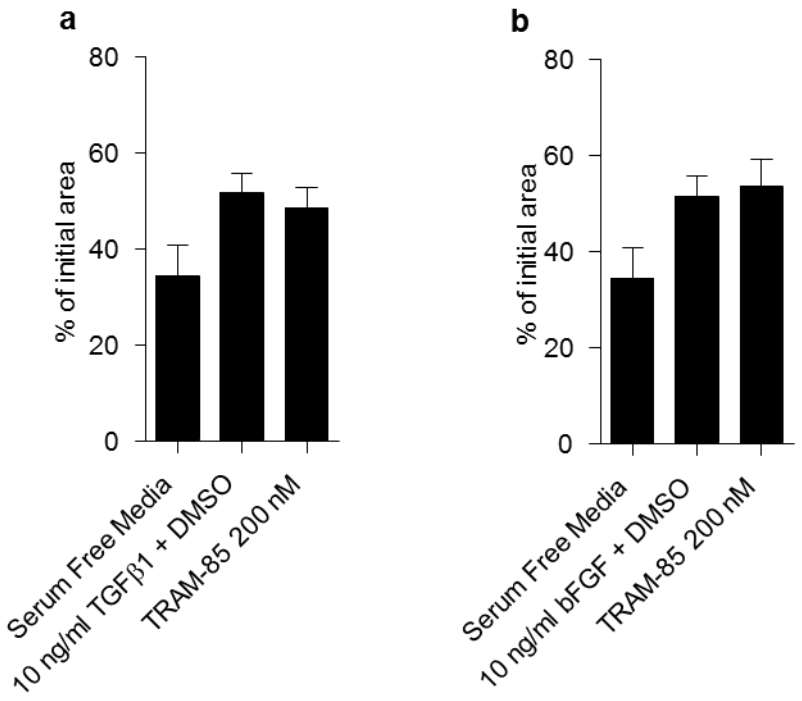

Figure 3-54. TRAM-85 does not inhibit myofibroblast contraction

Myofibroblast collagen gel contraction was increased following TGFβ1 and bFGF stimulation, but unlike TRAM-34 and ICA-17043, 24 hours of pre-treatment with TRAM-85 did not inhibit contraction

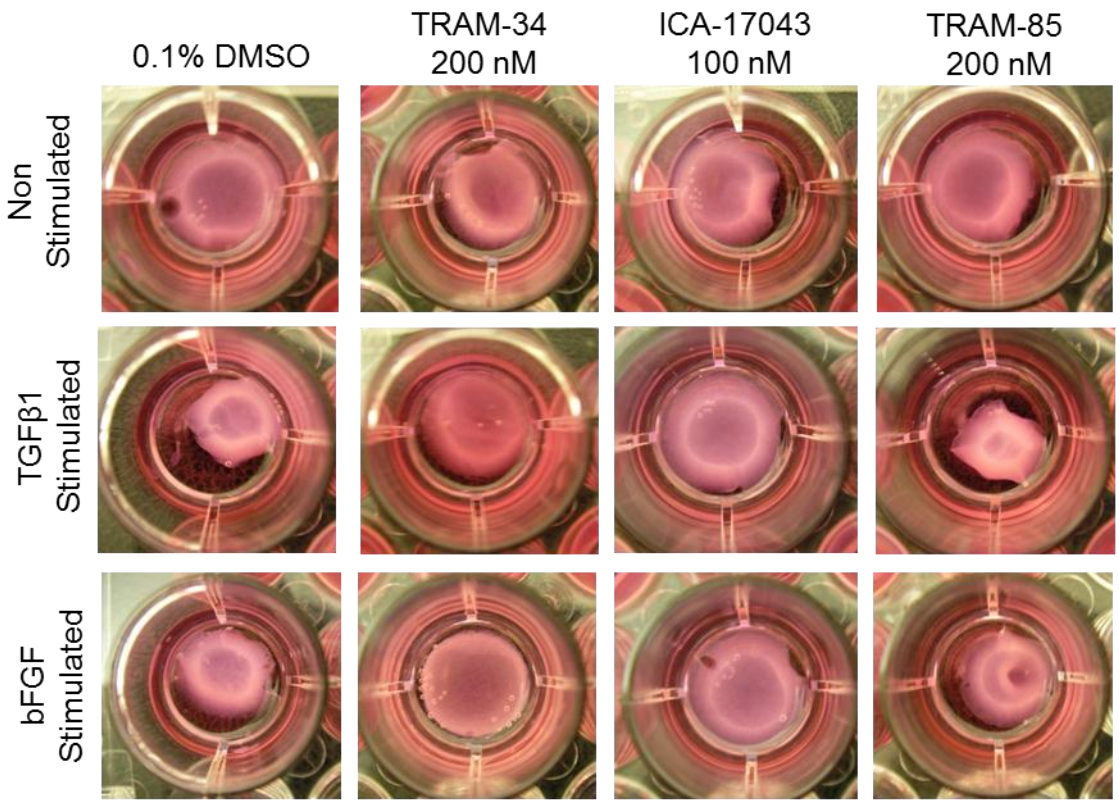

Figure 3-55. Myofibroblast collagen gel contraction

Pictures illustrate how the collagen gel contracted after TGFβ1 and bFGF stimulation. The collagen gels did not contract as much following pre-treatment with TRAM-34 or ICA-17043, whereas pre-treatment with TRAM-85 had no effect.

3.6.9 $K_{Ca}3.1$ inhibition decreases αSMA expression in human lung myofibroblasts

TGFβ1 is released constitutively by primary human lung myofibroblasts (see section **3.4.3**), and is known to increase αSMA expression(122,188,303). Because $K_{Ca}3.1$ block inhibits several TGFβ1-dependent responses in lung myofibroblasts, including myofibroblast contraction, it was hypothesised that $K_{Ca}3.1$ block may reduce the high constitutive expression of αSMA present in our cells. Using immunofluorescence the expression of αSMA in myofibroblasts following 48 hours of treatment with TRAM-34 (20 and 200 nM) was investigated. Interestingly αSMA expression was dose-dependently decreased in both NFC (n=4) and IPF (n=2) patients. No differences between donor types were found therefore data was pooled. In fact, TRAM-34 almost completely inhibited αSMA expression and stress fibres were much less apparent (**Figure 3-56**). Treatment with TRAM-7 or TRAM-85 (200 nM) did not inhibit αSMA expression.

Interestingly, ICA-17043 decreased the αSMA expression however statistics were not performed as this was only done in n=2 donors (**Figure 3-57**).

The results may indicate either that $K_{Ca}3.1$ blockade inhibits autocrine TGFβ1 secretion by the myofibroblasts resulting in a loss of αSMA stress fibres and filaments, or inhibits the TGFβ1-dependent cell signalling required for αSMA expression. This might then explain

the lack of contraction by the myofibroblasts following $K_{Ca}3.1$ blockade.

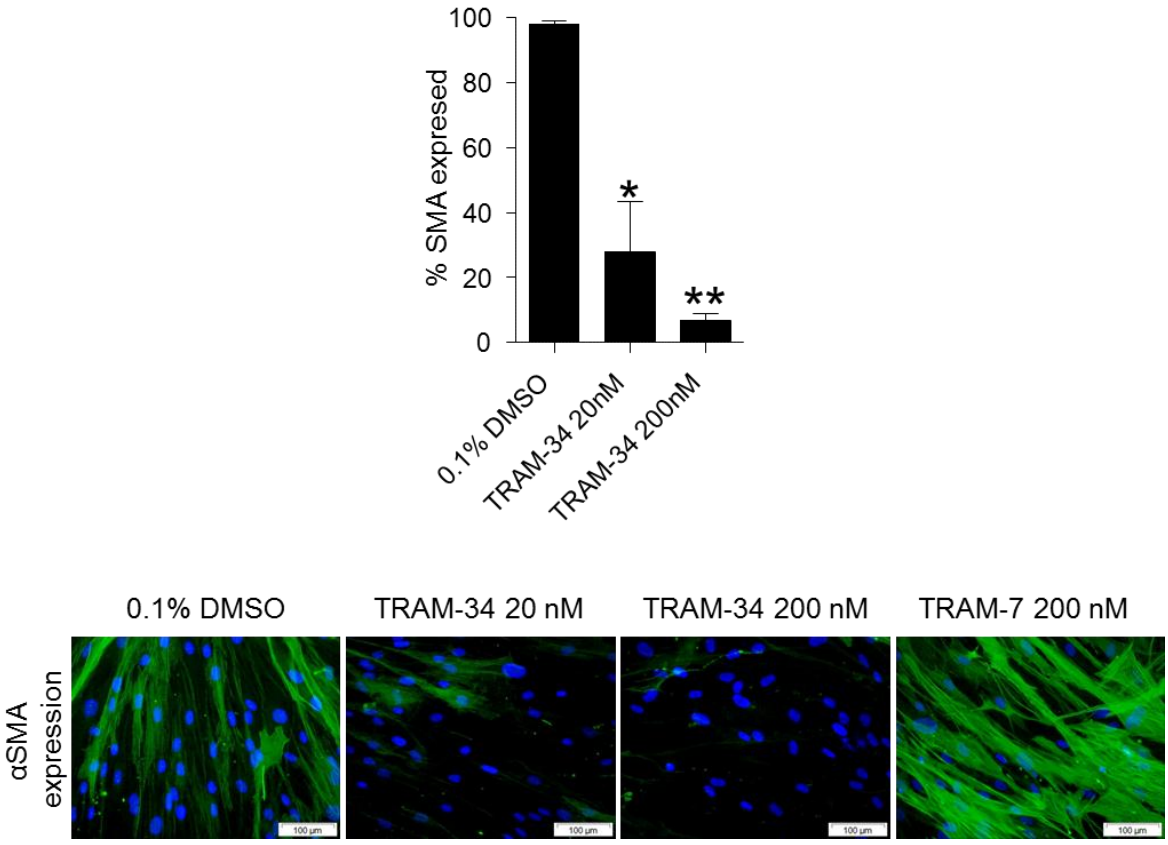

Figure 3-56. TRAM-34 inhibits αSMA expression in human lung myofibroblasts

Following 48 hours of incubation with TRAM-34 at 20 and 200 nM there was a dose dependent decrease in αSMA expression by NFC (n=4) and IPF (n=2) myofibroblasts (for the pooled data shown P=0.0003, repeated measures ANOVA), (*P<0.01, DMSO versus TRAM-34 20 nM and **P<0.001 for DMSO versus TRAM-34 200 nM, Bonferroni's multiple comparison test). The pictures illustrate the decrease in αSMA expression, green staining represents the αSMA and blue (DAPI) nuclei staining. Cells contain less αSMA stress fibres and there is barely any staining in the TRAM-34 200 nM picture. TRAM-7 200 nM did not inhibit αSMA expression or αSMA stress fibres and robust staining can clearly be seen.

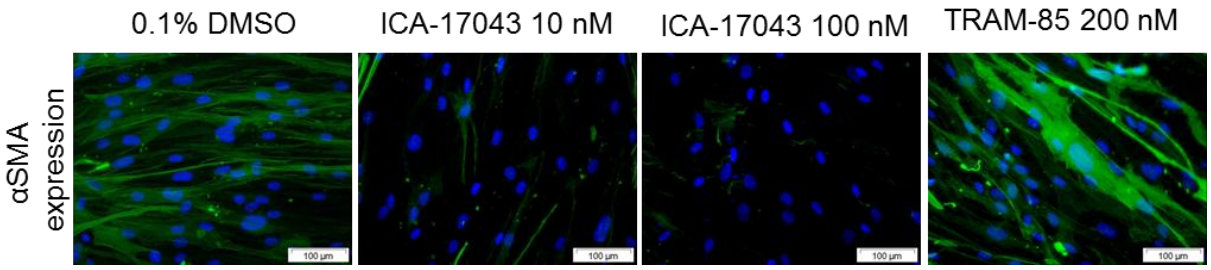

Figure 3-57. ICA-17043 inhibits αSMA expression in myofibroblasts

Pictures illustrate the decrease in αSMA expression, green staining represents the αSMA and blue (DAPI) nuclei staining. Cells contain less αSMA stress fibers and there is barely any staining following incubation with ICA-17043 100 nM. TRAM-85 200 nM did not inhibit αSMA expression and αSMA staining can clearly be seen.

3.6.10 The effect of $K_{Ca}3.1$ block on myofibroblast autocrine TGFβ1 secretion

To investigate whether $K_{Ca}3.1$ block inhibits autocrine TGFβ1 secretion by myofibroblasts we incubated the cells with either TRAM-34 or ICA-17043 for 24 hours. ICA-17043 significantly inhibited the autocrine secretion of TGFβ1 from both NFC (n=3) and IPF (n=3 donors, P=0.0431 for pooled data, repeated measures ANOVA). However, the effects were modest, and of uncertain biological significance (**Figure 3-58**), and TRAM-34 was without effect. TRAM-7 and TRAM-85 were also used and shown to be ineffective (**Figure 3-58)**. These data suggest that it is unlikely that the effects of $K_{Ca}3.1$ block on αSMA expression are due to the inhibition of autocrine TGFβ1 secretion, and make it more likely that there is inhibition of intracellular signalling events.

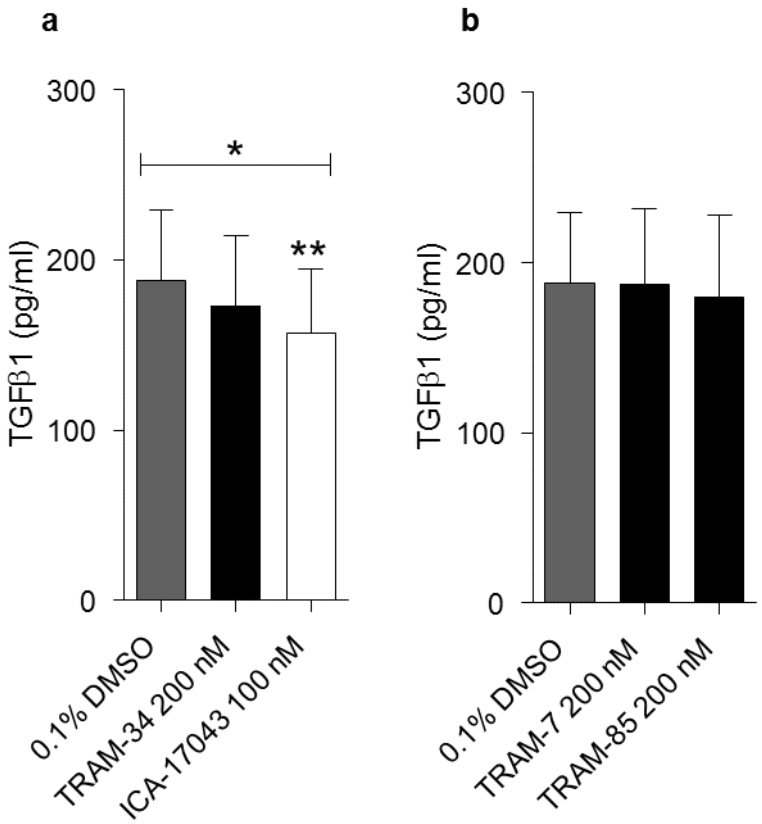

Figure 3-58. Autocrine secretion of TGFβ1 is attenuated by a $K_{Ca}3.1$ blockade

a) Human lung myofibroblasts from NFC (n=3) and IPF (n=3) patients secreted on average 187 pg/ml of TGFβ1. This secretion was significantly reduced following $K_{Ca}3.1$ blockade with ICA-17043 but not TRAM-34 (*P=0.0431, repeated measures ANOVA), (**P<0.05, DMSO versus ICA-17043 100 nM, Bonferroni's multiple comparison test). **b**) Neither TRAM-7 nor TRAM-85 has any significant effect on TGFβ1 autocrine secretion.

3.6.11 Chemokine secretion by human lung myofibroblasts

Using myofibroblast supernatants from both NFC and IPF donors chemokine production and the effects of $K_{Ca}3.1$ block were assessed. Cells were stimulated with either TGFβ1 (10 ng/ml), bFGF (10 ng/ml), or IFNγ plus TNFα (both 10 ng/ml) for 16 hours in the presence or absence of TRAM-34 or ICA-17043. Initially we examined the supernatants for CXCL10 (IP-10), CX3CL1 (Fractalkine), CCL5 (RANTES) and CCL11 (Eotaxin).

Myofibroblasts did not secrete detectable levels of CCL11 following 24 hours of either TGFβ1, bFGF or IFN-γ plus TNFα stimulation.

Levels of CCL5 were only increased following stimulation with both IFNγ and TNFα, but the increase was not significant (**Figure 3-59**).

Myofibroblast supernatants contained detectable levels of CXCL10 following 16 hours stimulation with IFNγ plus TNFα. Compared to media alone, IFNγ plus TNFα significantly increased the amount of CXCL10 released by myofibroblasts (P=0.0040). Neither TRAM-34 nor ICA-17043 were able to inhibit CXCL10 secretion (**Figure 3-60**).

Following 16 hours of incubation, human lung myofibroblasts also produced large amounts of CX3CL1 in media alone. CX3CL1

production was not significantly increased following stimulation with TGFβ1 (10 ng/ml), bFGF (10 ng/ml), IFN-γ plus TNFα (both 10 ng/ml), but none of these increases were statistically significant (**Figure 3-61**).

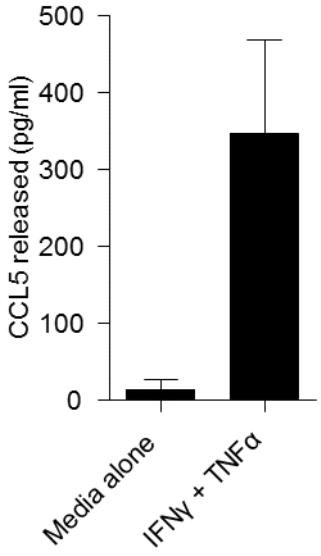

Figure 3-59. IFNγ and TNFα increased secretion of CCL5

IFN-γ and TNFα (both at 10 ng/ml) increased CCL5 production in human lung myofibroblast (n=3) following 16 hours stimulation although the increase was not significant.

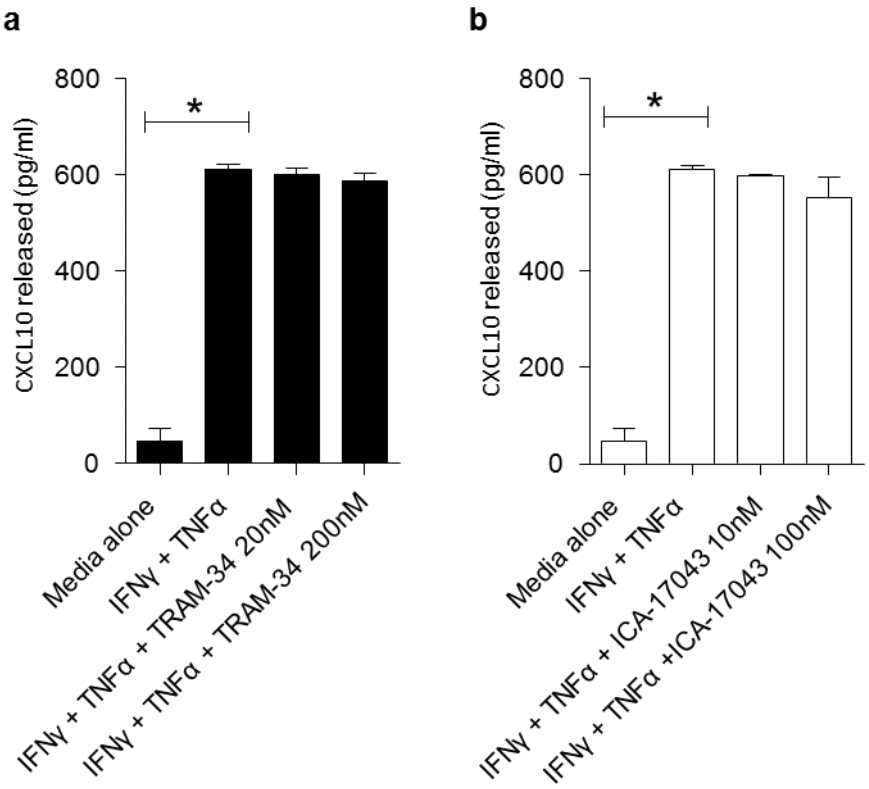

Figure 3-60. IFNγ and TNFα increased secretion of CX3CL1

a) and **b**) IFN-γ plus TNFα (both at 10 ng/ml) increased CXCL10 production in human lung myofibroblast (n=3) following 16 hours stimulation, *P=0.0040, t test. However, neither **a**) TRAM-34 nor **b**) ICA-17043 were capable of inhibiting its secretion.

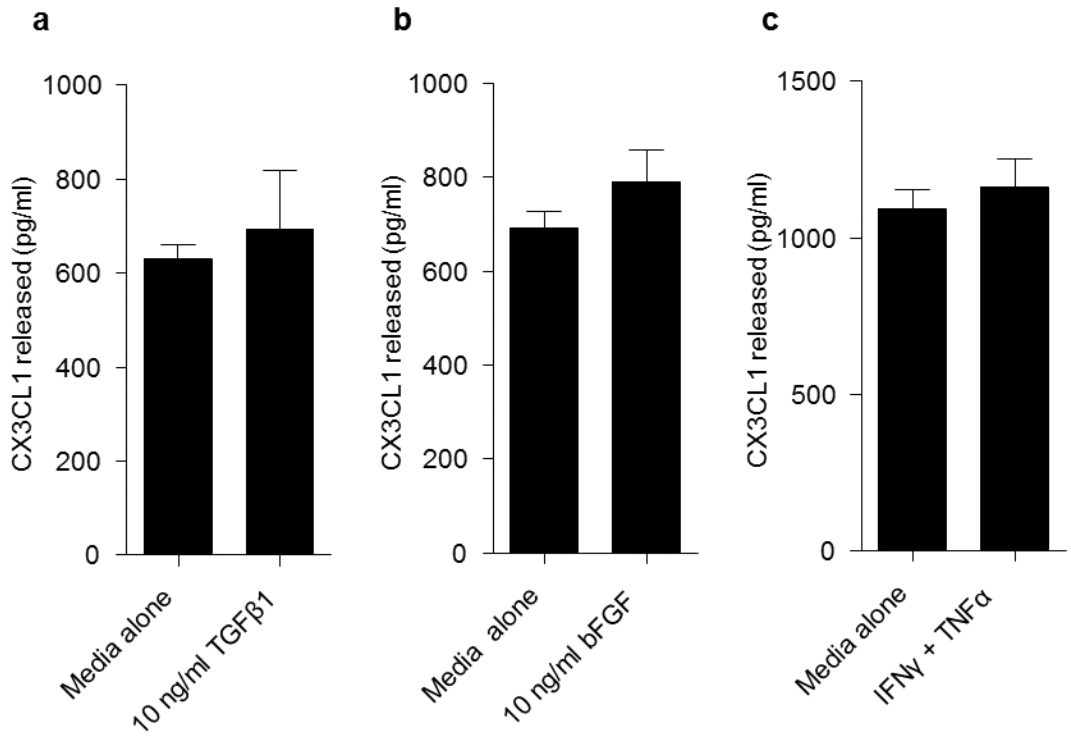

Figure 3-61. CX3CL1 production by human lung myofibroblasts

Human lung myofibroblast produce a substantial amount of CX3CL1 at baseline. Following either **a**) TGFβ1 (10ng/ml), **b**) bFGF (10 ng/ml), **c**) IFNγ plus TNFα (both 10 ng/ml) CX3CL1 production was not significantly increased.

4 Discussion

For the first time, it has been demonstrated that primary human lung myofibroblasts express the Ca^{2+}-activated K^+ channel $K_{Ca}3.1$ and that blocking this channel inhibits human lung myofibroblast function.

The role of the myofibroblast in IPF is paramount. These cells produce collagen and share features with both fibroblasts and smooth muscle cells, with evidence of a contractile phenotype and expression of αSMA. They localize to fibrotic foci and synthesise and deposit ECM proteins leading to the eventual destruction of alveolar-capillary units(11,178). Increases in myofibroblast numbers and fibrotic foci are associated with disease progression and a worsening prognosis(11). Targeting pro-fibrotic myofibroblast activity therefore offers the potential to slow down or halt the progression of IPF.

The widely accepted characterisation of a myofibroblast is that it co-expresses fibroblast-associated markers and αSMA fibres, but lacks the expression of the smooth muscle markers desmin and myosin(104,177). The cells developed in culture, in this study, strongly expressed both αSMA and two fibroblast markers, FSP and Thy-1, which are not expressed in smooth muscle cells(127,304). The cells were also negative for macrophage/monocyte and mesenchymal cell markers, CD68 and CD34. This indicated that there were no contaminating cells within the culture. In addition, a high proportion of the cells expressed functional $K_{Ca}3.1$ channels constitutively whereas these are rarely present in primary human

airway smooth muscle cells in the absence of TGFβ1 stimulation(275).

The expression of FSP and Thy-1 did not alter over passage although the cells began to lose their αSMA expression at passage 7, indicating a dedifferentiation from a myofibroblast to a fibroblast phenotype. The cells were therefore not used past passage 5. Myofibroblasts can vary in their phenotype and function depending on the lung region they were isolated. One study found that parenchymal fibroblasts were not only morphologically different to airway fibroblasts but displayed a more myofibroblast-like phenotype with increased αSMA expression and increased proliferation(126). This suggested that airway and parenchymal fibroblasts respond differently to injury and potentially control different lung activities. The same group went on to study the genomic differences between airway and parenchymal lung fibroblasts. They confirmed, using microarrays, that parenchymal lung fibroblasts are genomically distinct to airway fibroblasts, being myofibroblast-like and upregulating genes associated with actin binding and cytoskeletal organisation(110). Interestingly parenchymal fibroblasts exhibited significant increases in expression of TGFβ1 signalling molecules, SMAD3 and MAPK8, which are fundamental in myofibroblast differentiation(110). This work demonstrating that the cells cultured from human lung parenchyma exhibited features of a myofibroblast population is therefore highly consistent with these other

independent studies(110,126). It is also important to mention that the NFC myofibroblasts used in this study were isolated from lung resection tissue removed from lung cancer patients. Therefore, the tissue cannot be classified as entirely healthy. However, no morphological evidence of disease was evident, and so the myofibroblasts were classified as non-fibrotic. Although the drugs the donors were taking, priory to biopsy, were listed it was not possible to determine how these may affect the myofibroblasts used. However, as the cells had undergone 4 or 5 passages, it is assumed that any effects of the drugs should be minimal or non-existent.

A channel with properties resembling $K_{Ca}3.1$ has been described in mouse fibroblast cell lines(279), and $K_{Ca}3.1$ has been reported to be present in mouse renal fibroblasts(281). Here, it has been shown that $K_{Ca}3.1$ channel mRNA, protein and functional channels were expressed in myofibroblasts derived from both NFC and IPF donors. This was important to demonstrate as there are numerous examples of inter-species and intra-species heterogeneity with respect to cell phenotype. For example, rodent mast cells express robust Kir2.1 currents but these have never been seen in any human mast cell(305).

In both human and rat multiple splice variants of the $K_{Ca}3.1$ channel protein have been described. The predicted weight of the $K_{Ca}3.1$ channel is 48KDa; however, multiple splice variants of the $K_{Ca}3.1$ channel protein have been identified with molecular weights of

36, 33 and 32 kDa, and bands of 53kDa, perhaps relating to glycosylation have been reported frequently(275,297). Proteins isolated from human lymphoid tissues displayed two bands with molecular weights of 36 and 48 kDa. Similarly in mice and rats, bands specific for $K_{Ca}3.1$ channel are observed with molecular weights of 50, 48 and 25 kDa, indicating that splice variants are found in different species although the patterns may vary(297). Both human lung fibrocytes and airway smooth cells have demonstrated $K_{Ca}3.1$ channel protein with a molecular weight of 53 kDa. Using 3 different $K_{Ca}3.1$ channel antibodies, several different proteins of different molecular weights within human lung myofibroblasts were detected which have not previously been described. The $K_{Ca}3.1$ channel protein at a molecular weight of 48 kDa was detected with all three antibodies, which is described as the most dominant variant across species and tissues(297). However, dependent on the antibody, bands at 36 and 53kDa were also found consistent with human lung fibrocytes, smooth muscle cells and lymphoid tissue. The underlying mechanism generating these alternative splice variants has not to date been studied, however, it is likely that the alternative splicing of $K_{Ca}3.1$ channel protein plays a pivotal role in its physiological and pathophysiological function.

At baseline, human lung myofibroblasts expressed Kir2.0-like currents and these were significantly increased in IPF cells (42% NFC and 69% of IPF). Kir channels are strongly inwardly rectifying

channels selective for K^+. Typically Kir channels generate large K^+ conductance's at potentials negative to K^+ reversal potential, but permit less current flow at potentials positive to the K^+ reversal potential. Kir channels have been found in bronchial smooth muscle (306,307), and ventricular fibroblasts and myofibroblasts(308). In both of these cell types, it is implicated in regulating the resting membrane potential, proliferation and contractile responses(306-308). To date the channel has not been investigated in human parenchymal lung myofibroblasts or its role in IPF. These observations suggest that further investigation of its role in IPF would be interesting.

$K_{Ca}3.1$ channel currents were not evident in human lung myofibroblasts at baseline but were readily elicited following the addition of the $K_{Ca}3.1$ opener 1-EBIO in both NFC and IPF cells. Interestingly, $K_{Ca}3.1$ currents were present more frequently in IPF lung myofibroblasts and these currents were larger when compared to NFC lung myofibroblasts. This might reflect $K_{Ca}3.1$ up-regulation driven by the initiating disease insult in vivo, but the cells studied had been through 4 passages of culture, raising the possibility of an underlying disease-predisposing difference in myofibroblast $K_{Ca}3.1$ activity in patients with IPF. Surprisingly, although $K_{Ca}3.1$ currents were increased in IPF myofibroblasts, $K_{Ca}3.1$ mRNA was decreased. Chronic exposure of cells to the $K_{Ca}3.1$ opener 1-EBIO downregulates $K_{Ca}3.1$ mRNA expression(309), suggesting a negative-feedback

mechanism. It is therefore possible that the decreased mRNA expression signifies a failed attempt by IPF myofibroblasts to downregulate membrane channel expression. Whether the increased $K_{Ca}3.1$ plasma membrane expression in IPF myofibroblasts represents increased trafficking to the cell membrane or decreased turnover, requires further study.

The $K_{Ca}3.1$ channel was expressed in human lung tissue from both NFC and IPF patients. $K_{Ca}3.1$ expression co-localised to αSMA staining indicating the presence of myofibroblasts, which were primarily located in the dense fibrotic areas and fibroblast foci. Heavy $K_{Ca}3.1$ staining was also discovered in the IPF epithelium, perhaps indicating that the $K_{Ca}3.1$ channel could be involved in the process of EMT. Evidence of the $K_{Ca}3.1$ channel expression in human lung IPF tissue has not previously been reported. However, it has been reported in healthy tissues and tissues undergoing remodelling, and $K_{Ca}3.1$ channel blockers have demonstrated the ability to attenuate pathological processes. For example, $K_{Ca}3.1$ expression was increased in coronary vessels from patients with atherosclerosis(278), a process where thickening of the arterial wall is associated with VSMC activation and myofibroblast migration, proliferation and secretion(310). Mice reared with a genetic predisposition to atherosclerosis had reduced pathology when administered the $K_{Ca}3.1$ blockers TRAM-34 and clotrimazole, with suppressed VSMC proliferation and migration(278). In addition, a

swine model demonstrated that injury induced by balloon angioplasty, characterised by smooth muscle cell hyperplasis and subsequent restenosis, increased $K_{Ca}3.1$ channel mRNA and protein expression. Coating the balloons with TRAM-34 reduced subsequent restenosis(277).

TGFβ1 is a key mediator of fibrotic diseases. It plays an important role in fibroblast to myofibroblast differentiation(311), stimulates ECM protein production(105,134,135), and promotes epithelial-mesenchymal transition(199). Upon stimulation with TGFβ1, there was up-regulation of myofibroblast $K_{Ca}3.1$ mRNA expression, which was greatest in IPF-derived myofibroblasts (at least 10 fold). This is in keeping with previous work which found human ASM cells had increased $K_{Ca}3.1$ channel mRNA expression following 24 hours of TGFβ1 stimulation(275). TGFβ1 not only increased mRNA expression of the $K_{Ca}3.1$ channel in both NFC and IPF cells, it also increased frequency of cells expressing functional membrane $K_{Ca}3.1$ channels. Upon stimulation with TGFβ1 100% of IPF cells expressed $K_{Ca}3.1$ channels.

bFGF, another key mediator in fibrotic diseases, is a potent chemoattractant, mitogen and growth factor for myofibroblasts, and regulates extracellular matrix production and myofibroblast differentiation(160,208,210). In human lung myofibroblasts, it was found that bFGF stimulation led to up-regulation of myofibroblast

$K_{Ca}3.1$ mRNA expression, and although this was not significant, the increase was greatest in IPF donors (approximately 5 fold). bFGF also significantly increased the frequency of cells expressing $K_{Ca}3.1$ currents. These observations are in keeping with previous studies which demonstrate that bFGF upregulates $K_{Ca}3.1$ expression in several cell types. Both, bFGF-stimulated mouse renal fibroblasts and human lung ASM cells upregulated $K_{Ca}3.1$ channel mRNA in comparison to non-stimulated cells(275,281). The consistent upregulation of functional $K_{Ca}3.1$ channels by both TGFβ1 and bFGF suggests that the biological effects of these growth factors might rely heavily on $K_{Ca}3.1$ channel activity.

Myofibroblast proliferation was significantly increased by both bFGF and FBS. However, neither bFGF nor FBS-dependent proliferation was attenuated by $K_{Ca}3.1$ channel block, with either TRAM-34 or ICA-17043. Cell proliferation induced by bFGF relies on the P13K/AKT pathway, the RAS pathway and phosphorylation of SMAD2/3/4, which have all been shown to be Ca^{2+} independent, therefore $K_{Ca}3.1$ channel block might not be expected to inhibit proliferation(312-314). Previous work has shown that $K_{Ca}3.1$ channel block inhibits bFGF-stimulated proliferation in mouse renal fibroblasts(281). Yet, their method could not conclude that the results were from additional effects of $K_{Ca}3.1$ inhibition such as effects on cell volume regulation rather than proliferation(281). Nevertheless, these results demonstrate an important difference

between human lung myofibroblasts and mouse renal fibroblasts, and demonstrate the importance of studying cells from the species and tissue of interest.

Using a 2D wound healing assay the myofibroblast repair response was investigated. As this is only a 2D assay this does not necessarily reflect wound healing within the lung. A 3D assay including damage to the epithelial cells might be more (patho)physiological. Though, the 2D assay allows us to readily monitor the myofibroblast repair response to stress and pro-fibrotic mediators. The myofibroblast repair response was increased by bFGF and FBS, and both increased myofibroblast proliferation and migration(78,137,147). Both TRAM-34 and ICA-17043 inhibited myofibroblast wound repair. As neither blocked myofibroblast proliferation, it is likely that the effects seen were due to inhibition of myofibroblast migration into the wound. This would be in accordance with previous work demonstrating that $K_{Ca}3.1$ channel block inhibits the migration of many cells types, including the fibrocyte(298), a cell that contributes to the abundance of myofibroblasts found in the IPF lung(161). A migration assay was attempted using Transwell inserts, but this was poorly reproducible and therefore was not pursued. Consequently, the wound healing assay appeared to be the best method to assess myofibroblast migration.

In keeping with the literature, TGFβ1 significantly increased collagen secretion by both the NFC and IPF myofibroblasts. In contrast, bFGF had no effect on collagen secretion. TGFβ1-dependent collagen secretion was also markedly inhibited by $K_{Ca}3.1$ blockade. The fibrillar collagens, types I, II, III, V and XI account for the majority of excess extracellular matrix molecules accumulating in IPF tissue(2,184). TGFβ1 evokes Ca^{2+} waves in pulmonary fibroblasts which in turn amplified extracellular gene expression(315). This suggests that $K_{Ca}3.1$ channel block may inhibit the TGFβ1-induced Ca^{2+} waves through negation of the negative membrane potential generated by open $K_{Ca}3.1$ channels, and consequently inhibit collagen production and secretion. The ability of $K_{Ca}3.1$ block to inhibit the secretion of collagens and other potential ECM proteins could be vital in halting the progression of fibrosis in IPF lungs. Unfortunately, sircol assay technique does not detect the presence of collagen IV, which is also secreted by myofibroblasts(158).

Both bFGF and TGFβ1 increased human lung myofibroblast contraction. This ability of the cells to contract is an integral part of wound healing and an important factor leading to tissue contraction in fibrotic tissues including IPF lung. Increased concentrations of Ca^{2+} elicit rapid but transient responses in stress fibres, although myofibroblasts require long term contraction during tissue regeneration. Since $K_{Ca}3.1$ block also inhibited myofibroblast

contraction, it is likely that this also occurs through the disruption of Ca^{2+} signalling. This hypothesis will need testing in future work.

In addition, $K_{Ca}3.1$ channel block markedly inhibited myofibroblast αSMA expression which is also likely to contribute to the reduced contractile activity. The first theory behind this was that autocrine production of TGFβ1 was inhibited by the $K_{Ca}3.1$ blockers. However, the ELISA results were inconclusive as TRAM-34 did not inhibit production although ICA-17043 did. This work should be considered carefully as the experiments were only performed with a small number of donors. Further work is required to confirm the downregulation of αSMA by quantitative PCR and increased n numbers would be required to confirm whether $K_{Ca}3.1$ channel inhibition decreases autocrine production of TGFβ1. An alternative explanation could be that downregulation of αSMA occurs at the level of αSMA gene transcription which again could be confirmed using quantitative real time PCR.

To block $K_{Ca}3.1$ two distinct and selective blockers TRAM-34 and ICA-17043 were used(274). Importantly, TRAM-34 and ICA-17043 inhibited various cell processes at physiologically relevant concentrations. Thus, it takes 5-10x the K_d to inhibit almost all channels (K_d=concentration producing 50% block). The K_d for TRAM-34 is 20 nM(275) and for ICA-17043 6-10 nM(274). At 10x the K_d for both blockers, myofibroblast wound healing, collagen secretion and

contraction were significantly attenuated. At these concentrations both drugs are specific and not known to affect other ion channels, receptors or transporters(281,301). Furthermore, the effects of TRAM-34 and ICA-17043 on myofibroblast biology were not mimicked by TRAM-7 or TRAM-85, two molecules of similar structure to TRAM-34 which do not block $K_{Ca}3.1$ ion channels(276,281).

In view of the above discussion, it most likely that inhibitory effects of $K_{Ca}3.1$ blockers on myofibroblast function have occurred through the inhibition of K^+ flux through the $K_{Ca}3.1$ pore, which in turn has interfered with normal Ca^{2+} waves initiated by growth factor exposure. This is summarised in **Figure 4-1**.

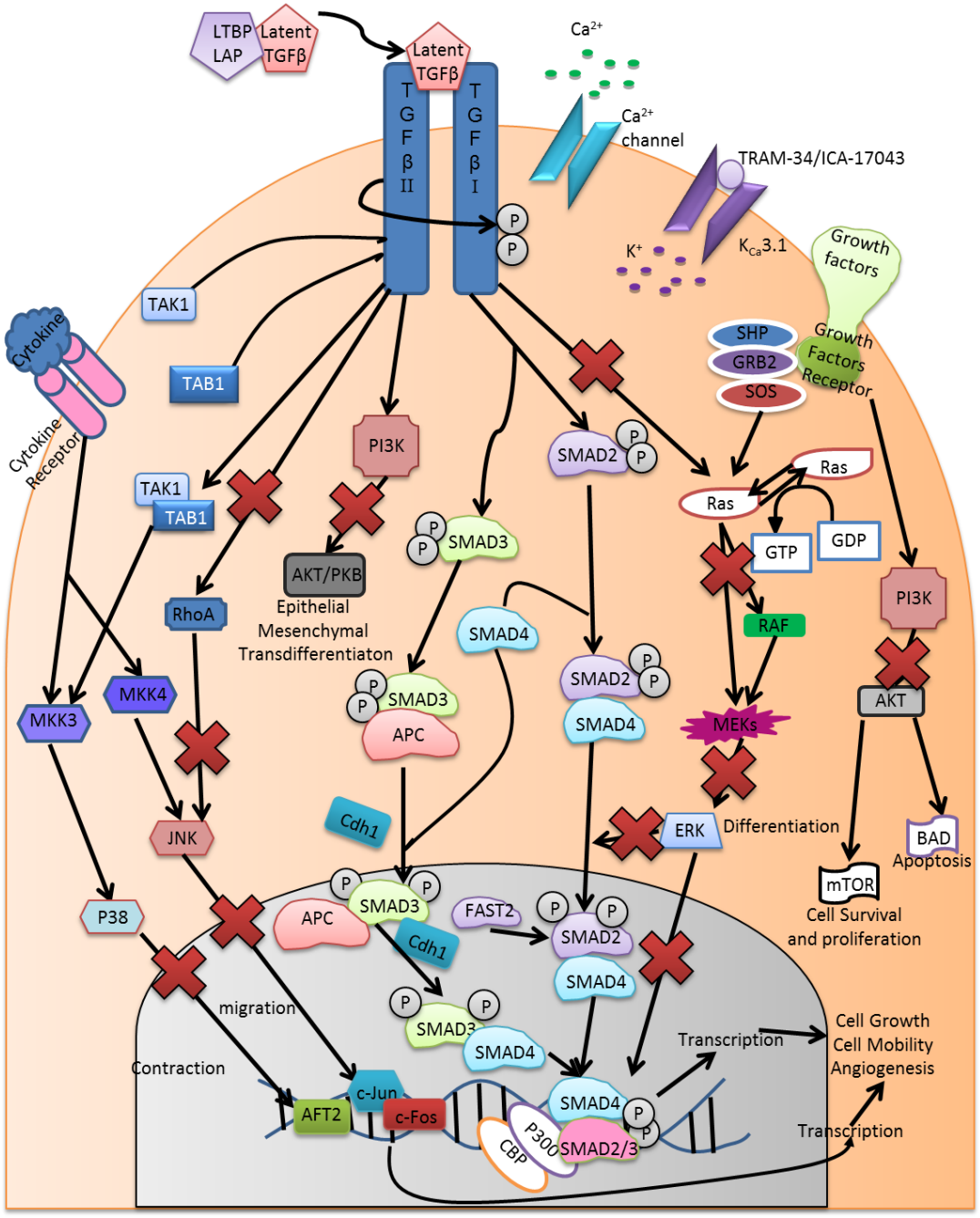

Figure 4-1. Processes which require an influx of Ca^{2+}

Processes that require an influx of Ca^{2+} and could potentially be blocked by $K_{Ca}3.1$ inhibition are highlighted with the red crosses. TGFβ1 causes immediate changes in Ca^{2+} influx, inducing Ca^{2+} release and intracellular Ca^{2+} oscillations which would most likely require the $K_{Ca}3.1$ channel(314).

Consequently, the majority of TGFβ1 signalling pathways could be inhibited by $K_{Ca}3.1$ channel however, SMAD phosphorylation is reportedly Ca^{2+} independent. Ca^{2+} influx is necessary for P38(316), RhoA(317) and Ras(318) activation. All pathways if inhibited could attenuate myofibroblast contraction, proliferation, migration and differentiation.

During this PhD, a collaboration with a group from the University of Glasgow who agreed to investigate the effectiveness of $K_{Ca}3.1$ blockade in the mouse model of bleomycin-induced pulmonary fibrosis. While this model does not induce the same myofibroblast foci seen in IPF, it is nevertheless useful for proof-of-principle studies aimed at inhibiting lung fibrosis(319).

The results from the Glasgow bleomycin studies are summarised in **Figure 4-2**. In brief, $K_{Ca}3.1$ immunostaining in the mouse matched that in human tissue in that it was widely expressed in both healthy mouse lung and in the fibrotic areas following bleomycin administration. As predicted from the vitro studies, TRAM-34 administered daily at a dose known to give relevant blood and tissue concentrations(281), improved survival and prevented weight loss, attenuated collagen deposition and reduced lung fibrosis. This protection was likely to have occurred at least in part through the inhibition of pro-fibrotic myofibroblast function. However, inhibition of other cells which express $K_{Ca}3.1$ such as alveolar epithelial cells and mast cells is possible. Furthermore, bleomycin-induced lung damage recruits fibrocytes which may also contribute to the fibrotic response. $K_{Ca}3.1$ inhibition markedly attenuates human fibrocyte migration(298), which may therefore, be relevant to the observed in vivo response.

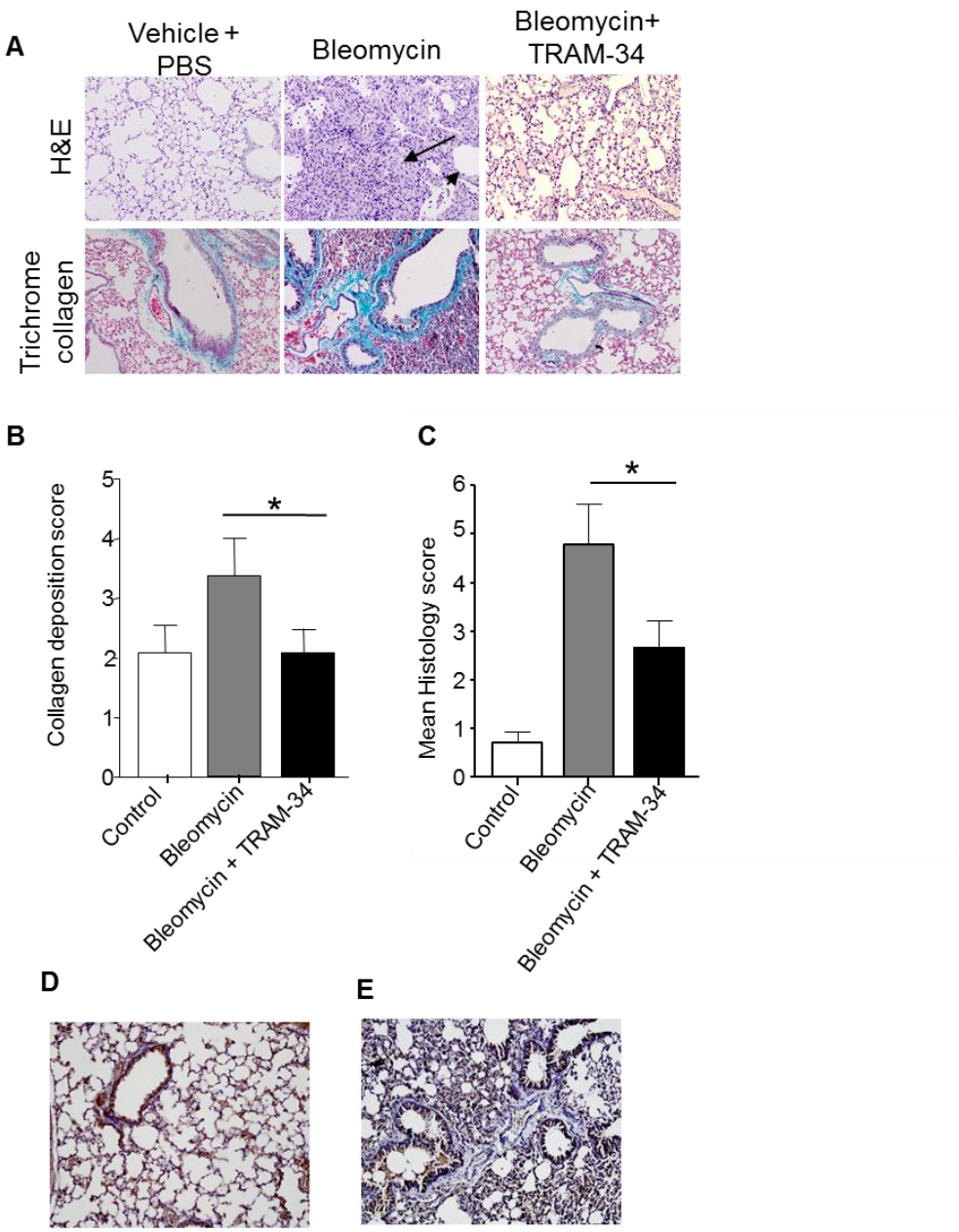

Figure 4-2. TRAM-34 attenuates bleomycin-induced lung fibrosis in vivo.

(**A**) Fibrosis was assessed in H&E-stained paraffin-embedded lung. In comparison to mice that received only vehicle and nasal PBS, bleomycin induced marked alteration of lung architecture, thickening of alveolar

septae (arrow head) and fibrotic foci (arrow). Treatment with intraperitoneal TRAM-for 21-days attenuated these bleomycin-dependent histological features of pulmonary fibrosis. (**B**) Collagen staining (Masson's trichrome stain) revealed increased collagen in lungs from mice exposed to nasal bleomycin, which was reduced by TRAM-34 treatment (*P*=0.046.)(**C**) A modified form of the score devised by Ashcroft et al was used to quantify the degree of histological visible lung fibrosis. TRAM-34 administration reduced the score induced by bleomycin alone (*P*=0.034). Immunohistochemical staining of $K_{Ca}3.1$ distribution in normal lung (**D**) and bleomycin exposed lung (**E**).

In summary, when taken together, the data indicate that the $K_{Ca}3.1$ channel may play a key role in the development of lung fibrosis, in both IPF and other lung disorders. $K_{Ca}3.1$ is an attractive pharmacological target as it appears to play a minor role in healthy physiology, but contributes significantly to tissue remodeling and fibrosis(266). $K_{Ca}3.1$ knockout mice are viable, of normal appearance, produce normal litter sizes, and exhibit rather mild phenotypes(276,282). High doses of TRAM-34 administered to rodents over many weeks are well tolerated(281), and the orally available $K_{Ca}3.1$ blocker, ICA-17043, has been administered to humans in phase 2 and 3 trials of sickle cell disease with minor side effects(265). There is therefore, the potential for the rapid investigation of $K_{Ca}3.1$ block in clinical trials of IPF and other fibrotic lung diseases.

4.1 Future Work

Previous work in primary human osteoblasts found TGFβ1 stimulation elicited rapid, transient and oscillatory rises in the intracellular Ca^{2+} concentration(314). This suggests intracellular Ca^{2+} signalling is an important component in TGFβ1 signal transduction pathways. Furthermore, TGFβ1 has been shown to evoke Ca^{2+} waves in human lung fibroblasts and that these waves increase collagen and fibronectin gene expression(315). It is therefore likely that both TGFβ1 and bFGF initiate an increase in intracellular Ca^{2+} concentrations in primary human lung parenchymal myofibroblasts, but further work is required to confirm this and to examine whether this is attenuated by $K_{Ca}3.1$ blockade. To investigate this, Ca^{2+} signalling in the myofibroblasts would be assessed upon TGFβ1 and bFGF stimulation ± $K_{Ca}3.1$ block using Ca^{2+} imaging techniques on single cells.

This study has also shown that $K_{Ca}3.1$ blockade inhibits many TGFβ1- and bFGF-dependent cell processes in human lung myofibroblasts, but the effects of $K_{Ca}3.1$ channel block on bFGF- and TGFβ1-dependent signal pathways are still unknown. Western blot and ELISA assays could be used to determine the magnitude and kinetics of the phosphorylation of the TGFβ1 receptor. It is unlikely that $K_{Ca}3.1$ channel block affects SMAD-2 phosphorylation and

transcription as previous work showed that intracellular Ca^{2+} is not required for these processes(314). However, this could be investigated along with other signalling pathways involving activation of P38, RhoA, and Ras.

Investigating the role of Kir currents in human lung myofibroblasts would be of interest. The work performed in ventricular fibroblasts and myofibroblasts suggests it plays a major role in fibroblast proliferation and contraction(308). Using Kir channel inhibitors such as Ba^{2+} and shRNA knockdown, proliferation assays and contraction assays could determine its role in IPF myofibroblasts.

The $K_{Ca}3.1$ channel was heavily expressed in the epithelium of IPF tissue. Thus, it is likely that the $K_{Ca}3.1$ channel plays a vital role in the process of EMT driven by TGFβ1. To investigate this, primary human airway epithelial cells and alveolar epithelial cells obtained from bronchial brushings and lung tissue respectively would be grown in the presence of TGFβ1. To assess EMT changes cell shape would be studied, looking for a shift from the typical epithelial morphology to a fibroblastic spindle-stellate shaped morphology. Using immunofluorescence and flow cytometry the loss of epithelial markers, E-Cadherin and Zo-1 and the induction of fibroblast markers Thy-1, FSP, vimentin and αSMA could also be investigated. If TGFβ1 induces EMT in human bronchial epithelial cells the effects of $K_{Ca}3.1$ block could be examined.

5 References

(1) Liebow AA. Definition and Classification of Interstitial Pneumonias in Human Pathology. ; 1975.

(2) Katzenstein AL, Myers JL. Idiopathic pulmonary fibrosis: clinical relevance of pathologic classification. Am J Respir Crit Care Med 1998 Apr;157(4 Pt 1):1301-1315.

(3) ATS, ERS. Idiopathic Pulmonary Fibrosis: Diagnosis and Treatment . International Consensus Statement. Am J Respir Crit Care Med 2000 February 1;161(2):646-664.

(4) Mueller-Mang C, Grosse C, Schmid K, Stiebellehner L, Bankier AA. What every radiologist should know about idiopathic interstitial pneumonias. Radiographics 2007 May-Jun;27(3):595-615.

(5) Raghu G, Weycker D, Edelsberg J, Bradford WZ, Oster G. Incidence and prevalence of idiopathic pulmonary fibrosis. Am J Respir Crit Care Med 2006 Oct 1;174(7):810-816.

(6) Flaherty KR, King TE,Jr, Raghu G, Lynch JP,3rd, Colby TV, Travis WD, et al. Idiopathic interstitial pneumonia: what is the effect of a multidisciplinary approach to diagnosis? Am J Respir Crit Care Med 2004 Oct 15;170(8):904-910.

(7) Raghu G, Collard HR, Egan JJ, Martinez FJ, Behr J, Brown KK, et al. An Official ATS/ERS/JRS/ALAT Statement: Idiopathic Pulmonary Fibrosis: Evidence-based Guidelines for Diagnosis and Management. Am J Respir Crit Care Med 2011 Mar 15;183(6):788-824.

(8) Schwartz DA, Helmers RA, Galvin JR, Van Fossen DS, Frees KL, Dayton CS, et al. Determinants of survival in idiopathic pulmonary fibrosis. Am J Respir Crit Care Med 1994 Feb;149(2 Pt 1):450-454.

(9) Gribbin J, Hubbard RB, Le Jeune I, Smith CJ, West J, Tata LJ. Incidence and mortality of idiopathic pulmonary fibrosis and sarcoidosis in the UK. Thorax 2006 Nov;61(11):980-985.

(10) Mannino DM, Etzel RA, Parrish RG. Pulmonary fibrosis deaths in the United States, 1979-1991. An analysis of multiple-cause mortality data. Am J Respir Crit Care Med 1996 May;153(5):1548-1552.

(11) King TE,Jr, Schwarz MI, Brown K, Tooze JA, Colby TV, Waldron JA,Jr, et al. Idiopathic pulmonary fibrosis: relationship between

histopathologic features and mortality. Am J Respir Crit Care Med 2001 Sep 15;164(6):1025-1032.

(12) Hubbard R, Johnston I, Britton J. Survival in patients with cryptogenic fibrosing alveolitis: a population-based cohort study. Chest 1998 Feb;113(2):396-400.

(13) Meltzer EB, Noble PW. Idiopathic pulmonary fibrosis. Orphanet J Rare Dis 2008 Mar 26;3:8.

(14) Selman M, King TE, Pardo A, American Thoracic Society, European Respiratory Society, American College of Chest Physicians. Idiopathic pulmonary fibrosis: prevailing and evolving hypotheses about its pathogenesis and implications for therapy. Ann Intern Med 2001 Jan 16;134(2):136-151.

(15) Harari S, Caminati A. IPF: new insight on pathogenesis and treatment. Allergy 2010 May;65(5):537-553.

(16) Baumgartner KB, Samet JM, Stidley CA, Colby TV, Waldron JA. Cigarette smoking: a risk factor for idiopathic pulmonary fibrosis. Am J Respir Crit Care Med 1997 Jan;155(1):242-248.

(17) Scott J, Johnston I, Britton J. What causes cryptogenic fibrosing alveolitis? A case-control study of environmental exposure to dust. BMJ 1990 Nov 3;301(6759):1015-1017.

(18) Billings CG, Howard P. Hypothesis: exposure to solvents may cause fibrosing alveolitis. Eur Respir J 1994 Jun;7(6):1172-1176.

(19) Iwai K, Mori T, Yamada N, Yamaguchi M, Hosoda Y. Idiopathic pulmonary fibrosis. Epidemiologic approaches to occupational exposure. Am J Respir Crit Care Med 1994 Sep;150(3):670-675.

(20) Han MK. High prevalence of abnormal acid gastro-oesophageal reflux in idiopathic pulmonary fibrosis. Eur Respir J 2006 Oct;28(4):884-5; author reply 885.

(21) Gauldie J, Jordana M, Cox G. Cytokines and pulmonary fibrosis. Thorax 1993 Sep;48(9):931-935.

(22) Arase Y, Suzuki F, Suzuki Y, Akuta N, Kobayashi M, Kawamura Y, et al. Hepatitis C virus enhances incidence of idiopathic pulmonary fibrosis. World J Gastroenterol 2008 Oct 14;14(38):5880-5886.

(23) Manika K, Alexiou-Daniel S, Papakosta D, Papa A, Kontakiotis T, Patakas D, et al. Epstein-Barr virus DNA in bronchoalveolar lavage

fluid from patients with idiopathic pulmonary fibrosis. Sarcoidosis Vasc Diffuse Lung Dis 2007 Sep;24(2):134-140.

(24) Mageto YN, Raghu G. Genetic predisposition of idiopathic pulmonary fibrosis. Curr Opin Pulm Med 1997 Sep;3(5):336-340.

(25) Wise AL, Schwartz DA. Pulmonary Fibrosis, Familial. 1993.

(26) Zantour B, Knani J, Boudawara N, Boussoffara L, Jerbi S, Hamza H, et al. Familial idiopathic pulmonary fibrosis associated with autoimmune polyendocrinopathy and epidermodysplasia verruciformis. Rev Pneumol Clin 2010 Apr;66(2):127-131.

(27) Alhamad EH. Familial interstitial lung disease in four members of one family: a case series. Cases J 2009 Dec 19;2:9356.

(28) Mason RJ, Schwarz MI, Hunninghake GW, Musson RA. NHLBI Workshop Summary. Pharmacological therapy for idiopathic pulmonary fibrosis. Past, present, and future. Am J Respir Crit Care Med 1999 Nov;160(5 Pt 1):1771-1777.

(29) Flaherty KR, Colby TV, Travis WD, Toews GB, Mumford J, Murray S, et al. Fibroblastic Foci in Usual Interstitial Pneumonia. American Journal of Respiratory and Critical Care Medicine 2003 May 15;167(10):1410-1415.

(30) Chandler PW, Shin MS, Friedman SE, Myers JL, Katzenstein AL. Radiographic Manifestations of Bronchiolitis Obliterans with Organizing Pneumonia Vs Usual Interstitial Pneumonia. Am J Roentgenol 1986 NOV 1986;147(5):899-906.

(31) King TE, Collard HR. Idiopathic Pulmonary Fibrosis. Available at: http://www.cyberounds.com/cmecontent/art295.html?pf=yes. Accessed 09/05, 2012.

(32) Douglas WW, Ryu JH, Schroeder DR. Idiopathic pulmonary fibrosis: Impact of oxygen and colchicine, prednisone, or no therapy on survival. Am J Respir Crit Care Med 2000 Apr;161(4 Pt 1):1172-1178.

(33) Raghu G, Depaso WJ, Cain K, Hammar SP, Wetzel CE, Dreis DF, et al. Azathioprine combined with prednisone in the treatment of idiopathic pulmonary fibrosis: a prospective double-blind, randomized, placebo-controlled clinical trial. Am Rev Respir Dis 1991 Aug;144(2):291-296.

(34) Johnson MA, Kwan S, Snell NJ, Nunn AJ, Darbyshire JH, Turner-Warwick M. Randomised controlled trial comparing prednisolone

alone with cyclophosphamide and low dose prednisolone in combination in cryptogenic fibrosing alveolitis. Thorax 1989 Apr;44(4):280-288.

(35) Douglas WW, Ryu JH, Swensen SJ, Offord KP, Schroeder DR, Caron GM, et al. Colchicine versus prednisone in the treatment of idiopathic pulmonary fibrosis. A randomized prospective study. Members of the Lung Study Group. Am J Respir Crit Care Med 1998 Jul;158(1):220-225.

(36) Raghu G, Brown KK, Bradford WZ, Starko K, Noble PW, Schwartz DA, et al. A placebo-controlled trial of interferon gamma-1b in patients with idiopathic pulmonary fibrosis. N Engl J Med 2004 Jan 8;350(2):125-133.

(37) King TE,Jr, Behr J, Brown KK, du Bois RM, Lancaster L, de Andrade JA, et al. BUILD-1: a randomized placebo-controlled trial of bosentan in idiopathic pulmonary fibrosis. Am J Respir Crit Care Med 2008 Jan 1;177(1):75-81.

(38) Demedts M, Behr J, Buhl R, Costabel U, Dekhuijzen R, Jansen HM, et al. High-dose acetylcysteine in idiopathic pulmonary fibrosis. N Engl J Med 2005 Nov 24;353(21):2229-2242.

(39) Kubo H, Nakayama K, Yanai M, Suzuki T, Yamaya M, Watanabe M, et al. Anticoagulant therapy for idiopathic pulmonary fibrosis. Chest 2005 Sep;128(3):1475-1482.

(40) Ziesche R, Hofbauer E, Wittmann K, Petkov V, Block LH. A preliminary study of long-term treatment with interferon gamma-1b and low-dose prednisolone in patients with idiopathic pulmonary fibrosis. N Engl J Med 1999 Oct 21;341(17):1264-1269.

(41) Shane E, Silverberg SJ, Donovan D, Papadopoulos A, Staron RB, Addesso V, et al. Osteoporosis in lung transplantation candidates with end-stage pulmonary disease. Am J Med 1996 Sep;101(3):262-269.

(42) Munson JC, Kreider M, Chen Z, Christie JD, Kimmel SE. EFFECT OF TREATMENT GUIDELINES ON THE INITIAL MANAGEMENT OF IDIOPATHIC PULMONARY FIBROSIS. Br J Clin Pharmacol 2010;9999(999A).

(43) Raghu G, Johnson W, Lockhart D, Mageto Y. Treatment of idiopathic pulmonary fibrosis with a new antifibrotic agent, pirfenidone - Results of a prospective, open-label phase II study. American Journal of Respiratory and Critical Care Medicine 1999 APR;159(4):1061-1069.

(44) Noble PW, Albera C, Bradford WZ, Costabel U, Glassberg MK, Kardatzke D, et al. Pirfenidone in patients with idiopathic pulmonary fibrosis (CAPACITY): two randomised trials. Lancet 2011 MAY 21;377(9779):1760-1769.

(45) Carter NJ. Pirfenidone In Idiopathic Pulmonary Fibrosis. Drugs 2011;71(13):1721-1732.

(46) Raghu G. Idiopathic pulmonary fibrosis: treatment options in pursuit of evidence-based approaches. Eur Respir J 2006 September 1;28(3):463-465.

(47) Collard HR, King TE,Jr. Treatment of idiopathic pulmonary fibrosis: the rise and fall of corticosteroids. Am J Med 2001 Mar;110(4):326-328.

(48) B. T. Society and S. O. Commitee. The diagnosis, assessment and treatment of diffuse parenchymal lung disease in adults. Introduction. Thorax 1999 Apr;54 Suppl 1:S1-14.

(49) Wells AU, Behr J, Costabel U, Cottin V, Poletti V. Triple therapy in idiopathic pulmonary fibrosis: an alarming press release. European Respiratory Journal 2012 April 01;39(4):805-806.

(50) McGrath EE, Millar AB. Hot off the breath: triple therapy for idiopathic pulmonary fibrosis-hear the PANTHER roar. Thorax 2012 FEB;67(2):97-98.

(51) Raghu G, Anstrom KJ, King TE, Jr., Lasky JA, Martinez FJ, Idiopathic Pulm Fibrosis Clinical. Prednisone, Azathioprine, and N-Acetylcysteine for Pulmonary Fibrosis. N Engl J Med 2012 MAY 24;366(21):1968-1977.

(52) Carbone R, Bottino G, Paredi P, Shah P, Meyer KC. Predictors of survival in idiopathic interstitial pneumonia. Eur Rev Med Pharmacol Sci 2010 AUG 2010;14(8):695-704.

(53) Collard HR, King TE, Bartelson BB, Vourlekis JS, Schwarz MI, Brown KK. Changes in clinical and physiologic variables predict survival in idiopathic pulmonary fibrosis. American Journal of Respiratory and Critical Care Medicine 2003 SEP 1 2003;168(5):538-542.

(54) Latsi PI, du Bois RM, Nicholson AG, Colby TV, Bisirtzoglou D, Nikolakopoulou A, et al. Fibrotic idiopathic interstitial pneumonia - The prognostic value of longitudinal functional trends. American Journal of Respiratory and Critical Care Medicine 2003 SEP 1 2003;168(5):531-537.

(55) Caminati A, Bianchi A, Cassandro R, Mirenda MR, Harari S. Walking distance on 6-MWT is a prognostic factor in idiopathic pulmonary fibrosis. Respir Med 2009 JAN 2009;103(1):117-123.

(56) Lettieri CJ, Nathan SD, Barnett SD, Ahmad S, Shorr AF. Prevalence and outcomes of pulmonary arterial hypertension in advanced idiopathic pulmonary fibrosis. Chest 2006 MAR 2006;129(3):746-752.

(57) Vignaud J, Allam M, Martinet N, Pech M, Plenat F, Martinet Y. Presence of Platelet-derived Growth Factor in Normal and Fibrotic Lung Is Specifically Associated with Interstitial Macrophages, While Both Interstitial Macrophages and Alveolar Epithelial Cells Express the c-sis Proto-oncogene. American Journal of Respiratory Cell and Molecular Biology 1991 December 01;5(6):531-538.

(58) Madtes DK, Busby HK, Strandjord TP, Clark JG. Expression of transforming growth factor-alpha and epidermal growth factor receptor is increased following bleomycin-induced lung injury in rats. American Journal of Respiratory Cell and Molecular Biology 1994 November 01;11(5):540-551.

(59) Khalil N, Oconnor R, Unruh H, Warren P, Flanders K, Kemp A, et al. Increased Production and Immunohistochemical Localization of Transforming Growth-Factor-Beta in Idiopathic Pulmonary Fibrosis. American Journal of Respiratory Cell and Molecular Biology 1991 AUG;5(2):155-162.

(60) Kline J, Schwartz D, Monick M, Floerchinger C, Hunninghake G. Relative Release of Interleukin-1-Beta and Interleukin-1 Receptor Antagonist by Alveolar Macrophages - a Study in Asbestos-Induced Lung-Disease, Sarcoidosis, and Idiopathic Pulmonary Fibrosis. Chest 1993 JUL;104(1):47-53.

(61) Zhang Y, Lee TC, Guillemin B, Yu MC, Rom WN. Enhanced IL-1 beta and tumor necrosis factor-alpha release and messenger RNA expression in macrophages from idiopathic pulmonary fibrosis or after asbestos exposure. The Journal of Immunology 1993 May 01;150(9):4188-4196.

(62) Mornex J, Martinet Y, Yamauchi K, Bitterman P, Grotendorst G, Chytilweir A, et al. Spontaneous Expression of the C-Sis Gene and Release of a Platelet-Derived Growth Factorlike Molecule by Human Alveolar Macrophages. J Clin Invest 1986 JUL;78(1):61-66.

(63) Higashiyama S, Abraham JA, Miller J, Fiddes JC, Klagsbrun M. A Heparin-Binding Growth-Factor Secreted by Macrophage-Like Cells that is Related to Egf. Science 1991 FEB 22 1991;251(4996).

(64) Rappolee D, Mark D, Banda M, Werb Z. Wound Macrophages Express Tgf-Alpha and Other Growth-Factors Invivo - Analysis by Messenger-Rna Phenotyping. Science 1988 AUG 5;241(4866):708-712.

(65) Inoue Y, King TE,Jr, Tinkle SS, Dockstader K, Newman LS. Human mast cell basic fibroblast growth factor in pulmonary fibrotic disorders. Am J Pathol 1996 Dec;149(6):2037-2054.

(66) Ando M, Miyazaki E, Fukami T, Kumamoto T, Tsuda T. Interleukin-4-producing cells in idiopathic pulmonary fibrosis: an immunohistochemical study. Respirology 1999 1999-Dec;4(4).

(67) Chiaramonte MG, Donaldson DD, Cheever AW, Wynn TA. An IL-13 inhibitor blocks the development of hepatic fibrosis during a T-helper type 2-dominated inflammatory response. J Clin Invest 1999 SEP 1999;104(6).

(68) du Bois RM. Strategies for treating idiopathic pulmonary fibrosis. Nat Rev Drug Discov 2010 Feb;9(2):129-140.

(69) Kasai H, Allen JT, Mason RM, Kamimura T, Zhang Z. TGF-beta1 induces human alveolar epithelial to mesenchymal cell transition (EMT). Respir Res 2005 Jun 9;6:56.

(70) Khouw IMSL, van Wachem PB, Plantinga JA, Vujaskovic Z, J.B. Wissink M, de Leij LFMH, et al. TGF-β and bFGF affect the differentiation of proliferating porcine fibroblasts into myofibroblasts in vitro. Biomaterials 1999 10;20(19):1815-1822.

(71) Raghu G, Masta S, Meyers D, Narayanan AS. Collagen Synthesis by Normal and Fibrotic Human Lung Fibroblasts and the Effect of Transforming Growth Factor-β. American Journal of Respiratory and Critical Care Medicine 1989 July 01;140(1):95-100.

(72) Strutz F, Zeisberg M, Renziehausen A, Raschke B, Becker V, van Kooten C, et al. TGF-beta 1 induces proliferation in human renal fibroblasts via induction of basic fibroblast growth factor (FGF-2). Kidney Int 2001 Feb;59(2):579-592.

(73) Henke C, Marineli W, Jessurun J, Fox J, Harms D, Peterson M, et al. Macrophage Production of Basic Fibroblast Growth-Factor in the Fibroproliferative Disorder of Alveolar Fibrosis After Lung Injury. Am J Pathol 1993 OCT;143(4):1189-1199.

(74) Latina MA. Interferon-gamma inhibits collagen synthesis by human tenon's capsule fibroblasts in vitro. Invest Ophthalmol Vis Sci 1992 1992-Nov;33(12).

(75) Solisherruzo JA, Brenner DA, Chojkier M. Tumor Necrosis Factor-Alpha Inhibits Collagen Gene-Transcription and Collagen-Synthesis in Cultured Human-Fibroblasts. J Biol Chem 1988 APR 25 1988;263(12).

(76) Postlethwaite AE, Seyer JM. Stimulation of Fibroblast Chemotaxis by Human Recombinant Tumor-Necrosis-Factor-Alpha (Tnf-Alpha) and a Synthetic Tnf-Alpha 31-68 Peptide. J Exp Med 1990 DEC 1 1990;172(6).

(77) Bonner JC. Regulation of PDGF and its receptors in fibrotic diseases. Cytokine Growth Factor Rev 2004 AUG 2004;15(4).

(78) Chaudhary NI, Roth GJ, Hilberg F, Mueller-Ouernheim J, Prasse A, Zissel G, et al. Inhibition of PDGF, VEGF and FGF signalling attenuates fibrosis. European Respiratory Journal 2007 MAY;29(5):976-985.

(79) Antoniu SA, Kolb MRJ. Intedanib, a triple kinase inhibitor of VEGFR, FGFR and PDGFR for the treatment of cancer and idiopathic pulmonary fibrosis. Idrugs 2010 MAY;13(5):332-345.

(80) Rubbiabrandt L, Sappino AP, Gabbiani G. Locally Applied Gm-Csf Induces the Accumulation of Alpha-Smooth Muscle Actin Containing Myofibroblasts. Virchows Archiv B-Cell Pathology Including Molecular Pathology 1991 1991;60(2).

(81) Lembach KJ. Induction of Human Fibroblast Proliferation by Epidermal Growth-Factor (Egf) - Enhancement by an Egf-Binding Arginine Esterase and by Ascorbate. Proc Natl Acad Sci U S A 1976 1976;73(1).

(82) Frazier K, Williams S, Kothapalli D, Klapper H, Grotendorst GR. Stimulation of fibroblast cell growth, matrix production, and granulation tissue formation by connective tissue growth factor. J Invest Dermatol 1996 SEP 1996;107(3).

(83) Pilewski JM, Liu LX, Henry AC, Knauer AV, Feghali-Bostwick CA. Insulin-like growth factor binding proteins 3 and 5 are overexpressed in idiopathic pulmonary fibrosis and contribute to extracellular matrix deposition. Am J Pathol 2005 FEB 2005;166(2):399-407.

(84) Murray LA, Argentieri RL, Farrell FX, Bracht M, Sheng H, Whitaker B, et al. Hyper-responsiveness of IPF/UIP fibroblasts: interplay between TGFbeta1, IL-13 and CCL2. Int J Biochem Cell Biol 2008;40(10):2174-2182.

(85) Ishida Y, Kimura A, Kondo T, Hayashi T, Ueno M, Takakura N, et al. Essential roles of the CC chemokine ligand 3-CC chemokine receptor 5 axis in bleomycin-induced pulmonary fibrosis through regulation of macrophage and fibrocyte infiltration. Am J Pathol 2007 MAR 2007;170(3).

(86) Capelli A, Di Stefano A, Gnemmi I, Donner CF. CCR5 expression and CC chemokine levels in idiopathic pulmonary fibrosis. European Respiratory Journal 2005 APR 2005;25(4).

(87) Huaux F, Gharaee-Kermani M, Liu T, Morel V, McGarry B, Ullenbruch M, et al. Role of Eotaxin-1 (CCL11) and CC Chemokine Receptor 3 (CCR3) in Bleomycin-Induced Lung Injury and Fibrosis. The American Journal of Pathology 2005 12;167(6):1485-1496.

(88) Moore BB, Murray L, Das A, Wilke CA, Herrygers AB, Toews GB. The role of CCL12 in the recruitment of fibrocytes and lung fibrosis. American Journal of Respiratory Cell and Molecular Biology 2006 AUG 2006;35(2).

(89) Pechkovsky DV, Prasse A, Kollert F, Engel KMY, Dentler J, Luttmann W, et al. Alternatively activated alveolar macrophages in pulmonary fibrosis-mediator production and intracellular signal transduction. Clinical Immunology 2010 OCT 2010;137(1).

(90) Yogo Y, Fujishima S, Inoue T, Saito F, Shiomi T, Yamaguchi K, et al. Macrophage derived chemokine (CCL22), thymus and activation-regulated chemokine (CCL17), and CCR4 in idiopathic pulmonary fibrosis. Respiratory Research 2009 AUG 29 2009;10:80.

(91) Isozaki T, Otsuka K, Sato M, Takahashi R, Wakabayashi K, Yajima N, et al. Synergistic induction of CX3CL1 by interleukin-1 beta and interferon-gamma in human lung fibroblasts: involvement of signal transducer and activator of transcription 1 signaling pathways. Transl Res 2011 FEB;157(2):64-70.

(92) Jiang D, Liang J, Campanella GS, Guo R, Yu S, Xie T, et al. Inhibition of pulmonary fibrosis in mice by CXCL10 requires glycosaminoglycan binding and syndecan-4. J Clin Invest 2010 Jun 1;120(6):2049-2057.

(93) Tager AM, Kradin RL, LaCamera P, Bercury SD, Campanella GS, Leary CP, et al. Inhibition of pulmonary fibrosis by the chemokine IP-10/CXCL10. Am J Respir Cell Mol Biol 2004 Oct;31(4):395-404.

(94) Burdick MD, Murray LA, Keane MP, Xue YY, Zisman DA, Belperio JA, et al. CXCL11 attenuates bleomycin-induced pulmonary fibrosis

via inhibition of vascular remodeling. American Journal of Respiratory and Critical Care Medicine 2005 FEB 1 2005;171(3).

(95) Belperio JA, Keane MP, Burdick MD, Lynch JP, Zisman DA, Xue YY, et al. Role of CXCL9/CXCR3 chemokine biology during pathogenesis of acute lung allograft rejection. Journal of Immunology 2003 NOV 1 2003;171(9).

(96) Huaux F, Liu TJ, McGarry B, Ullenbruch M, Phan SH. Dual roles of IL-4 in lung injury and fibrosis. Journal of Immunology 2003 FEB 15 2003;170(4).

(97) Saito F, Tasaka S, Inoue K, Miyamoto K, Nakano Y, Ogawa Y, et al. Role of interleukin-6 in bleomycin-induced lung inflammatory changes in mice. American Journal of Respiratory Cell and Molecular Biology 2008 MAY 2008;38(5).

(98) Arai T, Abe K, Matsuoka H, Yoshida M, Mori M, Goya S, et al. Introduction of the interleukin-10 gene into mice inhibited bleomycin-induced lung injury in vivo. American Journal of Physiology-Lung Cellular and Molecular Physiology 2000 MAY 2000;278(5).

(99) Saito A, Okazaki H, Sugawara I, Yamamoto K, Takizawa H. Potential action of IL-4 and IL-13 as fibrogenic factors on lung fibroblasts in vitro. Int Arch Allergy Immunol 2003 OCT 2003;132(2).

(100) Ziegenhagen MW, Zabel P, Zissel G, Schlaak M, Muller-Quernheim J. Serum level of interleukin 8 is elevated in idiopathic pulmonary fibrosis and indicates disease activity. American Journal of Respiratory and Critical Care Medicine 1998 MAR 1998;157(3).

(101) Gabbiani G, Ryan GB, Majno G. Presence of Modified Fibroblasts in Granulation Tissue and their Possible Role in Wound Contraction. Experientia 1971 1971;27(5).

(102) Kuhn C, McDonald JA. The roles of the myofibroblast in idiopathic pulmonary fibrosis. Ultrastructural and immunohistochemical features of sites of active extracellular matrix synthesis. Am J Pathol 1991 May;138(5):1257-1265.

(103) Zhang K, Rekhter MD, Gordon D, Phan SH. Myofibroblasts and their role in lung collagen gene expression during pulmonary fibrosis. A combined immunohistochemical and in situ hybridization study. Am J Pathol 1994 Jul;145(1):114-125.

(104) Desmouliere A, Geinoz A, Gabbiani F, Gabbiani G. Transforming growth factor-beta 1 induces alpha-smooth muscle actin expression in granulation tissue myofibroblasts and in quiescent

and growing cultured fibroblasts. J Cell Biol 1993 Jul;122(1):103-111.

(105) Raghow B, Irish P, Kang AH. Coordinate regulation of transforming growth factor beta gene expression and cell proliferation in hamster lungs undergoing bleomycin-induced pulmonary fibrosis. J Clin Invest 1989 Dec;84(6):1836-1842.

(106) Suganuma H, Sato A, Tamura R, Chida K. Enhanced migration of fibroblasts derived from lungs with fibrotic lesions. Thorax 1995 Sep;50(9):984-989.

(107) Eyden B. The myofibroblast: phenotypic characterization as a prerequisite to understanding its functions in translational medicine. J Cell Mol Med 2008 Jan-Feb;12(1):22-37.

(108) Ellabban NG, Lee KW. Myofibroblasts in Central Giant-Cell Granuloma of the Jaws - an Ultrastructural-Study. Histopathology 1983 1983;7(6).

(109) Schmittgraff A, Desmouliere A, Gabbiani G. Heterogeneity of Myofibroblast Phenotypic Features - an Example of Fibroblastic Cell Plasticity. Virchows Archiv-an International Journal of Pathology 1994 AUG 1994;425(1).

(110) Zhou X, Wu W, Hu H, Milosevic J, Konishi K, Kaminski N, et al. Genomic Differences Distinguish the Myofibroblast Phenotype of Distal Lung from Airway Fibroblasts. Am J Respir Cell Mol Biol 2011 Jul 14.

(111) Skalli O, Ropraz P, Trzeciak A, Benzonana G, Gillessen D, Gabbiani G. A monoclonal antibody against alpha-smooth muscle actin: a new probe for smooth muscle differentiation. J Cell Biol 1986 Dec;103(6 Pt 2):2787-2796.

(112) Skalli O, Pelte MF, Peclet MC, Gabbiani G, Gugliotta P, Bussolati G, et al. Alpha-smooth muscle actin, a differentiation marker of smooth muscle cells, is present in microfilamentous bundles of pericytes. J Histochem Cytochem 1989 Mar;37(3):315-321.

(113) Skalli O, Schurch W, Seemayer T, Lagace R, Montandon D, Pittet B, et al. Myofibroblasts from diverse pathologic settings are heterogeneous in their content of actin isoforms and intermediate filament proteins. Lab Invest 1989 Feb;60(2):275-285.

(114) Hudon-David F, Bouzeghrane F, Couture P, Thibault G. Thy-1 expression by cardiac fibroblasts: Lack of association with

myofibroblast contractile markers. J Mol Cell Cardiol 2007 MAY 2007;42(5).

(115) Saalbach A, Kraft R, Herrmann K, Haustein UF, Anderegg U. The monoclonal antibody AS02 recognizes a protein on human fibroblasts being highly homologous to Thy-1. Arch Dermatol Res 1998 JUL 1998;290(7).

(116) Saalbach A, Wetzig T, Haustein UF, Anderegg U. Detection of human soluble Thy-1 in serum by ELISA - Fibroblasts and activated endothelial cells are a possible source of soluble Thy-1 in serum. Cell Tissue Res 1999 NOV 1999;298(2).

(117) Gilles C, Polette M, Zahm JM, Tournier JM, Volders L, Foidart JM, et al. Vimentin contributes to human mammary epithelial cell migration. J Cell Sci 1999 DEC 1999;112(24):4615-4625.

(118) Abe S, Rhee SK, Osonoi M, Nakamura T, Cho BH, Murakami G, et al. Expression of intermediate filaments at muscle insertions in human fetuses. J Anat 2010 May 25.

(119) Shimizu K, Lopez-Ilasaca M, Li Y, Libby P, Mitchell RN, Minami M, et al. Response to Letter Regarding Article, "CC Chemokine Receptor-1 Activates Intimal Smooth Muscle–Like Cells in Graft Arterial Disease". Circulation 2010 June 15;121(23):e438-e438.

(120) Edelman AM, Higgins DM, Bowman CL, Haber SN, Rabin RA, Cho-Lee J. Myosin light chain kinase is expressed in neurons and glia: immunoblotting and immunocytochemical studies. Brain Res Mol Brain Res 1992 Jun;14(1-2):27-34.

(121) Wong JZ, Woodcock-Mitchell J, Mitchell J, Rippetoe P, White S, Absher M, et al. Smooth muscle actin and myosin expression in cultured airway smooth muscle cells. Am J Physiol 1998 May;274(5 Pt 1):L786-92.

(122) Chambers RC, Leoni P, Kaminski N, Laurent GJ, Heller RA. Global expression profiling of fibroblast responses to transforming growth factor-beta1 reveals the induction of inhibitor of differentiation-1 and provides evidence of smooth muscle cell phenotypic switching. Am J Pathol 2003 Feb;162(2):533-546.

(123) Schlossman SF, Boumsell L, Gilks W, Harlan JM, Kishimoto T, Morimoto C, et al. CD antigens 1993. Immunol Today 1994 Mar;15(3):98-99.

(124) Wenzel SE, Balzar S. Myofibroblast or smooth muscle: do in vitro systems adequately replicate tissue smooth muscle? Am J Respir Crit Care Med 2006 Aug 15;174(4):364-365.

(125) Wenzel SE, Trudeau JB, Barnes S, Zhou X, Cundall M, Westcott JY, et al. TGF-β and IL-13 Synergistically Increase Eotaxin-1 Production in Human Airway Fibroblasts. The Journal of Immunology 2002 October 15;169(8):4613-4619.

(126) Kotaru C, Schoonover KJ, Trudeau JB, Huynh ML, Zhou X, Hu H, et al. Regional fibroblast heterogeneity in the lung: implications for remodeling. Am J Respir Crit Care Med 2006 Jun 1;173(11):1208-1215.

(127) Thierry Simonart, Degraef C, Heenen M, Hermans P, Van Vooren J, Noel J. Expression of the fibroblast/macrophage marker 1B10 by spindle cells in Kaposi's sarcoma lesions and by Kaposi's sarcoma-derived tumor cells. J Cutan Pathol 2002;29(2):72-78.

(128) Jenkins,Cathleen, Milsted,Amy, Doane,Kathleen, Meszaros,Gary, Toot,Jonathan, Ely,Daniel. A cell culture model using rat coronary artery adventitial fibroblasts to measure collagen production. BMC Cardiovascular Disorders 2007.

(129) Eyden B, Banerjee SS, Shenjere P, Fisher C. The myofibroblast and its tumours. J Clin Pathol 2009 Mar;62(3):236-249.

(130) Grotendorst GR, Rahmanie H, Duncan MR. Combinatorial signaling pathways determine fibroblast proliferation and myofibroblast differentiation. The FASEB Journal 2004 March 01;18(3):469-479.

(131) Kothapalli D, Frazier K, Welply A, Segarini P, Grotendorst G. Transforming growth factor beta induces anchorage-independent growth of NRK fibroblasts via a connective tissue growth factor-dependent signaling pathway. Cell Growth Differ 1997 January 1;8(1):61-68.

(132) Tarantal AF, Chen H, Shi TT, Lu CH, Fang AB, Buckley S, et al. Overexpression of TGF-{beta}1 in foetal monkey lung results in Prenatal Pulmonary Fibrosis. Eur Respir J 2010 Mar 29.

(133) Goodwin A, Jenkins G. Role of integrin-mediated TGFbeta activation in the pathogenesis of pulmonary fibrosis. Biochem Soc Trans 2009 Aug;37(Pt 4):849-854.

(134) Yu L, Border WA, Huang Y, Noble NA. TGF-beta isoforms in renal fibrogenesis. Kidney Int 2003 Sep;64(3):844-856.

(135) Branton MH, Kopp JB. TGF-beta and fibrosis. Microbes Infect 1999 Dec;1(15):1349-1365.

(136) Lemaire I, Beaudoin H, Masse S, Grondin C. Alveolar Macrophage Stimulation of Lung Fibroblast Growth in Asbestos-Induced Pulmonary Fibrosis. Am J Pathol 1986 FEB 1986;122(2).

(137) Imamura M, Kanematsu A, Yamamoto S, Kimura Y, Kanatani I, Ito N, et al. Basic fibroblast growth factor modulates proliferation and collagen expression in urinary bladder smooth muscle cells. American Journal of Physiology - Renal Physiology 2007 October 01;293(4):F1007-F1017.

(138) Akers IA, Parsons M, Hill MR, Hollenberg MD, Sanjar S, Laurent GJ, et al. Mast cell tryptase stimulates human lung fibroblast proliferation via protease-activated receptor-2. American Journal of Physiology - Lung Cellular and Molecular Physiology 2000 January 01;278(1):L193-L201.

(139) Pesci A, Bertorelli G, Gabrielli M, Olivieri D. Mast-Cells in Fibrotic Lung Disorders. Chest 1993 APR 1993;103(4).

(140) Andersson CK, Andersson-Sjoland A, Mori M, Hallgren O, Pardo A, Eriksson L, et al. Activated MCTC mast cells infiltrate diseased lung areas in cystic fibrosis and idiopathic pulmonary fibrosis. Respiratory Research 2011 OCT 20 2011;12:139.

(141) Tangkijvanich P, Santiskulvong C, Melton AC, Rozengurt E, Yee HF. p38 MAP kinase mediates platelet-derived growth factor-stimulated migration of hepatic myofibroblasts. J Cell Physiol 2002 JUN 2002;191(3).

(142) Takeji M, Moriyama T, Oseto S, Kawada N, Hori M, Imai E, et al. Smooth Muscle α-Actin Deficiency in Myofibroblasts Leads to Enhanced Renal Tissue Fibrosis. Journal of Biological Chemistry 2006 December 29;281(52):40193-40200.

(143) Hertz MI, Henke CA, Nakhleh RE, Harmon KR, Marinelli WA, Fox JMK, et al. Obliterative Bronchiolitis After Lung Transplantation - a Fibroproliferative Disorder Associated with Platelet-Derived Growth-Factor. Proc Natl Acad Sci U S A 1992 NOV 1 1992;89(21).

(144) Grinnell F. Fibroblasts, myofibroblasts, and wound contraction. J Cell Biol 1994 Feb;124(4):401-404.

(145) Wynn TA. Cellular and molecular mechanisms of fibrosis. J Pathol 2008 Jan;214(2):199-210.

(146) Pierce EM, Carpenter K, Jakubzick C, Kunkel SL, Evanoff H, Flaherty KR, et al. Idiopathic pulmonary fibrosis fibroblasts migrate and proliferate to CC chemokine ligand 21. European Respiratory Journal 2007 June 01;29(6):1082-1093.

(147) Kanazawa S, Fujiwara T, Matsuzaki S, Shingaki K, Taniguchi M, Miyata S, et al. bFGF Regulates PI3-Kinase-Rac1-JNK Pathway and Promotes Fibroblast Migration in Wound Healing. Plos One 2010 AUG 17 2010;5(8):e12228.

(148) Huang M, Sharma S, Zhu LX, Keane MP, Luo J, Zhang L, et al. IL-7 inhibits fibroblast TGF-beta production and signaling in pulmonary fibrosis. J Clin Invest 2002 Apr;109(7):931-937.

(149) Leask A, Abraham DJ. TGF-beta signaling and the fibrotic response. Faseb Journal 2004 MAY 2004;18(7).

(150) Eickelberg O, Kohler E, Reichenberger F, Bertschin S, Woodtli T, Erne P, et al. Extracellular matrix deposition by primary human lung fibroblasts in response to TGF-beta 1 and TGF-beta 3. American Journal of Physiology-Lung Cellular and Molecular Physiology 1999 MAY 1999;276(5).

(151) Birchmeier C, Birchmeier W. Molecular aspects of mesenchymal-epithelial interactions. Annu Rev Cell Biol 1993 1993;9.

(152) Schuppan D, Schmid M, Somasundaram R, Ackermann R, Ruehl M, Nakamura T, et al. Collagens in the liver extracellular matrix bind hepatocyte growth factor. Gastroenterology 1998 JAN 1998;114(1).

(153) Tettamanti G, Grimaldi A, Rinaldi L, Arnaboldi F, Congiu T, Valvassori R, et al. The multifunctional role of fibroblasts during wound healing in Hirudo medicinalis (Annelida, Hirudinea). Biology of the Cell 2004 AUG 2004;96(6).

(154) Desmouliere A, Badid C, Bochaton-Piallat M, Gabbiani G. Apoptosis during wound healing, fibrocontractive diseases and vascular wall injury. Int J Biochem Cell Biol 1997;29:19-30.

(155) Fournier C, Kraft-Weyrather W, Kraft G. Survival, differentiation and collagen secretion of human fibroblasts after irradiation with carbon ions and X-rays. Physica Medica 1998 JUL 1998;14.

(156) Scottburden T. Extracellular-Matrix - the Cellular Environment. News in Physiological Sciences 1994 JUN 1994;9.

(157) Kelley J, Trombley L, Kovacs EJ, Davis GS, Absher M. Pulmonary Macrophages Alter the Collagen Phenotype of Lung Fibroblasts. J Cell Physiol 1981 1981;109(2).

(158) Lodish H, Berk A, Zipursky SL, et al. Section 22.3, Collagen: The Fibrous Proteins of the Matrix. Molecular Cell Biology. 4th ed. New York: W. H. Freeman; 2000.

(159) Laurent GJ. Lung Collagen - More than Scaffolding. Thorax 1986 JUN 1986;41(6).

(160) Kennedy S, Qin H, Lin L, Tan E. Basic Fibroblast Growth-Factor Regulates Type-i Collagen and Collagenase Gene-Expression in Human Smooth-Muscle Cells. Am J Pathol 1995 MAR;146(3):764-771.

(161) Andersson-Sjoland A, de Alba CG, Nihlberg K, Becerril C, Ramirez R, Pardo A, et al. Fibrocytes are a potential source of lung fibroblasts in idiopathic pulmonary fibrosis. Int J Biochem Cell Biol 2008;40(10):2129-2140.

(162) Kim JH, Jang YS, Eom K, Hwang YI, Kang HR, Jang SH, et al. Transtorming Growth Factor β1 Induces Epithelial-to-Mesenchymal Transition of A549 Cells. J Korean Med Sci 2007 10;22(5):898-904.

(163) Sanders YY, Kumbla P, Hagood JS. Enhanced myofibroblastic differentiation and survival in Thy-1(-) lung fibroblasts. Am J Respir Cell Mol Biol 2007 Feb;36(2):226-235.

(164) Rieder F, Brenmoehl J, Leeb S, Schölmerich J, Rogler G. Wound healing and fibrosis in intestinal disease. Gut 2007 January 01;56(1):130-139.

(165) Muro AF, Moretti FA, Moore BB, Yan M, Atrasz RG, Wilke CA, et al. An essential role for fibronectin extra type III domain A in pulmonary fibrosis. American Journal of Respiratory and Critical Care Medicine 2008 MAR 15 2008;177(6).

(166) Hu B, Wu Z, Phan SH. Smad3 mediates transforming growth factor-beta-induced alpha-smooth muscle actin expression. American Journal of Respiratory Cell and Molecular Biology 2003 SEP 2003;29(3).

(167) Tomasek J, Gabbiani G, Hinz B, Chaponnier C, Brown R. Myofibroblasts and mechano-regulation of connective tissue remodelling. Nature Reviews Molecular Cell Biology 2002 MAY;3(5):349-363.

(168) Dugina V, Fontao L, Chaponnier C, Vasiliev J, Gabbiani G. Focal adhesion features during myofibroblastic differentiation are controlled by intracellular and extracellular factors. J Cell Sci 2001 SEP 2001;114(18).

(169) Hinz B, Phan SH, Thannickal VJ, Galli A, Bochaton-Piallat M, Gabbiani G. The myofibroblast: One function, multiple origins. Am J Pathol 2007;170:1807-1816.

(170) Gabbiani G, Ryan GB, Statkov PR, Hirschel BJ, Majno G. Granulation Tissue as a Contractile Organ - Study of Structure and Function. J Exp Med 1972 1972;135(4).

(171) Wipff PJ, Rifkin DB, Meister JJ, Hinz B. Myofibroblast contraction activates latent tgf-beta1 from the extracellular matrix. J Cell Biol 2007;179:1311-1323.

(172) Hasegawa T, Nakao A, Sumiyoshi K, Tsuchihashi H, Ogawa H. SB-431542 inhibits TGF-β-induced contraction of collagen gel by normal and keloid fibroblasts. J Dermatol Sci 2005 7;39(1):33-38.

(173) Zhang HY, GharaeeKermani M, Phan SH. Regulation of lung fibroblast alpha-smooth muscle actin expression, contractile phenotype, and apoptosis by IL-1 beta. Journal of Immunology 1997 FEB 1 1997;158(3).

(174) Horowitz JC, Lee DY, Waghray M, Keshamouni VG, Thomas PE, Zhang H, et al. Activation of the pro-survival phosphatidylinositol 3-kinase/akt pathway by transforming growth factor-beta1 in mesenchymal cells is mediated by p38 mapk-dependent induction of an autocrine growth factor. J Biol Chem 2004;279:1359-1367.

(175) Zhang HY, Phan SH. Inhibition of myofibroblast apoptosis by transforming growth factor beta(1). American Journal of Respiratory Cell and Molecular Biology 1999 DEC 1999;21(6).

(176) Beasley D, Cohen RA, Levinsky NG. Interleukin-1 Inhibits Contraction of Vascular Smooth-Muscle. J Clin Invest 1989 JAN 1989;83(1).

(177) McAnulty RJ. Fibroblasts and myofibroblasts: their source, function and role in disease. Int J Biochem Cell Biol 2007;39(4):666-671.

(178) Willis BC, duBois RM, Borok Z. Epithelial origin of myofibroblasts during fibrosis in the lung. Proc Am Thorac Soc 2006 Jun;3(4):377-382.

(179) Brewster CE, Howarth PH, Djukanovic R, Wilson J, Holgate ST, Roche WR. Myofibroblasts and subepithelial fibrosis in bronchial asthma. Am J Respir Cell Mol Biol 1990 Nov;3(5):507-511.

(180) Phan SH. The myofibroblast in pulmonary fibrosis. Chest 2002 Dec;122(6 Suppl):286S-289S.

(181) Zhang K, Gharaee-Kermani M, Jones ML, Warren JS, Phan SH. Lung monocyte chemoattractant protein-1 gene expression in bleomycin-induced pulmonary fibrosis. J Immunol 1994 Nov 15;153(10):4733-4741.

(182) Chambers RC. Abnormal wound healing responses in pulmonary fibrosis: focus on coagulation signalling. EUROPEAN RESPIRATORY REVIEW 2008 December 1;17(109):130-137.

(183) Thannickal VJ, Horowitz JC. Evolving concepts of apoptosis in idiopathic pulmonary fibrosis. Proceedings of the American Thoracic Society 2006 2006-Jun;3(4).

(184) Ramos C, Montaño M, Garćıa-Alvarez J, Ruiz V, Uhal BD, Selman M, et al. Fibroblasts from Idiopathic Pulmonary Fibrosis and Normal Lungs Differ in Growth Rate, Apoptosis, and Tissue Inhibitor of Metalloproteinases Expression. American Journal of Respiratory Cell and Molecular Biology 2001 May 01;24(5):591-598.

(185) Thannickal V. Mechanisms of pulmonary fibrosis: role of activated myofibroblasts and NADPH oxidase. Fibrogenesis & Tissue Repair 2012;5:23.

(186) Darby I, Skalli O, Gabbiani G. Alpha-Smooth Muscle Actin is Transiently Expressed by Myofibroblasts during Experimental Wound-Healing. Laboratory Investigation 1990 JUL 1990;63(1).

(187) Brody AR, Bonner JC, Overby LH, Badgett A, Kalter V, Kumar RK, et al. Interstitial pulmonary macrophages produce platelet-derived growth factor that stimulates rat lung fibroblast proliferation in vitro. J Leukoc Biol 1992 Jun;51(6):640-648.

(188) Mattey DL, Dawes PT, Nixon NB, Slater H. Transforming growth factor beta 1 and interleukin 4 induced alpha smooth muscle actin expression and myofibroblast-like differentiation in human synovial fibroblasts in vitro: modulation by basic fibroblast growth factor. Ann Rheum Dis 1997 Jul;56(7):426-431.

(189) Selman M, Ruiz V, Cabrera S, Segura L, Ramirez R, Barrios R, et al. TIMP-1,-2,-3, and-4 in idiopathic pulmonary fibrosis. A prevailing nondegradative lung microenvironment? American Journal

of Physiology-Lung Cellular and Molecular Physiology 2000 SEP 2000;279(3).

(190) Tager A, LaCamera P, Shea B, Campanella G, Karimi-Shah B, Kim N, et al. The lysophosphatidic acid receptor LPA1 links pulmonary fibrosis to lung injury by mediating fibroblast recruitment and vascular leak. Inflammation Res 2007 JUN 2007;56.

(191) Bucala R, Spiegel LA, Chesney J, Hogan M, Cerami A. Circulating fibrocytes define a new leukocyte subpopulation that mediates tissue repair. Mol Med 1994 Nov;1(1):71-81.

(192) Moeller A, Gilpin SE, Ask K, Cox G, Cook D, Gauldie J, et al. Circulating fibrocytes are an indicator of poor prognosis in idiopathic pulmonary fibrosis. Am J Respir Crit Care Med 2009 Apr 1;179(7):588-594.

(193) Bellini A, Mattoli S. The role of the fibrocyte, a bone marrow-derived mesenchymal progenitor, in reactive and reparative fibroses. Laboratory Investigation 2007 SEP 2007;87(9).

(194) Epperly MW, Guo HL, Gretton JE, Greenberger JS. Bone marrow origin of myofibroblasts in irradiation pulmonary fibrosis. American Journal of Respiratory Cell and Molecular Biology 2003 AUG 2003;29(2).

(195) Hashimoto N, Jin H, Liu TJ, Chensue SW, Phan SH. Bone marrow-derived progenitor cells in pulmonary fibrosis. J Clin Invest 2004 JAN 2004;113(2).

(196) Mehrad B, Burdick MD, Zisman DA, Keane MP, Belperio JA, Strieter RM. Circulating peripheral blood fibrocytes in human fibrotic interstitial lung disease. Biochem Biophys Res Commun 2007 FEB 2 2007;353(1).

(197) Phillips RJ, Burdick MD, Hong K, Lutz MA, Murray LA, Xue YY, et al. Circulating fibrocytes traffic to the lungs in response to CXCL12 and mediate fibrosis. J Clin Invest 2004 AUG 2004;114(3).

(198) Wang CH, Huang CD, Lin HC, Lee KY, Lin SM, Liu CY, et al. Increased circulating fibrocytes in asthma with chronic airflow obstruction. Am J Respir Crit Care Med 2008 Sep 15;178(6):583-591.

(199) Willis BC, Borok Z. TGF-beta-induced EMT: mechanisms and implications for fibrotic lung disease. Am J Physiol Lung Cell Mol Physiol 2007 Sep;293(3):L525-34.

(200) Gai Z, Zhou G, Gui T, Itoh S, Oikawa K, Uetani K, et al. Trps1 Haploinsufficiency Promotes Renal Fibrosis by Increasing Arkadia Expression. J Am Soc Nephrol 2010 May 27.

(201) Rajasekaran SA, Huynh TP, Wolle DG, Espineda CE, Inge LJ, Skay A, et al. Na,K-ATPase Subunits as Markers for Epithelial-Mesenchymal Transition in Cancer and Fibrosis. Mol Cancer Ther 2010 May 25.

(202) Willis BC, Liebler JM, Luby-Phelps K, Nicholson AG, Crandall ED, du Bois RM, et al. Induction of epithelial-mesenchymal transition in alveolar epithelial cells by transforming growth factor-ss 1 - Potential role in idiopathic pulmonary fibrosis. Am J Pathol 2005 MAY 2005;166(5).

(203) Kim KK, Kugler MC, Wolters PJ, Robillard L, Galvez MG, Brumwell AN, et al. Alveolar epithelial cell mesenchymal transition develops in vivo during pulmonary fibrosis and is regulated by the extracellular matrix. Proc Natl Acad Sci U S A 2006 AUG 29 2006;103(35).

(204) Roberts AB, Sporn MB. Physiological Actions and Clinical-Applications of Transforming Growth-Factor-Beta (Tgf-Beta). Growth Factors 1993 1993;8(1).

(205) Lynch JP. Idiopathic Pulmonary Fibrosis. : CRC press; 2004.

(206) Pechkovsky DV, Hackett TL, An SS, Shaheen F, Murray LA, Knight DA. Human Lung Parenchyma but Not Proximal Bronchi Produces Fibroblasts with Enhanced TGF-{beta} Signaling and {alpha}-SMA Expression. Am J Respir Cell Mol Biol 2010 December 1;43(6):641-651.

(207) Burgess WH, Maciag T. The Heparin-Binding (Fibroblast) Growth-Factor Family of Proteins. Annu Rev Biochem 1989 1989;58.

(208) Davis M, Zhou M, Ali S, Coffin J, Doetschman T, Dorn G. Intracrine and autocrine effects of basic fibroblast growth factor in vascular smooth muscle cells. J Mol Cell Cardiol 1997 APR;29(4):1061-1072.

(209) Berndt A, Kosmehl H, Mandel U, Gabler U, Luo XM, Celeda D, et al. TGF beta and bFGF synthesis and localization in Dupuytren's disease (nodular palmar fibromatosis) relative to cellular activity, myofibroblast phenotype and oncofetal variants of fibronectin. Histochem J 1995 DEC 1995;27(12).

(210) Pintucci G, Moscatelli D, Saponara F, Biernacki P, Baumann F, Bizekis C, et al. Lack of ERK activation and cell migration in FGF-2-deficient endothelial cells. Faseb Journal 2002 FEB;16(2):598-+.

(211) Inoue Y, King TE,Jr, Barker E, Daniloff E, Newman LS. Basic fibroblast growth factor and its receptors in idiopathic pulmonary fibrosis and lymphangioleiomyomatosis. Am J Respir Crit Care Med 2002 Sep 1;166(5):765-773.

(212) Blotnick S, Peoples G, Freeman M, Eberlein T, Klagsbrun M. T-Lymphocytes Synthesize and Export Heparin-Binding Epidermal Growth Factor-Like Growth-Factor and Basic Fibroblast Growth-Factor, Mitogens for Vascular Cells and Fibroblasts - Differential Production and Release by Cd4+ and Cd8+ T-Cells. Proc Natl Acad Sci U S A 1994 APR 12;91(8):2890-2894.

(213) Dvorak A. Ultrastructural Analysis of Human Mast-Cells and Basophils. Human Basophils and Mast Cells: Biological Aspects 1995;61:1-33.

(214) Antoniades H, Bravo M, Avila R, Galanopoulos T, Nevillegolden J, Maxwell M, et al. Platelet-Derived Growth-Factor in Idiopathic Pulmonary Fibrosis. J Clin Invest 1990 OCT;86(4):1055-1064.

(215) Wangoo A, Haynes A, Sutcliffe S, Sorooshian M, Shaw R. Modulation of Platelet-Derived Growth Factor-B Messenger-Rna Abundance in Macrophages by Colchicine and Dibutyryl-Camp. Mol Pharmacol 1992 OCT;42(4):584-589.

(216) Shimizu S, Gabazza E, Hayashi T, Ido M, Adachi Y, Suzuki K. Thrombin stimulates the expression of PDGF in lung epithelial cells. American Journal of Physiology-Lung Cellular and Molecular Physiology 2000 SEP;279(3):L503-L510.

(217) Collins T, Ginsburg D, Boss J, Orkin S, Pober J. Cultured Human-Endothelial Cells Express Platelet-Derived Growth-Factor B-Chain - Cdna Cloning and Structural-Analysis. Nature 1985;316(6030):748-750.

(218) Gurujeyalakshmi G, Hollinger M, Giri S. Pirfenidone inhibits PDGF isoforms in bleomycin hamster model of lung fibrosis at the translational level. American Journal of Physiology-Lung Cellular and Molecular Physiology 1999 FEB;276(2):L311-L318.

(219) Daniels CE, Lasky JA, Limper AH, Mieras K, Gabor E, Schroeder DR, et al. Imatinib Treatment for Idiopathic Pulmonary Fibrosis Randomized Placebo-controlled Trial Results. American Journal of

Respiratory and Critical Care Medicine 2010 MAR 15;181(6):604-610.

(220) SABiosciences AQC. TGF-Beta Pathway. 2012; Available at: http://www.sabiosciences.com/pathway.php?sn=TGF_Beta_Pathway, 2012.

(221) Moustakas A, Pardali K, Gaal A, Heldin C. Mechanisms of TGF-β signaling in regulation of cell growth and differentiation. Immunol Lett 2002 6/3;82(1–2):85-91.

(222) Li W, Ding S. Small molecules that modulate embryonic stem cell fate and somatic cell reprogramming. Trends Pharmacol Sci 2010 1;31(1):36-45.

(223) Hong KM, Belperio JA, Keane MP, Burdick MD, Strieter RM. Differentiation of Human Circulating Fibrocytes as Mediated by Transforming Growth Factor-β and Peroxisome Proliferator-activated Receptor γ. Journal of Biological Chemistry 2007 August 03;282(31):22910-22920.

(224) Aidley D,J, Stanfield p,R. Ion Channels : molecules in action. Great britain: Cambridge University Press; 1996.

(225) Femini B. Recent Advances in Ion Channel Screening Technologies. Ion Channels: Springer Berlin Heidelberg; 2008. p. 1-25.

(226) Decoursey TE, Chandy KG, Gupta S, Cahalan MD. Two types of potassium channels in murine T lymphocytes. The Journal of General Physiology 1987 March 01;89(3):379-404.

(227) Barrett JN, Magleby KL, Pallotta BS. Properties of single calcium-activated potassium channels in cultured rat muscle. J Physiol 1982 Oct;331:211-230.

(228) Dartsch PC, Ritter M, Gschwentner M, Lang HJ, Lang F. Effects of Calcium-Channel Blockers on Nih 3t3 Fibroblasts Expressing the Ha-Ras Oncogene. Eur J Cell Biol 1995 AUG 1995;67(4).

(229) Su X, Wang Y, Zhang W, Zhao L, Li G, Deng X. Insulin-mediated upregulation of KCa3.1 channels promotes cell migration and proliferation in rat vascular smooth muscle. J Mol Cell Cardiol 2011 7;51(1):51-57.

(230) Hu L, Pennington M, Jiang Q, Whartenby KA, Calabresi PA. Characterization of the functional properties of the voltage-gated

potassium channel Kv1.3 in human CD4+ T lymphocytes. J Immunol 2007 Oct 1;179(7):4563-4570.

(231) Kessler W, Budde T, Gekle M, Fabian A, Schwab A. Activation of cell migration with fibroblast growth factor-2 requires calcium-sensitive potassium channels. Pflügers Archiv European Journal of Physiology 2008;456(5):813-823.

(232) Schilling T, Stock C, Schwab A, Eder C. Functional importance of Ca2+-activated K+ channels for lysophosphatidic acid-induced microglial migration. Eur J Neurosci 2004 Mar;19(6):1469-1474.

(233) Patel AJ, Lazdunski M. The 2P-domain K+ channels: role in apoptosis and tumorigenesis. Pflugers Archiv-European Journal of Physiology 2004 JUN 2004;448(3).

(234) Bertran GC, D'Alessio C, Kotsias BA. Ion channels in non excitable cells. Medicina (B Aires) 1995;55(5 Pt 1):449-456.

(235) Berridge MJ, Lipp P, Bootman MD. The versatility and universality of calcium signalling. Nat Rev Mol Cell Biol 2000 Oct;1(1):11-21.

(236) Meech RW, Standen NB. Potassium activation in Helix aspersa neurones under voltage clamp: a component mediated by calcium influx. J Physiol 1975 Jul;249(2):211-239.

(237) Greber UF, Gerace L. Depletion of calcium from the lumen of endoplasmic reticulum reversibly inhibits passive diffusion and signal-mediated transport into the nucleus. J Cell Biol 1995 Jan;128(1-2):5-14.

(238) Duffy S, Berger P, Cruse G, Yang W, Bolton SJ, Bradding P. The K+ channel iKCA1 potentiates Ca2+ influx and degranulation in human lung mast cells. J Allergy Clin Immunol 2004 Jul;114(1):66-72.

(239) Parekh AB, Putney JW. Store-Operated Calcium Channels. Physiological Reviews 2005 April 01;85(2):757-810.

(240) Gardos G. The function of calcium in the potassium permeability of human erythrocytes. Biochim Biophys Acta 1958 Dec;30(3):653-654.

(241) Vergara C, Latorre R, Marrion NV, Adelman JP. Calcium-activated potassium channels. Curr Opin Neurobiol 1998 Jun;8(3):321-329.

(242) Tharp DL, Bowles DK. The intermediate-conductance Ca2+ -activated K+ channel (KCa3.1) in vascular disease. Cardiovasc Hematol Agents Med Chem 2009 Jan;7(1):1-11.

(243) Schreiber M, Salkoff L. A novel calcium-sensing domain in the BK channel. Biophys J 1997 Sep;73(3):1355-1363.

(244) Ishii TM, Silvia C, Hirschberg B, Bond CT, Adelman JP, Maylie J. A human intermediate conductance calcium-activated potassium channel. Proc Natl Acad Sci U S A 1997 Oct 14;94(21):11651-11656.

(245) Fanger CM, Ghanshani S, Logsdon NJ, Rauer H, Kalman K, Zhou J, et al. Calmodulin mediates calcium-dependent activation of the intermediate conductance KCa channel, IKCa1. J Biol Chem 1999 Feb 26;274(9):5746-5754.

(246) Neylon CB, Lang RJ, Fu Y, Bobik A, Reinhart PH. Molecular cloning and characterization of the intermediate-conductance Ca(2+)-activated K(+) channel in vascular smooth muscle: relationship between K(Ca) channel diversity and smooth muscle cell function. Circ Res 1999 Oct 29;85(9):e33-43.

(247) Ghanshani S, Coleman M, Gustavsson P, Wu AC, Gargus jJ, Gutman GA, et al. Human Calcium-Activated Potassium Channel GeneKCNN4Maps to Chromosome 19q13.2 in the Region Deleted in Diamond–Blackfan Anemia. Genomics 1998 7/1;51(1):160-161.

(248) Khanna R, Chang MC, Joiner WJ, Kaczmarek LK, Schlichter LC. hSK4/hIK1, a Calmodulin-binding KCa Channel in Human T Lymphocytes. Journal of Biological Chemistry 1999 May 21;274(21):14838-14849.

(249) Bouhy D, Ghasemlou N, Lively S, Redensek A, Rathore KI, Schlichter LC, et al. Inhibition of the Ca2+-Dependent K+ Channel, KCNN4/KCa3.1, Improves Tissue Protection and Locomotor Recovery after Spinal Cord Injury. Journal of Neuroscience 2011 NOV 9 2011;31(45).

(250) Bradding P, Wulff H. The K+ channels K(Ca)3.1 and K(v)1.3 as novel targets for asthma therapy. Br J Pharmacol 2009 Aug;157(8):1330-1339.

(251) Grgic I, Kaistha BP, Hoyer J, Kohler R. Endothelial Ca+-activated K+ channels in normal and impaired EDHF-dilator responses--relevance to cardiovascular pathologies and drug discovery. Br J Pharmacol 2009 Jun;157(4):509-526.

(252) Pedersen KA, Schroder RL, Skaaning-Jensen B, Strobaek D, Olesen SP, Christophersen P. Activation of the human intermediate-conductance Ca(2+)-activated K(+) channel by 1-ethyl-2-benzimidazolinone is strongly Ca(2+)-dependent. Biochim Biophys Acta 1999 Aug 20;1420(1-2):231-240.

(253) Devor DC, Singh AK, Frizzell RA, Bridges RJ. Modulation of Cl- secretion by benzimidazolones. I. Direct activation of a Ca(2+)-dependent K+ channel. Am J Physiol 1996 Nov;271(5 Pt 1):L775-84.

(254) Singh S, Syme CA, Singh AK, Devor DC, Bridges RJ. Benzimidazolone activators of chloride secretion: potential therapeutics for cystic fibrosis and chronic obstructive pulmonary disease. J Pharmacol Exp Ther 2001 Feb;296(2):600-611.

(255) Sankaranarayanan A, Raman G, Busch C, Schultz T, Zimin PI, Hoyer J, et al. Naphtho[1,2-d]thiazol-2-ylamine (SKA-31), a new activator of KCa2 and KCa3.1 potassium channels, potentiates the endothelium-derived hyperpolarizing factor response and lowers blood pressure. Mol Pharmacol 2009 Feb;75(2):281-295.

(256) Strobaek D, Teuber L, Jorgensen TD, Ahring PK, Kjaer K, Hansen RS, et al. Activation of human IK and SK Ca2+-activated K+ channels by NS309 (6,7-dichloro-1H-indole-2,3-dione 3-oxime). Biochimica Et Biophysica Acta-Biomembranes 2004 OCT 11 2004;1665(1-2).

(257) Triggle D. The pharmacology of ion channels: with particular reference to voltage-gated Ca2+ channels. Eur J Pharmacol 1999 JUN 30;375(1-3):311-325.

(258) Gimenez-Gallego G, Navia MA, Reuben JP, Katz GM, Kaczorowski GJ, Garcia ML. Purification, sequence, and model structure of charybdotoxin, a potent selective inhibitor of calcium-activated potassium channels. Proc Natl Acad Sci U S A 1988 May;85(10):3329-3333.

(259) Sands SB, Lewis RS, Cahalan MD. Charybdotoxin Blocks Voltage-Gated K+ Channels in Human and Murine Lymphocytes-T. J Gen Physiol 1989 JUN 1989;93(6).

(260) Deutsch C, Price M, Lee S, King VF, Garcia ML. Characterization of High-Affinity Binding-Sites for Charybdotoxin in Human Lymphocytes-T - Evidence for Association with the Voltage-Gated K+ Channel. J Biol Chem 1991 FEB 25 1991;266(6).

(261) Wojtulewski JA, Gow PJ, Walter J, Grahame R, Gibson T, Panayi GS, et al. Clotrimazole in rheumatoid arthritis. Ann Rheum Dis 1980 Oct;39(5):469-472.

(262) Brugnara C, Gee B, Armsby C, Kurth S, Sakamoto M, Rifai N, et al. Therapy with oral clotrimazole induces inhibition of the Gardos channel and reduction of erythrocyte dehydration in patients with sickle cell disease. J Clin Invest 1996 MAR 1;97(5):1227-1234.

(263) Stocker JW, De Franceschi L, McNaughton-Smith GA, Corrocher R, Beuzard Y, Brugnara C. ICA-17043, a novel Gardos channel blocker, prevents sickled red blood cell dehydration in vitro and in vivo in SAD mice. Blood 2003 MAR 15 2003;101(6):2412-2418.

(264) Wulff H, Miller MJ, Hansel W, Grissmer S, Cahalan MD, Chandy KG. Design of a potent and selective inhibitor of the intermediate-conductance Ca2+-activated K+ channel, IKCa1: a potential immunosuppressant. Proc Natl Acad Sci U S A 2000 Jul 5;97(14):8151-8156.

(265) Ataga KI, Smith WR, De Castro LM, Swerdlow P, Saunthararajah Y, Castro O, et al. Efficacy and safety of the Gardos channel blocker, senicapoc (ICA-17043), in patients with sickle cell anemia. Blood 2008 APR 15 2008;111(8):3991-3997.

(266) Wulff H, Castle NA. Therapeutic potential of KCa3.1 blockers: recent advances and promising trends. Expert Rev Clin Pharmacol 2010 2010-May;3(3):385-96.

(267) Wulff H, Calabresi PA, Allie R, Yun S, Pennington M, Beeton C, et al. The voltage-gated Kv1.3 K(+) channel in effector memory T cells as new target for MS. J Clin Invest 2003 Jun;111(11):1703-1713.

(268) Ghanshani S, Wulff H, Miller MJ, Rohm H, Neben A, Gutman GA, et al. Up-regulation of the IKCa1 potassium channel during T-cell activation. Molecular mechanism and functional consequences. J Biol Chem 2000 Nov 24;275(47):37137-37149.

(269) Wolfle SE, Schmidt VJ, Hoyer J, Kohler R, de Wit C. Prominent role of KCa3.1 in endothelium-derived hyperpolarizing factor-type dilations and conducted responses in the microcirculation in vivo. Cardiovasc Res 2009 Jun 1;82(3):476-483.

(270) Grgic I, Eichler I, Heinau P, Si H, Brakemeier S, Hoyer J, et al. Selective blockade of the intermediate-conductance Ca2+-activated K+ channel suppresses proliferation of microvascular and

macrovascular endothelial cells and angiogenesis in vivo. Arterioscler Thromb Vasc Biol 2005 Apr;25(4):704-709.

(271) Shumilina E, Lam RS, Wolbing F, Matzner N, Zemtsova IM, Sobiesiak M, et al. Blunted IgE-mediated activation of mast cells in mice lacking the Ca2+-activated K+ channel KCa3.1. J Immunol 2008 Jun 15;180(12):8040-8047.

(272) Duffy SM, Cruse G, Cockerill SL, Brightling CE, Bradding P. Engagement of the EP2 prostanoid receptor closes the K+ channel KCa3.1 in human lung mast cells and attenuates their migration. Eur J Immunol 2008 Sep;38(9):2548-2556.

(273) Duffy SM, Lawley WJ, Conley EC, Bradding P. Resting and activation-dependent ion channels in human mast cells. J Immunol 2001 Oct 15;167(8):4261-4270.

(274) Cruse G, Duffy SM, Brightling CE, Bradding P. Functional KCa3.1 K+ channels are required for human lung mast cell migration. Thorax 2006 Oct;61(10):880-885.

(275) Shepherd MC, Duffy SM, Harris T, Cruse G, Schuliga M, Brightling CE, et al. K(Ca)3.1 Ca2+-Activated K+ channels regulate human airway smooth muscle proliferation. Am J Respir Cell Mol Biol 2007 NOV;37(5):525-531.

(276) Kohler R, Wulff H, Eichler I, Kneifel M, Neumann D, Knorr A, et al. Blockade of the intermediate-conductance calcium-activated potassium channel as a new therapeutic strategy for restenosis. Circulation 2003 Sep 2;108(9):1119-1125.

(277) Tharp DL, Wamhoff BR, Wulff H, Raman G, Cheong A, Bowles DK. Local delivery of the KCa3.1 blocker, TRAM-34, prevents acute angioplasty-induced coronary smooth muscle phenotypic modulation and limits stenosis. Arterioscler Thromb Vasc Biol 2008 Jun;28(6):1084-1089.

(278) Toyama K, Wulff H, Chandy KG, Azam P, Raman G, Saito T, et al. The intermediate-conductance calcium-activated potassium channel KCa3.1 contributes to atherogenesis in mice and humans. J Clin Invest 2008 Sep;118(9):3025-3037.

(279) Rane SG. A Ca2(+)-activated K+ current in ras-transformed fibroblasts is absent from nontransformed cells. American Journal of Physiology - Cell Physiology 1991 January 01;260(1):C104-C112.

(280) Pena TL, Rane SG. The fibroblast intermediate conductance K(Ca) channel, FIK, as a prototype for the cell growth regulatory

function of the IK channel family. J Membr Biol 1999 Dec 1;172(3):249-257.

(281) Grgic I, Kiss E, Kaistha BP, Busch C, Kloss M, Sautter J, et al. Renal fibrosis is attenuated by targeted disruption of KCa3.1 potassium channels. Proc Natl Acad Sci U S A 2009 Aug 25;106(34):14518-14523.

(282) Si H, Grgic I, Heyken WT, Maier T, Hoyer J, Reusch HP, et al. Mitogenic modulation of Ca2+ -activated K+ channels in proliferating A7r5 vascular smooth muscle cells. Br J Pharmacol 2006 Aug;148(7):909-917.

(283) Begenisich T, Nakamoto T, Ovitt CE, Nehrke K, Brugnara C, Alper SL, et al. Physiological roles of the intermediate conductance, Ca2+-activated potassium channel Kcnn4. J Biol Chem 2004 NOV 12 2004;279(46).

(284) Keira SM, Ferreira LM, Gragnani A, Duarte IdS, Santos, Isabel Anunciação Neves dos. Experimental model for fibroblast culture. Acta Cirurgica Brasileira 2004;19:11-16.

(285) Kaur D, Saunders R, Berger P, Siddiqui S, Woodman L, Wardlaw A, et al. Airway Smooth Muscle and Mast Cell-derived CC Chemokine Ligand 19 Mediate Airway Smooth Muscle Migration in Asthma. Am J Respir Crit Care Med 2006 December 1;174(11):1179-1188.

(286) Tennant JR. Evaluation of the Trypan Blue Technique for Determination of Cell Viability. Transplantation 1964 1964-Nov;2.

(287) Lowry OH, Rosebrough NJ, Farr AL, Randall RJ. Protein measurement with the Folin phenol reagent. The Journal of biological chemistry 1951 1951-Nov;193(1):265-75.

(288) Hamill OP, Marty A, Neher E, Sakmann B, Sigworth FJ. Improved patch-clamp techniques for high-resolution current recording from cells and cell-free membrane patches. Pflugers Arch 1981 Aug;391(2):85-100.

(289) Riss T, Moravec R. Comparison of Mtt, Xtt, and a Novel Tetrazolium Compound Mts for Invitro Proliferation and Chemosensitivity Assays. Mol Biol Cell 1992 SEP;3:A184-A184.

(290) Distler JHW, Jüngel A, Huber LC, Schulze-Horsel U, Zwerina J, Gay RE, et al. Imatinib mesylate reduces production of extracellular matrix and prevents development of experimental dermal fibrosis. Arthritis & Rheumatism 2007;56(1):311-322.

(291) Matsumoto H, Moir LM, Oliver BGG, Burgess JK, Roth M, Black JL, et al. Comparison of gel contraction mediated by airway smooth muscle cells from patients with and without asthma. Thorax 2007 OCT;62(10):848-854.

(292) Miki H, Mio T, Nagai S, Hoshino Y, Tsutsumi T, Mikuniy T, et al. Glucocorticoid-induced contractility and F-actin content of human lung fibroblasts in three-dimensional culture. Am J Physiol -Lung Cell Mol Physiol 2000 JAN;278(1):L13-L18.

(293) Woodman L, Siddiqui S, Cruse G, Sutcliffe A, Saunders R, Kaur D, et al. Mast Cells Promote Airway Smooth Muscle Cell Differentiation Via Autocrine Upregulation of Transforming Growth Factor Beta 1. Thorax 2008 DEC 2008;63:A51-A51.

(294) Kuzuya M, Cheng X, Sasaki T, Tamaya-Mori N, Iguchi A. Pitavastatin, a 3-hydroxy-3-methylglutaryl-coenzyme a reductase inhibitor, blocks vascular smooth muscle cell populated-collagen lattice contraction. J Cardiovasc Pharmacol 2004 JUN;43(6):808-814.

(295) Singer KH, Scearce RM, Tuck DT, Whichard LP, Denning SM, Haynes BF. Removal of fibroblasts from human epithelial cell cultures with use of a complement fixing monoclonal antibody reactive with human fibroblasts and monocytes/macrophages. J Invest Dermatol 1989 Feb;92(2):166-170.

(296) Chen M, Gorman S, Benson B, Singh K, Hieble JP, Michel M, et al. Small and intermediate conductance Ca²⁺-activated K⁺channels confer distinctive patterns of distribution in human tissues and differential cellular localisation in the colon and corpus cavernosum. Naunyn-Schmiedeberg's Archives of Pharmacology 2004;369(6):602-615.

(297) Ohya S, Niwa S, Yanagi A, Fukuyo Y, Yamamura H, Imaizumi Y. Involvement of Dominant-negative Spliced Variants of the Intermediate Conductance Ca2+-activated K+ Channel, KCa3.1, in Immune Function of Lymphoid Cells. Journal of Biological Chemistry 2011 May 13;286(19):16940-16952.

(298) Cruse G, Singh SR, Duffy SM, Doe C, Saunders R, Brightling CE, et al. Functional KCa3.1 K+ channels are required for human fibrocyte migration. J Allergy Clin Immunol 2011 12;128(6):1303-1309.e2.

(299) Ramos C, Becerril C, Montaño M, García-De-Alba C, Ramírez R, Checa M, et al. FGF-1 reverts epithelial-mesenchymal transition induced by TGF-β1 through MAPK/ERK kinase pathway. American

Journal of Physiology - Lung Cellular and Molecular Physiology 2010 August 01;299(2):L222-L231.

(300) Guo W, Shan B, Klingsberg RC, Qin X, Lasky JA. Abrogation of TGF-beta1-induced fibroblast-myofibroblast differentiation by histone deacetylase inhibition. Am J Physiol Lung Cell Mol Physiol 2009 Nov;297(5):L864-70.

(301) Jensen BS, Odum N, Jorgensen NK, Christophersen P, Olesen SP. Inhibition of T cell proliferation by selective block of Ca(2+)-activated K(+) channels. Proc Natl Acad Sci U S A 1999 Sep 14;96(19):10917-10921.

(302) Raghu G, Masta S, Meyers D, Narayanan AS. Collagen synthesis by normal and fibrotic human lung fibroblasts and the effect of transforming growth factor-beta. Am Rev Respir Dis 1989 Jul;140(1):95-100.

(303) Wicks J, Haitchi HM, Holgate ST, Davies DE, Powell RM. Enhanced upregulation of smooth muscle related transcripts by TGF beta2 in asthmatic (myo) fibroblasts. Thorax 2006 Apr;61(4):313-319.

(304) Hagood JS, Prabhakaran P, Kumbla P, Salazar L, MacEwen MW, Barker TH, et al. Loss of fibroblast Thy-1 expression correlates with lung fibrogenesis. Am J Pathol 2005 Aug;167(2):365-379.

(305) Bradding P, Okayama Y, Kambe N, Saito H. Ion channel gene expression in human lung, skin, and cord blood-derived mast cells. Journal of Leukocyte Biology 2003 May 01;73(5):614-620.

(306) Hibino H, Inanobe A, Furutani K, Murakami S, Findlay I, Kurachi Y. Inwardly Rectifying Potassium Channels: Their Structure, Function, and Physiological Roles. Physiological Reviews 2010 January 01;90(1):291-366.

(307) Oonuma H, Iwasawa K, Iida H, Nagata T, Imuta H, Morita Y, et al. Inward Rectifier K+ Current in Human Bronchial Smooth Muscle Cells. American Journal of Respiratory Cell and Molecular Biology 2002 March 01;26(3):371-379.

(308) Chilton L, Ohya S, Freed D, George E, Drobic V, Shibukawa Y, et al. K+ currents regulate the resting membrane potential, proliferation, and contractile responses in ventricular fibroblasts and myofibroblasts. American Journal of Physiology - Heart and Circulatory Physiology 2005 June 01;288(6):H2931-H2939.

(309) Koegel H, Kaesler S, Burgstahler R, Werner S, Alzheimer C. Unexpected Down-regulation of the hIK1 Ca2+-activated K+ Channel by Its Opener 1-Ethyl-2-benzimidazolinone in HaCaT Keratinocytes. Journal of Biological Chemistry 2003 January 31;278(5):3323-3330.

(310) Cai X, Chen L, Li L, Feng M, Li X, Zhang K, et al. Adiponectin Inhibits Lipopolysaccharide-Induced Adventitial Fibroblast Migration and Transition to Myofibroblasts via AdipoR1-AMPK-iNOS Pathway. Molecular Endocrinology 2010 January 01;24(1):218-228.

(311) Thannickal VJ, Lee DY, White ES, Cui Z, Larios JM, Chacon R, et al. Myofibroblast differentiation by transforming growth factor-beta1 is dependent on cell adhesion and integrin signaling via focal adhesion kinase. J Biol Chem 2003 Apr 4;278(14):12384-12389.

(312) Conus NM, Hemmings BA, Pearson RB. Differential Regulation by Calcium Reveals Distinct Signaling Requirements for the Activation of Akt and p70S6k. Journal of Biological Chemistry 1998 February 20;273(8):4776-4782.

(313) Kishaba Y, Matsubara D, Niki T. Heterogeneous expression of nestin in myofibroblasts of various human tissues. Pathol Int 2010 May;60(5):378-385.

(314) Nesti LJ, Caterson EJ, Li W, Chang R, McCann TD, Hoek JB, et al. TGF-?1 calcium signaling in osteoblasts. J Cell Biochem 2007;101(2):348-359.

(315) Mukherjee S, Kolb MRJ, Duan F, Janssen LJ. Transforming Growth Factor-beta Evokes Ca2+ Waves and Enhances Gene Expression in Human Pulmonary Fibroblasts. American Journal of Respiratory Cell and Molecular Biology 2012 JUN 2012;46(6).

(316) Ohanian J, Cunliffe P, Ceppi E, Alder A, Heerkens E, Ohanian V. Activation of p38 mitogen-activated protein kinases by endothelin and noradrenaline in small arteries, regulation by calcium influx and tyrosine kinases, and their role in contraction. Arteriosclerosis Thrombosis and Vascular Biology 2001 DEC 2001;21(12).

(317) Masiero L, Lapidos KA, Ambudkar I, Kohn EC. Regulation of the RhoA pathway in human endothelial cell spreading on type IV collagen: role of calcium influx. J Cell Sci 1999 OCT 1999;112(19).

(318) Rosen LB, Ginty DD, Weber MJ, Greenberg ME. Membrane Depolarization and Calcium Influx Stimulate Mek and Map Kinase Via Activation of Ras. Neuron 1994 JUN 1994;12(6).

(319) Moeller A, Ask K, Warburton D, Gauldie J, Kolb M. The bleomycin animal model: A useful tool to investigate treatment options for idiopathic pulmonary fibrosis? Int J Biochem Cell Biol 2008;40(3):362-382.